การวัดสังเกตุน้ำหนักรถบรรทุกในประเทศไทย และการประเมินสภาพโครงสร้างสะพานคอนกรีด

นาย ดวงมีชัย ดวนสุวรรณ

วิทยานิพนธ์นี้เป็นส่วนหนึ่งของการศึกษาตามหลักสูตรปริญญาวิศวกรรมศาสตรดุษฎีบัณฑิต
สาขาวิชาวิศวกรรมโยธา   ภาควิชาวิศวกรรมโยธา
คณะวิศวกรรมศาสตร์ จุฬาลงกรณ์มหาวิทยาลัย
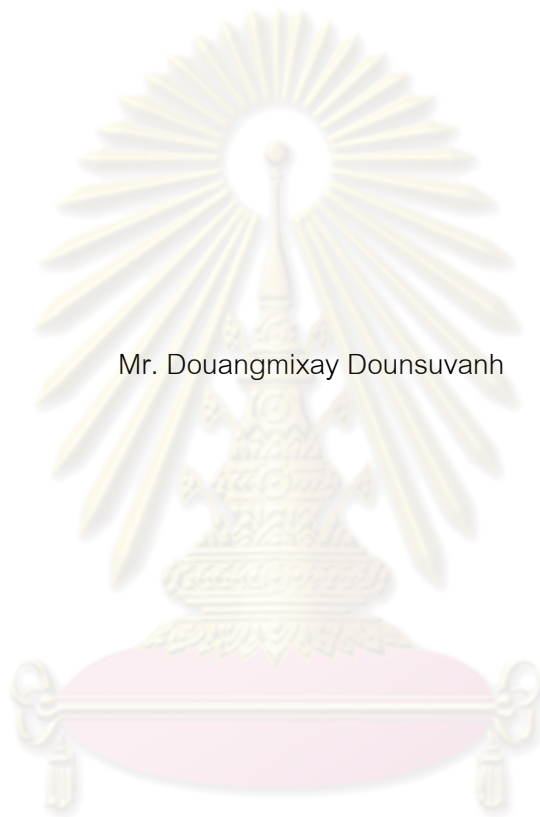ปีการศึกษา 2552

THAI TRUCK LOADING MONITORING AND ASSESSMENT OF EXISTING

CONCRETE BRIDGES

Mr. Douangmixay Dounsuvanh

A Dissertation Submitted in Partial Fulfillment of the Requirements

for the Degree of Doctor of Philosophy Program in Civil Engineering

Department of Civil Engineering

Faculty of Engineering

Chulalongkorn University

Academic Year 2009
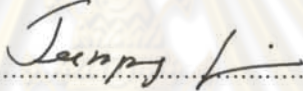
Thesis Title   THAI TRUCK LOADING MONITORING AND ASSESSMENT OF
                    EXISTING CONCRETE BRIDGES
By   Mr. Douangmixay Dounsuvanh
Field of Study   Civil Engineering
Thesis Advisor   Associate Professor Phoonsak Pheinsusom, D.Eng.
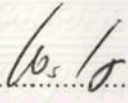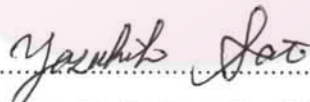Thesis Co-advisor   Associate Professor Yasuhiko Sato, D.Eng.

Accepted by the Faculty of Engineering, Chulalongkorn University in Partial Fulfillment of the Requirements for the Doctoral Degree

.... Dean of the Faculty of Engineering

(Associate Professor Boonsom Lerdhirunwong, Dr.Ing.)
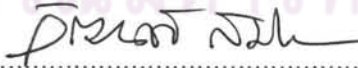
THESIS COMMITTEE

.... Chairman

(Associate Professor Teerapong Senjuntichai, Ph.D.)

.... Thesis Advisor

(Associate Professor Phoonsak Pheinsusom, D. Eng.)

.... Thesis Co-advisor

(Associate Professor Yasuhiko Sato, D. Eng.)

.... Examiner

(Associate Professor Boonchai Stitmannaithum, D. Eng.)

.... Examiner

(Assistant Professor Watanachai Smittakorn, Ph.D.)

.... External examiner

(Khampaseuth Thepvongsa, D. Eng.)

ดวงมีชัย ดวนสุวรรณ : การวัดสังเกตุน้ำหนักรถบรรทุกในประเทศไทย และการประเมินสภาพโครงสร้างสะพาน คอนกรีต. (THAI TRUCK LOADING MONITORING AND ASSESSMENT OF EXISTING CONCRETE BRIDGES) อ. ที่ปรึกษาวิทยานิพนธ์หลัก : รศ.ดร. พูลศักดิ์ เพียรสุสม, อ. ที่ปรึกษาวิทยานิพนธ์ร่วม : รศ.ดร. ยาสุนิโกะ ซาโต, 257 หน้า.

การตรวจสอบและประเมินความสามารถในการรับน้ำหนักของโครงสร้างสะพานเป็นสิ่งที่จำเป็นอย่างยิ่งในปัจจุบัน เนื่องจากสะพานที่ใช้กันอยู่ได้ผ่านการใช้งานต่อเนื่องมาเป็นเวลานานทำให้มีการเสื่อมสภาพ ในทางกลับกันปริมาณการจราจรและน้ำหนักบรรทุกของยานพาหนะมีค่าเพิ่มขึ้นจากในอดีต ในการที่จะประเมินความสามารถในการรับน้ำหนักของโครงสร้างสะพานเก่า จำเป็นจะต้องทราบน้ำหนักบรรทุกจริงของยานพาหนะ ดังนั้นการศึกษานี้ จะมุ่งเน้นการศึกษาในการพัฒนาเทคนิคในการตรวจวัดน้ำหนักรถ และเทคนิคในการประเมินโครงสร้างสะพานเก่าให้ถูกต้องและมีประสิทธิภาพ

ผลกระทบของน้ำหนักรถบรรทุกต่อโครงสร้างสะพานเป็นปัญหาสำคัญของประเทศไทยในปัจจุบัน เพราะโครงสร้างของสะพานในประเทศไทยได้ออกแบบตามมาตรฐานของ American Association of State Highway and Transportation Officials (AASHTO) แต่น้ำหนักรถบรรทุกจริงมีความแตกต่างจากน้ำหนักที่ใช้ในการออกแบบ และยังไม่มีข้อมูลน้ำหนักรถบรรทุกจริงที่เพียงพอในการพัฒนาแบบจำลองน้ำหนักรถบรรทุกที่ใช้ในการออกแบบสะพานของประเทศไทย ดังนั้นการศึกษานี้จึงได้พัฒนาวิธีการตรวจวัดน้ำหนักรถ โดยอิงตามวิธี Bridge Weigh-In-Motion (B-WIM) สำหรับอุปกรณ์ที่ใช้ มีราคาไม่สูงมาก ติดตั้งง่าย ผลการวิจัยนี้พบว่า มีความคลาดเคลื่อนในการประเมินน้ำหนักรวมของรถบรรทุก ร้อยละ 6 ถึง 10

การวิเคราะห์โครงสร้างคอนกรีตด้วยวิธี Nonlinear Finite Element Method (NLFEM) ทั่วไปไม่สามารถจำลองความเสียหาย และ รอยแตกร้าวได้ ในการศึกษานี้ ได้พัฒนาวิธีจำลองความเสียหายและรอยแตกร้าวของโครงสร้างคอนกรีตและคอนกรีตเสริมเหล็ก เพื่อนำไปใช้ในการประเมินโครงสร้างคอนกรีตเก่าที่มีจุดบกพร่องและรอยแตกร้าว เพื่อตรวจสอบวิธีจำลองที่นำเสนอ จึงได้วิเคราะห์คานคอนกรีต และคอนกรีตเสริมเหล็กที่มีจุดบกพร่อง จากการเปรียบเทียบพบว่า ค่าที่ได้จากวิธีที่นำเสนอมีความใกล้เคียงกับผลการทดสอบ

จากนั้นได้นำวิธีการที่นำเสนอไปวิเคราะห์โครงสร้างสะพานจริง ซึ่งสะพานที่วิเคราะห์เป็นสะพานคอนกรีตเสริมเหล็กจำนวน 3 สะพาน ซึ่งสะพานดังกล่าวได้ทำการเก็บข้อมูลความเสียหายและรอยแตกร้าวจากการตรวจสอบที่ภาคสนาม ผลจากการวิเคราะห์ด้วยวิธีที่นำเสนอนี้ ได้ทำการเปรียบเทียบกับวิธีการวิเคราะห์ที่ใช้กันอยู่ทั่วไป และผลจากการวัดจากภาคสนาม พบว่า วิธีการที่นำเสนอมีความใกล้เคียงกับผลทดสอบ ในขณะที่วิธีการที่ใช้กันทั่วไปนั้น มีความคลาดเคลื่อนมาก หลังจากนั้นได้นำวิธีการที่นำเสนอไปวิเคราะห์เพื่อประเมินสะพาน จำนวน 2 สะพานจากน้ำหนักรถบรรทุก ที่วัดมาได้ และ ทำการเพิ่มน้ำหนักจนกระทั่งสะพาน ถึงจุดรับกำลังประลัย จากการวิเคราะห์สรุปได้ว่า วิธีที่นำเสนอสามารถทราบถึงพฤติกรรมของโครงสร้างสะพาน และกำลังรับน้ำหนักสูงสุดของสะพาน ที่น่าเชื่อถือซึ่งกำลังที่ได้จากวิธีที่นำเสนอมีค่าน้อยกว่าวิธี NLFEM ทั่วไปแต่สูงกว่าวิธีมาตรฐาน ของ AASHTO

ภาควิชา........วิศวกรรมโยธา........... ลายมือชื่อนิสิต.......................................

สาขาวิชา........วิศวกรรมโยธา.......... ลายมือชื่อ อ.ที่ปรึกษาวิทยานิพนธ์หลัก.................

ปีการศึกษา........2552................... ลายมือชื่อ อ.ที่ปรึกษาวิทยานิพนธ์ร่วม.................

4871862121   : MAJOR CIVIL ENGINEERING

KEYWORDS: B-WIM TRUCK LOAD MONIOTRING SYSTEM/THAI TRUCK DATA/NLFEM/CONCRETE BRIDGE ASSESSMENT

DOUNGMIXAY DOUNSUVANH: THAI TRUCK LOADING MONITORING AND ASSESSMENT OF EXISTING CONCRETE BRIDGES. THESIS ADVISOR: ASSOC. PROF. PHOONSAK PHEINSUSOM, D.Eng., THESIS CO - ADVISOR: ASSOC. YASUHIKO SATO, D.Eng., 257 pp

At the present decades, bridge assessment and evaluation are the vital issues in Thailand. Due to that many old bridge structures are inclined and deteriorated. In the contrast, the present truck loads are heavier than previous truck loads. To evaluate the old bridge structure, the actual truck data have to be available. Therefore, this study has mainly studied on development truck load monitoring system, and assessment for existing bridges.

In Thailand, bridges have been designed by HS20-44 bridge design truck designed by AASHTO for many years, but the actual truck loads are greater than those the design truck. However, the data for local truck load has not been available to develop bridge truck load design for Thailand. Therefore, this study proposes an alternative truck load monitoring system based on the Bridge Weigh-In-Motion (B-WIM) algorithm. The system is inexpensive, no devices exposed on the road, and it is convenient in installation and maintenance. From results of testing monitoring actual truck load, the system estimates the GVW of the truck within 6% to 10% error.

Many constitutive models for nonlinear finite element method (NLFEM) for analysis concrete and reinforced concrete structures can not account for existing flaw/crack in old concrete and reinforced concrete (RC) members. In this study, the softening model for concrete and tension stiffening model for RC members are adopted to account for existing flaw/crack for analysis old concrete and RC structures. Some notched concrete and RC beams are analyzed to verify the proposed models which notch is assumed as an existing flaw. The analysis results of these examples are very close to the test results.

To apply the proposed models which existing flaw/cracks are accounted, three concrete slab bridges have been analyzed by 3D NLFEM. The analysis results obtained from the proposed models have then compared to truck test results and to general NLFEM results. The results obtained from the proposed models are closed to the test results, while the results by general NLFEM are much less than those of the test results. After that, two concrete slab bridges are continued to analyze evolution their capacity using the proposed models and using maximum truck load from monitored data. From the analysis results, the behavior and capacity of the bridges can be obtained reasonably which bridge capacity obtained from the proposed models is less than those from general NLFEM and higher than those from simplify method of AASHTO.

Department :   CIVIL ENGINEERING   Student's Signature :

Field of Study :   CIVIL ENGINEERING   Advisor's Signature :

Academic Year :   2009   Co-advisor's Signature :

ACKNOWLEDGEMENTS

CONTENTS

LIST OF TABLES

ศูนย์วิทยทรัพยากร

จุฬาลงกรณ์มหาวิทยาลัย

LIST OF FIGURES

page

CHAPTER I

INTRODUCTION

1.1 Introduction

The bridge structure is one of the most difficult structures in design and assessment, because the bridges are resisted to complicated loads and environments. The major loads applied to the bridges are dead load, live load, environmental loads (temperature, wind earthquake) and other loads (collision, emergency braking). The basic load combination is a simultaneous concurrence of dead load, live load, wind load, etc. The combinations involving other load components (earthquake, and collision forces) are required as the special case.

Live load covers a range of forces produced by vehicles moving on the bridge. The effect of live load depends on many parameters including truck weight, axle loads, axles configuration, span length, position of the vehicle on the bridge (transverse and longitudinal), number of the vehicles on the bridge, etc. The live load for bridge design must be specified properly relationship to vehicle crossing the bridges. In Thailand and many countries, bridge live load design has been adopted in the design specification from overseas countries. Sometimes design truck load from the specification is not proper to the actual local truck loads. This becomes critical issue when actual truck loads are higher than that design load. The bridges experiencing these higher loads are subjected to a higher risk of distress, damage, and possible failure. Therefore, actual local truck loads are very significant to the highway bridge engineers for bridge design, assessment, evaluation, and maintain.

For many years, truck weight measurement was conducted by stationary weigh scale with fixed location on the major highways which purpose of ensuring that trucks do not load exceedingly the legal limit weights of the transportation agency. This method is limited to detect overburdened trucks data because many drivers of overload truck intentionally avoid the scales, causing the results are biased to lighter weight trucks. Therefore, in recent decades, truck weight monitoring technology has been growing interested developing in many countries. In 1970s, Weight-In-Motion (WIM) system has been developed and became usefulness for truck load monitoring data. The major WIM systems can be categorized in to two approaches namely Road-

Surface Weigh-In-Motion (RS-WIM) system and Bridge Weigh-In-Motion (B-WIM) System. The RS-WIM system is the system where equipments are installed on the road surface. This system can also be categorized according to equipment types such as Bending Plate, or Load Cell WIM Systems with embedding on the road surface, and Piezoelectric Sensor WIM System with mounting on the road surface. The B-WIM is the system using instrumented bridge to monitor traffic trucks data. This system generally consists of devices such as: strain gauges or strain transducers attaching on the bottom of each bridge girders or bottom of slab bridges, axle detectors which are placed on the road surface. B-WIM system has many advantages over RS-WIM system such as it is convenient for installation, maintenance and inexpensive.

The assessment and evaluation (AE) of the existing bridge is major issue in the bridge engineering field at the present decades. It will provide necessary information of existing bridges: repair, rehabilitate, replace or demolish. The tasks of assessment and evaluation existing bridge structures can be separated in to two main tasks, the first one is assessment to know bridge condition (damaged and deteriorated rate of the bridge structure members), and the second is analysis modelling to evaluate the capacity of the bridge structure members to ensure safety performance to the traffic loads. Therefore, the accuracy of AE is according to information of bridge structure members (damaged condition) and analysis modelling of the bridge structure. There are many methods to estimate damage condition of the bridge structure members such as bridge inspection, structure identification techniques, etc. After damaged condition of bridge members are known, consequent works is the evaluation capacity of the bridges. The difficulty is that how to connect between the bridge condition from assessment works and evaluation capacity model of the bridge. The conventional method to evaluate bridge capacity is based on Manual for Condition Evaluation of Bridges of AASHTO, 1994. In this method, the bridge damage condition is interpreted as reduction factor to reduce bridge component strength. The main concept of this method is that the bridge will be safe if the strength of the bridge members is greater than effects induced by applied load (Rating factor is greater than one). However, it is still difficult to include actual damaged condition using this conventional method. Therefore, it is needed to find out the approach that can present actual bridge condition to reach more accuracy for evolution existing bridge.

The reinforced concrete (RC) bridge structure is the most complicated for AE, especially aged RC bridge structures; because the reinforced concrete structure has complicated behaviour, it is composed of two materials, concrete and steel reinforcement. The concrete is made of cement and natural material (sand, gravel and water) which it is very high capacity in compression force, but very low capacity in the tension; the steel bar is reinforced to enhance in tension forces. Many researches have clearly understood the behaviour of the concrete structure at the certain conditions, and successfully in the design. Many design codes have been developed using in the worldwide. However, the works for assessment and evaluation of the existing concrete structure is still under research; especially the deteriorated concrete bridges structures, because bridge is withstood to uncertain environment condition and traffic loads.

In Thailand, Bridge Design has been based on AASHTO specification, and design live load using HS20 – 44 loading, for many years. For the over loading case, it may be increased this design load up to 30 % to accommodate heavy trucks. However, there are still no any studies for increasing of the design load from the original specification. In fact, the actual trucks in the Thailand are also unlike the AASHTO truck model, and the legal limitation of vehicle weight in Thailand is different from USA definitely. Furthermore, at the present time, many bridges, especially concrete bridges types have been old and some are deteriorated.

Therefore, this study would like to study into two main parts, first part is to develop truck load monitoring system base on the concept of B-WIM system and test this system to monitor Thai truck data at the Bangkok city, second part is to develop models for 3D nonlinear finite element method (NLFEM) accounting for existing flaw/cracks to analysis diagnosis and evaluation existing concrete bridge.

1.2 Objective and Scope of the Research

1.2.1 The Objective of the Research

The main objectives of the research are as below:

1. To develop truck load monitoring system and to monitor actual local truck loading at Bangkok, Thailand.

2. To present actual Thai truck loading and its configuration from monitoring data, and compare the maximum observed truck loads to the bridge design loading of AASHTO, HS20-44 using simply analysis.

3. To adopt softening model of concrete and tension stiffening model of reinforced concrete accounting for existed flaw/crack at tension region for 3D nonlinear finite element analysis of reinforced concrete structures.

4. To apply proposed models for analysis diagnosis existing concrete bridge structures by 3D nonlinear finite element method which existing flaw/cracks are considered.

1.2.2 The Scope of the Research

Truck load monitoring system:

- Truck loading monitoring system will be based on B-WIM algorithm for this study, which the bridge is modeled as one dimension of beam element and truck is assumed in a constant speed crossing the bridge. For closed axles or axle group weight of truck is assumed as one point load applied to the bridge.

- Thai truck data (axle weight, axles groups weight, axles spacing, and gross vehicle weight (GVW)) from monitoring will be presented. Further more, the simplified analysis for short to medium span bridges will be used to observe the responses of heaviest truck from monitored data to HS20-44 truck loading of AASHTO.

Assessment existing bridges using NLFEM:

- The bridge geometry will be modeled in 3D, 20 nodes solid element for Nonlinear Finite Element Method. CAMUI program which developed at Laboratory of Engineering for Maintenance System, Hokkaido University will be used.

- The concrete and reinforcement properties are considered as the nonlinear material, constitutive models. The existed flaw/cracks at the tension zone of the members are accounted by adopting softening and tension stiffing models for concrete and reinforced concrete element, respectively.

- Two types of cracks at the tension region of old concrete bridge are considered, i.e. cracks mapping from site are called visible cracks, and small cracks which may can not be observed form the site, are calculated from bending member theory and called theoretical cracks.

- In this study, easting cracks are assumed to have the same width trough the depth of the effective tension region of the concrete structure members, and assumed to have no influence to the steel reinforcement property.

- Existing concrete slab bridges are used as case study for proposed models approach by 3D NLFEM. The bridge curbs and main slab are assumed to be full composite.

1.3 Methodology

The methodology in this research consists of literature review, field data collecting and testing, data simulation and model analysis as explaining in the following.

Literature review:

The truck load monitoring technologies, bridge assessment method, and NLFEM for reinforced concrete structure have been reviewed from many previous researches to be back ground of the study.

Data collection and field testing:

The field works are included truck load monitoring and inspection existing concrete slab bridges.

The system has tested using prestressed T-girder bridge at main highway, Bangkok Earthen Ring Road, near Bangkok metropolitan. The equipments for this monitored system are included such as strain gauges, data acquisition (DAQ), photoelectric sensors, CCTV, and PC computer. After system was calibrated properly, then the actual truck loads data were collected continually and saved to computer hard disk for further simulation.

Some existing concrete slab bridges, span 8 to 10 m at northern part of Thailand were selected foe inspection and testing. The bridge inspection was included such as detail visual inspection, crack mapping, and bridge dimension measurement. The testing works included such as material testing and non destructive load testing which these testing works were conducted with inspecting company.

Analysis and simulation:

The monitoring data that collecting from the site was further to simulate. The strains signal was filtered by lowpass filter. The program for simulation monitored data and deriving trucks was written using MATLAB code. The heaviest trucks from monitored data were compared to HS20-44 of AASHTO specifications by using simplify analysis to short and middle simple span bridge, range from 6 m to 35 m.

The material constitutive models of softening and tension stiffening are adopted to account for the existing flaw/crack at tension zone in concrete and RC

structures, and then the proposed models have installed to program code file of 3D NLFEM, CAMUI program which this program is originally developed at Maintenance System Laboratory, Hokkaido University. Then the proposed approach was verified by analysis notched concrete and RC beams. After the program was proved working properly, some existing concrete slab bridges span length between 8 m have been chosen to be case study for analysis diagnosis their behaviours.

1.4 Dissertation Organization

This dissertation consists of seven chapters. Chapter I presents a general introduction of the research motivation, objectives, scope and methodology of this research. Chapter II reviews previous research works related to the vehicle-bridge truck load, truck load monitoring system and B-WIM system, bridge evaluation, and NLFEM for concrete and RC structure. Chapter III describes the theoretical of WIM and B-WIM systems. The formulation, equipments for the system using in this study are also presented. Chapter IV presents the application of truck load monitoring system which developed in this study. Signal collection, calibration procedure, and final monitoring results for Thai truck data are also included in this chapter. Chapter V presents the NLFEM concept for analysis concrete and reinforced concrete structures. Concrete mechanical properties, crack in concrete and RC, and proposed models of tension softening and stiffening models for accounting for existing flaw/crack are also presented in this chapter. Then the notched concrete and RC beams are used to verify the proposed models. Chapter VI presents the application analysis diagnosis full scale concrete slab bridges using models derived from chapter V. Chapter VII summarizes the obtained results, and gives discussion on the effectiveness and limitations of the results in this study. In addition, further research is recommended in this chapter.

CHAPTER II

LITERATURE REVIEW

2.1 General

At the present decade, the major task in structural engineering can be divided into two challenging tasks. First challenging task is about new structural design. Due to the advanced technology has been developed; the accuracy, reliability, durability and economic for the new structures are needed. For many decades, the structural design approach has been developed increasingly. The design code for the structures since the beginning of 1990s was Working Stress Design (WSD) method, then at the middle of 1990s was Ultimate Load Design (USD) method, and at the present time is Load Resistant Factor Design (LRFD) method. The second challenging task is about how to maintain the existing structures. Even though the structures were designed by the same code, but they may be constructed at the different construction technique and located in different environments; i.e. in Thailand, the bridges have been designed by AASTHO standard specification, which this specification has been developed in United State of American (USA) according to USA conditions (Loading and environment); in fact, environment condition and actual truck loads in Thailand are differed from USA. In addition, the trucks at the present time are also different from the tucks at the time of bridges designed. Therefore, the evaluation of existing bridges is more complicated than that design new bridges. The researches about effect of local truck loads and evaluation for the existing bridges structures are important at the present.

This study, therefore, would like to develop the advanced technique for truck load monitoring system and evaluation of existing bridge structures. To study an existing bridge structures, the important information are the actual applied load during its service life, structure member conditions, and method of structure analysis. Therefore this research has been divided into two main parts, the first part is studied about truck loading monitoring system, the B-WIM technique has been adopted; and the second part is studied about assessment of existing bridges, 3D NLFEM has been used. The following sections will summary previous research works that related to these topics.

2.2 Literature Review for Truck Load Monitoring

2.2.1 Bridge Live Load, AASHTO Loading

The live load for bridge design has been developed continuously since the beginning of twentieth century. Nevertheless, it is still difficult to the bridge engineers to develop unique model for using in the worldwide. In the industrialized countries, such as Unite State of America, England, Australia, etc, their have conducted a lot of researches to develop live load model for their own bridge design specification. In accordingly, many counties which have less research have to base on codes or specifications from these industrialized countries. Using overseas specification, it is confused to the local engineers to accommodate between overseas design trucks and local regulation trucks.

The American Association of State Highway Officials (AASHO) Standard Specifications for Highway Bridges was first published in 1931 (Tonias, 1995), and it has been widely used for design of highway bridges in the USA and elsewhere. In 1973, the term of AASHO was changed to AASHTO (American Association of State Highway and Transportation Officials). The first published code was based on a train of truck which included truck loading such as H15-35 (15 tons truck), H20-35 (20 tons truck). The HS20 truck and semi-trailer combination was introduced in 1944, five truck classes were made in this year, H10-44 (20,000 lb/ 9,072 kg), H15-44 (30,000 lb/ 13,608 kg), H20-44 (40,000 lb/ 18,144 kg), HS15-44 (54,000 lb/ 24,494 kg), and HS20-44 (72,000 lb/32,659 kg). Together with these trucks, the lane loading configuration (Uniform distribution load combined with concentrated forces) was replaced for the train of the truck. Generally typical of truck loading governs for short simple span bridges, lane loading typically holds for long and continues span bridges. In the 1976, AASHTO Interim Specification modified this by requiring the bridges on Interstate Highway should also be able to carry an "Alternate Military Loading" consisting of two axles, 1.22m spacing and 10,608 kg for each axle load.

In 1986, AASHTO commissioned a major review of US bridge design practice, leading to the 1994 first edition of their Load and Resistant Factor Design of Bridge Specification (AASHTO LRFD). The most of this works was carried out by Nowak, such as Nowak and Hong, 1991; Nowak and Nassif, 1993; Nowak, 1993; Nowak, 1995, etc. The new AASHTO LRFD loading consists of design truck, HL93, coincident with lane loading. The design truck is effectively the old HS20-44 truck semi-trailer combination in SI unit. The axle load of 35.6, 142 and 142 kN of HS20-

44 become 35, 145 and 145 kN, respectively, and the axles spacing 4.3m and 4.1-9.1 m are adjusted to 4.3 and 4.3 – 9.0m, respectively. The design lane load, the old one is changed from 9.34 kN/m to 9.3 kN/m, and the concentrate (knife-edge) loads (116 kN for shear and 80.5 kN for bending moment) are changed to be 116 kN for shear and 85kN for bending moment, respectively. The design tandem or Military Loading consists of two 110 kN axle loads, with axle spacing of 1.2m.

2.2.2 Thai Truck Loading:

Transportation Regulation about truck loading in Thailand in 1991 has limited only the vehicle gross weight and axle loading (Department of Civil Engineering, Chulalongkorn University, 2003). The trucks loading are determined into four types such as: 6-wheel truck, 10-wheel truck, 18-wheel truck trailer combination and 18-wheel truck semi-trailer combination; and legal limit of gross weight of these trucks are 12 tons, 21 tons, 39.2 tons and 37.4 tons, respectively.

In 2005, Highway Transportation Department has issued new regulation of truck weigh which limited of axle and gross weight of vehicles, (Department of Highways, Thailand, 2005). The trucks have been classified in to 12 types; however the heavy weight trucks which may affect the bridge structures can be summarized in to five truck types such as: 6-wheel truck (15 tons), 10-wheel truck (25 tons), 12 wheel truck (30 tons), 18-wheel truck semi-trailer combination (45 tons), 18-wheel truck full-trailer combination (47 tons) and 22-wheel truck full-trailer combination (53 tons).

From the primary comparison between Thai truck loading and AASHTO, HS20-44 for bridge structure has indicated that the bridges with length less than 16m, HS20-44 loading is conservative, for the bridges with length less than 34m, bridge loading design should be 1.3 to 1.8 times of HS20-44 loading, and when the length of the bridges are increased, the maximum bending moment from multiple Thai truck loading trend to present more than HS20-44 loading (Phoonsak, 2003).

2.2.3 Truck Loading Monitoring System

Truck loading monitoring is very important to road and bridge engineers. In the past, truck data were collected by truck surveys, and weighting scale stations which were installed in the fixed location along major high ways. The usefulness data obtained from stations were limited, because many drivers of overload truck intentionally avoid the scales, causing the results are biased to lighter weight. Therefore in the early of 1970s, Weigh-In-Motion (WIM) technology, which can

estimate the vehicle weight during its moving, has been developed. WIM technology becomes usefulness, which can provide unbiased data. At the present time, many countries have been developing and applying this technology along their main highway such as USA, Canada, Australia, England, France, German, Slovenia, Hong Kong, etc (European Commission , 2001, 2001; Peter, 1995). The major WIM system for monitoring truck weight along highway can be categorized in to two approaches, namely the Road-Surface WIM (RS-WIM) system and under bridge structure systems. The under bridge structure system is based on measuring bridge response when truck passing over bridge, and this method can be based on dynamic or static structure systems. To estimate truck weigh which is base on static influence line method called Bridge Weigh-In-Motion (B-WIM) system, other which is based on dynamic bridge interaction called Moving Force Identification (MFI). However, MFI is still difficult in application, due to many parameters are involved in interaction between truck and bridge.

2.2.3.1 Roadway Surface WIM Systems

The RS-WIM system is used for measure vehicle weight and axles configuration in the slow speed, which equipments of system are embedded or stripped on the road surface at the appropriate location. The RS-WIM system called load cell WIM was first researched in the USA since 1950s by the Virginia State Department of Highway (Grant G. S, 2006). This system featured large concrete platform. The platform was supported by columns which bonded strain gauges. At the first time, there were many limitations in this system. In 1960s and 1970s, the digital computers made possible to handle some of limitations, and then the system has applied widely for truck weigh monitoring and screening over truck weigh along the highway in the USA. In the 1970's and 1980's RS-WIM system became commercially available. In the mid-1990's, WIM system started to be an object of study under contract with the American Federal Highway Administration (FHWA). A large quantity of WIM data has been collected within the Long-Term Pavement Performance program in the USA.

Some European countries developed WIM since 1970s such as France and United Kingdom (UK). Many counties have investigated the possibility of using WIM systems in the late 1980s. Early 1990s, a great demand arose for improved RS-WIM technology, more durable and accurate sensors, more powerful electronics, etc. Later, quality assurance of WIM data emerged as a growing need. Therefore, COST323

(Cooperation for Science and Technology), was initiated in 1992 as the first European co-operation action on WIM of road and vehicles. In addition, a large research project: 'WAVE' (Weighing in motion of Axles and Vehicles for Europe) commenced in 1996. This project has developed many new features of WIM (European Commission, 2001).

The most common technologies of RS-WIM are Piezo-electric sensors (Figure 2.1a), Bending Plates (Figure 2.1c), and Load cells (Figure 2.1b). The Piezo-electric sensors produce a voltage in proportion to the applied stress, from which axle truck loads can be calculated. The Bending Plate is measurement bending strain due to axle truck load, than the strain convert to axle truck load. Less common is Load cells, which measure weight via hydraulic pressure change or compressive strain of axle truck load (Schultz, 2006). A limitations of RS-WIM systems are measuring vehicle axle weights at slow speeds leading to be inconvenient for collecting truck data. For the permanent systems, it is costly of installation and maintenance. The equipments of system are also exposed to road surface. The error level about 15% to 20%. At the present time RS-WIM is developed and widely used in many countries, new researches still effort to increase the accuracy and measure vehicles in speed.

a.) Piezo-electric sensors   **b.)** Load cells

c.) Bending plate
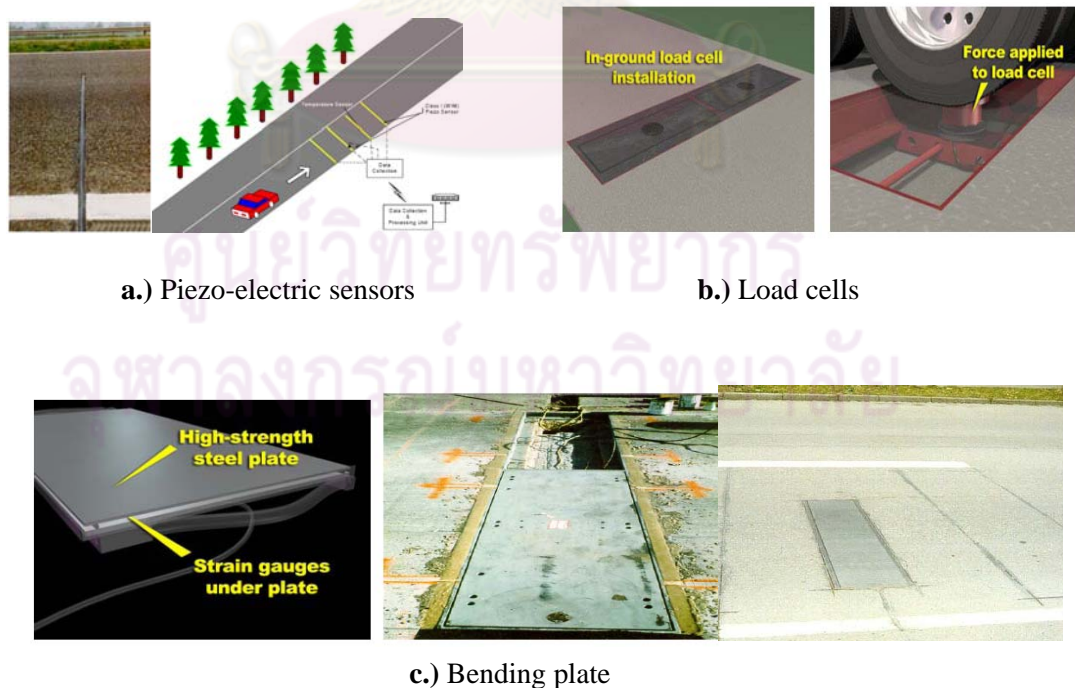
Figure 2.1 Road surface WIM systems (European Commission, 2001)

2.2.3.2 Bridge Truck Load Monitoring System

The main disadvantages of the RS-WIM system are interruption traffic during installation, exposure to road surface, un-durability etc. To overcome these disadvantages, truck load monitoring using bridge structure has been developed. The mathematical model for interaction between bridge and structures can be done by two approaches such as structural static approach and structural dynamic approach. The static structure model is called Bridge Weigh-In-Motion (B-WIM) system and dynamic structure model is call Moving Fore Identification (MFI) system.

Bridge Weigh-In-Motion (B-WIM) System:

The B-WIM system is the process weighting the trucks travelling on the bridges, by measuring the deformation of a bridge and the use of the measurements to estimate the attributes of passing traffic loads (European Commission , 2001). This technology generally consists devices as: strain gauges or strain transducers attaching on the bottom of each bridge girders or bottom of slab bridge, axle detectors placing on the road surface, data acquisition equipment for covering strain gauges and axle detector signals, and personal computer for recording the data (Figure.2.2). The strain gauges or transducers were provided to measure bending strain of bridge girders, and axle detectors provide to measure speed and axles spacing of trucks, these information then can be used to estimate axle weight through the application of an algorithm, the Gross Vehicle Weight (GVW) can be summed up of axle's weight. The algorithm obtains truck axle weight by comparing theoretical models to measured responses.
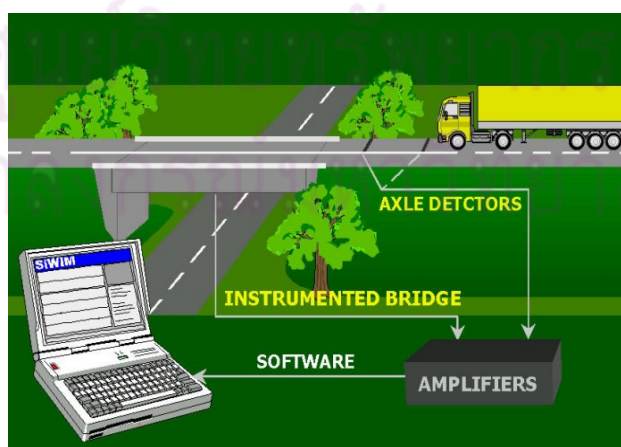
Figure 2.2 Layout of conventional B-WIM system (European Commission, 2001)

B-WIM system was firstly developed by F. Moses in 1970s, concept of using bridges as scales to weigh trucks during moving across the bridge. This becomes the pioneer of B-WIM technology (Moses, 1979). The system by Moses consisted devices such as button box, tape switches, strain gauges, and instrument van. The accuracy of the system in the GVW is about 10% to 15%. The system is more accuracy in estimating the GVW than individual axle weight and the axle group load (tandem and triple). The vehicle velocity is another extremely important parameter for accuracy of B-WIM system.

In 1986, Peters developed truck loading monitoring system by using culverts in Australia (Peter, 1986, 1995). The basic principle is similar to the algorithm of B-WIM as Moses. The system consists of strain transducer attached at the bottom surface of the culvert deck transversely at midspan to record the bending strain caused by the passage of the vehicle axles. Vehicle speed, axle number and spacing were recorded by axle detector installed on the road surface. The total culvert bending strain is summed up individual strain gauge similar to a theoretical bending moment influence line. The site condition selection is very important to minimize weighing errors, the selection of culvert should consider such as: single span box culvert less than 2.7 m, a smooth and flat road surface, little skew, pavement cover more than 200mm but less than 1500mm. The error of this system has been found to estimate static GVW within +/- l0%, and the individual axle weight within +/- 15%.

In 1990s, B-WIM has been popular research in Europe. As a rapid increase in road traffic and a major expansion in the number and size of heavy goods vehicles has occurred on European road. In addition, there is pressure from freight companies to increase truck weights and dimensions. It is of particular concern that such heavy vehicles are aggressive for bridges and pavements and that a significant number of trucks are illegally overloaded. To enhance the system management of highway transportation and demand of the traffic data for development road ands bridges structures in European road net work, thus, a proposal for a large research project, 'WAVE' (Weigh in motion of Axles and Vehicles for Europe) was submitted in March 1995 by a consortium of 11 partners from 10 countries such as France, England, German, Sweden, Slovenia etc. Under WAVE project, several bridges of different type were instrumented to enhance B-WIM system. The method was extended to short concrete slabs, box culverts, long-span bridges, including box girders and orthotropic decks. A new approach, no axle detector system was

developed for short span concrete slab bridge and orthotropic steel deck bridges. Subsequently, this concept is called Free of Axle Detector B-WIM (FAD B-WIM) (Zidaric, 2005). The basic algorithm for B-WIM developed in WAVE is also similar to Moses system which bases on measurement responses and theoretical bridge influence line. The error for GWV can be less than 10%, however the major accuracy is depended on bridge type, smoothing of the road surface, selection of bridge influence line and calibration procedure.

In Japan, Ojio and Jamada (2005) proposed a method of axle-detector-free B-WIM called the reaction force method by using steel plate girder bridges. In Japan, steel plate girder bridges is popularly using for medium span highway bridges. At the end of the steel plate girders, vertical stiffeners are put for supported bearing (Ojio, and Yamada, 2005). The strain gauges can be attached on theses end vertical stiffeners at both sides of the bridge to be both axle detector and axle truck load signal. The velocity of the trucks is estimated by comparison of strain signals on both sides of the bridge. When truck crosses the bridge, sharp edges will occur in the reaction force response wave. The amount of the edges is corresponding to linear to independent axle weight. Axle spacing is estimated by the interval of axle; the truck classes are classified by axle spacing. The error of this B-WIM, reaction force method for estimation of axle spacing is bout 5%, for GVW is 15%.

Moving Force Identification Systems:

The B-WIM technology calculates based on static algorithm. A technique to estimate the vehicular loads from the dynamic interaction between bridge and vehicle is called Moving Force Identification (MFI) those of mathematical parameters of the bridge and vehicle must be complicated than static method.

Law and Chan (1997) were developed the theory of moving force identification on the basis of the modal superposition principle, and assuming the force as a step function in a small time interval. A method is developed to identify the force in the time domain, which it called 'Moving forces Identification: A Time Domain Method (TDM). The simulation of both one and two forces moving on a simply supported beam is used to evaluate the method. An experiment with a model car moving on a simply supported beam is performed to simulate the vehicle bridge interaction. Both the simulations and the experimental results show that the method is effective, and acceptable results can be obtained by combining the use of data from

bending moment and acceleration measurements. However, the proposed method is noise sensitive, especially in identifying more than one moving force.

Chan et al. (2000) were studied of forces identification using Prestressed concrete bridges. The Time Domain Method (TDM) was implemented for this study. Field measurement was carried out using an existing prestressed concrete bridge. Two-axle heavy truck was hired for the calibration test of field measurements. The dynamic bending moments of the test bridge deck were acquired by both calibration vehicle and in-service vehicles. The special case of force identification considering prestressing concrete bridge forces in the identification process was also studied. The results show that the equivalent axles load and gross weight are accepted, the percentage of errors are between 2% to 5%. Therefore, the proposed method of moving load identification is valid for applying in the prestressed concrete bridges. However, this testing can estimate only two axle trucks.

2.3 Literature Review for Assessment and Evaluation of Existing Concrete Bridge.

Bridge Assessment and Evaluation:

In Thailand and many countries in the world, aged and deteriorated bridges have been increased every year. In addition, some bridges have been deteriorated faster than usual. This is becoming main issue to highway agencies to evaluate their bridges performance. A rational bridge management is vital required advanced technology to categorize actual condition of bridge structure components accurately. The bridge assessment and evaluation (BAE) is the tool for bridge management system. BAE system may be involved in two steps, the first one is classification bridge structure member condition, and the second one is model to evaluate bridge capacity. Bridge structure condition can be done by visual inspection, Non Destructive Evaluation (NDE), Destructive Evaluation (DE), Load testing, and structure damage identification. The estimation of bridge capacity can be done by model analysis, or full load testing.

AASHTO Manual for Condition Evaluation of Bridge (AASHTO, Manual 1994), is guideline for conventional bridge inspection and evaluation. Five types of bridge inspection are recommended in the manual such as: (a) Initial inspection, (b) Routine inspection, (c) Damage inspection, (d) In-depth-Inspection and (e) Special

inspection. Generally bridge inspection task is included many testing methods such as NDE, DE, full scale load testing etc. The information from bridge inspection will be used for decision bridge structure member strength. Then the bridge capacity can be estimated by load rating equation which the result will be presented as rating factor (RF). The methods of load rating of the bridge members recommended in the manual are Allowable Stress Design (ASD), Strength Design (SD) and Load Resistant Factor Rating (LRFR).

Stalling, and Yoo (1993) were performed test on three short span, two lanes steel bridges. Tests were conducted with stationary and moving test trucks placed on the bridges one at a time and side by side. Wheel load distribution factors were calculated from the result of the stationary truck-test, and impact factors were calculated from the result of moving truck test. The test results indicated that the response the calculation girder strain using simplify method from the code were consistently larger than measurement values. The rating factors from testing are 49% to 90% larger than those determined by ASD of the AASHTO. This is due to that the bridge are included the benefit effects such as three-dimensional characteristics of bridges, composite action, support restraint, and stiffness of secondary structures.

Huria et al. (1994) were rating existing concrete slab bridge by different approach such as conventional AASHTO approach, 3D linear finite element method (LFEM), and 3D nonlinear finite element method (NLFEM). The AASHTO was using equivalent slab width for loading distribution, the bridge capacity were evaluated by ASD and SD. For finite element method, the layer shell element was modelled for bridge geometry. The NLFEM is accounted for material nonlinear model. The results indicated that the rating factor result from LFEM is higher than the result of SD (AASHTO method) two times, and the result from NLFEM is higher than the result of SD more than three times. However, SD and LFEM methods can not investigate failure mechanism of the bridge. The NLFEM can present failure behavior of the concrete bridge.

Law et al. (1995) developed a method of assessing the load currying capacity as well as structure condition of a T-beam bridge deck based on dynamic vibration approach. The approach aims to apply for assessment and evaluation existing bridges which reinforcing steel in the structure members is not known. Both full scale static and dynamic test were employed to this task. The result indicated that is possible to use bridge vibration response to assess the condition of the concrete structure. The

percentage of reinforcement in the main beam was estimated from dynamic testing, and then load carrying capacities of the bridge structure can be implied.

Hu and Shenton (2003) presented the method of damage identification in a two span continues beam using static-based damage identification. The procedure is redistribution of dead load in the structure when damage occurs to determine the location of damage in the structure. Damage is presented by a finite length section of reduced flexural rigidity in the beam. Damage is identified by minimizing the error between measured strains and strains computed from finite element model of damaged structure. The solution is obtained by using genetic algorithm.

Nonlinear finite element method (NLFEM) for concrete structure:

The most difficulty to the bridge engineers is studying the behavior of existing concrete bridges, because the concrete is inelastic material since at initial applied loading. Beside of the knowledge of the bridge structure, the knowledge of the concrete mechanics is also vital. This section needs to brief reviewing how the finite element method (FEM) can be used to analyze concrete structures. The conventional analysis and design of the concrete structure is assumed that the concrete is linear material, the secant modulus is used as material stiffness, and the tension strength of the concrete is neglected. But in the reality, concrete will occur the micro crack at the small applied load (about 30% of ultimate compressive strength, f_c') (Jiang, 1995), this leading to concrete behaves as nonlinear material. In the recent decades, the computation technology and knowledge of mechanical properties of the concrete material have been developed; the real nonlinear behavior of concrete material have been employed to analysis model, and tension strength of the concrete also can be accounted and greatly important in reinforced concrete structure. One of the most effective computational tool to accounting for nonlinear behavior of concrete is using nonlinear finite element method (NLFEM). Using this approach, the computational and experimental results can be matched closely.

The pioneer researchers for NLFEM analysis of concrete structures were Ngo and Scordelis (1967). Their paper has greatly exerted impact to subsequent research works. In their paper, the concrete and steel reinforcement were both modeled by triangle elements. Elastic-plastic of the material behavior was assumed for concrete in compression and steel reinforcement's elements. Linear elastic fracturing model was used for concrete in tension. The reaction between concrete and reinforcing bars was modeled as bond element. Bond elements in the form of bond link element are

inserted at the concrete and steel interface. In addition, Ngo and Scordelis purposefully incorporated an inclined crack into the mesh during the mesh generation stage (location of the crack had been pre-determined from experiments). Linkage elements are inserted to connect the nodal pairs at the two surfaces across the crack. The linkage elements are able to simulate the aggregate interlock and dowel action across the crack. This analysis concept is a pioneer for discrete crack model for NLFEM of concrete structure.

At the later year, Nilsson (1968) was also presented NLFEM analysis of concrete structure which the crack propagation in the concrete elements can be presented as discrete crack. His concept is that cracks are not introduced in the mesh generation stage. The crack will be happened when the tension force is exceeded tension strength of the concrete. The crack is defined along an element edge which is the most nearly normal to the principal tension direction, and is modeled by establishing two disconnected nodes across the crack width. Finite element mesh geometry is not changed, but crack are forced to propagate along the element edge, therefore the crack patterns are depended also on the mesh geometry. This concept of crack prorogation may not be reality, because actual cracks may occur in the direction perpendicular to the principle tension stress. However this paper is significant to further for finite element modeling of discrete cracks approach.

The alternative smear crack approach for NLFEM analysis of concrete structure was proposed by Rashid (1968). The main concept of this technique is that the constitutive properties of the concrete material in un-crack will be changed after crack occurred. The crack will be propagated when principal tension stress of concrete element exceeds tensile strength of the concrete, and the material stiffness at the direction of principal stress will be reduced. This paper is the great pioneer to smear crack approach on NLFEM of the concrete structure, and it is being popular used at the present.

In additional to smear crack model, Schnobrich (1977) was proposed model of element whose steel reinforcement is smeared over concrete elements at the around reinforcement region (effective zone), and then concrete and steel are combined in the single element called reinforced concrete (RC) element. The embed steel in RC element is introduced as steel ratio. This approach is bringing many benefits that the elements number of the FEM model are reduced, the computational time is also reduced.

In the discrete element, the steel bar is modeled as truss element, and the interaction between concrete and reinforcement steel is modeled by bond link element, or contract element. The interaction property is introduced by constitutive model of bond link or contract element model. In smeared steel reinforcement element (RC element), the effect of interaction between concrete and steel reinforcement is indirectly accounted as tension stiffening model (Gilbert and Warnner,1978). In the Gilbert paper, the effect of the tension capacity of the concrete after crack was investigated for reinforced concrete slab, they stated that after concrete crack, descending tension strength of the concrete is greatly important.

From the pioneer research, the difficulties for NLFEM of concrete and RC structure have been further studied. The major issues is accounting for nonlinear and crack propagation behavior of the concrete and the FEM mesh size. Hillerborg et al. (1976) was applied fracture mechanics, called fictitious crack model, to explain nonlinear at post crack of the plain concrete. The main concept of fictitious crack model is that the area under softening curve of stress and crack width is the fracture energy of the concrete. This energy is a constant value and depends on concrete properties, and the region of the crack tip is defined as fracture process zone which assume to process in the narrow discrete region. In the reality the fracture process zone of concrete may not be processed continually, and not necessary developed is narrow region line as Hillerborg concept. Therefore, Bazant and Oh (1983) was proposed crack band theory by the concept that the effect of crack is smeared over the effective element width (crack band width) which has the dimension about three times of maximum aggregates. This concept is called crack band theory.

The smear RC element (steel smear over the concrete) and smear crack model have many advantages over discrete model, especially for analysis large scale structure. Therefore this concept has been widely developed in the worldwide and successfully used for analysis large scale structure models. The accuracy of the analysis is mainly depended on selection of material constrictive models. Vecchio and Colin (1986) proposed the modified compression field theory for analysis shear wall. The concept of Vecchio and Colin model is that when crack occurs in element, it not only tensile strength of concrete in the normal crack direction is reduced but also compression strength in parallel to crack direction is reduced as well.

Okamura and Maekawa (1991) published greatly report on NLFEM analysis of the concrete structures using smear crack concept. Many constitutive models were

developed and presented such as constrictive elasto-plastic and fracture model to account for inelastic behavior of the concrete at beginning of the applied load, tension stiffing model for accounting in tension force in reinforced concrete element, shear transfer model, etc. All of these models are independent on the FEM mesh size. Maekawa et al. (2003) also published text book of Nonlinear Concrete Mechanics. In this text book, various NLFEM analysis cases and experiments results of concrete structure have been presented. Smear crack concepts is proved and most acceptable for application.

NLFEM for analysis of the concrete and reinforced concrete structure has been developed in the world wide; however, most of these models have been developed based on the specimens at the laboratory. This means that the concrete structures are in good condition, and assumed no any existing flaw/crack before applied analysis load. In the actual situation, existing concrete structure may be deteriorated, existed flaw/crack, corrosion etc. However, models for NLFEM for analysis existing concrete bridge structure are not yet existed.

2.4 Summary

An AASHTO standard was issued at early of 1930s, which the design truck was H20-35. In 1940s, HS20-44 has been introduced, and this truck becomes popular using to the design bridges in USA and elsewhere. Thailand and some other countries which have no their own codes have adopted AASHTO standard for design their bridges.

Actual truck load data is main information for development bridge design specification. The WIM system is new technology which can provide many usefulness. The WIM systems which are mounted on the road surface called RS-WIM system. However, it has many limitations for RS-WIM system, i.e., high cost, difficulty in installation, high error etc. Other system is using the bridge for monitoring truck load data, some of the limitation from RS-WIM system have been improved. The bridge system can be based on structural dynamic approach called MFI, or structural static approach called B-WIM.

MFI technique can estimate both static and dynamic of the vehicle axle load and more accuracy than B-WIM algorithm, but most of the researches were successful conducting in the laboratory. It is still difficult in the practice for monitoring normal traffic load. The disadvantages of conventional B-WIM system are that axle detector

stripped on road surface leading to poor durability, difficult and unsafe during installation. Even though, the FAD B-WIM system can be overcome some weaknesses of conventional B-WIM, but this system can be applied only some typical bridges. Therefore, the main purpose of this study would like to develop truck load monitoring technique based on B-WIM and monitor actual truck load in Thailand. The photoelectric sensor will be used for more accurate and facilities for axle detectors, the system has no any equipment exposed to road way surface. CCTV will be used for observing and classifying of the actual trucks. The detail for this part will be presented in chapter 3 and chapter 4 in this study.

The conventional approach to evaluate the capacity of bridge structure members is using AASHTO Manual, or by direct load testing. In the manual, it recommends that the bridge can be modelled by simplify or equivalent approach, and the damage condition of bridge members can be represented by reduction factors. The capacity of concrete bridge member may be calculated by WSD, or USD. At the recent years, the NLFEM for the concrete structure has been developed, the nonlinear behaviour of the RC structure represented more reality. Therefore, the capacity of the concrete bridge members may also be known by using NLFEM.

AASHTO Manual approach is overestimated, and the bridge structure could not be modelled exactly as actual bridge condition (damage of the bridge element). Direct load test may be costly and ruin the bridge structure. The general NLFEM model could not account for existing flaw/crack in the existing concrete structure. Therefore in this study would like to find out advanced approach to assess deteriorated concrete bridge structure by using smear crack concept of 3D NLFEM, the concrete bridge structure is model as material nonlinear approach which existing flaw/crack will can be accounted. The softening model will be adopted for existing flaw/ crack in concrete element, and the tension stiffening model will be adopted for existing flaw/ crack in existing reinforced concrete element. The detail and procedure of the propose approach will be presented in chapter 5 to chapter 6 in this study.

CHAPTER III

TRUCK LOADING AND MONITORING SYSTEM

3.1 General

Heavy trucks cause a great damage to road pavements and bridge structures. Therefore, truck weight control is needed to reduce the illegal overloaded vehicles and to preserve the roads and bridges infrastructure. New design truck load for highway transportation are also needed to meet the requirement of transportation system at the present time. To fulfil in these requirements, new advanced technology of load control and truck data collection is vital to highway engineering. At the previous time, load control and truck load data collection had been done by static weigh scale station. This traditional weigh scales station can not accommodate high volumes of truck traffic and the results are biased to lighter weight trucks. In early year, 1790s new technology called WIM systems have been developed in United State and later 1980s, and 1990s this technology has developed and practiced in Australia, and European countries, respectively. At the present time, this technology is spreading out to many countries in the world such as Canada, Japan, China, Korea, etc.

The new technologies for truck load monitoring are RS-WIM, and B-WIM system. However, the B-WIM system has more advantages over RS-WIM system. The B-WIM technology can estimate the vehicle weight during its crossing the bridge in normal traffic speed, and it can provide large volume of truck data. In Thailand, truck load data are not yet available to develop local bridge design truck load model. The effect of the actual local truck load on the bridge has not been studied yet. The comprehension of design truck, legal limit truck and actual traffic truck loads is not yet clear to the practice engineers. Therefore, this section would like to be one that research about truck load monitoring system which based on B-WIM technique, and providing some truck data for Thailand. The below sections will present vehicle loads, WIM system and B-WIM system using in this study.

3.2 Vehicular Loads

Vehicular loads involved in the bridge structures are design truck, permitted truck, and actual truck loads. The design trucks mean un-permanent moving loading

that assumed to design for bridge structures. The design truck load must be proper to actual truck crossing the bridge. Local trucks are the actual traffic truck crossing the bridges, they must induce bridge stress less than design truck and have weight not exceed legal limit truck weigh.

Design truck:

The AASHTO truck loading is popular used to design bridge in USA, and many counties including Thailand. At early publication of AASHO (1935), the design truck loads for the bridges were used train of trucks, H20-35 and H15-35 (Figure 3.1).
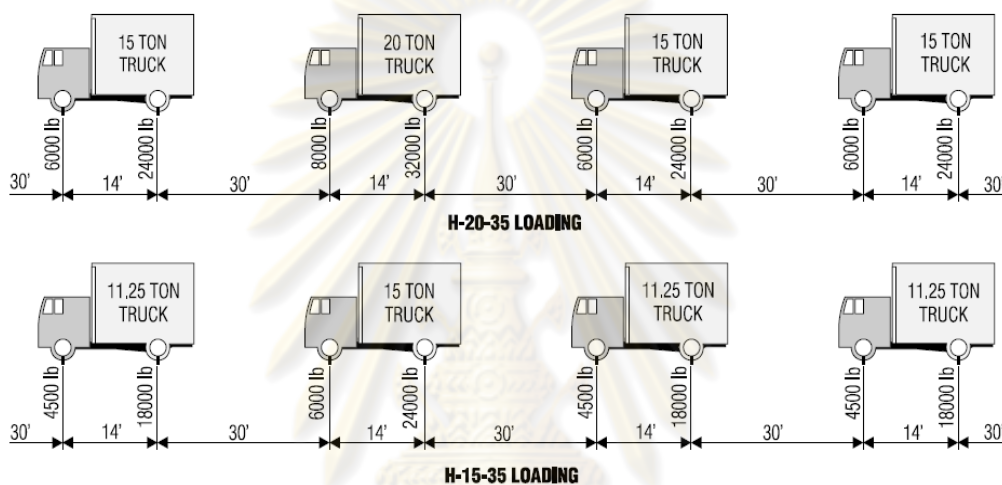
Figure 3.1 H15-35 and H20-35 of AASHO 1993 (Tonias, 1995)

As the highway trucking industry grew, many bridges began to evidence overstressing in structural components. In 1944, design trucks of AASHTO were developed, called as H and HS trucks (Figure. 3.2a). These design trucks were created with two and three axles, respectively. The distance between axles of HS are varying from 14 to 30 ft (4.27 to 9.14 m), it is used to create a live loading situation which will induce maximum moment in a span. For simply supported bridges, this value will be the 14 ft minimum. In continuous spans, however, the distance between axles is varied to position the axles at adjacent supports in such as to create the maximum negative moment. Normally, H and HS trucks are suitable for short, simple span bridges. For long and continues span bridge, AASHTO standard has developed a uniform distributed load combined with a concentrated force. These forces alter for moment and shear computations, and called as H and HS lane loading (Figure. 3.2b). For the bridge that design for military load in the Unstated State, at later year 1976, the alternative military track load was developed (O' Connor, 2000).
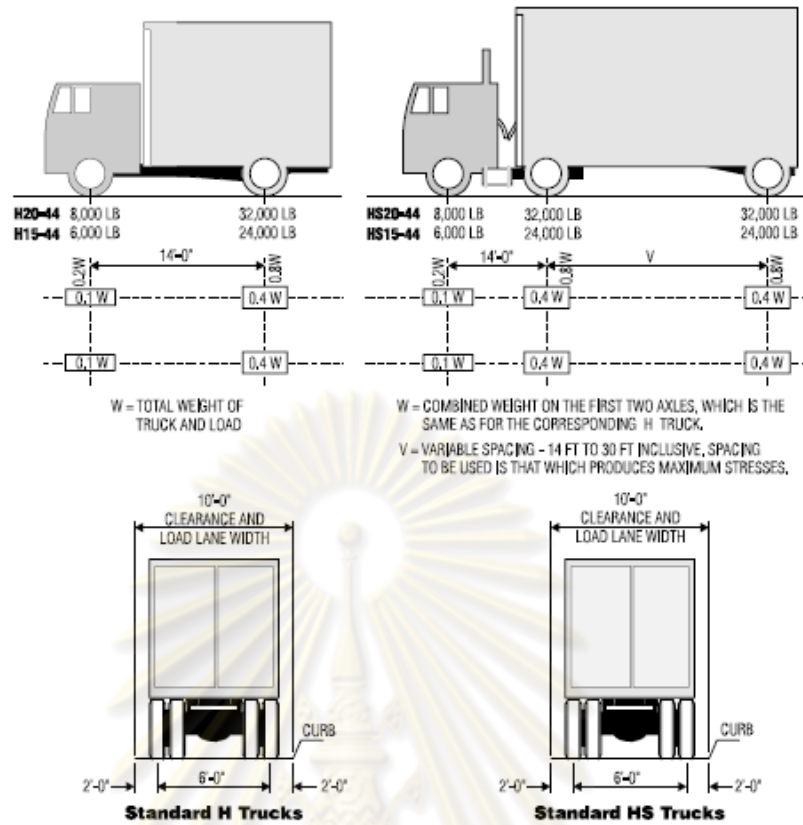
Figure 3.2a AASHTO H & HS20-44 truck loading (AASHTO, 2002)
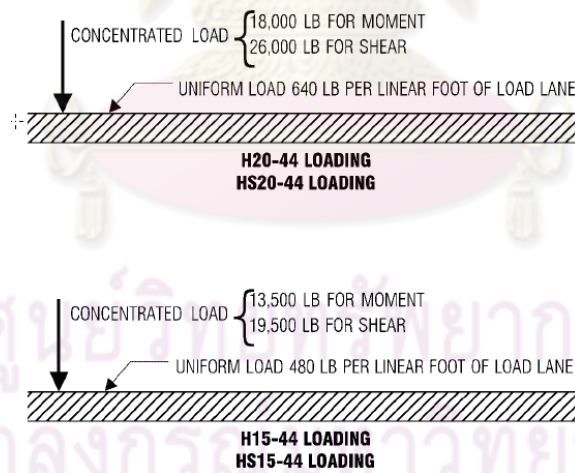
Figure 3.2b AASHTO H & HS-20-44 Lane loading (AASHTO, 2002)

The H and HS design trucks dominated the core standard in the United States until AASHTO Load Resistant Factor Design (LRFD) specifications became widely accepted since 1990s. In the AASHTO LRFD specifications, the HL-93 live load is used. The HL-93 is composed of a truck (identical to HS20-44) or a tandem, combined with a lane load of 0.64 kip/ft (9.34 KN/m), see Figure. 3.3.
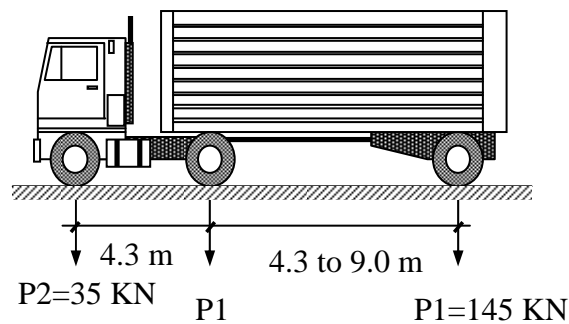
Figure 3.3a HL-93 of AASHTO LRFD truck loading (AASHTO LRFD,1998)
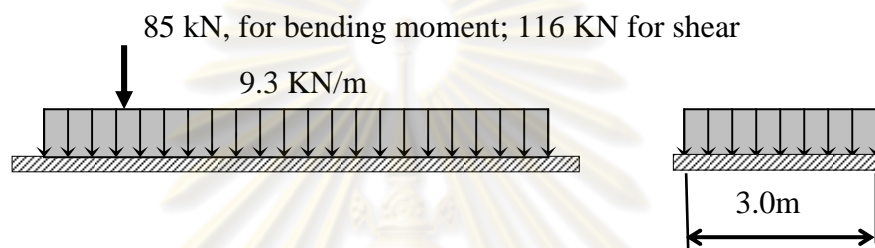
Figure 3.3b HL-93 of AASHTO LRFD Lane loading (AASHTO LRFD, 1998)
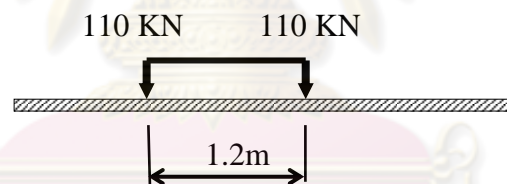
Figure 3.3c HL-93 of AASHTO LRFD Military loading (AASHTO LRFD, 1998)

As it has seen that the design truck load for the bridge from AASHTO bridge design standard has been developed and increased. This is due to that the road traffic at the present time is increased heavier than that at the previous time. HL-93 bridge design truck of new specification, AASHTO LRFD is believed to be conservative for traffic load. In USA, this specification has been replaced completely for new design bridge from 2002. However, for many existing bridge in United State which have been designed by old AASHTO standard specification; nevertheless, HS20-44 still remains for rating these existing bridges. In some states in USA and some countries, which design engineers are not yet comprehensive with new design specification, AASHTO LRFD, are still using AASHTO Standard specification.

Two axles, 4-wheel truck
Maximum GVW = 7,500 kg

1500 kg   6000 kg

Two axles, 6-wheel truck
Maximum GVW = 10,000 kg

2000 kg   8000 kg

Three axles, 6-wheel truck
Maximum GVW = 13,500 kg

1500 kg   6000 kg   6000 kg

Three axles, 10-wheel truck
Maximum GVW = 18,000 kg

2000 kg   8000 kg   8000 kg

Three axles, 10-wheel truck
Maximum GVW = 18,00 kg

3200 kg   7200 kg 7200 kg

Simi trailer, 18-wheel truck
Maximum GVW = 32,400 kg

3200 kg   7200 kg   7200 kg   7200 kg   7200 kg

⊙ Single wheel   ⊚ Double wheels

Figure 3.4 Legal limit trucks in 1960s (Sokuan, 1963)

Legal limit truck in Thailand:

There are a great variety of vehicles in the actual used on the highway. In the legal limit trucks are only representative types of heavies' trucks which given by the Department of Highways. In Thailand, at the early years 1960s, there were six standards vehicle truck types (Somkuan Watakeekul, 1963), which were allowed in the regulation. Both gross load and axle load of each truck type are limited to the maximum value as show in the Figure. 3.4.

At later year in 1991, these legal limit trucks have been verified and increased as shown in the Figure. 3.5 below.

Two axles, 6-wheel truck
Maximum GVW = 12,000 kg

3000 kg   9000 kg

Three axles, 10-wheel truck
Maximum GVW = 21,000 kg

4200 kg   82000 kg 82000 kg

Simi trailer, 18-wheel truck
Maximum GVW = 37,400 kg

4600 kg   8200 kg   8200 kg   8200 kg   8200 kg

Trailer , 18-wheel truck
Maximum GVW = 39,200 kg

4600 kg   82000 kg 82000 kg 9100 kg   9100 kg
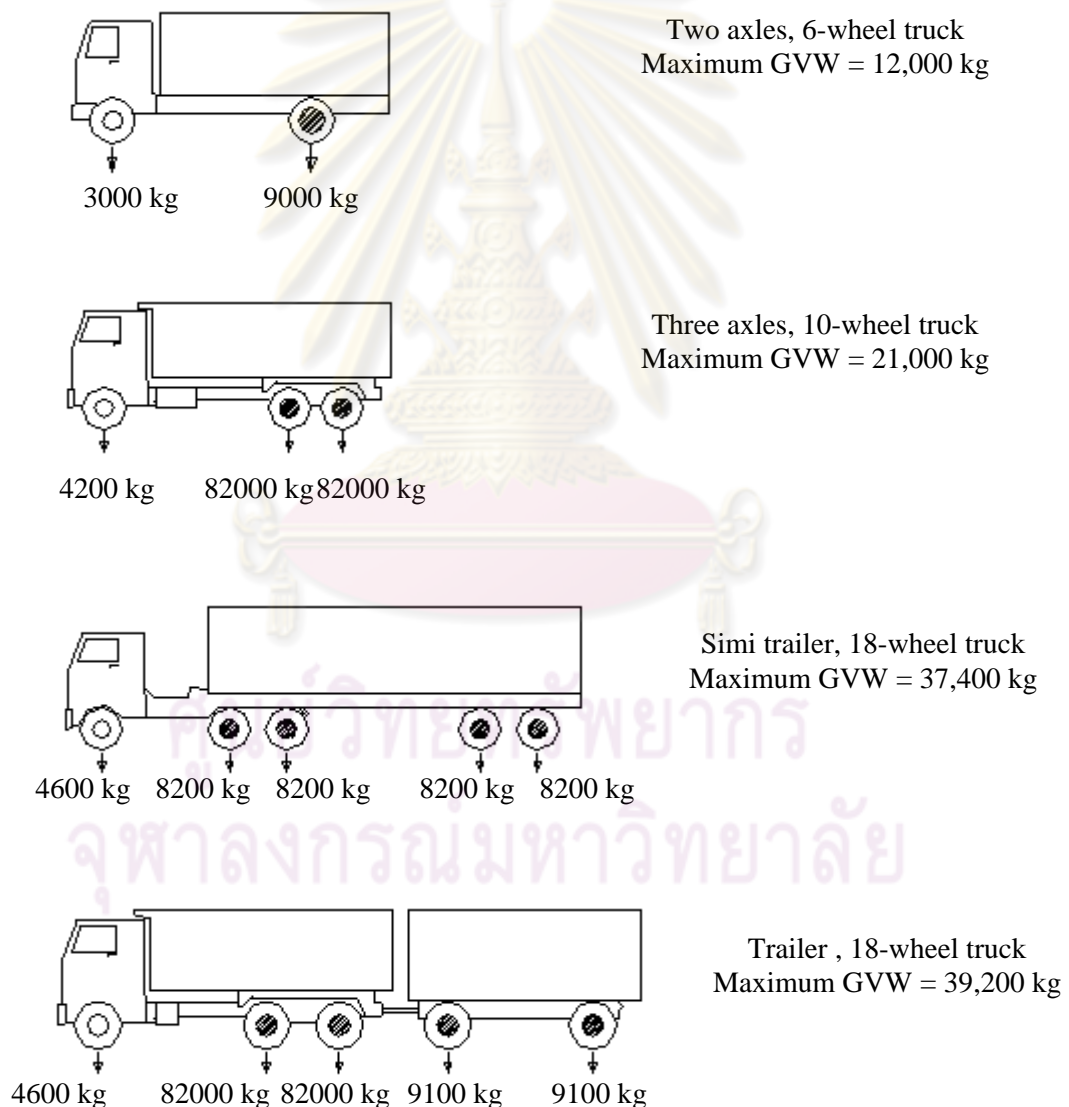
Figure 3.5 Legal limit trucks in 1991 (Department of Civil Engineering, 2003)
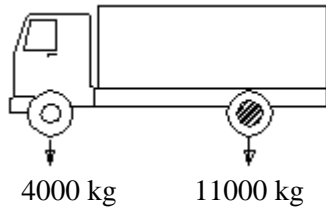
Two axles, 6-wheel truck
Maximum GVW = 15,000 kg

4000 kg   11000 kg
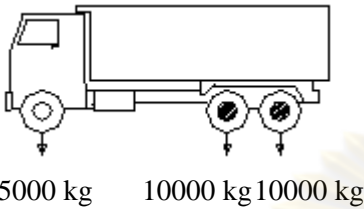
Three axles, 10-wheel truck
Maximum GVW = 25,000 kg

5000 kg   10000 kg 10000 kg
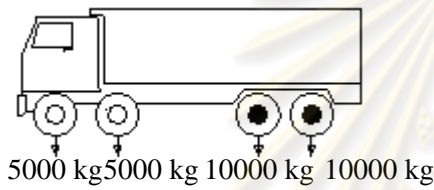
Three axles, 12-wheel truck
Maximum GVW = 30,000 kg

5000 kg 5000 kg 10000 kg 10000 kg
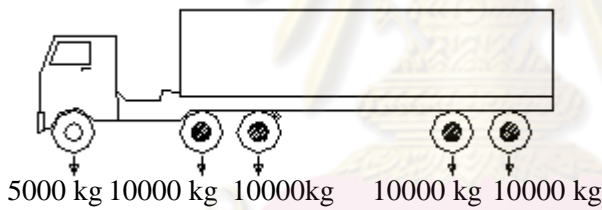
Simi trailer, 18-wheel truck
Maximum GVW = 45,000 kg

5000 kg 10000 kg 10000kg   10000 kg 10000 kg
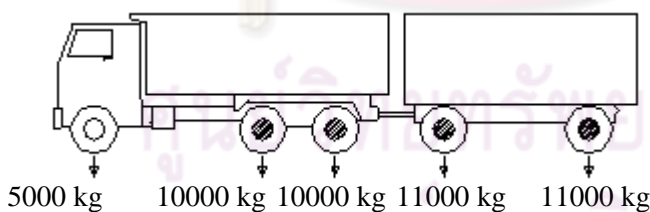
Trailer , 18-wheel truck
Maximum GVW = 47,000 kg

5000 kg   10000 kg 10000 kg 11000 kg   11000 kg
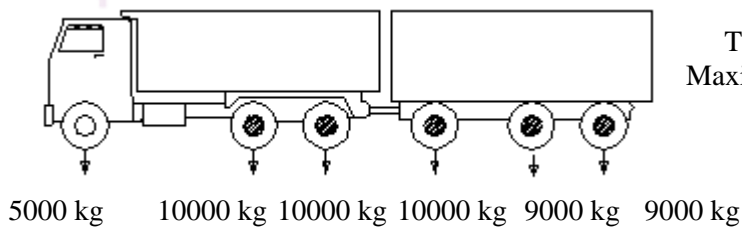
Trailer, 22-wheel truck
Maximum GVW = 53,000 kg

5000 kg   10000 kg 10000 kg 10000 kg 9000 kg   9000 kg

Figure 3.6 Legal limit trucks in 2005 (Department of Highways, Thailand 2005)

At the recent years, transportation companies have again proposed to increase the legal limit truck weight for economic of transportation term. Therefore the Department of Highways of Thailand has to increase the legal limit trucks again in 2005. For example legal limit weight of 10-wheel truck in 1990s was 21 tons, in 2005 the legal limit weight of this truck has been increased to 25 tons, and legal limit weights of other types also have been increased similarly. However, these legal limit trucks are still not yet defining for spacing of axles (see the Figure. 3.6).

Local truck:

The actual vehicles or local trucks load are different from that design truck in many aspects, i.e. the different in the axles spacing, the gross load, the distribution of the load among the axles, etc. The variation of truck parameters is also producing different effects to the bridge structures. Therefore, the different between design and actual loads is one of the important issues to the bridge engineers. To design bridge proper with actual situation, it is not easy, because the stress produced by vehicles loads are influenced by many factor such as span length of the bridges, gross weight of vehicle, wheel based length of the vehicles, number of axels, axle spacing, distribution of the gross weight among the axle, the growing of the future truck, etc. In addition, the actual truck may also often differ from legal limit truck; mostly they are loaded heavier than legal limit truck weight. In Thailand, actual truck is not the same as design truck, and always loaded more than legal limit truck.

As mention in the above, in actual situation, truck loading is still being the major issue to the highway bridge engineers in Thailand. The design truck load is lighter than actual trucks. The freight companies always require increasing legal limit truck weight at early years. Moreover, the actual local trucks are always loaded heavier than legal limit truck weight. But many bridges have been designed by old truck load model, HS20-44 of AASHTO. To deal with this problem, it is not easy, the truck load control system along the highway is needed, and the local truck load model for the bridge design must be developed to ensure capturing the actual present and future trucks. The difficulty for this works is that the actual truck load data in Thailand are still not enough to develop new local design truck load. Therefore, the works for collecting actual truck load data must be done first. This research would like to develop technology to monitoring/collecting the truck load data that support for further works such as development local design truck load model.

3.3 Static Weighing Scale

Before WIM System has been appeared, static weigh scale station was the only way to weighing the overload trucks. Conventionally, there are two types of the static scale station, stationary platform scale and portable wheel load scale. The way to using both types of static scales is that the highway officials have to intercept interested vehicles and divert to static weighing area which provided beside on the road way.

Platform scale consists of the rigid scale frame without bending, load cells, junction boxes, and weight indicator. The strain gauges are attached on the load cells, as the truck rolls on the scale, the compress changes strain resistance proportionally to the applied load. These traditional scales are available in a wide range of sizes and weighing capacities. A platform scale gives a typical maximum permissible error band of 0.5% for the gross vehicle weight.

Figure 3.7 Static platform scale (www.siwim.com)

Portable wheel load scales have been developed to allow for measuring wheel load individually, the axle loads as well as gross vehicle weight are summed of individual wheel load. They are mostly used for spot checks. Each wheel is measured individually, but their precision is somewhat lower than platform scales.

Compared to a WIM system, a static scale can store and retrieve additional information on customers, products, vehicle registrations, suppliers and destinations. However, as vehicles must be stopped on the scale, the weighing system is time consuming and inconvenient for drivers. WIM systems overcome this problem, but their calibration and testing still depends on the information supplied by a reliable static weighing scale. In Thailand and many countries which WIM is not available are still using these static systems.

3.4 Roadway Surface Weigh-In-Motion (RS-WIM) System

The RS-WIM system is the system that measures static truck load by sensors mounted on the roadway surface. According to the devices types, RS-WIM systems are consisted of three types such as bending plates, piezoelectric sensors, and load cells. There are also three promising sensor technologies that are currently being tested but have not been widely used: 1) quartz, 2) fiber optic, and 3) seismic. (McCall et al., 1997). The differences among them are measurement accuracy, initial cost and maintenance cost. The following sections will be brief summary of each technology.

Bending plate:

Bending Plate WIM system utilizes plates with strain gauges bonded to the underside. As a vehicle passes over the bending plate, the dynamic strain will be measured by the strain gauges. The static load is estimated using the measured dynamic load and calibration parameters. This system is classified as an ASTM type I, II, III, or IV (see Table 3.1) system depending on the intended use of the device and the number of scales placed in the lane.
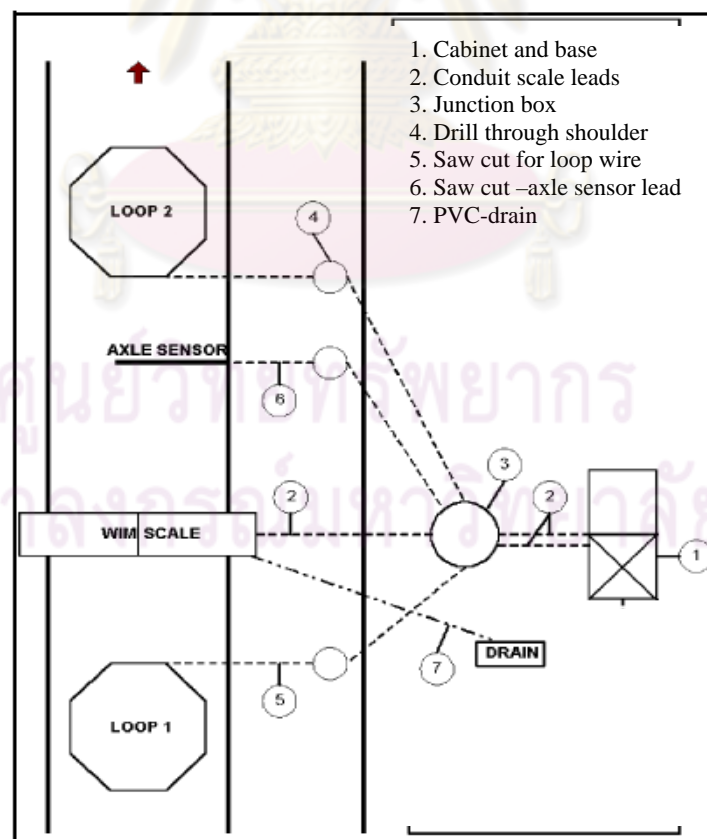
Figure 3.8 Bending Plate system layout (McCall et al., 1997)

Bending Plate WIM system consists of at least one scale and two inductive loops (see Figure 3.8). The scale is placed in the travel lane perpendicular to the direction of travel. The inductive loops are placed upstream (loop 1) and downstream (loop 2) from the scale. The loop 2 is used to detect vehicles and to alert the system of an approaching vehicle. The vehicle speed, which is used to determine the axle spacing, can be determined by axle sensor. An example of the layout for a bending plate WIM system is shown in Figure 3.8 (McCall et al., 1997).

Piezoelectric sensors:

Piezoelectric WIM system utilizes piezo sensor to detect a change in voltage caused by pressure exerted on the sensor by an axle and measure the axle weight. As a vehicle passes over the piezo sensor, the system records the electrical charge created by the sensor and calculates the dynamic load. The static load is estimated using the measured dynamic load and calibration parameters. This system is classified as an ASTM Type I or II (see Table 3.1) depending on the intended use of the device and the number of sensors placed in the lane. The layout of the system is also similar manner to bending plate. The difference is only replacing the piezoelectric sensor to bending plate.

Load cell:

Load Cell WIM system utilizes a single load cell with two scales to detect an axle and weighs both the right and left sides of the axle simultaneously. As a vehicle axle passes over the load cell, the system records the weights measured by each scale and sums them to obtain the axle weight. This system is classified as an ASTM Type I, II, III, or IV system depending on the site design. The layout of the system is also similar manner to bending plate.

The Accuracy of WIM:

The performance of a WIM system is depended on calibration method, devices manufacturing and many influence factors. The most important is system calibration. The calibration by test vehicles make repetitively running over the test site, and the resulting WIM data is processed and compared with static weight measurements of the same vehicles. Alternatively, vehicles taken randomly from the traffic are weighed statistically and used to assess the WIM system accuracy. The accuracy class of the system can be classified according to standard specification. The most widely used is standard specification of the American Society for Testing and Materials (ASTM) which issued in 1990s, called "Standard Specification for Highway Weigh-in-Motion

(WIM) Systems with User Requirements and Test Method" (McCall et al., 1997). In this standard, WIM system has been classified as type I, II, III, or IV (see Table 3.1) according to their application and user requirements for each type of system. Table 3.1 shows functional performance requirements for WIM systems for each class type. Type I and II may be required for traffic data collection for highway management, truck load model, etc, while type III and IV are required for truck weigh enforcement. The three systems of WIM (Bending plate, load cell, and piezoelectric sensor) have different speed ranges, data gathering capabilities, and intended applications, i.e Bending plate and load cell systems can be fall into type III for truck speed 24 km/h for two lanes road (McCall et al., 1997).

RS-WIM is used in the worldwide, many types of sensor are developed aiming to meet the accuracy, durability of sensor, and weighting at high speed truck. Compare B-WIM, however RS-WIM system requires the most controlled environment (smooth, level pavement), costly equipment, set up, and calibration. There are more limitations and influence factors such as road surface roughness, vehicles speed, balance of tire and wheel, tire inflation pressure, etc. The effective using this system is at the low speed truck, 6 to 15 km/h, (McCall et al., 1997).

Table 3.1 WIM Systems classification by ASTM (McCall et al., 1997)

Function	Tolerance for 95% Probability of Conformity				
	Type I	Type II	Type III	Type IV	
				value >= kg (lb)*	± kg (lb)
Wheel Load	± 25%	NA	± 20%	2,300 (5,000)	100 (250)
Axle Load	± 25%	± 30%	± 15%	5,400 (12,000)	200 (500)
Axle-Group Load	± 25%	± 20%	± 10%	11,300 (25,000)	500 (1,200)
GVW	± 25%	± 15%	± 6%	27,200 (60,000)	1,100 (2,500)
Speed	± 2 km/h (1 mph)				
Axle Spacing	± 150 mm (0.5 ft)				

* Low values are not normally a concern in enforcement

3.5 Application of WIM Data

WIM data is very important to National Road Administrations, it can provide traffic truck data and truck parameters (GVW, Axle weight, axle spacing). These information can be also using in terms of engineering field, i.e. development of design

codes for pavements and bridges, assessment of existing bridges and road, etc. The requirements in accuracy of WIM systems will vary depending on their final application. For the traffic statistics: traffic and road monitoring, and road infrastructure and design; high-speed WIM can achieve accuracy in the range of 10% to 25% or type I and II of ASTM (see Table 3.1) which is fully accepted in these applications.

WIM data has many advantages in the bridge engineering such as development of bridge live load model, evaluation of existing bridges, study dynamic impact, fatigue and monitoring. In early 1990's, WIM data was used to review the traffic load model specified in the Eurocode, (Jacob, 2005). This model is based on traffic statistics collected at various WIM facilities in European countries. New bridge design truck load of Canadian bridge design code has been derived from data that monitoring from WIM system. Nowak (1994) has observed effect of the truck load with design truck of AASHTO for 75 years, the traffic truck load data is also taken from WIM system. Miao (2002) has derived bridge live load model for short span bridge using 10 years Hong Kong WIM data.

3.6 Bridge Weigh In Motion (B-WIM) system

At the beginning of the development for truck load monitoring system, RS-WIM was firstly developed in the USA in 1950s; however, there were many problems having been noted. As an alternative to RS-WIM systems, Moses (1979) developed the concept of using bridges as scales to weigh trucks in motion. B-WIM system has several advantages compared to RS-WIM systems. One of them is that limits activity required on the pavement results in a reduction in inconvenience to road users, and it reduces the cost of installation and maintenance.

In the 1970's in the USA, the Federal Highway Administration (FHWA) started studying the use of B-WIM systems to acquire WIM data. Moses (1979) introduced an algorithm based on the assumption that a moving load will cause a bridge to bend in proportion to the product of the load magnitude and a reference curve representative of the bridge behaviour, the influence line. In the 1980's, Peters developed a more effective system for weighing trucks using culverts, known as Culvert-WIM system (Peters, 1986). Both the American and Australian systems have been used for commercial applications on bridges and culverts. In the 1990's, B-WIM systems were developed in Ireland, Slovenia and Japan (Jacob, 2005; Ojio, 2000).

Recent progress through the European COST323 action, the WAVE project (European Commission, 2001) and other researches have led to significant improvements in the performance of B-WIM systems. Research from WAVE also reveals that many of the difficulties observed with B-WIM systems in the past can be resolved by the new or updated algorithms and by using modern devices, and more powerful computers.

B-WIM system generally consists devices such as: strain gauges or strain transducers attaching on the bottom of each bridge girders or bottom of slab bridge, axle detectors placing on the road surface of each lane road, and data acquisition equipments processing signal of strain and axle truck. The information from these devices then using computer processing can be converted to truck parameters, axle weight, and the gross vehicle weight (GVW).

Moses B-WIM 1979:

As result, Moses (1979) developed a system that used instrumented bridge girders combined with axle detectors to predict the axle and gross weight of trucks in motion. This prediction is based on the fact that a moving load will induce bending strain in the bridge girders then converts the strain to bending moment in proportion to the product of the value of the influence line and the axle load magnitude. An influence line is defined as the bending moment at the point of measurement (at middle span of each girder) due to a unit axle load moving along the bridge. Moses proved that weight predictions were feasible and results were repeatable when using a calibration truck. The system described by Moses was the pioneer of B-WIM system and nowadays it is widespread in the USA and elsewhere.

The Moses algorithm composed of strain gauges attached on the bottom of the bridge girders at midspan, tape switches installed on the road way surface prior to the bridge, and bottom box which controlled by an operator at the road side. When a truck was seen, an operator depressed a bottom box to alert the system operation. Instrumented bridges used for B-WIM was multiple girders bridge. All girders are usually identical, though some differences in section modulus can appear in edge members. The simplest bridge to apply Moses' algorithm would be a single span bridge with no skew. A single bridges span less than 18 m is preferred to predict axle weights. A larger span, over 24 m, would be preferable for determining GVW. However, Moses recommended that other bridges could be used for WIM system,

once an influence line of the bending moment can be obtained and the relation between measurements and this influence line is reliable.

Australia Culvert-WIM (Peter, 1985):

In 1980s, the same concept of the B-WIM has been researched in Australia by using culvert instated (see Figure 3.9) (Peter, 1986). The basic principle consists of relating the bending strains in a culvert deck caused by the passage of a vehicle overhead to the axle weights of that vehicle. The relationship is established by recording the strains induced by a vehicle whose axles have been weighed statically. In addition to axle weights, vehicle speed, axle number and spacing, and the date and time of the event are recorded by axle detector located on road surface. The strains at each gauge are summed up to obtain a characteristic response similar to a theoretical bending moment influence line. Figure 3.10 shows the characteristic for moment response of a four meter span culvert to a four-axle truck. Typical peaks can be seen in the figure corresponding to individual axles of the vehicle.
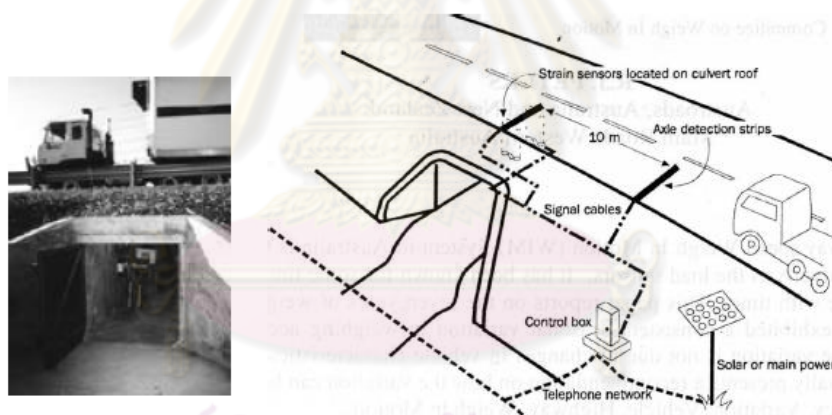
Figure 3.9 Typical Australia Culvert-WIM system (Peter, 1986)

The Australian experience over twelve years has identified a number of site specific factors which can have an effect on the overall accuracy of a culvert based system. The following guidelines have been established for the selection of an 'ideal' Culvert in order to minimize weighing errors: single span reinforced concrete box culvert, precast, 'uncracked' and less than 2.7m in span; a smooth road surface; a straight and flat road; culvert square to the road or a little skew is tolerable; pavement cover more than 200 mm but less than 1500 mm on top of the culvert
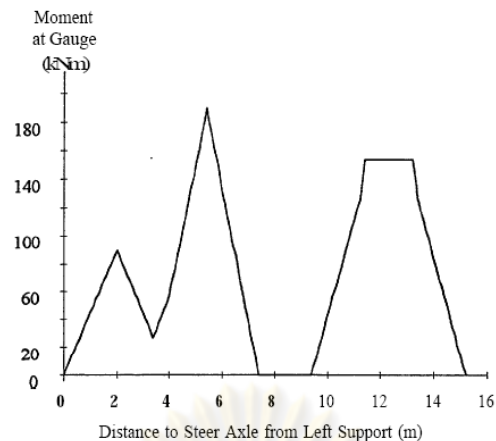
Figure 3.10 Bending moment of 4-Axle truck by Culvert-WIM (Peter, 1986)

European B-WIM:

B-WIM system has been tested in many countries in Europe in 1990s under the WAVE project. The system has been tested for different type of bridges and climates. Some bridge types have been selected such as slab bridge, and orthotropic bridge. It is found that these types of bridges can be used with out axle detectors mounded on the road surface.

In the Slovenia, the system has been tested in the concrete slab bridges with span length 8m to 25m. Test on this type of bridge can be done without axle detectors placed on the road way, due to the slab bridge type is more sensitive to truck load. The strain gauges can be added more at the near both side supports section to record the axle truck signal representing axle detectors. This system was than called Free Axle Detector B-WIM system (FAD B-WIM). Final accuracy was found to be strongly related to a number of parameters such as: influence line, calibration methods, road unevenness and bridge skew (Jacob, 2005).

Free of axle detector (FAD) algorithm has been also developed for orthotropic bridges by Dempsey et al. in 1998 (European Commission, 2001). Velocity, number of axles and axle spacings are all calculated from the strain readings underneath the bridge at two different longitudinal locations. The values obtained for these parameters are not as accurate as axle detectors mounted on the road surface, but FAD systems are a solution to sites where installation of road sensors or road closure is not feasible. The prediction of axle and gross vehicle weights must allow for inaccurate estimates of axle spacings and velocity to some extent. This initial error can be reduced by using optimization techniques.

Research in the WAVE project of B-WIM can be divided into five areas: (a) increment accuracy for typical bridges, (b) extension of B-WIM to orthotropic decks, (c) extension of the range of application of B-WIM, (d) dynamic analysis of typical bridges and (e) calibration. The results of many tests, it became evident that the parameters with the highest influence on final accuracy are (European Commission, 2001): selection of influence line, accurate assessment of vehicle velocity, dynamics of vehicles and bridge, bridge surface roughness and calibration methods. According to the experience reported from WAVE, many helpful suggestions are given for B-WIM. Therefore in this study has also carefully selected instrument bridge site such as simple and short span bridge, two lanes and one traffic direction, smooth road surface to reduce dynamic effect.

B-WIM in this study:

The main problem of conventional B-WIM system is that the axle detector is exposed on the bridge road leading to poor durability, difficult and unsafe during installation of the system. In addition, the system reflecting to the truck drivers, they may avoid the system that is monitoring them. Many recent studies in European countries have attempted to develop a FAD B-WIM system. However, the FAD can be applied only some bridge types such as orthotropic deck bridges, thin slab bridges (Jacob, 2005), or steel girder bridges with vertical stiffeners above the supports (Ojio, 2005). In reality, many highways of interest do not have such bridge types.

This study would like to develop truck loading monitoring system, and test to monitor truck load at Bangkok, Thailand. The B-WIM as Moses algorithm will be adopted. The system described this study includes strain transducers (strain gauges), photoelectric sensors to detect truck axles, and a CCTV. Some advantages over conventional system are that no equipment is exposed on the road surface and the system does not interrupt traffic while the equipment is being installed. The CCTV is used to increase the accuracy of the system's classification of truck types. The detail of the system and test results will be presented at the chapter four. The idea of the system can be applicable to any type of bridges. For this study, the T-Girder Prestressed bridge will be used.

3.6.1 B-WIM Formulation

As we know that the basis theory of B-WIM is referred to Moses 1979 algorithm. This algorithm has been used and modified to real application in the

worldwide. Many researches have developed this system concept in the later years; however, most of those are developed new system devices such as powerful computers, transducer, data acquisition, axle detectors, calibration processes and testing system to difference type of the bridges. Therefore, the system in this study is also adopted as Moses algorithm for calculation axle truck loads.

The principal concept of B-WIM is that the static theoretical response (bending moment influence line) equals to the measurement response at the same point and in the same interval of time, minimization this correlation, axle load then can be derived. It notes that the truck configuration needs to be prior known from axle detector. The detail of its formulation is presented as follow:

If a vehicle is considered at a certain static position on the bridge, and assuming that each girder has a strain transducer in the longitudinal location at midspan. The relation between strain and bending moment at girder i, M_i is given by:

$$M_i = S_i \sigma_i = E S_i \varepsilon_i \qquad ..... (3.1)$$

E - Modulus of elasticity

ε_i - Strain transducer at girder i

S_i - Section modulus of girder i.

Total bending moment in the bridge can be found by summing of the individual girder moment.

$$M = \sum_{i}^{n\_girders} M_i = \sum_{i}^{n\_girders} E S_i \varepsilon_i \qquad ..... (3.2)$$

If E and S_i are the same for each girder, total bending moment can be written as:

$$M = E S \sum_{i}^{n\_girders} \varepsilon_i \qquad ..... (3.3)$$

Thus the sum of the bending strain is proportional to the gross bridge bending moment. E and S are constant and independent from position of the axles of truck.

40
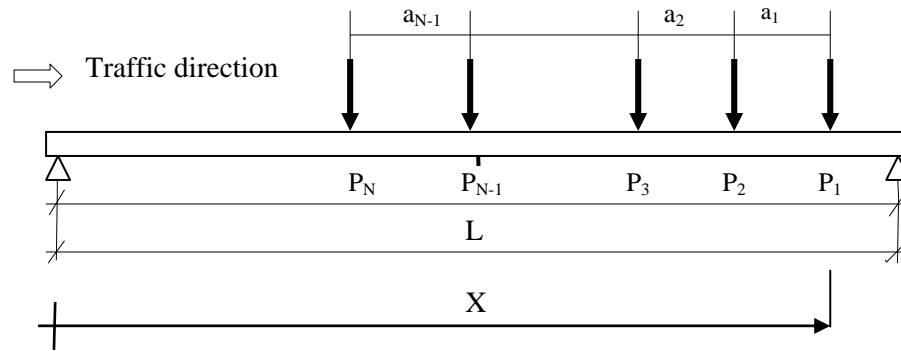
Figure 3.11 Location of axle truck load on the bridge span (Moses, 1979)

Figure 3.11 shows the static axles position of vehicle moving on the simply supported bridge. For different position of the truck axles, the total bending moment at any bridge section can be related to the individual of axle weight for each position. In the beam theory, the number of unknowns for each truck equals to the number of axles, *N*, and this can be calculated from a known of strain records corresponding to *N* different positions of the truck axles along the bridge. This system of equations can be established from influence line of the bending moment. The ordinate of the influence line indicates the bending moment for a unit axle load located at a certain point along the bridge. Considering a vehicle with axle weights are $P_1, ..., P_N$ and corresponding axle spacing $a_1, ..., a_{N-1}$. as shown in Figure 3.11. Then, the bending moment can be expressed for any location *X* of the first axle (*X* is the position of first axle measured from the first support) as follow:

$$M(X) = P_1 I(X) + P_2 I(X - a_1) + P_3 I(X - a_1 - a_2) +$$
$$... + P_N I(X - a_1 + a_2 - ... - a_N) \quad\quad ..... (3.4)$$

Or

$$M(X) = \sum_{i=1}^{N} P_i I(X - \sum_{j=1}^{j-1} a_j) \quad\quad ..... (3.5)$$

Where *I( )* is the influence line ordinate, and a_j is the spacing between axle *j* and (*j-1*).

As in the actual, when truck crossing the bridge, the vehicle axle's position along the bridge will be altered by the time. Therefore, the theoretical bending moment can be expressed as function of time. Using the velocity and axle spacing, we can also write the influence line for each axle as a function of time. By summing the effects of each axle the expected static bending moment can be written as:

$$M(t_k) = \sum_{i=1}^{N} P_i I_i(t_k) \qquad\qquad ….. (3.6)$$

In which $M(t_k)$ = bending moment at gauge location; t_k = time increment; $I_i(t_k)$ = gross bending moment influence line at gauge location for i^{th} axle at time t_k.

Calculate the static axle loads and GVW:

In the reality, bridge response is not static, however it oscillates around static equilibrium response as shown in Figure 3.12.
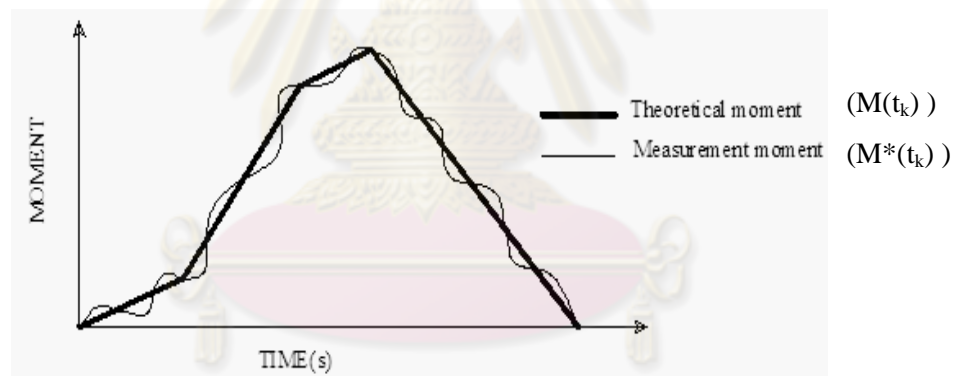
Figure 3.12 Theoretical static bending moment $M(t_k)$ and measured bending moment $M^*(t_k)$(Moses, 1979)

The main purpose is to estimate axle static weight. According to Mose's algorithm, the dynamic part can be filtered out by defining an error function, φ, that is different between the expected static bending moment, $M(t_k)$, and the measure bending moment from recorded strain, $M^*(t_k)$ as:

$$\varphi = \sum_{k=1}^{T} \left[M(t_k) - M^*(t_k) \right]^2 \qquad\qquad ….. (3.7)$$

Substituting for the theory bending moment, $M(t_k)$ from Eq 3.6, given

$$\varphi = \sum_{k=1}^{T}\left[\sum_{i}^{N} P_i I_i(t_k) - M*(t_k)\right]^2 \qquad \ldots.. (3.8)$$

Where, T is the number of scan while the truck is on the bridge. A minimum condition for the error function can be imposed by:

$$\frac{\partial \varphi}{\partial P_i} = 0 \qquad i = 1,2,3,\ldots, N \qquad \ldots.. (3.9)$$

This gives:

$$\sum_{k=1}^{T}\left[2(\sum_{i}^{N} P_i I_i(t_k) - M*(t_k))(I_j(t_k)\right] = 0 \qquad \ldots.. (3.10)$$

and re-ordering:

$$\sum_{k=1}^{T}\left[\sum_{i}^{N} P_i I_i(t_k)\right] I_j(t_k) = \sum_{k=1}^{T} M*(t_k)I_j(t_k) \quad \ldots.. (3.11)$$

$$j=1,2,\ldots, N \text{ (N is the number of axles)}$$

The equation in the matrix form:

$$[F]_{NxN}[P_i]_{Nx1} = [M]_{Nx1} \qquad \ldots.. (3.12)$$

$$[F]_{NxN} = I_i(t_k)I_j(t_k) \qquad \ldots.. (3.13)$$

$$[M]_{Nx1} = \sum_{k=1}^{T} M*(t_k)I_j(t_k) \qquad \ldots.. (3.14)$$

Where:

$[P]_{Nx1}$ is the vector of unknown axles weight

$[F]_{NxN}$ is a matrix depended on influence line, axle spacing and speed

$[M]_{Nx1}$ depend on the same measure strain

Finally, axles weight $[P]$ can be solved by:

$$[P_i]_{Nx1} = [F]^{-1}_{NxN}[M]_{Nx1} \qquad \ldots.. (3.15)$$

The gross vehicle weight (GVW) is found by summing axle weight

$$GVW = \sum_{i=1}^{N} P_i \qquad\qquad \text{….. (3.16)}$$

3.6.2 Equipment or Devices for B-WIM System.

The main equipments for the B-WIM are consisted such as the strain gauge or transducers, axle detectors, data acquisition and PC computer. Each of these devices will be explained in the following section.

Strain gauge/ Strain transducers:

Strain gauges or strain transducers provide to measure strain of deformation of the bridge girder or slab caused by passing of vehicle axles, which are attached to the main bottom surface of the main bridge girder or slab.

(a) Layout   **(b)** Typical configuration
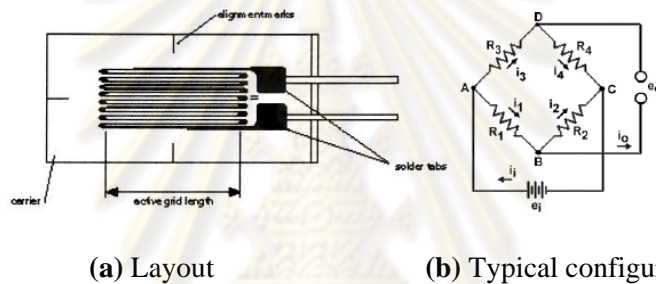
Figure 3.13 Strain gauge (Tokyo Sokki, 2005)

The bonded metallic strain gauge is the most widely used, which consists of a very fine wire or, metallic foil arranged in a grid pattern (Figure 3.13). In this figure, R_1, R_2, R_3, and R_4 represent resistors, and e_o and e_i are the excitation voltage powering the wheatstone bridge and the voltage measured by the DAQ system. The measured voltage, e_i, can be obtained by applying Ohm's laws, resulting in Equation 3.17. As strain is applied to the gauge, its resistance value changes, causing a change in the voltage at e_i.

$$e_i = \left(\frac{R_2}{R_2 + R_3} - \frac{R_1}{R_1 + R_4} \right) e_0 \qquad\qquad \text{….. (3.17)}$$

Metallic or foil gauge is mostly used for steel or PC bridges, and carefully used for concrete bridge. The concrete bridge may contain hair crack, the reading strain will be inaccurate. For the concrete structure, strain transducer can be used, and

this device can be reusable. In this study quarter bridge TML-90 foil gauge was used, because the tested bridge was PC bridge. There are also benefits for using PC bridge as instrumented bridge. Because there are no crack is in the PC bridge, and surface preparing and installation of gauges is more easier than steel surface.

Axle Detector:

The axle detector is used for providing information such as velocity, axle spacing, number of vehicle axles, and classification of the trucks. The traditional system, axle detectors are placed on the road surface. These detectors can be removable (tape switches, pneumatic tubes) or permanent (low-grade piezo-electric sensors or other built-in pavement sensors). From many testing have been reported that the axle detectors represent the most vulnerable part of any B-WIM system. New development FAD B-WIM system identifies axles purely by measuring strain in appropriate locations of the bridge structures. The initial estimation of the axle spacing and speed from FAD are not as accurate as from direct measurement, and FAD system can be achieved only soft slab bridge, orthotropic deck bridge, and steel plate girder bridge with stiffeners.

Figure 3.14 shows two types of removable sensor, i.e. pneumatic tubes and tape switches. Both types are placed on the road surface and they are more economical than a permanent solution. Their installation requires less time and traffic delays than other sensors embedded in the pavement. However, they are more exposed to traffic aggressiveness and they are not recommended in sites with high traffic densities.

(a) Tape switches axle detector   **(b)** Pneumatic axle detector

Figure 3.14 Axle detector mounted on road surface
(European Commission, 2001)

Permanent sensors for axle detector are developed in the various types. The most commonly used, known as a triboelectric cable, contains cores which induce a charge when they rub together and the cable is temporarily distorted by the passage of a vehicle. An increasingly popular variant on this is the piezo-electric cable which contains piezo-electric material such as polarized ceramic powder, Figure 3.15.

Though piezoelectric axle detectors embedded in a groove in the road generally provide a longer life than those mounted on the road surface, however they can fail in various ways. Piezo-electric cable is relatively expensive and needs carefully installation and calibration. Installation and maintenance are time consuming and interruption traffic flow. Moreover it is damage the road surface.
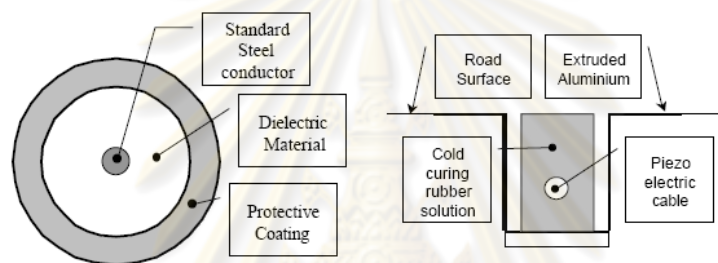
(a) Piezo electric cable cross section   **(b)** Permanent of Piezo electric cable

Figure 3.15 Permanent of axle detector (Gonzalez, 2001)

Photoelectric sensor:

To overcome the conventional axle detector, the photoelectric sensor is used in this study. The advantages of this device are that the photoelectric sensor can be installed at wherever convenience of the road side, bridge barriers, parapet, etc. Normally the photoelectric sensor is produced for detecting the objects in its path. It is used in to various fields such as in the factory, automatic door, detecting car at the car park, etc. Basically, there are three types of the photoelectric sensor such as trough beam model, reflecting model and diffuse reflecting (see Figure 3.16). The through beam model is consist of transmitter and receiver sets. This model can use for detecting the objects up to 300 m. The reflecting model consists of one set of transmitter sensor and one set of reflecting. Mostly reflecting model is using for distance about 3 m to 10 m. The other, diffuse reflecting has only single set of the transmitter, but it can detect the object only 3 m away from transmitter.

(a) Through beam model   **(b)** Reflecting model   **(c)** Diffuse reflecting model
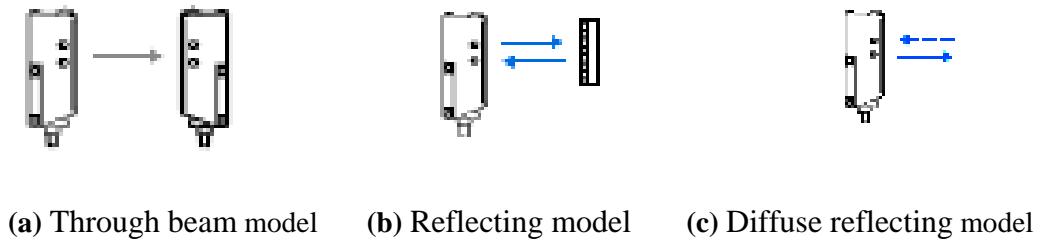
Figure 3.16 Typical of Photoelectric sensors (Omron Industrial Automation, 2006)

The input voltage requiring for photoelectric sensors is about 5v to 30v, which depends on the manufactures. In this study, the through beam model, E3SC of Omron is used. Two sets of photoelectric sensors were installed at both ends of bridge supports. Each set of sensor consists of a transmitter and a receiver installed at the road sides. A transmitter and a receiver must be installed at the same level, and the sensor beam (from transmitter to receiver) aligns perpendicular of the traffic direction. It will trigger when the axles truck passing through the sensor beam, then signal of wheels truck can be recorded. Figure 3.17 shows the signal of the 3-axle truck that proved by photoelectric sensors. For the detail of application with B-WIM system will be presented in the next chapter.
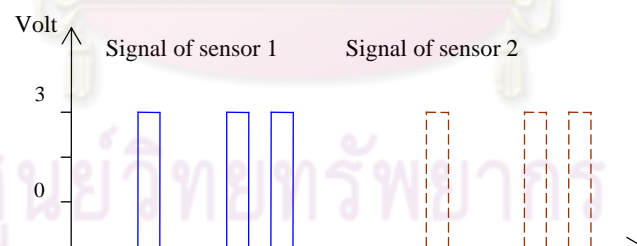
Figure 3.17 Signal provided by photoelectric sensor

The photoelectric sensor has many advantages over mounted on the road axle detectors (Removable sensors and permanent sensor). It is inexpensive, convenient in installation and maintenance. It does not interrupt traffic during installation.

CCTV:

One issue of conventional B-WIM system is that can not collect some information of the passing vehicle such as vehicle manufacturing, vehicle plate

number, etc during monitoring. However, CCTV can be added to B-WIM for providing this information. Therefore, CCTV is also included for system in this study. The detail of installation and results will present in chapter 4.

Data acquisition:

The data acquisition (DAQ) is using for convert analog signal to digital signal data from the stain gauges and axle detector sensors. These signal data are in term of the voltages. Information on voltages can be acquired in two different ways: one writing data to a binary file and another to an ASCII file. The latter allows graphical output and checking of the system in real time, but it requires more storage space. The binary format is generally used when collecting data for long periods.

In this study, data acquisition unit (DAQ), SCXI-1520 of National Instrument was used for processing strain signal. The data signal is saved to computer hard disk as ASCII file. The detail will be presented in the chapter 4.

3.6.3 Selection of Instrumented Bridges

At the first time tested by Moses, the preferred instrumented bridge is simple short span steel bridge. At the later years, the B-WIM system has been tested to many types of the bridge structure. If the approach road surface to the bridge is smooth, optimal results can be expected on spans of around 10 m in length. Such bridges are also easy to instrument and calibrate. If the density of heavy traffic is low and the axle weights are less important than the gross weights, spans over 30 meters can be also used. It should be kept in mind that longer spans and dense traffic increase the probability of having more vehicles on the bridge simultaneously which has unfavourable effects on the accuracy of weighing results for the systems. Generally, the type of the bridge (steel girders, prestressed concrete girders, reinforced concrete girders or concrete slab) and skewness up to 30° can provide acceptable results. Nevertheless, it is recommended to perform some simple preliminary site measurements and to make the final decision when the calibration results are available.

Traditionally, the bridges recommended for using the system should have characteristics such as span length 8m to 25m; bridge type: Steel girder bridge, Orthotropic deck bridge, Concrete slab bridge, etc; good or smooth bridge surface condition; one or two lanes is more preferred. In this study; therefore, the prestressed concrete I-Girder, and simply supported bridge is used. The span length is 20m, two traffic lanes and traffic running in the same direction.

3.6.4 System Calibration

The calibration of the system is very important step for B-WIM, it must be done after system has completed installation. It can be used by preparing trucks of known weight, or by using normal traffic trucks. Using traffic truck needs to stop interested normal trucks when they crossing instrumented bridge, and use moveable static scale to get actual weight. The European specifications of WIM recommended that 2 trucks, one 2 or 3-axle rigid and one 4 to 5 axle trailer or semi-trailer can be used by runing 10 times with at less 3 different speeds (COST 323, 1999).

Due to that 3-axle truck (standard ten wheels truck of Thailand) is the most popular in Thailand. Therefore in this study, the 3-axle truck has been used for calibration system. The calibration has been done by running over bridge more then ten times with different speeds.

3.6.5 Accuracy of the B-WIM System.

The accuracy of the B-WIM system is mainly depended on the bridge site condition, measurement of velocity, the calibration method and selection of theory influent line. The most influence to this algorithm is the dynamic force of the moving vehicles. This dynamic impact is mainly depended on road surface roughness. If the roughness of the road surface is more high, the dynamic force will be high as well, the accuracy of truck load data from the B-WIM system is more unreliable. The classification of the accuracy is can be referred to ASTM standard for WIM system as in section 3.4 in this chapter, or according to the European Specification for WIM (European Commission, 2001). The original test testing by Moese 1979, the error estimation for individual axle and axle group load were about 15% to 20%, respectively, and GVW is about 10% to 15%. In Australia, Culvert-WIM system has been founded to typically estimate static gross vehicle weight within ±10%, and the individual axle weights within ±15% at 95% confidence limits. The more accuracy is improved in Culvert-WIM due to that culvert is less vibrated than bridge (Peter, 1986). The new development and testing of B-WIM by WAVE project at the European countries the accuracy can be improved up to ±10% for single, axle group weight and GVW (European Commission, 2001).

The need of the accuracy also depend on purpose of the data will be used. For the bridge and load model, the class II of ASTM standard is acceptable. Aiming of this study would like to develop B-WIM for studying actual truck load influence to the bridge structures, and collecting actual truck load data for development of truck

load model in bridge design and assessment, therefore the class II of ASTM standard may be acceptable.

3.7 Summary

Most of the truck load for the bridge design in the world has been influence from AASHTO standard specification, which this model has been first publish since 1930s. Due to increasing the needs of the transportation; therefore, the bridge design truck load model from the specification for the present time has been developed and heavier than earlier model. However, many countries in the world still have not studied and developed their truck model. In Thailand, most of the bridges have been design by HS20-44 of AASHTO. Even though the legal trucks have been increased sine 1960s to 2005s, but the truck load model is still referred to HS20-44 of AASHTO. Because, the actual truck load data may not be available, the bridge design truck has not been developed. Therefore, the first aiming of this study would like to develop the truck load monitoring system.

The WIM system can be based on two techniques that RS-WIM and B-WIM. The RS-WIM is the first development since 1950s in the U.S., and then spreading to many countries in the world. However RS-WIM is has many limitations; therefore, the B-WIM has been developed for alternative technique at the first also in U.S.A in 1970s. The B-WIM later has developed and practiced in many countries. The major countries that effort for development this system are American, Australia, and some European countries. Several testing and understanding of B-WIM system has been found in Europe under WAVE project. New algorithm such as FAD B-WIM has been developed. The conventional system faces problem with axle detectors. The new system for FAD B-WIM can be used only for thin slab and orthotropic bridges.

The system in this study is adopted the same as traditional method at the step of estimation of axle weight. However some new devices are included to make system to be more effectively. Photoelectric sensor has been used to detect vehicle axles, and a CCTV has been added to the system for recording trucks photo during monitoring. This system has no any equipment exposed on the road surface and the system does not interrupt traffic while the equipments are installed. The proposed system is expected to be simply, inexpensive, and can apply to any type of bridges.

CHAPTER IV

MONITORING TRUCK LOAD IN BANGKOK

4.1 General

As explaining in previous chapter, the B-WIM system weighs the trucks during they travel across the bridge. This technique is the most acceptable and successful for long-term monitoring of truck load data. It is popularly used in United States, Canada, Australia, and many countries in Europe. The conventional B-WIM system consists of strain gauge attached to the bottom of bridge girders at midspan and tape switches placed on the bridge's road surface to detect axle's truck. The main problem of the traditional system is that the axle detector is exposed on the bridge road, which leads to poor durability, difficult and unsafe during installation; moreover, a system reflecting to the truck drivers, they may aware that the system is monitoring them. Many recent studies have attempted to develop a Free Axle Detector (FAD) B-WIM system. However, the present FAD B-WIM system can be applied to only few type of bridges such as orthotropic deck bridges, thin slab bridges, and steel girder bridges with vertical stiffeners above the supports.

This study proposes an alternative B-WIM technique for monitoring truck load data. It is more convenient for installation and maintenance, because some new devices are added. The photoelectric sensor has been used for axle detector, which it does not interrupt traffic. CCTV has been added to the system for recording trucks photo during monitoring which it can improve accuracy for truck classification. Then the system has been tested and monitored actual truck load at near Bangkok city.

The devices including in this system are:
1. Computer
2. Data acquisition (DAQ), SCXI 1521B
3. Strain gauges, PL-90, TML
4. CCTV
5. CCTV card
6. Sensor for axle detector, E3S-T11 of Omron
7. DAQ for photoelectric sensors, NI USB 609
8. Power amplifier, DC 10 to 30 V

4.2 Instrumented Bridge and System Installation

4.2.1 Instrumented Bridge

The instrumented bridge in this study is located on the Bangkok Eastern Ring Road (BK-ERR) in the eastern part of Bangkok. This is the main highway link between Thailand's southern and north-eastern (NE) regions (see Figure 4.1). Most of the heavy trucks use this highway to avoid entering the Bangkok city center.
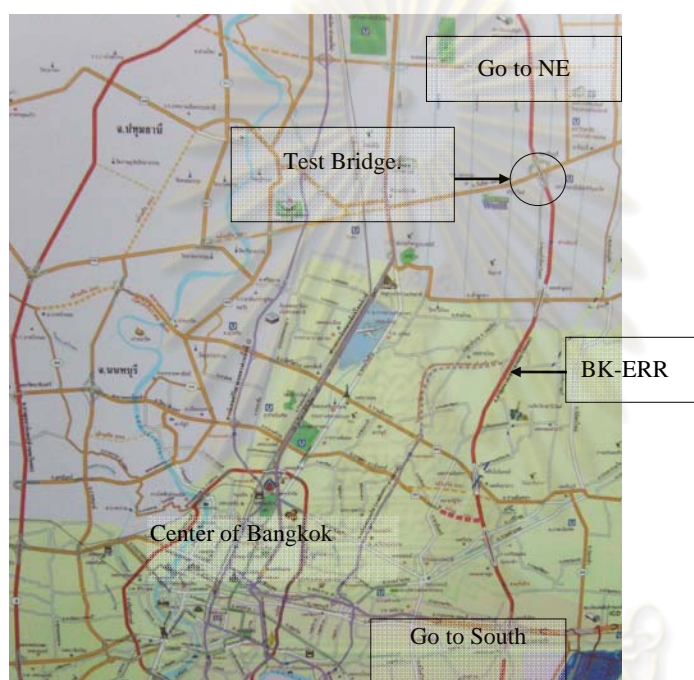
Figure 4.1 Map of tested bridge

Normally, a steel-girder bridge or thin-slab bridge with a span between 8 m to 25 m is preferred for the installation of a B-WIM system, because such bridge is more sensitive to truck loads (Zidaric, 2005). Since most of the bridges on this highway are prestressed concrete (PC) bridges, hence a PC I-girder bridge was selected for this test. The selected bridge has 6 girders, as shown in Figure 4.2b, a total length of 20 m, a support span of 19.4 m, and a total width of 11.9 m (see Figure 4.2a). The bridge has two lanes of traffic, each lane is 3.5 m in width, in the same traffic direction. The sidewalk is 2.4 m wide and located above G1, from left to right. The road surface is very smooth (see Figure 4.3). Both sides of the bridge have concrete railing parapets with 2 m high. Traffic is very dense during the day time, because many small cars use this highway during this time.
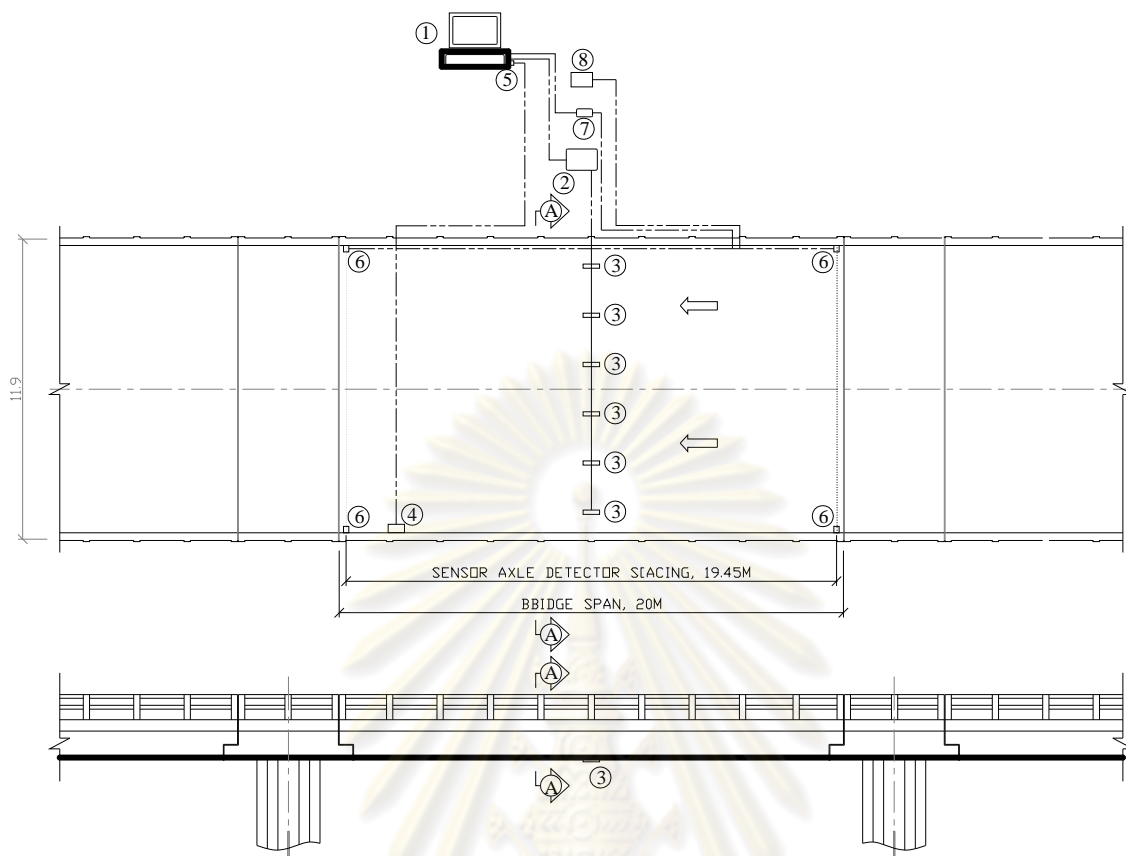
(a) Instrumented bridge plane and elevation
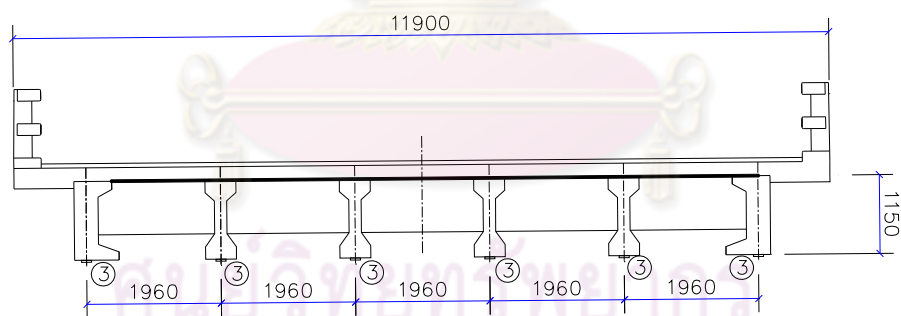
(b) Section A-A

1. Computer
2. Data acquisition (DAQ), SCXI 1521B
3. Strain gauges, PL-90, TML
4. CCTV
5. CCTV card
6. Photoelectric sensor for axle detector, Omron E3S-T11
7. DAQ for photoelectric sensor, NI USB 609
8. Power amplifier DC 10 to 30 V

Figure 4.2 Instrumented bridge plan

Figure 4.3 Pictures of tested bridge

4.2.2 System Devices and Installation

The devices for this monitoring system include a computer, strain gauges, a data acquisition (DAQ) unit for measuring the signal from the strain gauges, a CCTV, photoelectric sensors, and a DAQ for the photoelectric sensors. Figure 4.2 shows the locations of these devices on the bridge.

Strain gauge:

Bridge bending deformation due to axle's truck load can be measured by strain gauges. Reinforced concrete bridge usually will have crack, the strain transducer will be used. For the prestressed concrete bridges, crack will not be allowed, the strain gauge or reusable strain transducer can be used. In this study, instrumented bridge is PC I-girders, therefore the strain gauges for concrete-TML-PL-90 of Tokyo Sokki-have been used. Figure 4.4 shows quarter bridge circuit of TML gauges. The strain gauges have installed at bottom of midspan section (see Figure 4.5), two strain gauges for each bridge girder. The purpose attaching two strain gauges in each girder for ensuring strain signal being correctly. The advantages of PC bridges are very convenience to install strain gauges and not damage the bridge girders.
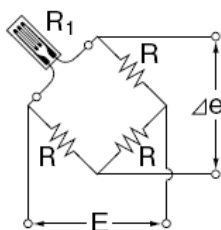
E: Existing voltages
R: Resistance before strain generation
Δe: Output voltage due to strain
ΔR: Resistance change due to strain
$R1 = R + \Delta R$

Figure 4.4 Strain gauges circuit (Tokyo Sokki, 2005)

Figure 4.5 Pictures of strain gauges installation

Data acquisition:

A data acquisition unit (DAQ) (SCXI-1520, National Instrument) is used to record the strain signal at a sampling rate of 1 kHz (1000 samples per second). This high sampling rate is recorded, because the noises will be filtered after data collecting. This strain data were filtered the noise using a separate program by a low-pass filter with a cut-off frequency of 25 Hz. This cut off frequency is most appropriated after calibrating.

Figure 4.6 Picture of data acquisition

Photoelectric sensor for axle detector:

Two sets of photoelectric sensors were installed at the both end of bridge for detecting truck velocity and truck axles. The sensors were attached to the bridge parapets at both ends

of the bridge, as shown in Figure 4.2a (devices 6). The sensors were 25 cm above the surface of the bridge road (Figure 4.7). Each set of photoelectric consists of an emitter and a receiver. The sensor emitter and a receiver can detect in the distance up to 30 m. The bridge in this study was only 11.4 m wide, so the emitter and the receiver were distant only 11.4 m. The sensor was an on/off device that registered "On" when the wheels of a truck passed through the beam between the emitter and receiver, and "Off" at all other times. The sensor's output signal was 3V when "On" and 0V when "Off," as shown in Figure 4.8. The DAQ uses to convert the analog signal to the digital signal and saved it to the computer at a sampling rate of 1000 Hz. Figure 4.8 shows an example of a signal for 3-axle truck, where $\triangle t$ is the time between the first sensor detecting the first axle and the second sensor detecting the same axle, $\triangle t1$ is the time between axle one and axle two at the first sensor, $\triangle t2$ is the time between axle two and axle three at the first sensor, and $\triangle t3$ is the time indicating the signal width of the truck wheel at the level of the sensor beam. For detecting other truck types are also follow the same manner. Because the distance and times between the sensors are known, by assuming that the truck's velocity is constant while crossing the bridge, the truck's velocity and axle spacing can be estimated. The width of the truck wheel at the level of the sensor signal also can be used to detect the vehicle type such as for a large truck the wheel truck width is between 80-90 cm, for small truck is 70-80 cm, and pick-up or small car is less than 70 cm. The truck type can be further classified according to the axle spacing, the width of the truck wheel, and the axle number.

Photoelectric sensors (6.5cm x2cm)   Sensor house

Figure 4.7 Pictures of installation photoelectric sensors
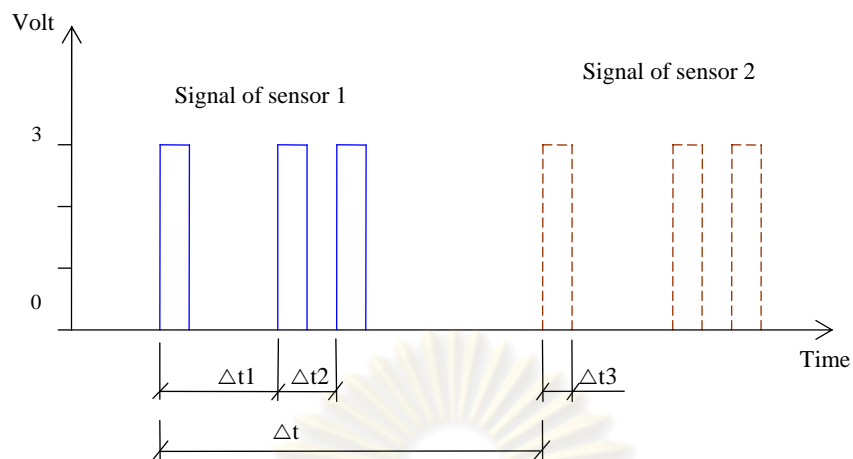
Figure 4.8 Example of axle sensor signal for a 3-axle truck

CCTV:

The CCTV was installed beside the bridge to record trucks photo crossing the bridge. This data were also saved to the computer. After all devices are completely installed and connected to PC computer (see Figure 4.9), video from CCTV and signal from sensors will be displayed on the computer screen. Figure 4.10 shows the computer screen displaying the strain signal, axle sensor signals and the CCTV video while monitoring trucks.

Figure 4.9 Pictures after installation of device completed
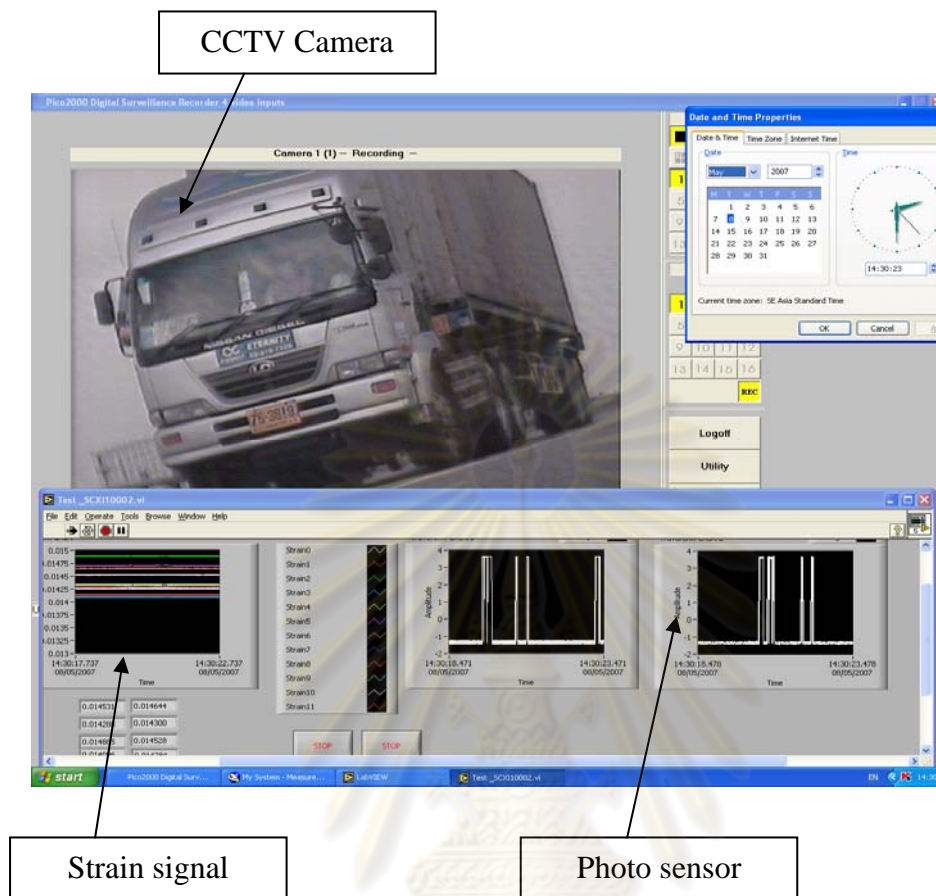
Figure 4.10 Computer processing collecting data
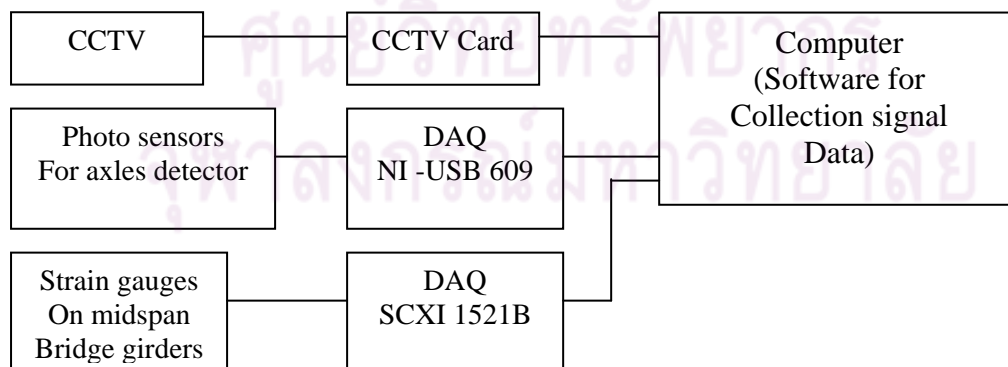
Figure 4.11 Collection data chart

4.3 Signal Analysis and Calculation Procedure

When system has been installed properly, all the devices will process the signal through the DAQ to convert the signal to be digital and save to PC computer as showing in the Figure 4.11. The LabVIEW commercial program has been used for processing the signal data from DAQ to computer. The system continually record data and save to files in the defined folders. After the all signal data have been saved, the second step is signal analysis and estimation truck load. This step can be done separately at the office. The following is explained the steps of data analysis and deriving truck load.

Calculation Procedure:
1. Analysis the data, filter strain data by low pass filter using cut off freq. 25 Hz.
2. Calculate truck speed and axles spacing of the truck from the photoelectric sensor signals by assuming that the truck velocity is in constant during crossing the bridge.
3. Consider truck class according to truck axle configuration and CCTV camera.
4. Calculate induced strain and define transverse position of truck, then determine calibration factor. Transverse position of truck is determine such that if the strain at middle girder higher than edged girder, truck will be at bridge center and vice versa.
5. Calculation individual axle load and axle group using B-WIM formulas, for gross vehicle weigh (GVW) is summed up of each individual axle load and axle group.

Truck speed calculation:

The way to calculate velocity of truck is that first the distance between sensors is known, e.g. 19.45 m. When the truck across the bridge the signals of the truck wheels will be recorded as shown in Figure 4.12, the time interval of truck axle between photoelectric sensor set one at approach bridge and set two at the out of bridge, $\triangle t$ can be calculated by assuming truck velocity is constant, than the velocity can be calculated by simple formulation by below equation, Eq. (4.1).

$$V_n = S / \Delta t_n \qquad \text{.......(4.1)}$$

Where,

V_n : The velocity of tuck number n

S : The distance between two sets of sensors, prior known

Δt_n : The time interval of axle truck from sensor set one to sensor set two recording by photoelectric sensor.

For the axle spacing can than be calculated by Eq. (4.2).

$$X_{ij} = V_n * \Delta t_{ij}$$

.......(4.2)

Where,

X_{ij} : The axle spacing between axle i^{th} and axle j^{th}

V_n : The truck velocity calculation from Eq. (4.1)

Δt_{ij} : The time interval of axle i^{th} to axle j^{th} recording by photoelectric sensor.
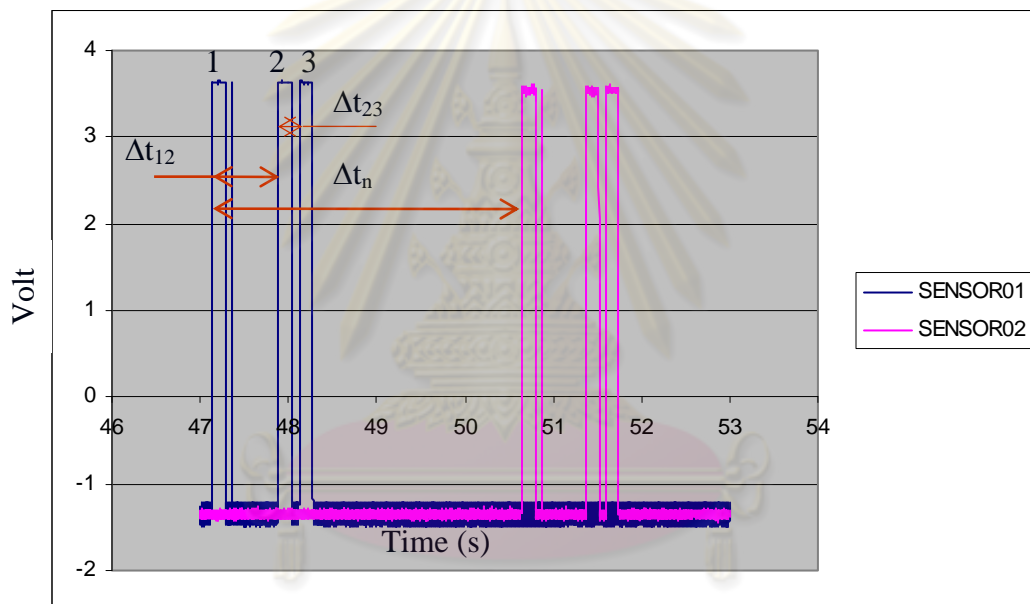
Figure 4.12 Signal of the 3-axle truck recording by sensor

The example results of the calculation velocity and axle spacing of three-axle truck are presented in the Table 4.11.

Table 4.1.1 Calculation of velocity for 3-axle truck

Sensor distance, S	Δt_n	V_n		Δt_{12}	X_{12}	Δt_{23}	X_{23}
m	s	m/s	km/h	s	m	s	m
19.450	3.540	5.494	19.780	0.578	4.168	0.238	1.307

Signal filtering:

Normally, strain gauge signal data without filtering will include noise. This noise is mostly due to electrical signal. The way to get rid of the noise can be done by two methods. First is done during collecting the data; however, this method may make computer more slowly. The second method may be done after signal recorded to data files. Due to the strain signal were collected in high frequency, therefore the noise was filtered after signal recorded by using MATLAB program. The low pass filter with cut off frequency 25 Hz has been used, the signal result before and after noise filtering are shown in the Figure 4.13.
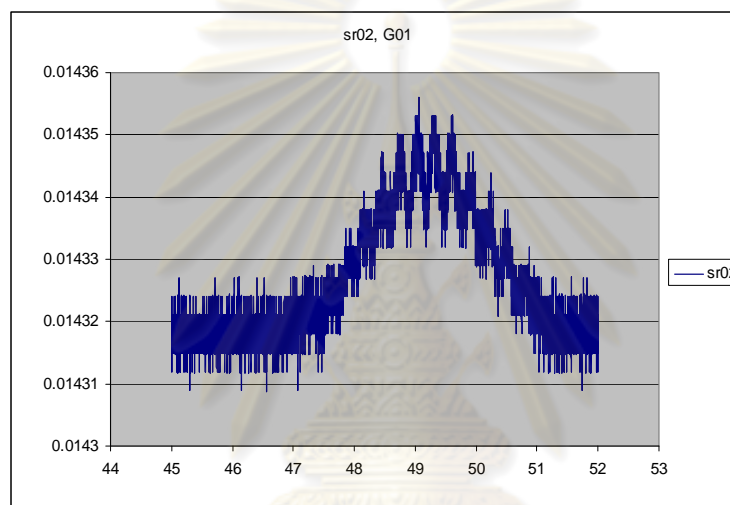
(a) Strain signal before filtering
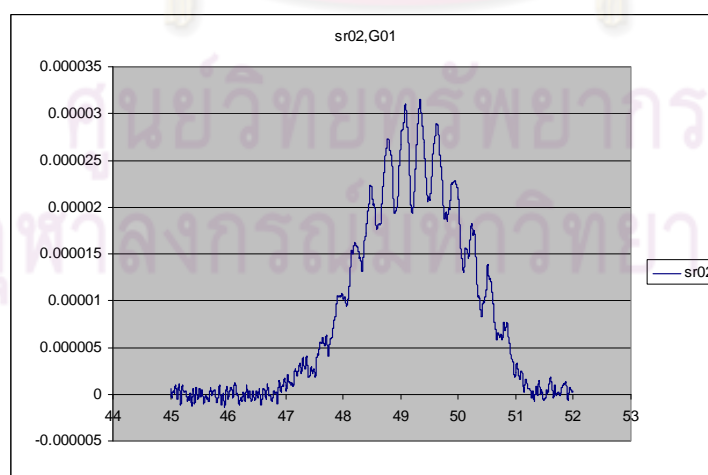
(b) Strain signal after filtering

Figure 4.13 Strain signal before and after noise filtering

Calculation of axle weight and GVW:

Truck parameters were defined and strain gauges data were filtered, the system is still difficult to distinguish closed peak of strain signal for axle group. Therefore, for closing axles group load (two and three axles groups) are assumed to be one point load contributed to the bridges structure. The Figure 4.14 shows the assumption of load for 3-axle truck distribution on the bridges.
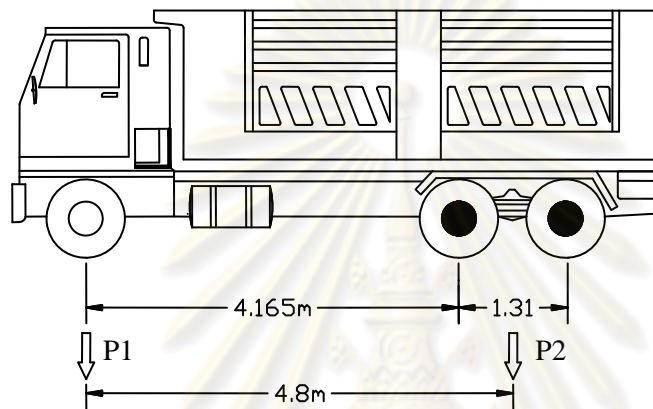
Figure 4.14 Contribution of three axle load to the bridges

After the truck velocity and distribution of the axle loads on the bridge have been defined, then the axle weights can be calculated by B-WIM formulations as presented in section 3.6.1. For example of the 3-axle truck, and assumed two point load distributed to the bridge girder, the matrix of the unknown axle load, P_i will be remained two unknown, P_1 and P_2 as shown in below system equation, Eq. (4.3).

$$\sum_{k=1}^{T}\begin{bmatrix} I_{1(tk)}I_{1(tk)} & I_{1(tk)}I_{2(tk)} \\ I_{2(tk)}I_{1(tk)} & I_{2(tk)}I_{2(tk)} \end{bmatrix}\begin{bmatrix} P_1 \\ P_2 \end{bmatrix} = \sum_{k=1}^{T} M^*_{(tk)}\begin{bmatrix} I_{1(tk)} \\ I_{2(tk)} \end{bmatrix} \quad \ldots..(4.3)$$

The equation 4.3 is the same as equation 3.11 in chapter 3 for N (unknown axle load) is equal to two.

And the GVW is summed up of individual axle weight, Eq. (4.4)

$$GVW = P_1 + P_2 \qquad \ldots..(4.4)$$

4.4 System Calibration

The stiffness of bridge girders was calculated by data (concrete modulus, and section dimension) from the bridge construction drawings and on site measurement. Due to site factors (Cai, 2002), the actual bridge stiffness may be stiffer then the theoretical stiffness. This difference can be known by calibration. According the recommendation from European specifications about the calibration of WIM system, the system calibration can be done by running known information truck for about ten times at different speeds. In this test, a 3-axle truck (standard ten wheels truck of Thailand) with a known load and axle configuration was used for calibrating the system. The GVW of calibration truck was about 25 tons, and its configuration as shown in Figure 4.15. This calibration has been done by running the truck over the bridge twelve times, eight times in the center lane (left lane) and four times in the edge lane (right lane), at four different speeds: 20 km/h, 40 km/h, 60 km/h, and 80 km/h. From this calibration, the calibration factor of the bridge stiffness is 1.30 when a truck travels on the center lane and 1.25 when a truck travels on the edge lane. This difference indicates the affect of transverse position of the truck, when the truck is on the bridge center, the truck load may be distributed to all bridge girders than when the truck is on the edge lane. The way to determine the truck transverse position is done by comparing measurement strain at the middle girder and edge girder of the bridge, if the induced strain at middle girder is higher than edge girder, the truck position is assumed on bridge center, and vice visa. Figure 4.16 (a) and (b) show the theoretical and measurement moments at midspan section before and after applied calibration factor.

4.3 m   1.3 m

5000.00 kg   9650.00 kg   9550.00 kg

GVW = 24200.00 kg
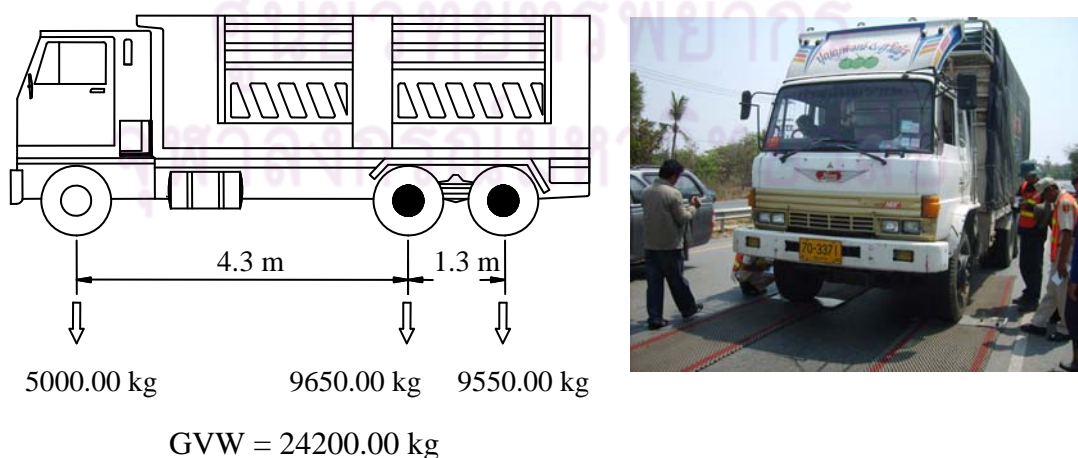
Figure 4.15 Calibration truck configuration and photo
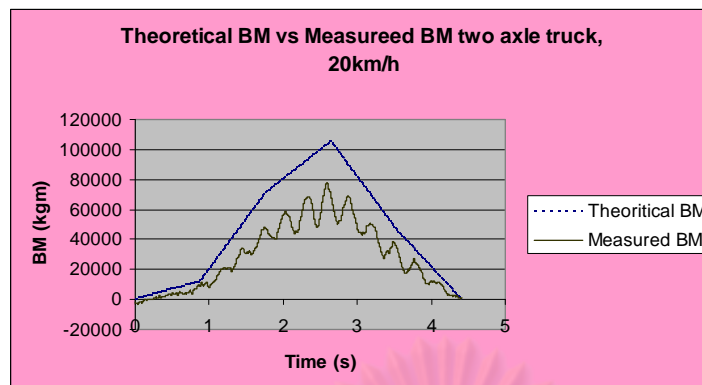
(a) Theoretical and measured before using applying calibration factor
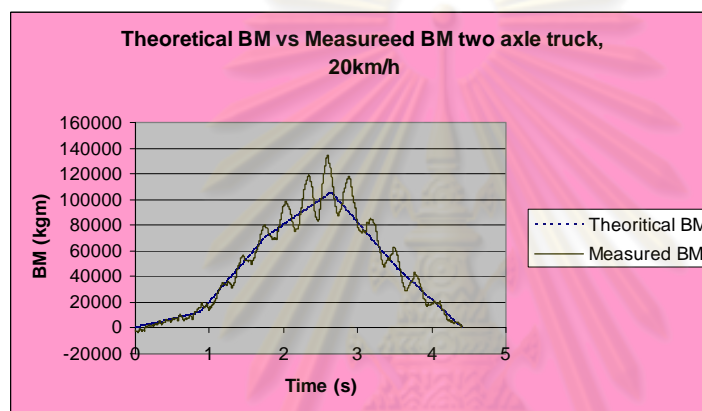
(b) Theoretical and measured after using applying calibration factor

Figure 4.16 Comparing theoretical and measured bridge bending moment

The results of all running calibration truck at different speed are presented in the Table 4.12. The results presented in the table are included first axle spacing, *A* and second axle spacing, *B* (see Figure 4.15); first axle load, P_1; axle group load, P_2; and GVW. The error in the estimation of axle group load is less than 10%.

Figure 4.17 shows the comparison of axle configurations of calibration truck which calculated from the system using signal from photoelectric sensors, and actual axle configurations. The calculation method is as explaining in section 4.3. As shown in the figure, it is found that the error in estimation of axle spacing from the system was less than 1.5%. The values of 4.13 m and 1.3 m in this figure are actual axle spacing of calibrated truck.

Figure 4.18 shows the error of estimation the calibration truck load after applied the calibration factor. The error in the estimation of axle load and axle group load are less than 13%, and the error in gross vehicle weight (GVW) is less than 10%.

Table 4.1.2 Results of running calibration truck

No	speed	Axle spacing		P1	P2	GVW	Differ for GVW	Position of truck
	m/s	A(m)	(B)m	kg	kg	kg	%	
1	5.53	4.19	1.32	4,537.64	20,757.54	25,295.18	4.53%	Middle lane
2	7.88	4.15	1.31	5,209.90	20,118.91	25,328.80	4.66%	Middle lane
3	11.46	4.13	1.31	4,599.61	18,695.87	23,295.48	3.74%	Middle lane
4	12.27	4.10	1.30	5,380.21	17,340.30	22,720.51	6.11%	Middle lane
5	15.79	4.14	1.31	4,352.37	17,396.78	21,749.15	10.13%	Middle lane
6	16.36	4.14	1.31	4,504.22	17,169.30	21,673.53	10.44%	Middle lane
7	17.86	4.14	1.30	4,519.13	17,709.75	22,228.88	8.15%	Middle lane
8	18.11	4.15	1.30	4,642.36	17,816.42	22,458.78	7.20%	Middle lane
9	11.51	4.14	1.32	5,458.51	19,977.59	25,436.10	5.11%	edge lane
10	12.07	4.16	1.32	5,476.56	21,099.30	26,575.86	9.82%	edge lane
11	14.14	4.16	1.32	4,795.41	21,769.53	26,564.94	9.77%	edge lane
12	17.43	4.15	1.31	5,290.02	19,669.90	24,959.92	3.14%	edge lane

Actual calibration truck, P1= 5,000 kg, P2= 19,200 kg
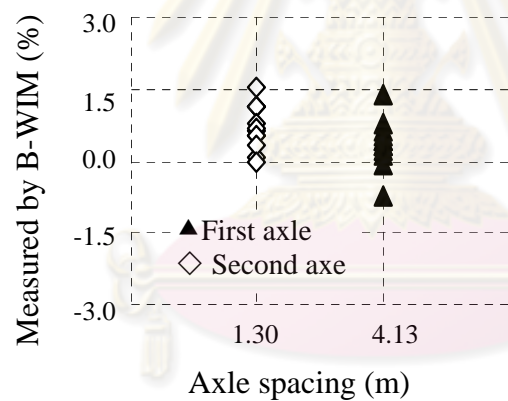
Figure 4.17 Error of evaluation of
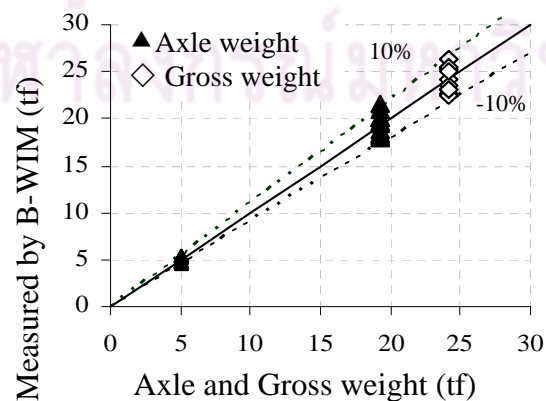
Figure 4.18 Error of evaluation of truck

4.5 Calculation Procedure and Program for System

        The calculation software for simulating long-term monitoring data was written by the author using MATLAB languages. Figure 4.19 is a flowchart of the calculation procedure. The procedure is as follows: filter the strain data, identify trucks by total bridge strains that are higher than 40 micro strain (if the strains is less than this value, it will be small cars or pick-up which GVW may less than 5 tons), calculate the truck parameters (velocity, axle spacing, and truck type), estimate the axle load and gross weight of the truck using the B-WIM algorithm. The results for each truck type are then saved to the output data files. Trucks of interest can be verified using the CCTV video, especially those with trucks heavy loads. This is a very useful and accurate method for verifying the truck type.
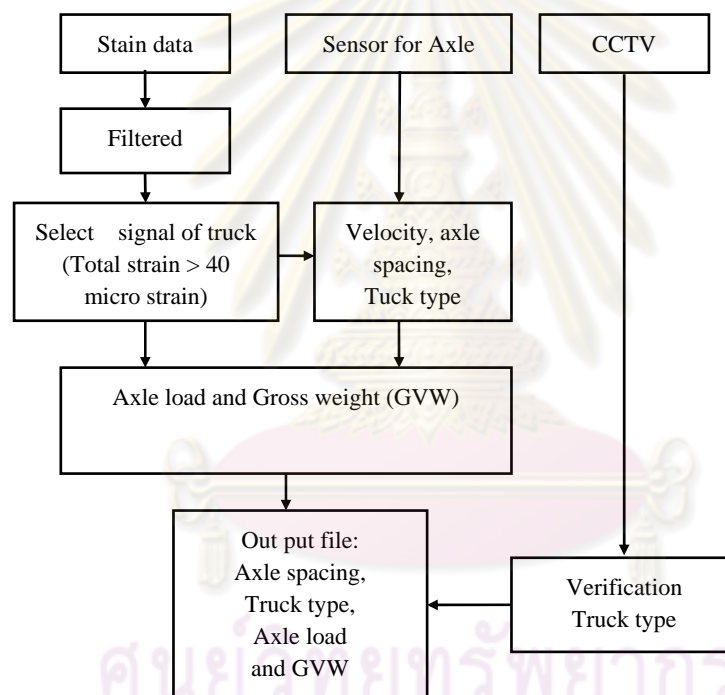
Figure 4.19 Flowchart of truck data analysis and calculation

4.6 Results of the Monitoring Truck Data

        Actual Thai trucks were monitored at the BK-ERR highway, as mentioned in section 4.1. Because this highway is near Bangkok city, traffic is very heavy, particularly during the day when many small cars use it. The main purposes of this study were to test the system and primarily investigated of actual Thai truck configurations and loads. Therefore, a total of about ninety hours of data were collected at night from 9: 30 p.m. to 6: 30 a.m. in May, 2007. A total of 10,621 trucks were derived from this monitored system, as shown in Figure 4.20.

Only those trucks that had a GVW of more than 5 tons were investigated. From these test results, the trucks were classified into seven types. The relative frequency of GVW for loaded truck and configuration of each truck type are presented in Figure 4.21 though Figure 4.27 at the below. For convenience, the truck types were given name as 2-axle trucks (TR-02), 3-axle trucks (TR-05), 4-axle semi-trailers (TR-07), 5-axle semi-trailers (TR-09), 6-axle semi-trailers (TR-10), 5-axle trailers (TR-11), and 6-axle trailers (TR-12).

Figure 4.20 shows that most of the trucks on this highway are 2-axle trucks (TR-02, amount about or 42%), 3-axle trucks (TR-05, about 27%), and 5-axle semi-trailers (TR-09, about 21%). There are few trucks for 4-axle semi-trailers (TR07, 2%), and 6-axle trailers (TR-12, 0.3%). For trucks 6-axle semi-trailers (TR-10) and 5-axle trailers (TR-11) are about 3% for each. It also can be observed that tuck TR-09 is more popular used than TR-10, while configuration of these trucks are different only rear axle group, two-axle group (tandem) for TR-09, and three-axle group for TR-10.

Total number for each truck type

TR-02 = 4,487 trucks

TR-05 = 2,896 trucks

TR-07 = 212 trucks

TR-09 = 2,269 trucks

TR-10 = 325 trucks

TR-11 = 401 trucks

TR-12 = 31 trucks

Total trucks = 10,621 trucks
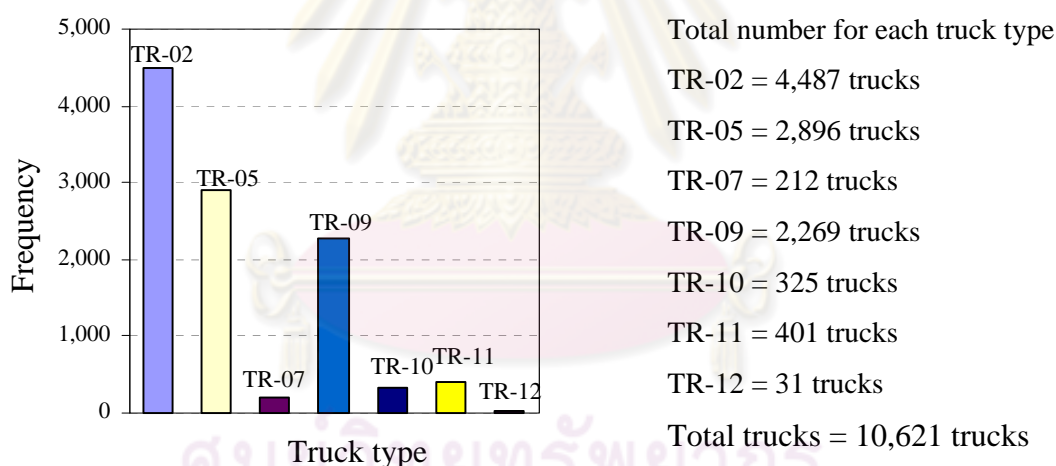
Figure 4.20 Total number of trucks monitored at BK-ERR

Figure 4.21a shows the relative frequency of GVW for loaded truck type TR-02, which ranges between 8 tons and 19 tons with total number of 4,040 trucks; the lower GVW may indicates empty trucks and not include in this figure. The dividing line for empty trucks and loaded trucks condition is selected by judgment (low GVW are assumed as empty trucks), and COV of GVW for data loaded trucks are considered less than 0.3, (Wang, T. L., et al., 2005). Because, high value of COV, it mean that truck load data are very varied. However, most of the GVW for TR-02 trucks ranged between 10 and 13 tons, and only few trucks (less

than 4%) had a GVW above 15 tons, which is the over legal limit load (legal limit of GVW is 15 tons) defined by the Department of Highways, Thailand. The mean value (MV), standard deviation (SD), and coefficient of variation (COV) for axle loads and GVW for loaded trucks of TR-02 are also given in Table 4.2a. The MV for first axle, second axle, and GVW are 3.36 tons, 7.63 tons, and 10.99 tons, respectively. The axle spacing for TR-02 truck is given in Table 4.2b as statistic values, and the graph of axle spacing distribution is presented in the appendix A-2. The median value (MD) of axle spacing is 5.07 m with standard deviation (SD) and coefficient of variation (COV) 0.93, and 0.19, respectively.

(a) Relative frequency of GVW for TR-02   **(b)** Configuration of TR-02
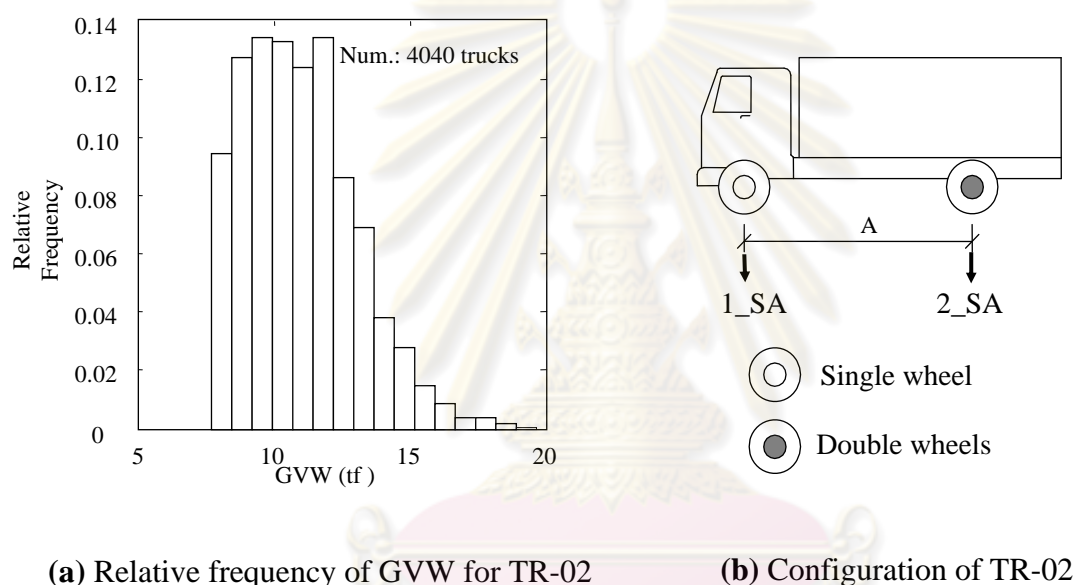
Figure 4.21 TR-02: **(a)** Relative frequency of GVW, **(b)** Configuration

Table 4.2a Axle weights for loaded truck , TR-02

Axle weight	MV (tons)	SD	COV
1_SA	3.36	0.88	0.26
2_SA	7.63	1.89	0.25
GWV	10.99	2.03	0.18

MV- mean value (tons), SD- standard deviation,

COV- coefficient of variation

Table 4.2b Axle configuration for TR-02

Axle spacing	MD (m)	SD	COV
A	5.07	0.93	0.19

MD- median (m), SD- standard deviation,

COV- coefficient of variation

Figure 4.22a shows the relative frequency of GVW for loaded trucks, TR-05, which ranges from 15 tons, light GVW trucks are not included in the graph. The condition selecting loaded truck is the same manner as indicating for TR-02. The maximum GVW is about 30 tons, while the GVW legal limit for this truck type is 25 tons (Department of Highways, 2005). The monitoring data indicate that most trucks are loaded under the legal load limit, with only 4% (in total TR-05 truck data) above the legal limit. Loading from closed spacing axles have been assumed as one axle group load (one point load). Therefore, axle weight data for TR-05 are given as the mean value (MV) of single axle (SA) and two-axle group (AG) weights. The statistical values (MV, SD, and COV) of axle weights and GWV for loaded trucks are shown in Table 4.3a, which MV for first axle (1_SA), axle group (2_AG), and GVW are 4.3 tons, and 16.44 tons, and 20.72 tons, respectively. The axle spacing data are listed in Table 4.3(b). The MD of the first axle spacing, A, is 4.12 m, and spacing of individual axle in tandem (two-axle group), B, is 1.30 m. The COV of this spacing is very small (0.06), indicating that the two-axle group spacing data are mostly that 1.30 m. This axle spacing data also agreed with data collected from factories in Thailand.
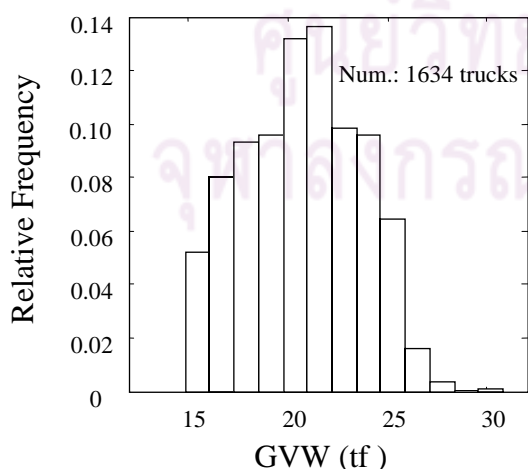
(a) Relative frequency of GVW for TR-05   **(b)** Configuration of TR-05
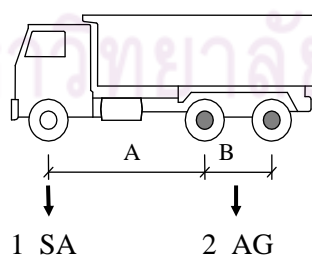
Figure 4.22 TR-05: **(a)** Relative frequency of GVW, **(b)** Configuration

Table 4.3a Axle weights for loaded truck , TR-05

Axle weight	MV (tons)	SD	COV
1_SA	4.30	1.88	0.24
2_AG	16.44	2.80	0.17
GVW	20.72	2.93	0.14

SA- single axle, AG- axle group (or tandem)

Table 4.3b Axle configuration for TR-05

Axle spacing	MD (m)	SD	COV
A	4.12	0.49	0.12
B	1.30	0.08	0.06
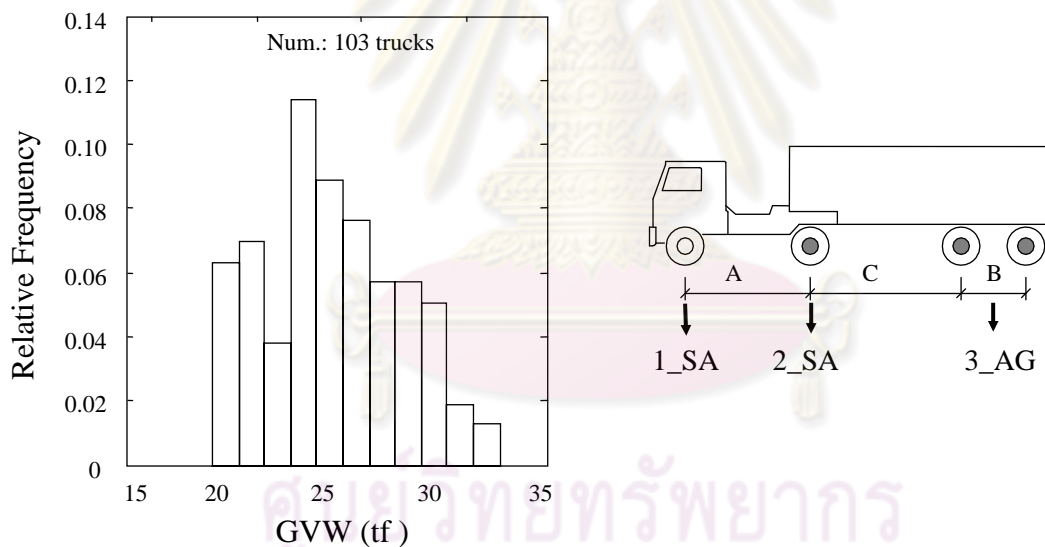
(a) Relative frequency of GVW for TR-07   **(b)** Configuration of TR-07

Figure 4.23 TR-07: **(a)** Relative frequency of GVW, **(b)** Configuration

Figure 4.23a shows the relative frequency of GVW for the TR-07 trucks which has only 2% of the total monitored data. This figure shows loaded trucks which GVW are more than 20 tons. And the maximum GVW for the TR-07 group was about 33 tons. This truck type is not existed in the list of legal limit trucks (Department of Highways, 2005). Table 4.4a shows the data of axle, axle group weights, and GVW, which the mean value (MV) are 3.78

tons, 9.26 tons, 12.77 tons, and 25.81 tons for first axle, second axle, third axle group weights, and GVW, respectively. Observing from these data, TR-07 truck is not too heavy truck load. The axle spacing for TR-07 truck type is listed in Table 4.4b. The median (MD) of A, B, and C (see Figure 4.23b) are 3.75, 1.35, and 8.07, respectively. The SD of the axle spacing, C is 1.41. It is seen that this value is higher than one because the data of this spacing is so variable, which the minimum and maximum values are varying from 3.3 m to 9.9 m (see appendix A-2 for axle distribution graph).

Table 4.4a Axle weights for loaded truck , TR-07

Axle weight	MV (tons)	SD	COV
1_SA	3.78	0.84	0.22
2_SA	9.26	1.94	0.21
3_AG	12.77	3.08	0.24
GVW	25.81	3.30	0.13

Table 4.4b Axle configuration for TR-07

Axle spacing	MD (m)	SD	COV
A	3.75	0.88	0.22
B	1.35	0.10	0.07
C	8.07	1.41	0.18

Figure 4.24a shows the relative frequency of GVW for the TR-09 group, and only loaded trucks are selected, which GVW are more than 25 tons. The condition for empty and loaded truck is also the same as explaining at the above. The maximum GVW for TR-09 is about 50 tons, while the legal GVW limit is 45 tons (Department of Highways, 2005). The peak of the frequency graph for highest GVW values indicates that most of the loaded trucks in the TR-09 group weighed about 39 tons. However, only a few trucks, less than 3% of total TR-09 truck data, were above the legal weight limit. This truck type is very important, because it is heavy loading truck and popular using in Thailand. The axle and axle group weight, and GVW data are also given in Table 4.5a, which MV are 4.79 tons, 14.26 tons, 17.84 tons, and 36.89 tons, respectively. All COV of axle weights data are also about 0.22. Observing from GVW and axle weights data, it can be seen that TR-09 truck is one very

heavy truck load. The configuration of truck is shown in Figure 4.24b, consisted single steering axle, and two tandems axles. The MD value of the spacing between the last leading axle to the first trailing axle (distance of C) is 7.2 m, and its SD value is 1.28 (see Table 4.5b). The SD value for axle spacing C is more than one, because of the wide range of the spacing data (between 3 m and 9 m). The graphs of axle spacing distribution are presented in the appendix A-2. The spacing for individual axles in tandems of heading is about 1.3 m, which the same as data collected from factories in Thailand (Chula Civil Dept. Report, 2003).
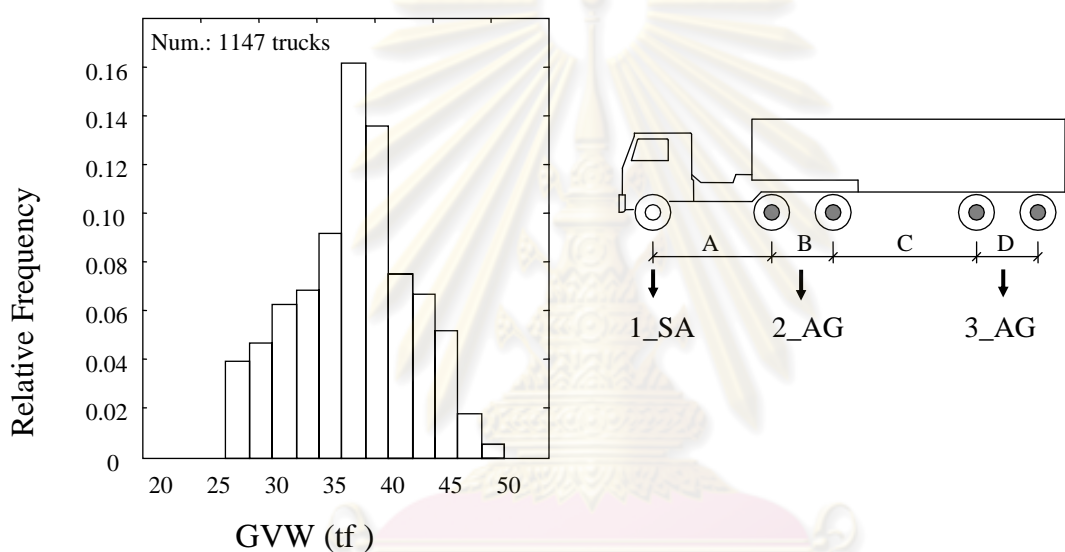
(a) Relative frequency of GVW for TR-09   **(b)** Configuration of TR-09

Figure 4.24 TR-09: **(a)** Relative frequency of GVW, **(b)** Configuration

Table 4.5a Axle weights for loaded truck , TR-09

Axle weight	MV (tons)	SD	COV
1_SA	4.79	1.04	0.22
2_AG	12.26	3.36	0.24
3_AG	17.84	4.06	0.23
GVW	36.89	5.03	0.14

Table 4.5b Axle configuration for TR-09

Axle spacing	MD (m)	SD	COV
A	3.36	0.24	0.07
B	1.30	0.05	0.04
C	7.20	1.28	0.19
D	1.35	0.06	0.05

Figure 4.25a shows the relative frequency of GVW for the TR-10 trucks and this figure includes only loaded trucks that GVW are more than 25 tons, and the maximum GVW of 58.1 tons. The legal GVW limit for this truck type is 50.5 tons (Department of Highways, 2005). The configuration of the TR-10 truck is different from the TR-09 truck only that trailing for TR-10 is three-axle group (see Figure 4.25b), while TR-09 is tandem. Axle weights for TR-10 truck consist of single axle, tandem axle, and three-axle group weights, with MV 5.62 tons, 17.66 tons, and 23.96 tons, respectively (Table 4.6a). The mean value of GVW is 47.24 tons. In this monitored data, this truck type is heaviest truck load. However, the numbers of this truck type is only 3% of total truck data. The axle spacings for this truck type are also the same as those for the TR-09 trucks (see Table 4.6b), for which the SD of axle spacing C is 1.26, and the MD of the spacing for the individual axle in axle groups are also the same as those for the TR-09 trucks with 1.3 m for heading and 1.35 m for trailing axles. These axle distribution graphs are also presented in appendix A-2.
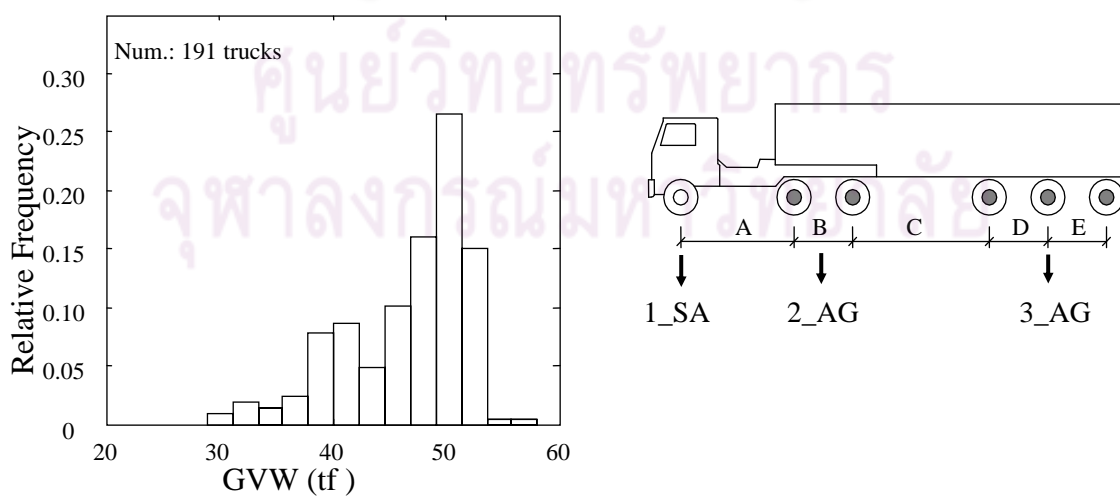
(a) Relative frequency of GVW for TR-10　　　**(b)** Configuration of TR-10

Figure 4.25 TR-10: **(a)** Relative frequency of GVW, **(b)** Configuration

Table 4.6a Axle weights for loaded truck , TR-10

Axle weight	MV (tons)	SD	COV
1_SA	5.62	1.06	0.22
2_AG	17.66	2.75	0.16
3_AG	23.96	3.51	0.15
GVW	47.24	4.57	0.10

Table 4.6b Axle configuration for TR-10

Axle spacing	MD (m)	SD	COV
A	3.37	0.25	0.08
B	1.30	0.07	0.05
C	6.26	1.26	0.22
D	1.35	0.07	0.05
E	1.35	0.07	0.05

Figure 4.26a shows the relative frequency of GVW for the TR-11 trucks, which GVW for loaded trucks are more than 30 tons. This truck type is a combination of a TR-05 truck and a trailer. The legal GVW limits for these truck types is 47 tons (Department of Highways, 2005), while the maximum GVW values in this monitored data is up to 50 tones. However, less than 3% of the total TR-11 truck data those are overloaded (have a GVW exceeding the legal limit). Observing the peak of the graph in Figure 26a, it is indicated that most of the GVW for loaded trucks are about 44 tons. The statistics values of axle weights, and GVW for TR-11 truck are given in Table 4.7a, which MV weights of single steering axle, tandem, tow single axles of trailing, and GVW are 4.63 tons, 18.52 tons, 8.88 tons, 9.06 tons, and 41.09 tons, respectively. This truck type is one heavy truck load in Thailand that may generate more loads to bridge structures, especially for medium and long span bridges. The axle spacings of the leader trucks for the TR-11 truck is also the same as those of the TR-05 group trucks, which MD for A and B are 4.12 m and 1.30 m, respectively (see Table 4.7b). The trailing axle spacings has SD values less than one, it indicates that this spacing does not much vary.
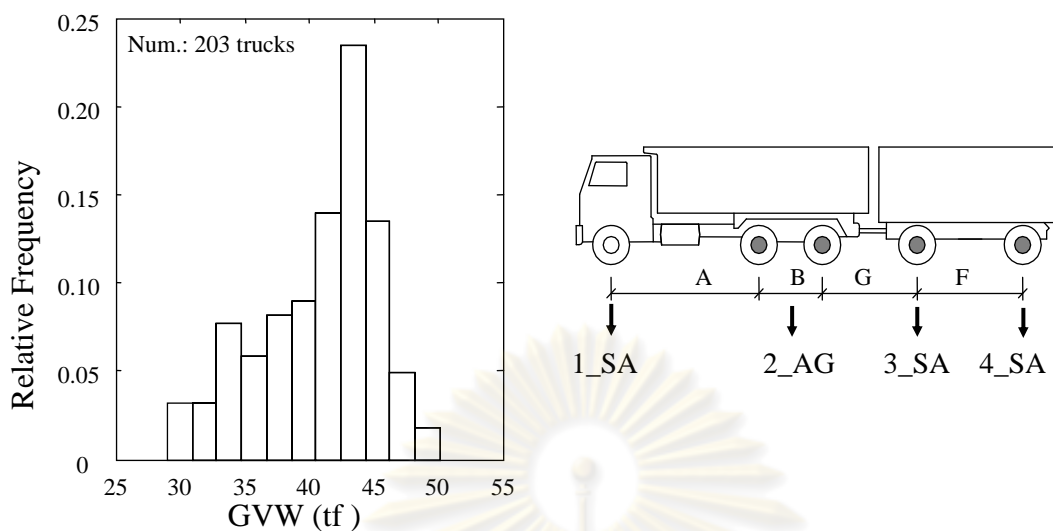
(a) Relative frequency of GVW for TR-11   **(b)** Configuration of TR-11

Figure 4.26 TR-11: **(a)** Relative frequency of GVW, **(b)** Configuration

Table 4.7a Axle weights for loaded truck , TR-11

Axle weight	MV (tons)	SD	COV
1_SA	4.63	1.11	0.24
2_AG	18.52	2.26	0.12
3_SA	8.88	1.92	0.22
4_SA	9.06	1.87	0.21
GVW	41.09	4.23	0.10

Table 4.7b Axle configuration for TR-11

Axle spacing	MD (m)	SD	COV
A	4.12	0.23	0.06
B	1.30	0.07	0.05
G	4.38	0.30	0.07
F	4.40	0.30	0.06

Figure 4.27 shows the figure for the TR-12 trucks. There are a few numbers for TR-12 trucks in this monitored data (only 0.3% of total monitored data). The loaded trucks have been selected with GVW higher than 30 tons, and only 7 loaded trucks can be observed. Therefore its data are not enough to present the graph of relative frequency of GVW. However, it can summary that the maximum GVW from monitored data is 54 tons, while the legal GVW limits is 53 tons (Department of Highways, 2005). The data of axle and axle group weights for loaded trucks are listed in Table 7a, which the MVs are 4.88 tons, 19.29 tons, 9.45 tons and 14.23 tons, and MV of GVW is 47.85 tons. In Table 4.8a, the COV for trailing axles are 0.38 and 0.35, which is greater than 0.3. This may be due to that some trucks were full loading for heading truck but empty for trailing trucks. This truck type is the heaviest truck in the list of legal limit truck (Department of Highways, 2005). In this monitoring, however, only little number has been found. This truck type is one heavy truck load in Thailand, it may important for bridge structure. Therefore it may suggest furthering monitoring to observe. The configuration of this truck type is similar as that TR-11 truck, it is different only that the trailing axles for the TR-12 truck consisted of a single axle and tandem (see Figure 27 and Table 4.8b).
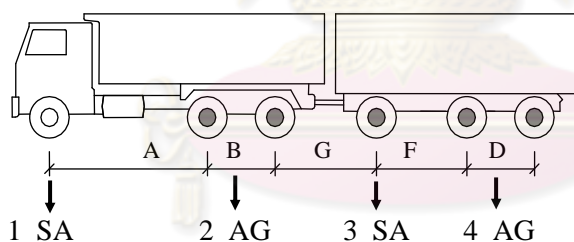
Figure 4.27 TR-12: Configuration

Table 4.8a Axle weights for loaded truck , TR-12

Axle weight	MV (tons)	SD	COV
1_SA	4.88	1.04	0.21
2_AG	19.29	2.92	0.15
3_SA	9.45	3.62	0.38
4_AG	14.23	4.93	0.35
GVW	47.85	7.36	0.15

Table 4.8b Axle configuration for TR-12

Axle spacing	MV (m)	SD	COV
A	4.14	0.30	0.07
B	1.30	0.06	0.05
G	4.39	0.37	0.10
D	1.35	0.05	0.04
F	3.42	0.36	0.11

From the above truck data, the configurations (axle spacing) of trucks are varied depend on truck type, which can be observed from the SD of axle spacing. SD of axle spacing for TR-02 is 0.93, which indicates that axle spacing data quite large varies between maximum and minimum value (this truck varying from 3 m to 6 m). This due to the TR-02 groups are two axle trucks, their axles may consist of four wheels and six wheels, the length of different amount of wheel truck may alter also. For three axles truck (TR-05), and leader truck for TR-11 and TR-12 trucks are similar configuration, which SD of first axle spacing is less than 0.5, and MD of first axle spacing is 4.12 m, the varying of this axle spacing is between 3.3 m to 5 m. The different configuration of these truck groups may due to such trucks may consist of three axles six wheels, three axles ten wheels, busses, etc. The SD of axle spacing between heading and trailing of semi-trailer truck types, TR-07, TR-09, and TR-10 are higher than one, and MD are higher than 7 m. The varying of axle spacing for theses truck groups are between 3.5 m to 9 m. this is due to the configuration of semi-trailer groups consist of different length. However, for individual axle spacing in axle groups for different truck type are similar, which is about 1.3 m for three axle truck group, and heading of semi-trailer groups; and 1.35 m for trailing of semi-trailer and trailer groups.

Each truck type can be grouped by loaded and empty trucks, which dividing line condition for loaded and empty trucks is explained in the above by judgment from GVW distribution and COV. Most of trucks from this monitoring loaded under legal limit. Each truck type has only about 3% loaded higher than legal limit. Observing relative frequency of the GVW, for two axles truck (TR-02) most of loaded trucks are about 10 tons, TR-05 (about 21 tons), TR-07 (about 24 tons), TR-09 (about 36 tons), TR-10 (about 50 tons), TR-11 (about 44 tons), TR-12 (about 50 tons). All truck are heavy truck load, accept TR-02 group. Few overloaded trucks were seen in this monitored data, this may due to that there is the weight

control station on this highway. All of this data are evident that the proposed system is applicable.

4.7 Observing of Heaviest Monitored Trucks to HS20-44

To investigate over loaded trucks, the heaviest trucks in each truck type from the monitored data were compared to the HS20-44 standard design truck in the AASHTO. HS20-44 consists of truck loading and lane loading, but for bridges with spans shorter than 35m, only truck loading is considered because it induces a greater load on such bridges than lane loading (Colin O'Connor and Peter A. S, 2000). Small and medium bridges in Thailand have been designed according to the HS20-44 design truck. The GVW of this truck model is 32 tons. The three axles have loads of 3.5 tons, 14.2 tons, and 14.2 tons, respectively. The axle spacings are 4.3 m between the first and second axles, and 4.3 to 9.1 m between the second and third axles (Figure 4.28). The monitored trucks (Thai trucks) in this test shown in Table 4.2 to 4.8 above have axle configurations that do not differ much from that of the HS20-44 design truck, varying between 4.1 and 9 m (from center to center for axle group). However, the axle weight and GVW of the heaviest loaded truck in each monitored truck group, except the TR-02 group, are higher than those of the HS20-44 truck.
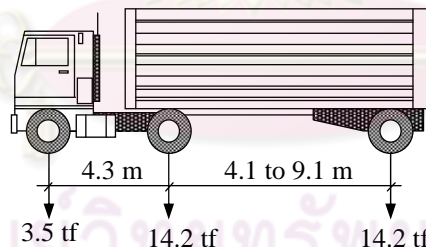
Figure 4.28 HS20-44 (AASHTO) truck

Table 4.9 shows the axle weights of the heaviest for the monitored trucks and the HS20-44 design truck. The individual axle weight in axle group is assumed as equal load. The GVW of each heaviest truck type is a sum of axle weights. It is seen that only the TR-02 truck has a GVW that is less than that of the HS20-44 design truck. The GVW of heaviest TR-10 truck is almost twice that of the HS20-44 design truck. Steering axle weights for all heaviest trucks are higher than 3.5 tons, which those of HS20-44. Weights of individual axles are less than 14.2 tons; however, axle group weights of heaviest trucks (sum of

individual axle weight in axle group) for each truck type are higher than second and third axle of the HS20-44 truck. For example, the heaviest for two-axle group is up to 26 tons, and the heaviest for three-axle group is up to 30 tons, while the axle load of the standard design truck is 14.2 tons.

Table 4.9 Axle weights of each heaviest truck (tons)

TR	1	2	3	4	5	6
HS20-44	3.5	14.2	14.2	-	-	-
TR-02	4.3	15.3	-	-	-	-
TR-05	4.7	13.1	13.1	-	-	-
		26.2				
TR-07	4.0	11.1	9.3	9.3	-	-
			18.6			
TR-09	5.1	10.0	10.0	12.3	12.3	-
		20.0		24.6		
TR-10	4.7	11.6	11.6	10.0	10.0	10.0
		23.2		30.0		
TR-11	4.5	11.4	11.4	11.1	11.6	-
		22.8				
TR-12	5.3	9.7	9.7	13.7	8.1	8.1
		18.4			16.2	

Another way to compare these heaviest Thai trucks with the HS20-44 truck is to compute the maximum bending moment for simply span bridges with a length between 5 m and 35 m. The bridges are assumed to have a single lane and a one truck presented for span less than 20 m, a single lane and train truck with distance 8 m (front bumper of following truck to rear bumper of preceding truck, or approximately 11 m from first axle of following truck to last axle of preceding truck) presented for higher span length. The maximum bending moment of the monitored Thai truck versus that of the HS20-44 truck for different bridge spans are shown in Figure 4.29. In the graph, the victual axis is the bending moment with unit (tf.m)x100, i.e number 1,2, 3, … mean that these value need to multiple by 100 to be 100, 200, 300, …. Tons.m.   The graph shows that the effects of the heaviest Thai truck types— TR-05, TR-09, TR-10, TR-11, and TR-12—are exceeded by those of the HS20-44 truck. For spans less than 15 m in length, the maximum moment is induced by the trucks in the TR-05 and TR-10 groups, and this maximum moment is about 48% greater than that of the

HS20-44 truck. On longer spans, the maximum moment is induced by the trucks in the TR-10 and TR-11 groups. This bending moment is about 40% greater than that of the HS20-44 truck. Both the axle weight and the axle configuration of the trucks are very important for bridge structures. For example, in this calculation, the GVW of a TR-05 truck is a little bit less than that of the HS20-44 truck but induces more maximum moment. The GVW of a TR-07 truck is a little bit more than that of the HS20-44 truck but induces less maximum moment. In the graph, 1.5HS20-44 means that the effects of HS20-44 are multiplied by a factor of 1.5. This graph is higher values than all other graphs for the heaviest of the monitored trucks, implying that, due to current truck loads, the 1.5 factor may be needed to increase the standard design truck. This effect, however, requires further study.
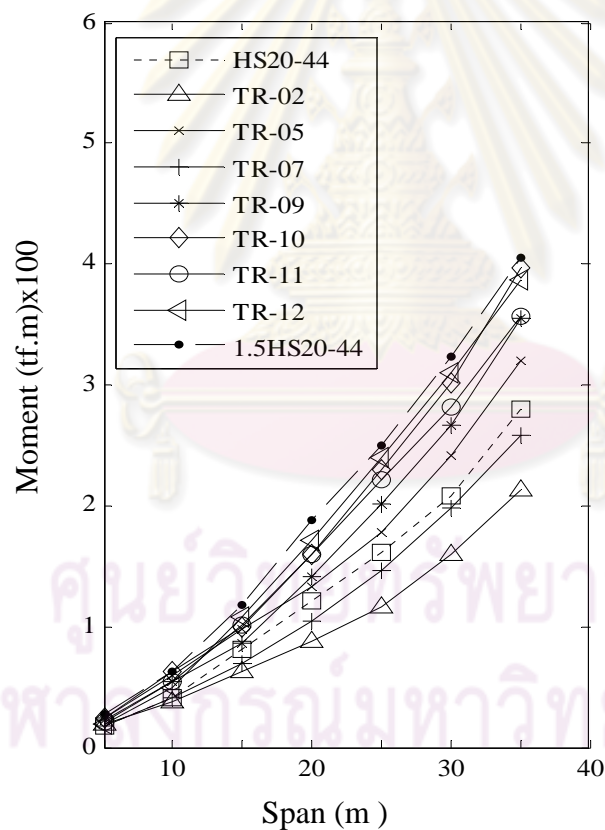
Figure 4.29 Maximum bending moment of the heaviest of the monitored truck and HS20-44 versus bridge span

Figure 4.30 shows shear force at support of maximum trucks from monitored data and HS20-44 for different bridge span, 5 m to 35 m. The graphs of shear force also are indicated

that the effects of the heaviest monitored truck, TR-05, TR-09, TR-10, TR-11, and TR-12, exceeded those cause by HS20-44 truck. For shear which span length less than 10m, TR-05 will be critical truck load, abut 23% higher than HS20-44 truck; and for longer bridges span, the maximum shear will be induced by TR-10 and TR-12, about 32% higher than HS20-44 truck. And, it is seen that the shear forces for 1.5HS20-44 are highest at all bridge spans.
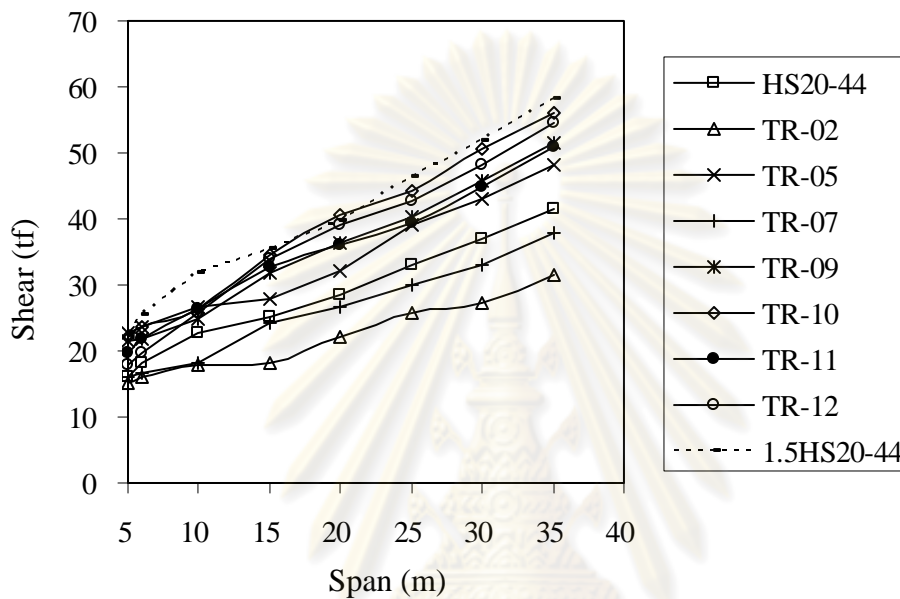
Figure 4.30 Maximum shear force of the heaviest of the monitored trucks
and HS20-44 versus bridge span

4.8 Summary

In this chapter, the detail of the B-WIM system developed in this study has been presented in the detail. The system has been tested and truck load data have been monitored. All monitored truck load data also are presented, and the heaviest monitored truck have been observed to HS20-44 of AASHTO. The overall results are summary in the following.

In this study, an alternative system of truck load monitoring based on the B-WIM system was developed. The proposed system consists of devices such as strain gauges, photoelectric sensors, and a CCTV. The system is uncomplicated and inexpensive, but it can provide reliable truck load data. No equipment is exposed on the road surface reflecting to the truck drivers leading to receive unbiased data. The installation does not interrupt traffic, which means that the system is easy to install and maintain. From the calibration truck, the error in estimation of axle spacing is less than 2%, the error in estimation of axle weight and axle group weight is less than 13%, and error in estimation of the GVW is within 6% to 10% .

The Bangkok Eastern Ring Road (BK-ERR) in Thailand was selected for monitoring actual truck configurations and loads. The results of this test can classify the actual trucks into seven types. The configurations of trucks can be grouped such as 2-axle truck, 3-axle truck, semi-trailer truck, and full trailer truck. The varying of truck configurations is given as standard deviation (SD) of axle spacing. The median value of axle spacing for 2-axle truck is about 5 m, and the 3-axle truck are about 4.1 m, and 1.3 m. The axle spacing of semi-trailer truck groups are very varied with SD higher than one; however, the individual axle spacing in axle groups for each truck type are similar by median value is 1.30 m for heading truck, and 1.35 m for trailing truck. This individual axle spacing in axle groups is also agreed with data collected from manufacture in Thailand. The frequencies of GVW of each truck type are also presented. Most of the truck loaded less than the legal GVW limit as seen that the mean value of GVW from monitored data are such as 2-axle truck about 11 tons, 3-axle truck about 20 tons, 4-axle truck about 25 tons, 5-axle truck about 55 tons, etc. It can be observed only 3% in each truck type that loaded higher than the legal limit. This may due to the weight control station on this highway.

Based on nominal analysis of a one-lane, short- to medium-span bridge, with span length between 5 m to 35 m, all of the heaviest of the monitored trucks (or actual Thai trucks) generate loads on bridges that are higher than that of the HS20-44 design truck. The heaviest truck load can reach as high as 48% and 35% for bending moment and shear forces, respectively above that of the HS20-44 design truck. The effects of truck loads on bridges are produced not only by the axle weight but also the axle spacing, which is not legally defined in Thailand.

CHAPTER V

NLFEM FOR ANALYSIS OF CONCRETE STRUCTURE

5.1 General Remark

Nonlinear Finite Element Method (NLFEM) for the reinforced concrete (RC) structures is growing interest in the civil and mechanical engineer at the present decades. This is due to that the numerical analysis technique and high speed computer make it possible to analyze nonlinear behavior of concrete. By using the NLFEM, the characteristics of the concrete can be assessed with some degree of the accuracy.

The analysis of RC structure is the most complex then other structure. The complex are raised due to such that the structure system is composed of concrete and steel reinforcement, the mechanical interaction (bond) between these two materials is very complex; concrete itself is composed of aggregate, cement paste, water and void which its behavior is nonlinear. Concrete exhibits progressive cracking under increasing load, which is difficult to model. Concrete properties are also influenced by many factors. i.e. environment, thermal, loading, etc. Therefore, it is difficult to model reality behavior of concrete. Most of the concrete models parameters are based on the empirical rules established by interpretation from the laboratory. Using numerical approach, there are three approaches to account for crack propagation in the concrete and RC structures such as discrete crack, smear crack, and embedded crack. For the large scale structure analysis, the smear crack model is more appropriated.

In this study, NLFEM for analysis existing concrete structure will be studied which the existing flaw/crack at tension region (or existing flexural crack for flexural member) of concrete and RC member will be considered into the constitute models. Hence, in this chapter some mechanical properties and general constitutive models of concrete will be summarized. The constitutive models of softening and tension stiffening accounting for existing flaw/crack at tension region for analysis old concrete and RC structure will be derived.

5.2 Basic Mechanical Properties of Concrete

Concrete is the composite material. It consists of coarse aggregate, sand, anhydrate cement, cement gel, gel pore, air void and water. The mechanical property

of concrete is really complex. Very fine cracks (microcracks) exist at the interface between coarse aggregates and cement paste, even prior to application of the load on the concrete. Due to microcracks existed, concrete is nonlinear material and very low in tension strength. In the structural engineering, the concrete can be considered as a homogenous and isotropic continuum at before crack state of exerted loading, after this state concrete can be assumed as inelasticity behavior (Jiang, 1995).

Compression of concrete:

The stress-strain curve of the concrete subjected to uni-axial compression (Figure 5.1(*a*)) shows a linear-elastic behavior up to about 30 percent of the ultimate compressive strength *fc′* (defined by ASTM C192), because under short-term loading the microcracks in the interfacial transition zone remain undisturbed. For stresses above this point, the curve shows a gradual increase in curvature up to about 0.75*fc′* to 0.9*fc′*, where upon its bends is more sharply, almost becoming flat, at *fc′*. Beyond this peak, stress-strain curve is descending until the concrete crushed. From the shape of the stress-strain curve it seems that, with a stress level that is between 30 to 50 percent of *fc′*, the microcracks in the interfacial transition zone show some extension due to stress concentration at the crack tips; however, no cracking occurs in the mortar matrix (Mehta and Moterio, 2006). Until this point, crack propagation is assumed to be stable in the sense that crack lengths rapidly reach their final values if the applied stress is held constant. With a stress level between 50 to 75 percent of *fc′*, some near aggregate surfaces start to form mortar crack. When the available internal energy exceeds the required crack-release energy, the rate of crack propagation will increase and the system will become unstable. This happens at the compressive stress levels above 75 percent of *fc′*, when complete fracture of the test specimen can occur by bridging of the cracks between the matrix and the interfacial transition zone.

Figure 5.1(b) shows the plot between volumetric strain, $e_v = e_1 + e_2 + e_3$, vs stress, this volume strain is increased almost linearly up to the stress level of about 75 to 90 percent of *fc′*. At this point the direction of the volume change is reversed, resulting in a volumetric expansion near or at *fc′*.

The typical of the crushing strain is still not obvious, but the ultimate strain (strain at peak curve) is roughly 0.002 (0.0018 ~ 0.0025) (Jaing, J.J, 1995). This value is all so similar all for all concrete of low, normal and high strength concrete, (W. F. Chen 1982).

The ultimate compressive strength fc' is obtained from standard ASTM cylinder (300mm in high and 150mm in diameter) test at aged of 28 days. This compressive strain is one of the most important in the mechanical property of concrete. The compressive strength can also be interpreted to other mechanical properties of concrete, such as tensile strength, modulus of elasticity.
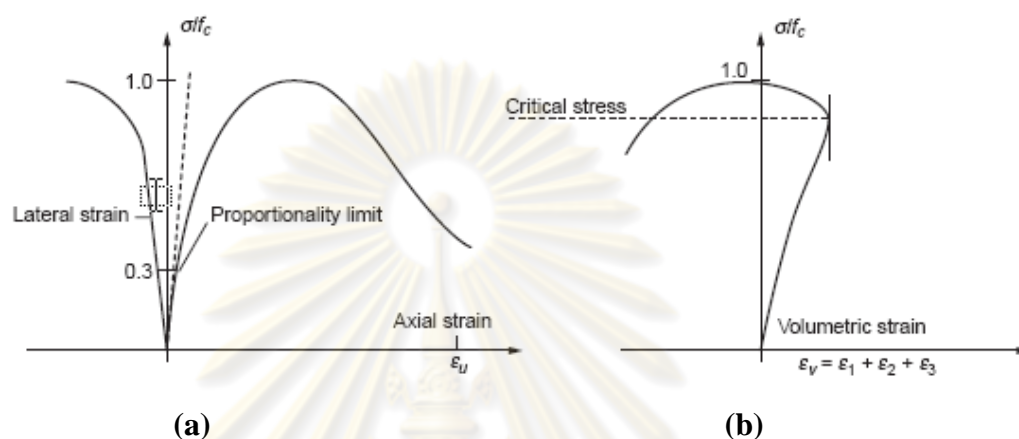
Figure 5.1 Plots of compressive stress vs. (a) axial and lateral strains, and (b) volumetric strains. (W. F. Chen 1982)

Modulus of concrete:

Since the stress-strain of the concrete is nonlinear, its elastic modulus varies with the intensity of the stress. In the practice, elastic modulus of concrete is defined into three types such as initial, secant and tangent modulus. Initial modulus is the slope of the stress-strain diagram at the original of the curve. The secant modulus is given by the slope of a line drawn from the origin to a point on the curve corresponding to a 40 percent stress of the failure load. The tangent modulus is given by the slope of a line drawn tangent to the stress-strain curve at any point on the curve. Secant modulus and initial modulus are mostly used for NLFEM.

The elastic modulus values used in concrete design computations are usually estimated from empirical expressions that assumes direct dependence of the elastic modulus on the ultimate strength of the concrete, fc' and density of the concrete, w_c. In actually this is the secant modulus.

ACI 318 $\qquad$ $E_c = w_c^{1.5} 0.043 \sqrt{f_c'}$ $\qquad$ MPa $\quad$ …..(5.1)

CEB (1990) $E_c = 2.15x10^4 \left(f_{cm} / 10 \right)^3$ MPa   …..(5.2)

Where E_c : Elastic modulus of the concrete

w_c : Unit weight (in between 1500 for 2500 kg/m^3)

f'_c : Concrete cylinder compressive strength (MPa)

f_{cm} : Mean value of concrete cylinder compressive strength (MPa)

Piossion ratio:

Poission ratio ,ν for concrete under uni-axial compressive loading ranges from about 0.15 to 0.22. Under uniaxail loading, the ratio, ν remains constant until approximately 80 percent of fc', at with stress the appearance Poission's ratio begin to increase. At the unstable phase, ν may be up to 0.5.

Uni-axial –Tension of concrete:

Concrete is very poor in the resistant the tension stress; however in recent years, the tensile properties of the concrete is significant to Nonlinear Finite Element Analysis (NFEA) for concrete and RC structures.

The shape of the stress-strain curve, the elastic modulus, and the Poisson's ratio of concrete under uni-axial tension are similar to those under uni-axial compression. However, the uni-axial tension state of stress is much less than the compressive states of stress. The tensile stress is the major cause of crack in the concrete. The direction of crack propagation in uni-axial tension is normal to the stress direction (Chen, 1982). The initiation and growth of every new crack will reduce the available load-carrying area, and this reduction causes an increase in the stresses at critical crack tips.

The stress-strain curve in the tension is almost linear up to peak load, Figure 5.2. The tension stress less than about 60 percent of the uni-axial tension strength, f_t, the creation of the new crack is negligible, due to the interval of the stable crack propagation, the linearity will be up to 70 percent of f_t (Chen, 1982). Beyond this state (point A and B) stress-strain curve is bended from linear to nonlinear ascending up to peak stress. After peak load, point B, the non-linear behavior starts to deviate varies between the studies performed in the literature (Hakhan T, 2006).
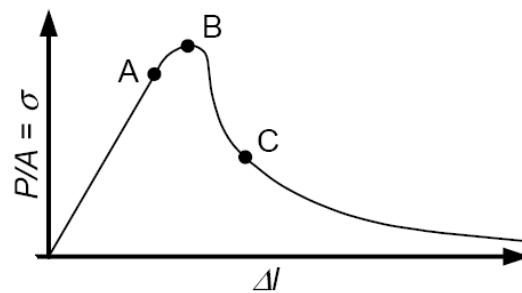
Figure 5.2 Tension stress vs strains curve. (Hakan T, 2006)

The tensile strength of the concrete, f_t, is normally obtained from standard splitting test of the concrete cylinder with the same dimension as compressive test specimen, however many researches stated that it can be approximately about 8 to 15 percent of compressive strength. The practice codes have given these relationships as below (Jaing, 1995).

ACI $\qquad$ $f_t = 0.5\sqrt{f_c{}'}$ $\qquad$ MPa $\qquad$ …..(5.3)

CEB $\qquad$ $f_t = 0.3\left(f_c{}'\right)^{2/3}$ $\qquad$ MPa $\qquad$ …..(5.4)

And rupture strength

ACI $\qquad$ $f_r = 0.7\sqrt{f_c{}'}$ $\qquad$ MPa $\qquad$ …..(5.5)

CEB $\qquad$ $f_r = 0.79\sqrt{f_c{}'}$ $\qquad$ MPa $\qquad$ …..(5.6)

f'_c : Concrete cylinder compressive strength (MPa)

f_t : Tensile strength of the concrete (MPa)

f_r : Modulus of the rupture of the concrete (MPa)

Biaxial and Multi-axial stress in concrete:

For the behavior of the concrete subjected to loads more than one direction, it will be depended on the loads direction and ratio applied loads. To understand this behavior of the concrete, many previous studies have been tested in biaxial load cases such as compressive – compression, compressive – tension, tension-tension. The most clearly to explain the concrete behavior   in biaxial is tested by Kupfer, et al (1969).

The stress strain curves for their test results are shown in Figure 5.3, for concrete under (a) biaxial compression, (b) combined tension compression, and (c) biaxial tension.

(a) Biaxial compression   (b) Combined tension compression

(c) Biaxial tension
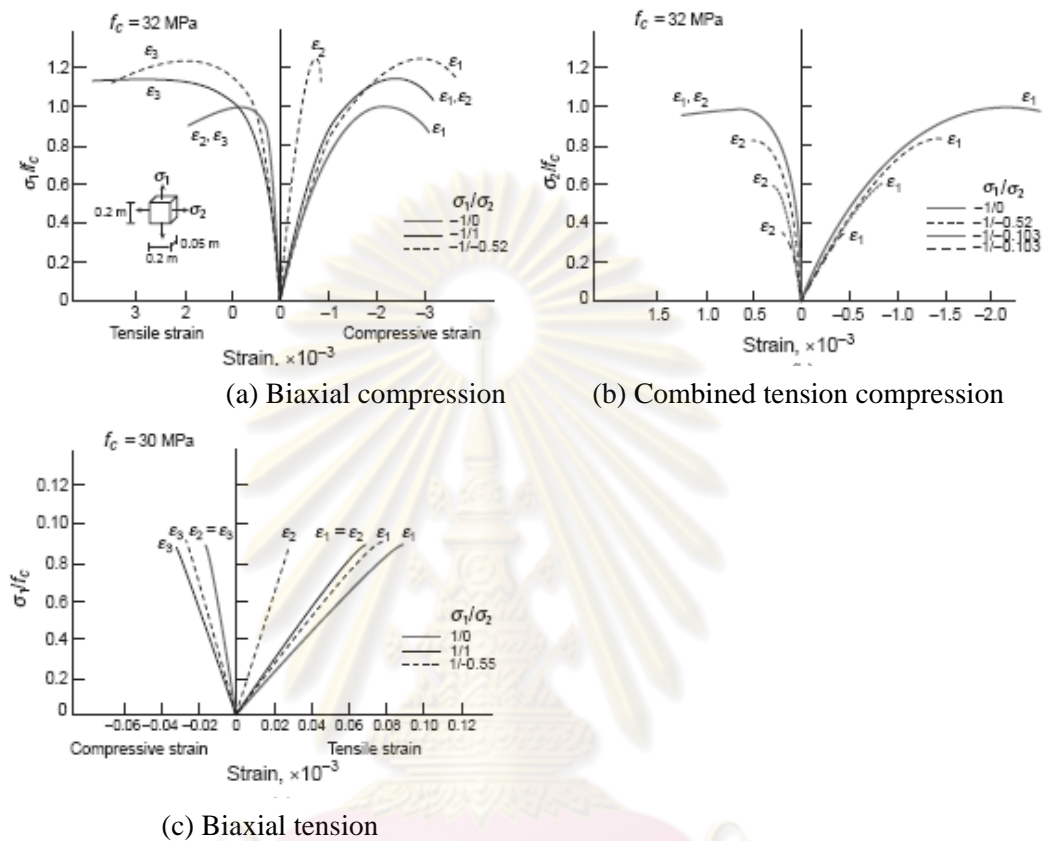
Figure 5.3 Experimental stress-strains curve. (Kufer, et al, 1969)

The test data show that the strength of concrete subjected to biaxial compression in Figure 5.3(a) may be up to 27 percent higher than the uni-axial strength. For equal compressive stresses in two principal directions, the strength is increased approximately 16 percent. Under biaxial compression-tension, Figure 5.3(b), the compressive strength decreased almost linearly as the applied tensile strength increased. From the biaxial strength envelope of concrete, Figure 5.3(c) it can be seen that the strength of concrete under biaxial tension is approximately equal to the uni-axial tensile strength.

The behavior of concrete under multi-axial stresses is very complex. There are no standard tests for concrete subjected to multi-axial stresses (Mehta and Moterio, 2006). However, some previous studies have been tested for standard cylinder by

using fluid pressure as lateral applies stress (Confined lateral, $\sigma_2 = \sigma_3$). Increase in lateral pressure brings very significant increase in ductility, as well as strength, and it found the relationship for the strength of concrete cylinder as Eq. (5.7) .

$$\sigma_1 = f_c' + 4.1\sigma_3 \qquad \qquad \ldots..(5.7)$$

Where

σ_1 : Axial compression strength of confined specimen (MPa)

σ_3 : Lateral confining pressure (MPa)

5.3 Cracking in Concrete and Reinforced Concrete

Causes of the crack in reinforced concrete member can be classified by two main categories, namely crack caused by external applied load, and those which occurred independently of the load (Reonart 1997). The flexural crack and inclined shear crack are main types of crack caused by external load. Flexural cracks are formed in the tensile zone of the member, and have a wedge shape. Inclined shear crack is usually developed in the thin web beam when subjected to high shear force. This study will derive model accounting for existing flaw/crack in concrete and RC members, and only cracks at the tension zone will be discussed which is mainly flexural crack, because this type of crack is mostly found in old concrete and RC structures. However; if flaws/cracks are found in other region, the other models are needed to develop which this is out off the scope of this study.

5.3.1 Cracking in Concrete Element

Concrete is a brittle materials type (low tensile strength material). At the recent decades, many researches have afforded to understanding cracking behavior of the brittle materials. The cracking behavior of this material is explained clearly by fracture mechanics theory. The successful fracture mechanics theories are theory of Griffith and Iwin. The crack modes of brittle material have generally stated in to three modes called modes I, II and III as shown in Figure 5.4. Mode I is cracking uni-axial tension crack; mode II is shear crack and mode III is out off plane shear or tear crack due to torsion.

From the development of the fracture theory and applying to concrete structure, cracking in the concrete can be modeled by both Linear Elastic Fracture Mechanics (LEFM), and Nonlinear Fracture Mechanics (NLFM) theories (Karihaloo,

1995; Van Mier, 1997). However, NLFM model is more appropriated for explaining post cracking in the concrete structures; because after cracking, concrete behavior is nonlinear. The successful NLFM models are such as fictitious crack model, and crack band model which are presented in the following.

mode I   mode II   mode III
(opening)   (sliding)   (tearing)
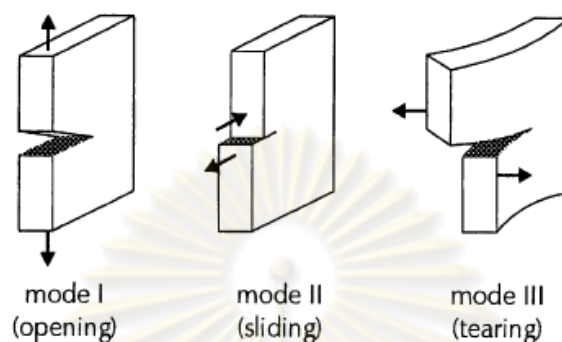
Figure 5.4 Cracking modes due to Griffith, (Van Mier, 1997)

Nonlinear Fracture Mechanic Fictitious crack model of concrete:

The first NLFM for concrete was proposed by Hillerborg et al. (1976), which called Fictitious Crack Model (FCM) for analyzing crack growth in cementitious composites. Unlike plastic metals, the closing stresses in the fracture process zone of concrete are not constant and the intensity factor mode one (K_I) is zero. In fact the idea is simple, when the concrete subjected to tension stress, the stress in the concrete is increased from zero up to f_t (tension strength of the concrete) and crack will be formed in concrete. This crack is not immediately stress free, but some tension capacities remain perpendicular to the crack face which is can be modeled by softening descending curve. The carrying capacity of concrete after cracking depends on crack width. Increasing the crack width, the stress transfer over the crack gradually decreases. Therefore tension strength of the concrete can be divided in to two parts, before cracking and after cracking. Before cracking, stress-strain diagram of the concrete is linear, after cracking this diagram is nonlinear softening in the function of the crack width (Figure (5.5 (a) and (b)).

In the fictitious crack model, there are two material parameters such as (i) the stress function (stress is a function of displacement, $\sigma(w)$), and (ii) the area under the tension softening curve which is the concrete fracture energy G_F , Eq. (5.9).

$$G_F = \int\limits_{f_t}^{0} w(\sigma)d\sigma \equiv \int\limits_{0}^{w_o} \sigma(w)dw \qquad \qquad .....(5.9)$$

Where f_t is the uni-axial tension strength limit of the material, and w_o is the critical crack tip opening displacement of the pre-exist crack.

In a finite element analysis of the concrete structure using FCM, some material parameters of the concrete are known by testing that are uni-axial tensile strength of the concrete, f_t, fracture energy G_F, and limit crack opening w_o. From the previous study, the fracture energy, G_F of normal concrete is about 0.05 to 0.11 N/mm (Maekawa 2003), and $w_o= \alpha GF/ft$ (α is constant parameter, according to Hillerborg et al, 1976, $\alpha=18/5$). When the normal tensile stress in an element attains the level f_t, at particular load, the corresponding nodes are released and defined as fracture zone. The nodes of element at fracture zone are assumed to tension softening stress strain displacement $\sigma(w)$. The fracture zone and the nonlinear zones are the same, since the material outside of the fracture process zone is assumed to be linear elastic. As the insertion of the $\sigma(w)$ distribution at the released nodes, the re-meshing of the elements is needed. This technique is also called discrete crack concept.

(a) Stress –strain before crack   (b) Stress –strain after crack
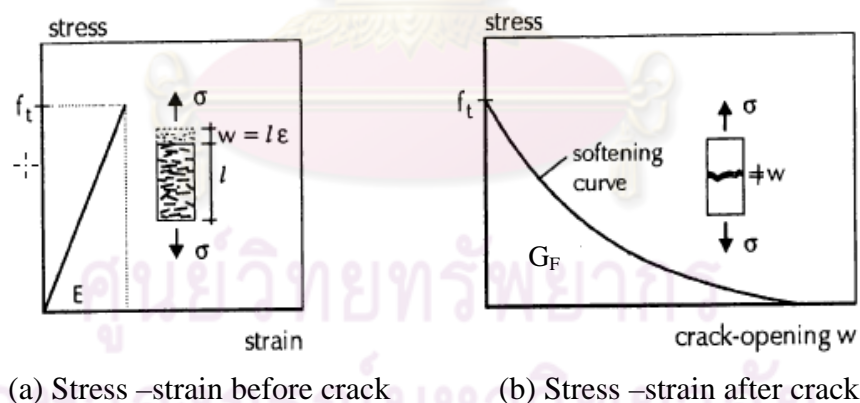
Figure 5.5 Fictitious crack model, (Van Mier, 1997)

Nonlinear fracture theory of crack band model of concrete:

As the microcracking and bridging in the process zone of concrete is not continuous and it is not necessarily developed in a narrow discrete region in line with the continuous traction free crack, it has been argued that the tension strength softening function in displacement, $\sigma(w)$ can be equaled well approximation by a

tension strength softening function in strain softening relation, $\sigma(\varepsilon)$. This strain is not related to the inelastic deformation, w (crack width), and fracture energy, G_F; but the ultimate strain at completed rupture, ε_o (critical strain) is related to critical crack width w_o. In other words, ε_o is can be defined by a fracture criterion. The fracture zone is assumed to process in the vicinity crack region, not in the certain line, which this concept is called crack band theory or crack band model (CBM). This technique can eliminate the spurious mesh dependence when uses in NLFEM. This technique was first developed by Bazant (1976), and further developed by Bazant and Cedolin (1979), and Bazant and Oh (1983) (Karihaloo, 1995). The basic idea of CBM is that after the concrete reaches the tension strength, f_t, the softening behavior of the concrete is smeared through fracture process zone, this zone is distributed over band width h. In the FEM, the microcracks are assumed to be smeared over an element, h is element size normal to crack direction. The whole element fractures when the uni-axial tension strength limit is reached. This technique is also called smeared crack approach.
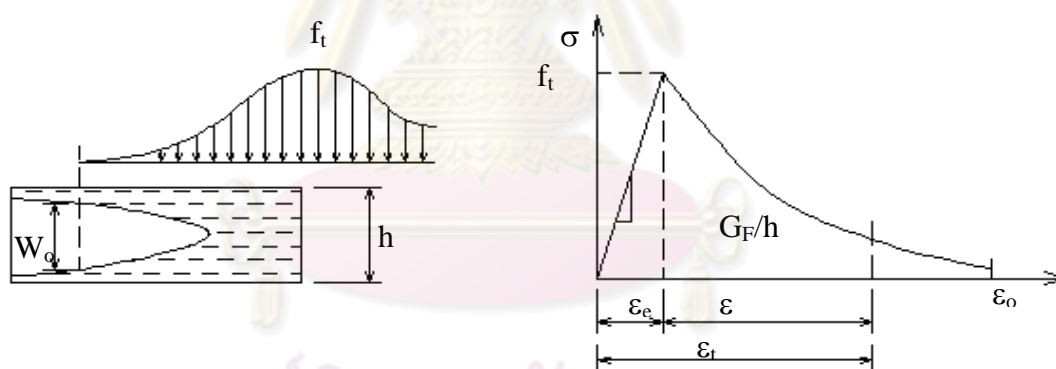
Figure 5.6 Crack band model (Karihaloo, 1995)

Returning the relationship between ε, w, and G_F as shown in Figure 5.6, the total strain is defined by $\varepsilon_t = \varepsilon_e + \varepsilon$, where ε_e is the elastic strain, ε is the strain when concrete formed process zone. Assuming all cracks smeared over h are initially parallel to one another. The tension strength of concrete in this region, h will be gradually decreased and vanished when total strain reaches critical strain, ε_o. The strain softening curve can be approximated as function of linear descending (Bazant

and Oh, 1983), or exponential (Reinhart, 1986). The fracture energy, G_F is the area under strain softening curve multiplied with h and can be defined by below equation.

$$G_F = h \int_0^{\varepsilon_o} \sigma(\varepsilon)d\varepsilon \qquad \qquad .....(5.10a)$$

The critical cracking strain is

$$\varepsilon_o = \frac{w_o}{h} \qquad \qquad .....(5.10b)$$

Where:

G_F : Concrete fracture energy (N/mm)

w_o : Critical crack opening (mm)

ε_o : Critical strain

$\sigma(\varepsilon)$: Stress at softening curve, which is a function of strain

h: Crack band width

Bazant and Oh (1983) recommended a value of h is approximately equaled to *3g*, where *g* is the maximum aggregate size. It is can be also possible to assume *h>3g* for the analysis of the large concrete structures, but the softening σ(ε) relation must be adjusted in order to ensure that the energy dissipation, G_F is unaltered.

The crack band model has many advantages over fictitious crack that the elements topology are not changed during crack propagation, the computation time is reduced, and it is suitable for analysis large scale structure, etc.

5.3.2 Cracking in RC Element

Crack is also unavoidable in reinforced concrete structure even at the normal service load. Due to that the strain of the steel is higher than that of the concrete; whenever strain at the reinforced concrete (RC) member exceeds the cracking strain of the concrete, crack will be formed. The crack behavior in the RC is quite more complex then in plain concrete members, because there are steel bars in RC member. Cracking in the reinforced concrete member has a major influence on structural performance, including tension and bending stiffness, energy absorption capacity, ductility, and corrosion resistant of the reinforcement (Oh and Kang, 1988).

5.3.2.1 Crack Width and Crack Spacing in flexural member

Cracks begin to occur when the stress at the tension member reaches the tension strength of the concrete, or stress at the tension face reaches ruptured strength

of the concrete for the flexural member. It is quite difficult to estimation crack width and crack spacing in reinforced concrete due to mechanics of composing between steel reinforcement and concrete is very complex. Different investigators have used different procedure to estimate cracking and its spacing. Many of those may used either of procedures such as: simplified analytical procedure to determine tensile stress in the concrete, analytical compounded with experimental works, and formulation totally based on test results (Pinhasena, 2002).

Gergely & Lutz (1968) proposed crack width prediction formulations based on computer statistical analysis of a large number of test results from different sources. Many combination of variable were tried, and it was very difficult to obtain equation that fitted all data. The important parameters which effected the crack width were found such as tensile force, number of bar, concrete cover, and steel stress. In that the steel stress is the most important. Then Gergely & Lutz proposed the formulation for prediction crack width at the tension face of the concrete fiber as the below equation.

$$w_{t,max} = 0.012\beta f_s \sqrt[3]{c_c A}\, 10^{-3} \quad \text{(mm)} \qquad \dots (5.11)$$

Where

$w_{t,max}$: Maximum crack width at tension face of concrete fiber, in mm.

β : ratio of distance between neutral axis and tension face to distance between neutral axis and centroid of reinforcing steel (taken as approximately 1.20 for typical beams in buildings).

f_s : steel reinforcement stress, ksc.

c_c: thickness of cover from tension fiber to center of bar closest thereto, mm.

A: average effective area of concrete in tension around each bar ($A=A_e/n$, where n is the number of bar), in mm^2.

ACI committee 224 has also recommened the formulation developed by Gergely & Lutz for design and control cracking in the reinforced concrete structure. ACI committee is adopted as Eq. (5.12).

$$w_{t,max} = 0.013z \qquad \dots (5.12)$$

And
$$z = f_s \sqrt[3]{c_c A}\, 10^{-3} \qquad \dots (5.13)$$

In ACI 318-89 code does not include a formula to compute explicitly crack width under service loads. There is calculated a limit of z-value as a means to control crack widths. This approach emphasizes the important influence of steel reinforcement details on the control of cracking, rather than the direct prediction of crack width.
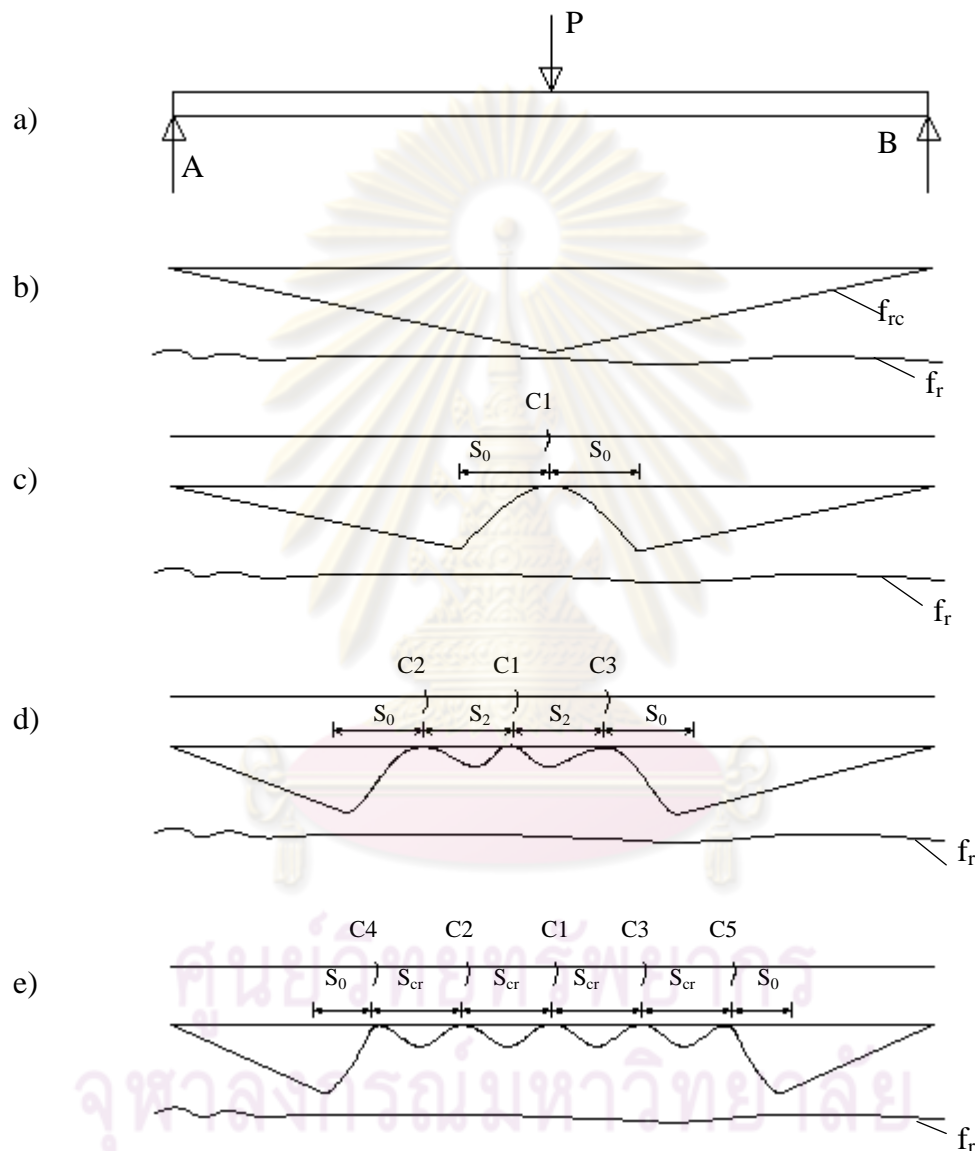
Figure 5.7 Crack developed in flexural member (Piyasena, 2002)

Crack propagation in the tension and flexural member can be categorized in three states of crack such as primary crack, second crack and stabilized crack. At first and second states, crack width and its spacing will be variable. At theses states, if applied load is increased, crack width will be increased, while crack spacing will be

reduced (Pynhasena, 2002). Many research have evidenced that the first crack will be occurred at where the maximum strain in the concrete member reached the tensile strength of the concrete, the second crack mostly will be occurred at the distance between l_t and $2l_t$ (l_t is the envelopment length) from first crack. At the stabilized state, crack spacing is not much vary from the second state, it mostly has spacing also between l_t and $2l_t$. The different formulas for predict crack spacing from the previous researches are depended on the formulas for predict envelopment length. Figure 5.7 shows the cracks propagation in flexural member subjected to applied one point load, P at near the middle span. When applied load is gradually increased, and stress in the tension face of the concrete at maximum moment reached tensile strength of concrete, first crack will be occurred as Figure 5.7c. Figure 5.7d is assumed second cracking state, and Figure 5.7e is stabilized crack state.   Where s_o is equal to envelopment length L_t. s_2 is a spacing of the second crack sate, s_{cr} is the stabilized crack spacing, f_r is the rupture strength of the concrete, and f_{rc} is the stress in the concrete due to applied loading.

5.3.2.2 Behavior of Crack Section

The cracks in the reinforced concrete members are formed whenever stress at the member in tension region is exceeded tension strength of the concrete. This section will study characteristic of the stress and stain at the crack face. In actually, width of crack is the slip of the concrete at the crack face (Oh and Kim, 2007), therefore the analytical approach is deriving crack width from the slip due to different between steel and concrete strains at the crack face (Somayaji, 1983; Oh and Kim, 2007).

Governing equation at the crack face:

When the concrete member is subjected to unaxial tension, and crack is presented as edged face of tension member, the stress and strain will be distributed as shown in the Figure 5.8. At section x from the crack face, the applied load P will be carried by concrete matrix as P_{cx}, and by steel as P_{sx}. The equilibrium equation is

$$P = P_{cx} + P_{sx} \qquad \qquad .....(5.14)$$

In the elastic state, $P_{cx} = A_c E_c \varepsilon_{cx}$, and $P_{cx} = A_s E_s \varepsilon_{cs}$,   where $A_s E_s = n A_s E_s \rho$, then Eq. (5.14) can be written as:

$$P = A_c E_c (\varepsilon_{cx} + \varepsilon_{sx} n\rho) \qquad .....(5.15)$$

Where

P: Total applied load (kg)

P_{cx}: Load carried by concrete at section x (kg)

P_{sx}: Load carried by reinforcement steel at section x (kg)

A_c: cross section area of concrete (cm2)

A_s: cross section area of steel (cm2)

E_c: modulus of elasticity of concrete (ksc)

ε_{cx}: strain of concrete at section x

ε_{cx}: Steel strain at x section from the crack face

n: Ratio of modulus of elasticity between steel and concrete

ρ: Reinforced steel ratio As/Ac

At the crack face, x=0 and P_{cx} is zero. P_{cx} will be maximum at the distance x= l_t from the crack face. Where l_t is the transfer length which is defined by the condition that at section x=l_t, the strain of the steel and concrete will be equaled to each other. The local slip due to crack, S_x can be defined as the total different elongations between the reinforcement and the concrete matrix measured over the length between section x and the center of the segment. The total crack width, w_x will be equaled to $2S_x$.

$$s_x = \int_x^{L/2} (\varepsilon_{sx} - \varepsilon_{cx}) dx \qquad .....(5.16)$$

By differentiation Eq. (5.16) with respect to x and substituting Eq. (5.15) into this equation, then differentiation again, the basic governing differential equation of the bond stress and slip will be obtained as Eq. (5.17).

$$\frac{d^2 s_x}{dx^2} - \frac{(1+n\rho)\sum_o}{A_s E_s} f_{bx} = 0 \qquad .....(5.17)$$

Where, Σ_o is the steel bar perimeter. Eq. (5.17) is the basic relationship between second derivative of local slip S_x and local bond stress f_{bx}. The analytical

model of bond slip, stress, crack width and crack spacing can be derived by solving this equation. Different investigators may solve this equation in different ways.
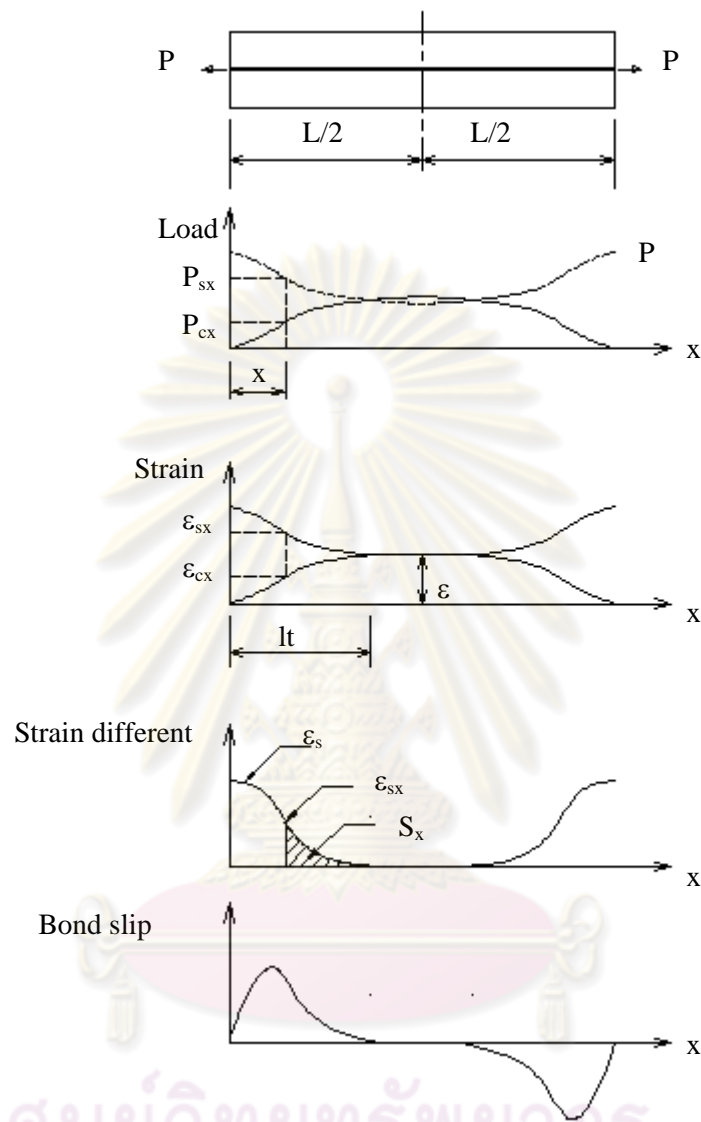
Figure 5.8 Distribution of stress strain at crack face

According Somayaji (1982) solving Eq. (5.17), he gave assumption as

$$\frac{d^2 s_x}{dx^2} = Ae^x + Be^{-x} + C \qquad \qquad \ldots\text{(5.18)}$$

Solving Eq. (5.18) and solution of bond slip is in the form

$$s_x = Ae^x + Be^{-x} + C\frac{x^2}{2} Dx + E \qquad \qquad \ldots\text{(5.19)}$$

Where A, B, C, D, E are constant determine from boundary conditions (see Somayaji, 1983).

And the transfer length is

$$l_t \;=\; K_p \; \frac{P_{tran}}{\sum_0} \qquad\qquad\qquad .....(5.20)$$

Where, P_{tran} is the transfer load at the concrete and steel interface. Kp is constant determine from the testing, (Somayaji defined as 0.0055 mm^2/N). The crack spacing is vary between $2l_t$ to l_t, and the crack width is equal to two time of the slip at crack face, $S_{x=0}$ ($S_{x=0}$ defined by Eq. 5.19) as below equation.

$$w_{av} = 2s_{x=0} \qquad\qquad\qquad .....(5.21)$$

5.4 Cracking Model of Concrete for NLFEM

There are two approaches that present cracking in the finite element analysis of RC structure, the discrete crack approach and the smear crack approach. The concept of smeared model was first introduced by Rashid (1968), and discrete crack model by Ngo and Schordelis (1967) (Kwak, 1991). In the discrete crack model, a crack is introduced as a geometric entity and re-meshing is required. In contrast, the smear crack model, topology of the original finite element mesh remains preserved.

The discrete crack approach introduces an actual gap in the finite element mesh at the location of a crack by using an interface element. It achieves this by doubling and separating the nodal coordinates lying along individual crack paths. This implies continuous change in mesh topology when crack propagation is considered. In the past, the re-meshing process has been a tedious and difficult job, (Figure 5.9a).

In the smear crack model, cracks are modeled by changing the average constitutive relations of stress and strain over some tributary area within the finite element (Figure 5.9b). This approach was introduced by Rashid in 1968, and becomes the most popular using in the finite element analysis of reinforced concrete members. However, there are some arguments that the smear crack model can not present the reality line of crack, the finite element analysis using smear crack is dependent on the size of the finite element mesh. Despite of these arguments, the smear crack approach is the most widely used approach in practice. The size-dependency effect of smear

crack approach has been investigated. As Bazant and Oh (1983) has introduced crack band model (CBM) from the fracture mechanics theory, Kwak (1991) proposed model of the mesh independent as given limit strain relating to the element mesh size. ACI committee (1995) summarized that there are three major reasons for adopting this approach, those are convenient in computation procedure, distributed damages in general and densely distributed parallel cracks in concrete structures, crack in concrete is not straight but highly tortuous which is closely to crack band.

Due to smear crack has many benefits over discrete crack, and in this study is aiming to analyze to assess full scale bridge structure, therefore the smear crack approach will be adopted in this study.
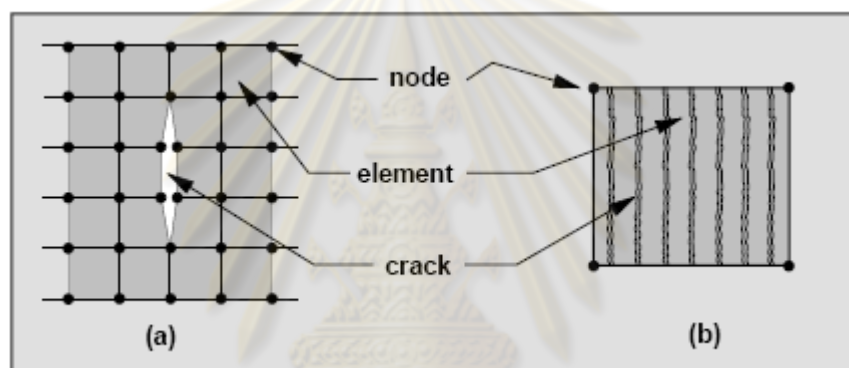
Figure 5.9 Cracking in FEM model, a) Discrete crack, b) Smear crack
(Kwak, 1991)

5.5 NLFEM and Material Model in CAMUI
5.5.1 Program Outline

In the present study, the 3D nonlinear finite element program "CAMUI" developed at the Laboratory of Engineering for Maintenance System of Hokkaido University is used. Three dimensional 20 nodes iso-parametric solid element, which contains 8 Gauss points, can be used for represent of plain and reinforced concrete elements. The nonlinear iterative procedure is controlled by the modified Newton-Raphson method (Withit, 2004). In the procedure, the convergence is adjust by values of $\Sigma(Residual\ force)^2/\ \Sigma(Internal\ force)^2$ or $\Sigma(Residual\ displacement\ due\ to\ residual\ force)^2/\ \Sigma(Increment\ of\ displacement\ in\ all\ element)^2$. The limit value is set to 10^{-6} through a sensitivity analysis. Figure 5.10 shows location of nodes and Gauss point of

elements. The smear crack concept and fixed crack model were adopted in the this 3D NLFEM program.

20 nodes   8 Gauss point
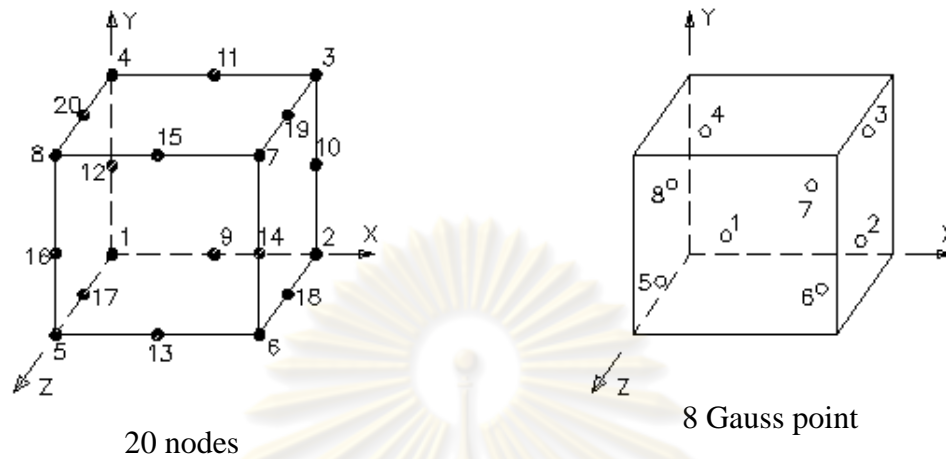
Figure 5.10 3D solid elements, 20 nodes and 8 Gauss points (Withit, 2004)

5.5.2 Material Constitutive Model in CAMUI

(1) The 3D Elasto-Plastic Fracture for Uncracked Concrete

Concrete nonlinearity cannot be described simply by plasticity since the theory of plasticity postulates no softening of the total stress-strain curve with constant stiffness along the unloading path. Softening along loading and unloading paths is usually observed even under higher confinement. Plasticity theory alone is not sufficient to cover this loading and unloading behavior. Softening and reduction in unloading stiffness are thought to result from continuum fracturing damage though dispersed micro-cracks, which degrades the energy absorption capacity. To take into account both plasticity and continuum damage, the 3D Elasto-Plastic Fracture Model is available to describe concrete in the pre-cracking range. The uncracked concrete is conceptually modeled as an assembly of infinitesimal elasto-plastic components. Concrete elasticity is modeled as a spring while plasticity is modeled as a slider. The fracturing damage is conceptually modeled as a broken spring. The total stress is integrated from the internal stresses of all undamaged spring components. Since elastic strain is directly proportional to interval stress developed in the undamaged components, it is adopted to describe the evolution of plasticity and damage. The

Elasto-Plastic Fracture Model divides concrete nonlinearity into continuum damage and plasticity.

The adopted failure criteria that acted in agreement with Niwa's model in tension-compression zone and Aoyanagi and Yamada's model in tension-tension region were extended to three-dimensional criteria by satisfying boundary conditions (Okamura, 1991).

When the first crack occurred, the stress of concrete element in the global coordinate system will be considered in the local coordinate system based on crack plane for calculation. The uni-axial stress in perpendicular direction to crack plane within the local coordinate system was calculated by Reinhardt's tension-softening model. Besides, in other two directions, which were parallel to crack plane, the model proposed by Vecchio & Collins (1983) was used for the local stress-strain relationship (Withit, 2004). Shear stress acted on the plane intersecting perpendicularly with a crack, was computed by using the average shear stiffness between shear stiffness of crack plane and shear stiffness from the concrete, which did not contain any cracks. Also, a simplified model of shear transfer model developed by Li and Maekawa et al was used in the present program (Withit, 2004).

(2) Tension Stiffening Model for Cracked Reinforced Concrete Element

Once cracks are generated in concrete, the anisotropy becomes significant so that the stress-strain relationship takes on an orthogonal anisotropy in the direction normal to cracks. This means that the stress-strain relationship has to be modelled respectively in the directions parallel as well as normal to cracks and in shear direction.

Owing to bond of concrete to the reinforcing bars, the concrete continues to support a part of the tensile force even after cracking has taken place in the reinforced concrete. Even though the concrete ceases to support the tensile force at the plane of cracking, in between the cracks the concrete continues to bear the part of the tensile force transmitted from the reinforcing bars through the bond action.

This makes the stiffness of reinforced concrete remain higher than that of the reinforcing bars alone. This phenomenon can be expressed by making the concrete to carry the tensile force after the generation of cracks. In the modeling of the cracked concrete, it is convenient if it is unrelated to the spacing of cracks, the direction of reinforcing bars and the reinforcement ratio.

It is for this reason that the model is expressed by the relation between the average stress and the average strain of concrete as shown in Figure 5.11.

Okamura et al.'s model

$$\sigma = f_1 \left(\frac{\varepsilon_{tu}}{\varepsilon} \right)^c \qquad \qquad .....(5.22a)$$

Where c: Coefficient defined by bond property (=0.4 for deformed bar, =0.2 for welded bar)
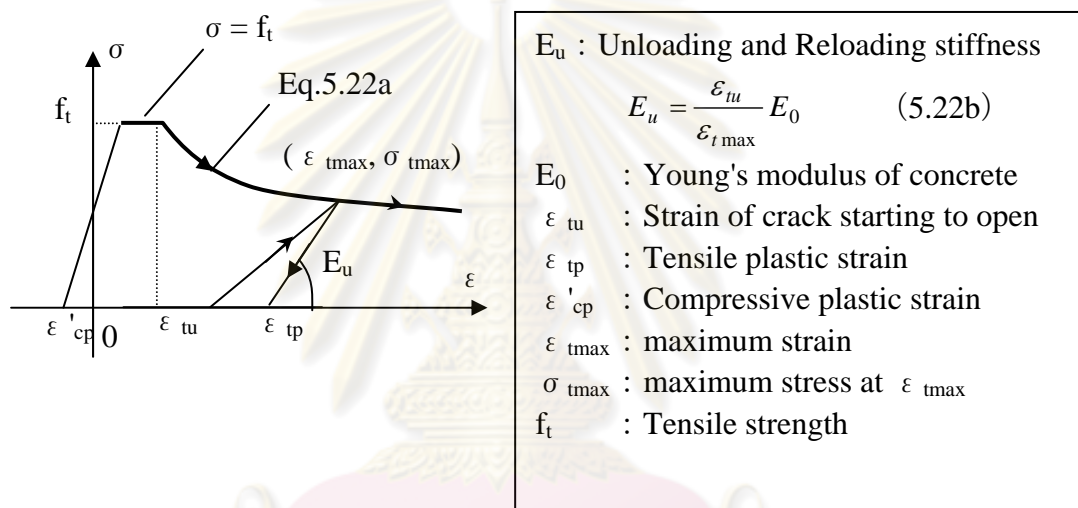
Figure 5.11 Tension stiffening model (Withit, 2004)

(3) Tension Softening Model for Cracked Concrete Element

On inspecting the stress-elongation diagram of deformation controlled uni-axial tensile test of concrete, a few features can be distinguished: the stress increase linearly with deformation up to about 60% of the maximum attainable stress; then deformation increases more than proportionally with respect to the stress; the stress reaches the maximum, for example, the tensile strength; and finally, a steep fall in stress occurs with increasing deformation until a certain deformation is reached where the two parts of the specimen are separated. This behavior means that after the tensile strength is reached, a large deformation can occur where stress transfer is still possible. Tension test of concrete had been conducted. The function, which is a product of an

algebraic and exponential term, was used for fitting of the test result. Figure 5.12 shows the outline of the model.

$$\frac{\sigma}{f_t} = \left\{ 1 + \left(c_1 \frac{\varepsilon}{\varepsilon_0} \right)^3 \right\} \exp\left(-c_2 \frac{\varepsilon}{\varepsilon_o} \right) - \frac{\varepsilon}{\varepsilon_o} \left(1 + c_1^3 \right) \exp\left(-c_2 \right) \qquad \ldots.(5.23)$$

Where $c_1 : 3$, $c_2 : 6.93$ as normal concrete
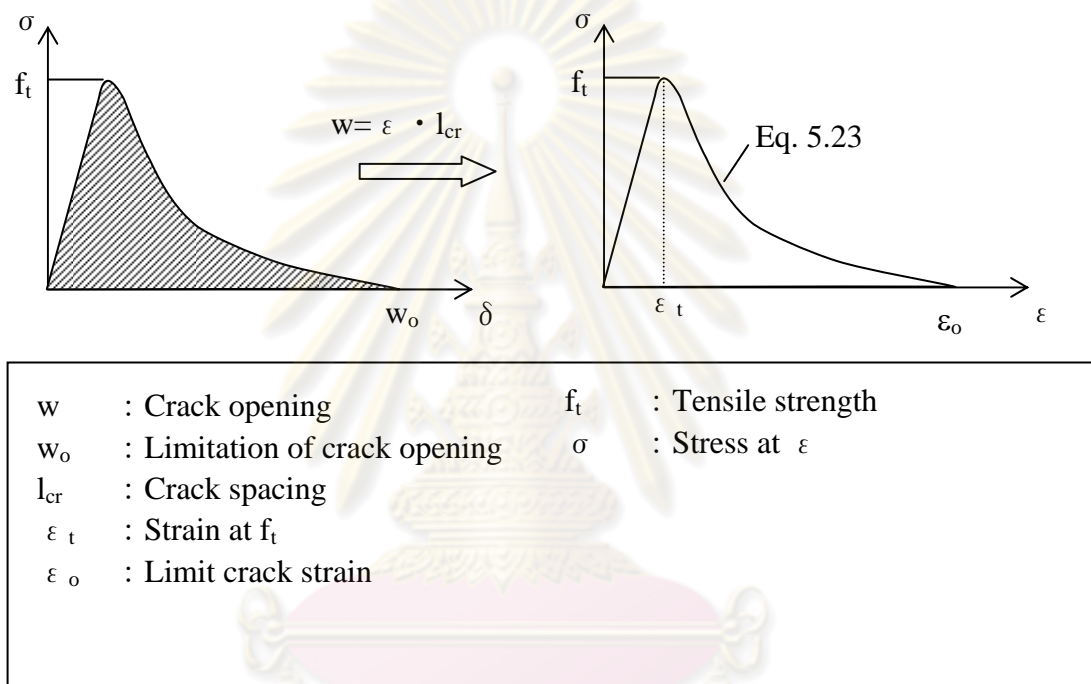
Figure 5.12 Tension softening model (Withit, 2004)

(4) Compression Model for Cracked Element

The directions of principle strains in the concrete deviated somewhat from the directions of principle stresses in concrete. However, it remains a reasonable simplification to assume that the principle strain axes and the principle stress axes for the concrete coincide. The principle compressive stress in the concrete (σ) was found to be a function not only of the principle compressive strain (ε) but also of the co-existing principle tensile strain (ε_t). Thus, cracked concrete subjected to high tensile strains in direction normal to the compression is softer and weaker than concrete in a

standard cylinder test. The relationship is shown below. The Vacchio & Collins's model is shown in Figure 5.13.

$$\varepsilon \leqq \varepsilon_p$$

$$\sigma = f_c' \left[2\left(\frac{\varepsilon}{\varepsilon_0}\right) - \left(\frac{\varepsilon}{\varepsilon_0}\right)^2 \right] \quad \text{------ (Eq.5.24)}$$

$$\varepsilon_p < \varepsilon \leqq 2\varepsilon_0$$

$$\sigma = \frac{f_c'}{\beta} \left[1 - \left(\frac{\varepsilon - \varepsilon_p}{2\varepsilon_0 - \varepsilon_p}\right)^2 \right] \quad \text{----- (Eq.5.25)}$$

$$\varepsilon_p = \varepsilon_0 / \beta$$

$$\beta = 0.85 + 0.27 \cdot \varepsilon_t / \varepsilon$$

ε_t : Tensile strain in orthogonal to crack

ε_0 : Strain at compressive strength($2f_c/E_c$)

ε : Compressive strain
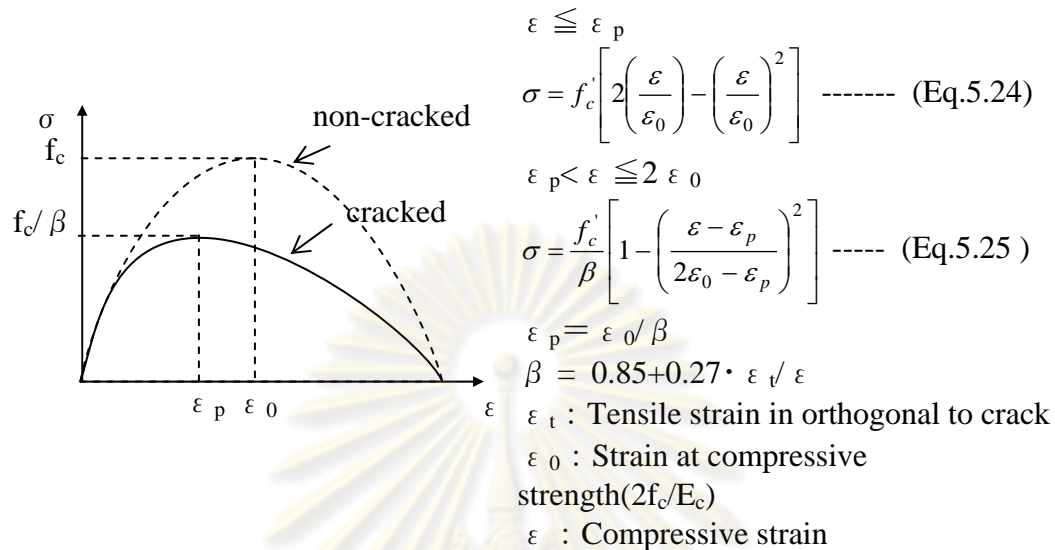
Figure 5.13 Vecchio & Collins's Model (Withit, 2004)

(5) Shear Transfer Model (Averaged Shear Stiffness Model)

The shear transfer behaviors have been reported as complicated phenomena and complex formulations have been utilized. It is possible to explain the complicated phenomena in appearance by some assumptions, which are verified by the experimental procedures. In the simplified equation, it was found that the shear and compressive stresses transfer across a crack are governed not by the magnitude of crack displacements but by the direction or the ratio of the crack displacements. The compressive strength is the only parameter to influence this relationship. And, the effect of concrete strength is implicitly taken into account if the shear stress is normalized by the shear capacity. The relationship between the normalized shear stress and the direction of crack displacement is shown in Figure 5.14

In the case of second and third cracks occurred, the active crack model that considers the change of concrete element by focusing on the crack width was adopted. However, since this method cannot apply when 2 non-interesting cracks occur at the same time, the concrete model for the crack in parallel direction and averaged shear stiffness model had to be applied.

τ_{st} : Shear transferred stress at crack

γ_{cr} : Shear strain by relative shear displacement along to crack

ε_t : Strain in orthogonal direction to crack plane

f_{st} : Shear transferred strength at crack

$$f_{st} = 3.8 f_c'^{1/3} \ \text{(MPa)}$$

f_c' : 1d compressive strength of concrete

G_{cr} : Shear stiffness at crack plane

G_c : Shear stiffness of concrete between cracks

G_t : Average shear stiffness of cracked concrete

γ : Average shear strain in cracked concrete (γ_{cr})

τ : Average shear stress in cracked concrete

$$\tau_{st} = f_{st} \frac{\beta^2}{1+\beta^2} \qquad \text{(Eq. 5.26)}$$

$$\text{Where } \beta = \gamma_{cr} / \varepsilon_t$$

$$G_{cr} = \tau_{st} / \gamma_{cr}$$
$$G_t = 1/\left(1/G_{cr} + 1/G_c\right)$$
$$\tau = G_t \cdot \gamma$$

Figure 5.14   Shear transfer model (Averaged shear stiffness model)
(Withit, 2004)

In terms of average shear stiffness model, stress calculated in the sub crack coordinate system was converted to the active crack coordinate system. And, from this shear stress and shear strain in the active crack coordinate system, the stiffness of the whole region could be obtained. The compression-tension model was the same as already stated above. Moreover, in the case of several sub cracked occurred, this method was adopted to only the sub crack that had a largest strain component in the perpendicular direction to dominant crack (direction 2) after strains within the global coordinate system were converted to each sub crack coordinate system.

(6) Model for Steel Reinforcement

The constitutive model for reinforcing bar in concrete was modelled based both on the properties of bare bars and on the effect of the bond to concrete, at this

point, tri-linear model presented by Maekawa et al (1991) expressing the strain hardening was adopted as shown in Figure 5.15.
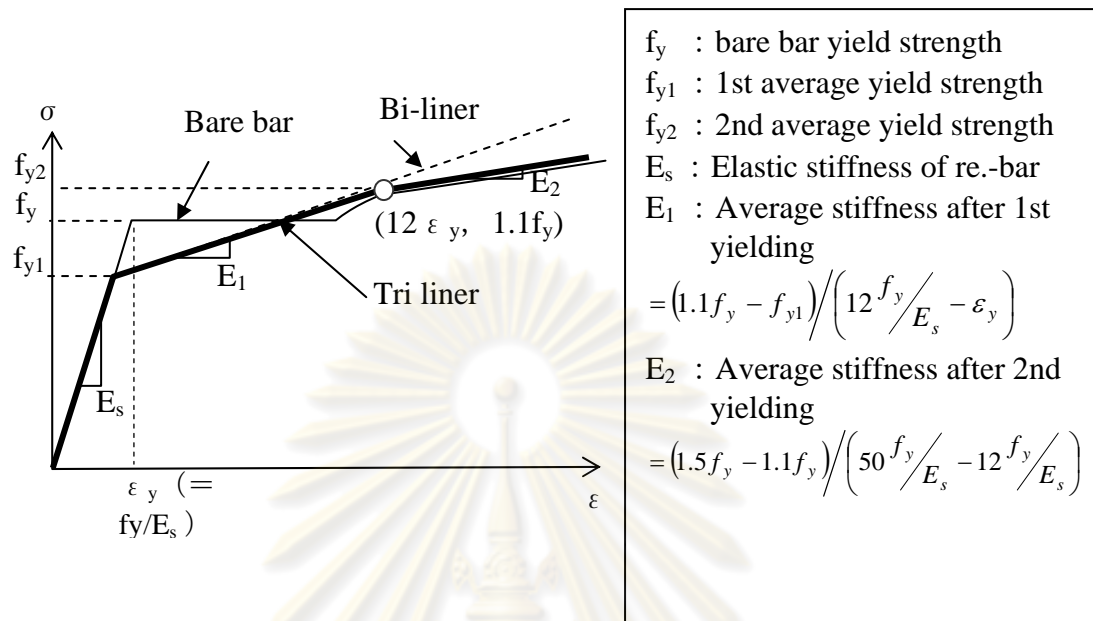
Figure 5.15 Tri-linear reinforcement bar model (Withit, 2004)

5.6 Tension Softening Model for Existing flaw/Cracks in Concrete Element
5.6.1 Concept and Development of Tension Softening Model

The development of the concrete softening model has been raised from the fracture mechanics theory as indicating in the section 5.3.1. After post cracking state, the softening descending will be occurred, the area under the softening curve are the fracture energy G_f for discrete crack model, and fracture energy density g_f for smear crack model (Figure 5.16) (Kwak, 1991).

The fracture energy, G_f is amount of energy required to crack in one unit of area of a continuous crack, and this value is considered as a material property. The definition of the fracture energy is as in the section 5.3.1.

$$G_F = \int_0^{w_o} \sigma(w)dw \qquad \qquad \text{.....(5.27)}$$

Where w is crack opening displacement at the process zone as explain in FCM theory in the above section.
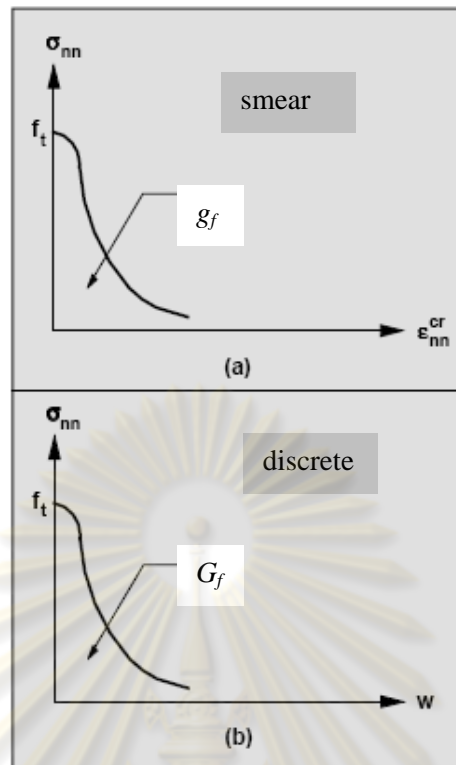
Figure 5.16 Strain softening of concrete a) Smear crack, b) Discrete crack
(Kwak, 1991)

As explaining in the section 5.3.1, for crack band theory, the fracture energy, G_f can be smeared over element band width and called as fracture energy density, g_f and can be calculated by the below equation.

$$g_f = \int_0^{\varepsilon_0} \sigma(\varepsilon)d\varepsilon \qquad \text{.....(5.28)}$$

In the smeared crack concept, w can be represented by a crack strain which acts over a certain width within the finite element called the crack band width h. If crack is perpendicular to the element side, the value h will equal to that element size, l_r. Since w is the accumulated crack strain within element, this is represented by the following relation, Eq. (5.29).

$$w = \int_0^{l_r} \varepsilon dl \qquad \text{.....(5.29)}$$

Assuming that the microcracks are uniformly distributed over the element, the total crack opening within element can be written as

$$w = \varepsilon l_r \qquad \qquad \text{.....(5.30)}$$

Where ε is total strain ($\varepsilon = \varepsilon_u + \varepsilon_c$)

And the fracture energy density, g_f can be written also as

$$g_f = \int_0^{\varepsilon_0} \sigma(\varepsilon)d\varepsilon = \frac{G_f}{l_r} \qquad \qquad \text{.....(5.31)}$$
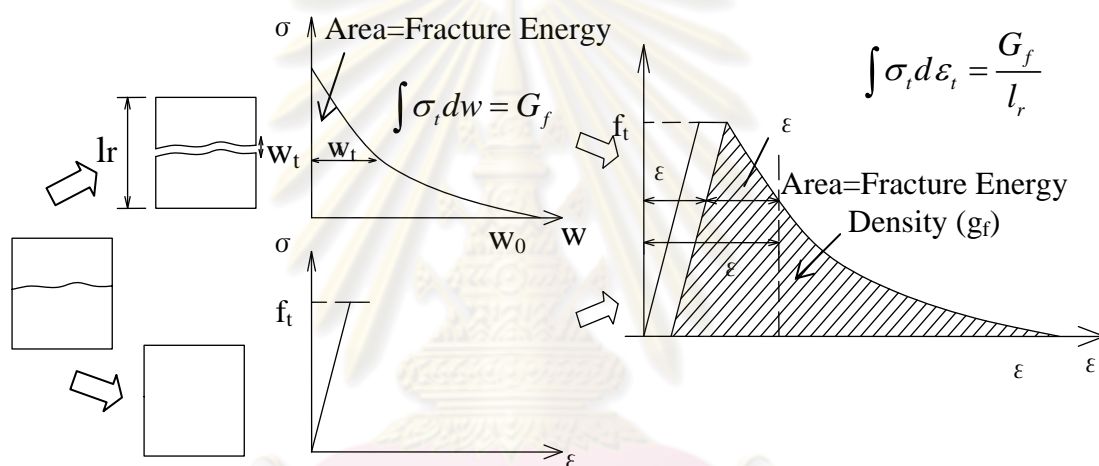
Figure 5.17 Softening behavior FEM of concrete (Maekawa, et al, 2003)

Observing of Eq. 5.31, the crack characteristic depends on the selection of the element size, the element type, the element shape, the integration scheme and the problem type to be solved. Many research have been investigated the accuracy of the FEM result when the element size is varied.

Bazant and Oh has proposed CBM, and assumed softening curve as linear function (Figure 5.18) (Kwak, 1991). The two basic assumptions of the model are that the band width of the fracture zone, h is about to three times of the maximum aggregate size and that the concrete strains are uniform within the band width. For FEM, h is the element size, l_r. The limit crack strain, ε_o is related to limit crack opening, w_o through element size l_r. As explaining in the above, the fracture energy and limit crack opening are material parameters and $w_o = \alpha G_f/l_r$. The α is constant

coefficient, and alters among investigators. Bazant and Oh (1983) has given $\alpha=2$, therefore limit cracking strain can be written as:

$$\varepsilon_0 = \frac{w_o}{l_r} = \frac{2G_f}{f_t l_r} = \frac{2g_f}{f_t} \qquad \qquad .....(5.32)$$
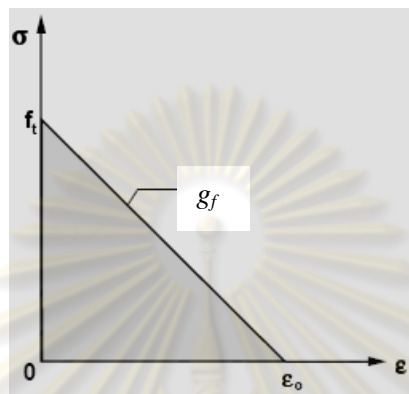
Figure 5.18 Softening model by Bazant and Oh, 1983 (Kwak, 1991)

Other popular softening branch for the tensile strain softening behavior of concrete is as Hillerborge, et al (1976) (Kwak, 1996), a bilinear descending function (Figure 5.19). The limit crack opening is $w_o=\alpha G_f/l_r$, with $\alpha=18/5$, similar to Eq. 3.52, limit cracking strain can be written as:

$$\varepsilon_0 = \frac{18G_f}{5 f_t l_r} \qquad \qquad .....(5.33)$$
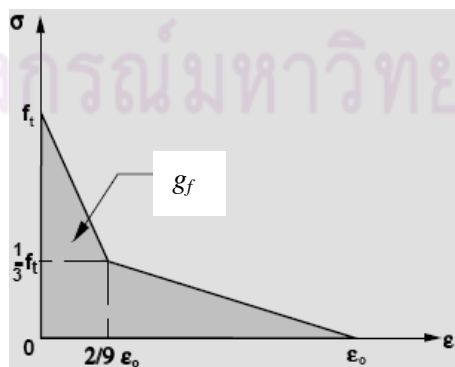
Figure 5.19 Bilinear softening model by Hillerborg 1976

Maekawa et al, 2003 proposed strain softening curve in the power function as Eq. (5.34). The coefficient c varies with element size as following formula.

$$\sigma = f_t \left(\frac{\varepsilon_{tu}}{\varepsilon_c} \right)^c \qquad \qquad .....(5.34)$$

From the experimental investigation, the value c is related to element size, l_r, as below:

l_r (mm)	c
70	0.6
140	0.9
170	1.6
230	2.5
500	5.5
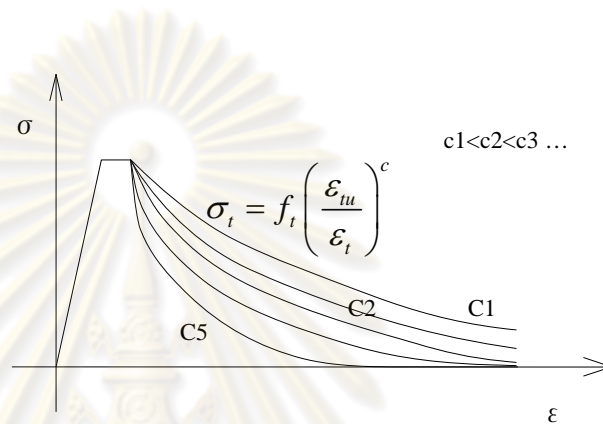
Figure 5.20 Softening model by Maekawa et al (2003)

Hordjik (1991) proposed the softening model in exponential function as Eq. (5.35) (Cervenka, 2001). This model is also using in the original CAMUI program (see Eq. (5.23)).

$$\frac{\sigma}{f_t} = \left\{ 1 + \left(c_1 \frac{\varepsilon}{\varepsilon_o} \right)^3 \right\} \exp\left(-c_2 \frac{\varepsilon}{\varepsilon_o} \right) - \frac{\varepsilon}{\varepsilon_o} \left(1 + c_1^3 \right) \exp\left(-c_2 \right) \qquad .....(5.35)$$

The FEM element size is controlled by the limit cracking strain which can be written as (Cervenka, 2001):

$$\varepsilon_0 = \frac{w_0}{l_c} = 5.14 \frac{G_f}{f_t l_c} \qquad \qquad .....(5.36)$$

Where, l_c is the relative length of element size that related to orthogonal crack direction (see Figure 5.21). In Eq. (5.36), it mean that coefficient $\alpha = 5.14$.
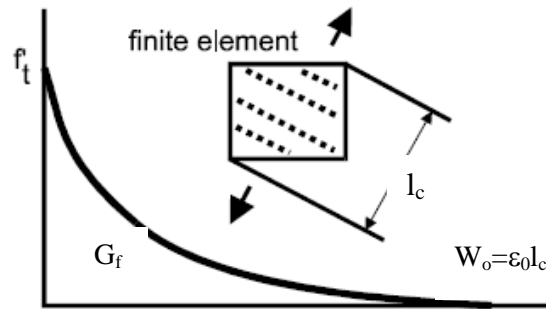
Figure 5.21 Softening model (Cervenka, et al 2001)

5.6.2 Tension Softening Model for Existing Flaw/Crack Element

As explaining in the above, the limit cracking strain is related to the element size. Consequently, the softening law in terms of strains for the smeared model is calculated for each element individually, while the crack-opening law is preserved. To account for crack in the existing concrete structure, exponential softening model and limit crack opening as Hordjik (Eq. (5.35) and 5.36) will be adopted. It is the same concept of crack band theory by Bazant and Oh; however, linear and bilinear model of softening is most appropriated for small element of FEM (Kwak, 1996). In the large scale analysis as concrete bridge structure, it may be inconvenient to mesh small element size. Therefore for large scale analysis and large element size are needed, the model as Maekawa (Eq.(3.54)) and Hordjik (Eq. (3.55)) are appropriated.

In this study, to account for existing crack in concrete member, it is assumed that the existing crack (or flexural crack) width w_i is known from the crack inspection (Crack mapping). From the concept of smear crack, the crack width can be converted to be smear crack strain over defined element as Figure 5.22, and defined as below:

$$\varepsilon_{cri} = \frac{\sum w_i}{L_{ct}} \qquad \text{…..(5.37a)}$$

Where w_i: the total crack width measured at the crack vicinity.

L_{ct}: equals to size of element at the crack vicinity for FEM. This element size can be selected independently due to Maekawa and Hordjik softening models. For Hordjik model, L_{ct} is the same as l_c (relative length of element size that related to orthogonal crack direction)

ε_{cri}: The crack stain that smeared over the element size, L_{ct}. This value is also defined as damage level of element that cracks existed.

Due to elastic recovery, the total strain of crack element normal to L_{ct} is equal to summation of cracking strain (ε_{cri}) and elastic recovering strain (ε_{er}). Assuming that elastic recovery stiffness (E_{er}) is approximately equal to or less than initial elastic strain of concrete (E_c). Therefore, the elastic recovery strain can be approximately defined as Eq.(5.37b) below:

$$\varepsilon_{er} = \frac{f_t}{E_c}\left\{1+\left(c_1\frac{\varepsilon_{cri}}{\varepsilon_o}\right)^3\right\}\exp\left(-c_2\frac{\varepsilon_{cri}}{\varepsilon_o}\right) - \frac{\varepsilon_{cri}}{\varepsilon_o}\left(1+c_1^3\right)\exp\left(-c_2\right) \quad.....(5.37b)$$

And the total strain of crack element, ε_{tci} can be calculate by below question

$$\varepsilon_{tci} = \varepsilon_{cri} + \varepsilon_{er} \quad.....(5.37c)$$

The remaining tensile strength capacity of the damaged element, than can be calculated by substituting ε_{tci} back to Eq. (3.35).

$$\frac{\sigma_{tci}}{f_t} = \left\{1+\left(c_1\frac{\varepsilon_{tci}}{\varepsilon_o}\right)^3\right\}\exp\left(-c_2\frac{\varepsilon_{tci}}{\varepsilon_o}\right) - \frac{\varepsilon_{tci}}{\varepsilon_o}\left(1+c_1^3\right)\exp\left(-c_2\right) \quad.....(5.38)$$

σ_{tci} is remaining tensile strength of the concrete for damage element (Figure 5.22). It is mean that the vicinity of the existing crack, the capacity of the concrete in tension will be reduced proportional to the crack width which is implied as ε_{cri}. It is seen that if ε_{tci} reaches limit cracking strain ε_o, the tensile strength of damaged element will be vanished.

Existing crack

L_{ct}

Flaw/Crack smeared to damaged element (COD element)
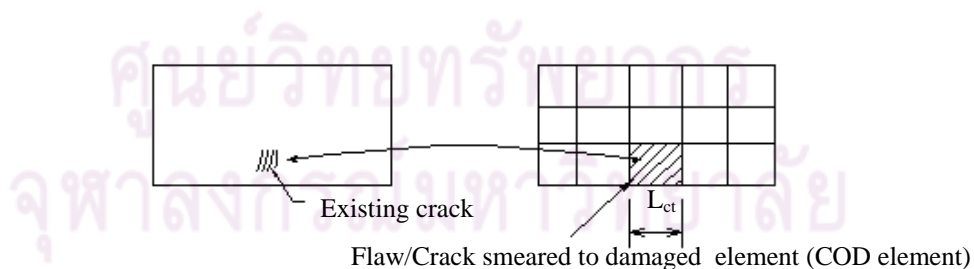
Figure 5.22 Concept of smeared existing crack

The way to apply Eq. (5.38) to the NLFEM, it is needed to define the remaining material stiffness of the damaged element. In the concept of the mechanics of the material, the model of material stiffness can be either or combined of damaged model, and plastic model (Figure 5.23a and 5.23b).
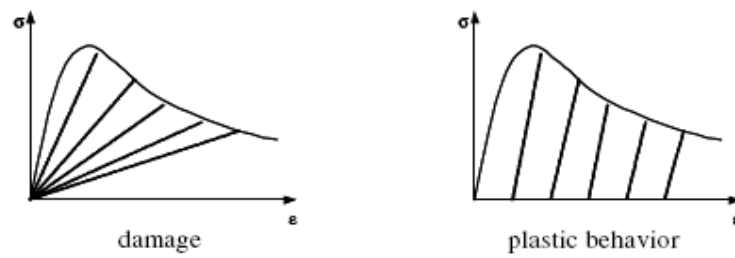
Figure 5.23a Concept of damage and plasticity model

Or combined models

Figure 5.23b Concept combination model (Tao, 2005)
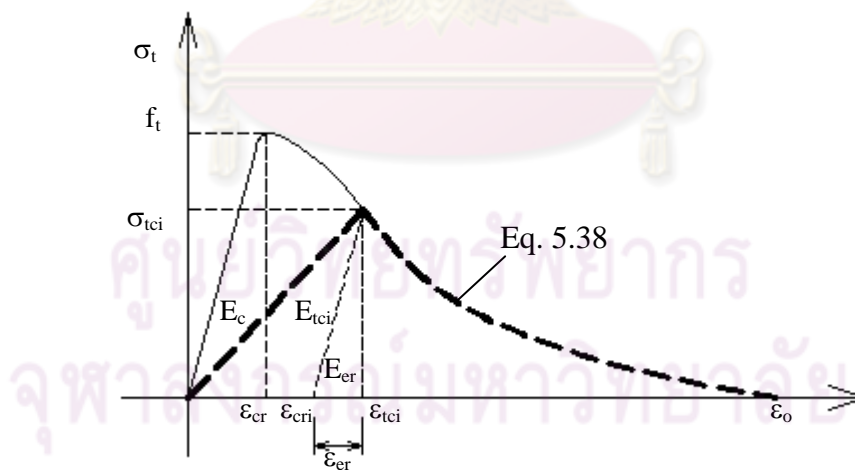
Figure 5.24 Tension softening for damaged concrete element (COD element)

For simplicity, in this study the stiffness of the damaged element has been assumed as the concept of the damaged model. Therefore, the remaining tensile strength of the concrete and the material stiffness of the existing flaw/crack element will be reduced in the direction orthogonal to the existing crack in the same manner as

damage model (Figure 23(a) left). The remaining material stiffness of existing crack element (damaged element), E_{tci} can be simply calculated as below equation and the stress-strain path of constitutive law will be followed as thick dash line in Figure 5.24.

$$E_{tci} = \frac{\sigma_{tci}}{\varepsilon_{tci}} \qquad\qquad .....(5.39)$$

5.7 Tension Stiffening Model for Existing Cracking in RC Element
5.7.1 Tension Stiffening Model, Concept and Development

Once the crack generated in the reinforced concrete structure, the anisotropy becomes significant so that the stress-strain relationship takes on the orthogonal anisotropy in direction normal to cracks. The concrete continues to support a part the tensile force even cracking has been generated. The stiffness of RC is higher than that of the reinforcing bar alone. This effect is called Tension Stiffening for smear RC element. This effect is very significant to behavior of the reinforced concrete structures. As shown in the Figure 5.25, concrete is assumed to behave like elastic material until its tensile strength is reached (the applied load equals to P_{cr}), so the straight line defines initially the stress–strain curve called the state I. In the post-cracking range of decay curve is adopted and called state II (the applied load is between P_{cr} to P_m). After this point, it is called state III or stabilized crack state. The characters of the curve in the state II and III is depended on effect of stiffening model.
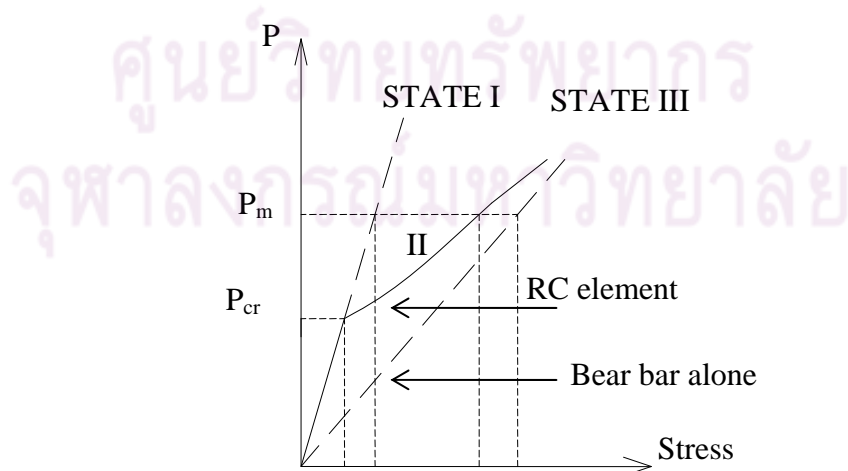
Figure 5. 25 Tension stiffening effect on RC element (Kwak, 2001)

    The tension stiffening effect is accounted by increasing the average stiffness of an element which has relatively large dimension when compared with the size of the cracked region. The tension stiffness is increased by using an average stress-strain relation which includes a descending branch in a tension region. While defining the strain softening branch of the tension stiffening model, several analytical models have been developed, and these models can be classified into three groups: (1) the models defined with the function of the tensile strength of concrete such as the Collins model (1986) (see Figure 5.26 (a)), and the Maekawa model (2003) (see Figure 5.26 (b)); (2) the models based on the assumed bond stress–slip relation as model of Kwak (2001) (see Figure 5.26 (d)); and (3) the models constructed from the average strains of steel such as model of Renata (2008) (see Figure 5.26 (c)).
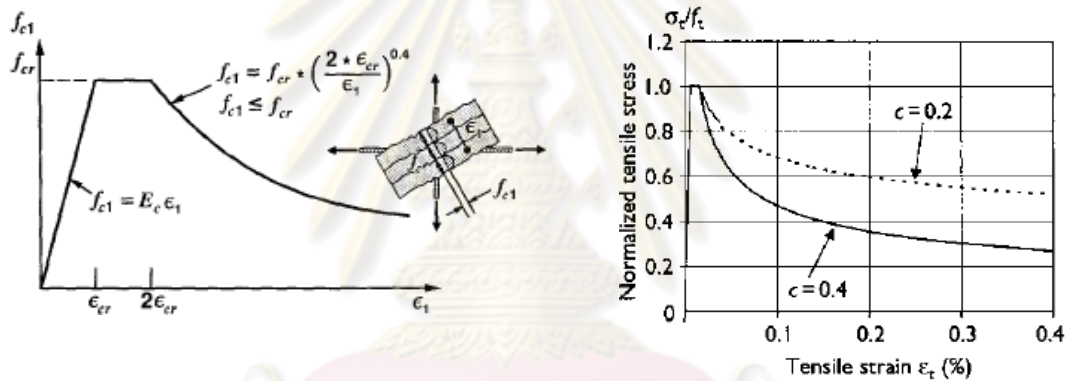
a), Tension stiffening, Collin (1986)   **b)**, Tension stiffening, Maekawa (2003)
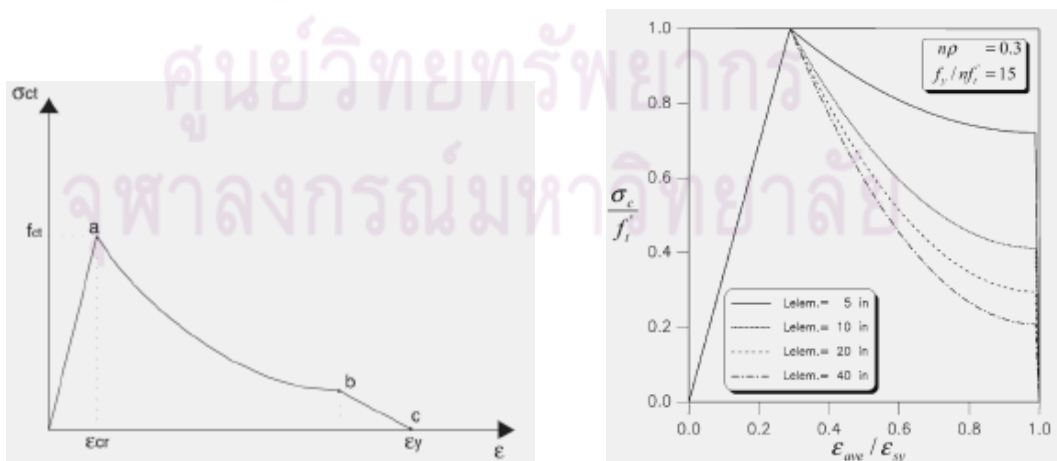
c), Tension stiffening, Renata (2008)   **d)**, Tension stiffening, Kwak (2001)

Figure 5.26 Tension stiffening model from different developers

In Figure 5.26, it can be observed that models of Collin (1986) and Maekawa (2003) have similar characteristic, the tension stiffening effect still remains in a small portion even member strain reached yielding strain of the steel. While other models, tensile stiffening effect will be vanished when member strain reached yielding strain of the steel reinforcement. However, all of the models are acceptable and used world wide. The model of group one is popular used in the Unite State, Canada, and Japan; while model of group two and three are popular used in Australia and Europe.

The model of Maekawa (2003) is element size independent, and not complicated. Therefore, this model will be adopted in this study for existing crack reinforced concrete element.

5.7.2 Tension Stiffening Model for Analysis Existing Flaw/Crack in RC Element

Even though many tension stiffening model have been developed for analysis RC structure; however, the model accounting for existing crack in RC element is not seen yet. In this section, model of Maekawa (2003) will be adopted for existing crack RC element. As similar concept of smear crack approach in concrete, the existing crack will be smeared in the crack vicinity and this vicinity will be defined as damage RC element (RED) (Figure 5.27). The tension stiffening effect and material stiffness of RED element will be reduced corresponding to total crack width at element region. Other elements which are out off crack vicinity will be still defended as normal elements and using normal tension stiffening constitutive law.
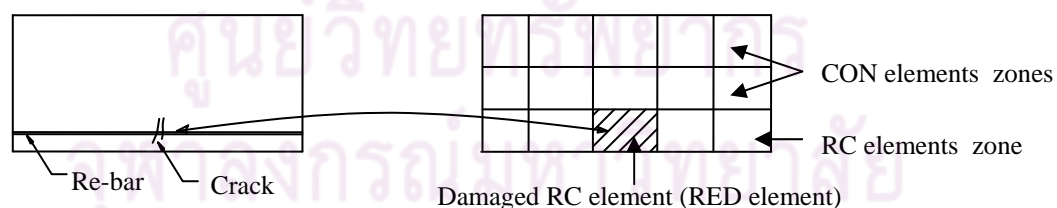
Figure 5.27 Smear of existing crack for RED element

The behavior of crack in RC element is more different and complex than those of crack in concrete element; therefore, the method to account for crack in RC element is also different from concrete element. The detail accounting for existing crack in RC element will be presented in the following section.

Existing crack strain distribution in crack RC element:

When crack occurred in RC elements, the strain of concrete at the crack face will be zero and gradually increases until at x equal to transfer length, l_t. At $x = l_t$, the strain of the concrete will equal to strain of the steel (Figure 5.28). In contrast, the strain of reinforcing steel will be highest at the crack face and gradually decreases until at section x equal to transfer length, then it will be constant and equal to strain of concrete (Kwak, 2001). If the element size in the reinforcement direction has length L, and assumes that the initial crack happened at $L/2$, then the elongation of RC element for $L/2$ will can be calculated as below equation:

$$\Delta L = \int_0^{l_t} (\varepsilon_s(x) - \varepsilon_c(x))dx + \int_{l_t}^{L/2} \varepsilon_{s1}dx \qquad \dots\dots (5.40)$$
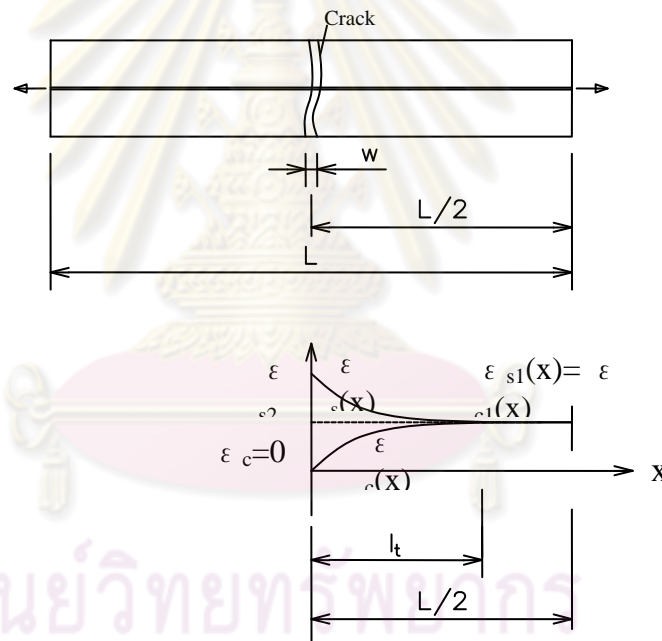
Figure 5.28 Strain distribution of crack in RC

Where,

> L: Element length (FEM length) along reinforcement direction
>
> l_t: Transfer length (The length that occur slip between steel and concrete)
>
> ε_{s2}: Strain of the steel at crack face
>
> ε_{sx}: Strain of the steel at location x
>
> ε_{cx}: Strain of the concrete at location x

ε_{s1}: Strain of the steel at un-slip length at $l_t < x <= L/2$ (the same as concrete)

The slip of element, s will be occurred at along the transfer length and can be calculated as the following equation.

$$s = \int_0^{l_t} (\varepsilon_s(x) - \varepsilon_c(x))dx = \frac{w_{in}}{2} \qquad \text{..... (5.41)}$$

Where,

w_{in}: existing crack width

s: bond slip, and it is also equalled to crack width divided by 2.

The elongation of steel strain at x for $l_t < x <= L/2$ is constant and can be calculated by below formula:

$$\int \varepsilon_{s1}(x)dx = \varepsilon_{s1}(\frac{L}{2} - l_t) \qquad \text{..... (5.42)}$$

Substituting Eq. (5.41) and (5.42) into Eq. (5.40), the elongation of RED element due to existing crack for segment of $L/2$ will be:

$$\Delta L = \frac{w_{in}}{2} + \varepsilon_{s1}(\frac{L}{2} - l_t) \qquad \text{..... (5.43)}$$

The average crack strain (smear crack strain) over RED element due to existing crack can be calculated as

$$\varepsilon_{cri} = \frac{\Delta L}{L/2} = \left(\frac{w_{in}}{2} + \varepsilon_{s1}(\frac{L}{2} - l_t) \right) \bigg/ \left(\frac{L}{2} \right) \qquad \text{..... (5.44)}$$

At this state, there are unknown parameter such as l_t, and ε_{s1}, these values will be defined by the following assumption. For the reinforced concrete member subjected to axial tension load, P; at the sections $x > l_t$, which the strain of steel bar equals to strain of concrete, the equilibrium relationship of applied load can be written as:

$$(A_s E_s + A_c E_c)\varepsilon_{s1} = P \qquad \text{..... (5.45)}$$

And strain of both steel and concrete can be calculated as:

$$\varepsilon_{s1} = \varepsilon_{c1} = \frac{P}{(A_s E_s + A_c E_c)} \qquad \text{..... (5.46)}$$

Where A_s, A_c are area of reinforcing steel and concrete matrix, respectively. E_s, E_c are modulus of elastic of reinforcing steel and concrete, respectively.

For the transfer length in this study will be taken as in the section 5.3.2 in this chapter which proposed by Somayaji (1983), and Kwak (2001).

$$l_t = k_p \frac{N_c}{(\phi_o)} \qquad \text{..... (5.47)}$$

Where N_c is transfer load, and can be calculated as:

$$N_c = A_c E_c \varepsilon_{s1} \qquad \text{..... (5.48)}$$

ϕ_o: Steel perimeter

ρ: Ratio of steel reinforcement and concrete section, As/Ac

k_p: Constant parameter, which used as Kwak (2001) has valued of 3.69 mm^2/kg

The above equations are derived from the crack of the RC bar subjected to uni-axial tension. For extension this concept to the bending member, slab or beam, the effective tension region of the flexural member can be used (CEB-FIP 1990), (Kwak, 2001). The tension region of the flexural member can be implied as axial tension and has the area as Figure 5.29, which given by CEB code. As it has been known that when the stress reached tension strength of the concrete, crack will be formed, it means that the stress of the concrete matrix in RC member will be between or less than the concrete strength, f_t. Therefore, for the maximum case of stress at un-slip region, it can assume that the tension stress is equal to tensile strength of concrete f_t (Kwak, 2001). The tension force acting on this effective area can be implied as $P_T = f_t A_{c,ef} (1 + n p_{ef})$, where P_T is tension force at effective tension area ($A_{c,ef}$), p_{ef} is steel ratio at effective tension area ($p_{ef} = A_s / A_{eff}$), and n is ratio of elastic modulus of steel and concrete. Then transfer length and element strain at un-slip section, ε_{s1} can be calculated as following formulations.

The strain at un-slip zone:

$$\varepsilon_{s1} = \varepsilon_{c1} = \frac{f_t A_{c,ef}(1+n\rho_{ef})}{(A_s E_s + A_{c,ef} E_c)} \qquad \dots \text{(5.49)}$$

And   the enveloped length (slip length):

$$l_t = k_p \frac{A_{c,ef} f_t}{(\phi_o)} \qquad \dots \text{(5.50)}$$

Where, f_t is the tensile strength of the concrete. $A_{c,ef}$ is an effective area of the concrete in tension zone which defined by CEB-FIP (1990) and can be calculated as shown in Figure 5.29.

$$A_{c,ef} = 2.5b(h-d) = 1/4bh \qquad A_{c,ef} = 2.5(c+\varphi/2)$$
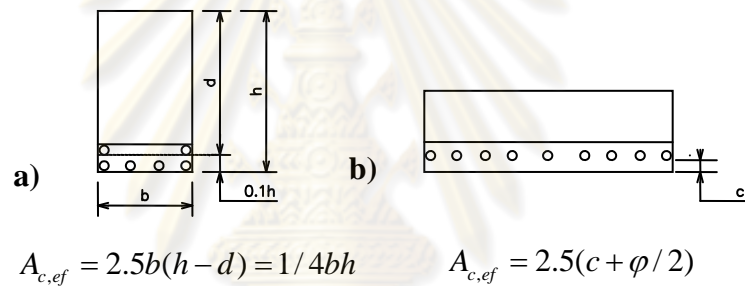
Figure 5.29 Effective area, a) for beam and b) for slab, CIB-FIP1990

Independent of element mesh size for RED element:

As indicated at the above, the affect of crack for the tension stiffening is related to transfer length, l_t and element size, the effect of single existing crack will be in vicinity of about $2l_t$. However, sometime size for RED element needs to be small and much less than two times of transfer length, the crack vicinity $2l_t$ can be also divided more than one RED element as the following reasons (Figure 5.30).

$$L \sim 2l_t$$
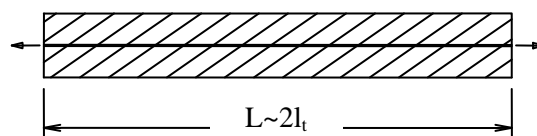
Figure 5.30 Damaged element size equal to $2l_t$

1. As in the above procedure, the width of damaged reinforce concrete element (RED) in orthogonal crack direction will be about $2l_t$ (Figure 5.30).

And the cracking strain within element will be

$$\varepsilon_{cri} = \frac{w_{in}}{2l_t} = \frac{w_{in}}{L} \qquad\qquad ..... (5.51)$$

2. If the length of $2l_t$ is divided into more than one element as shown in Figure 5.31, each elements within dimension of $2l_t$ will be influenced by the same cracking strain, ε_{cri} which is calculated by Eq. (5.51).
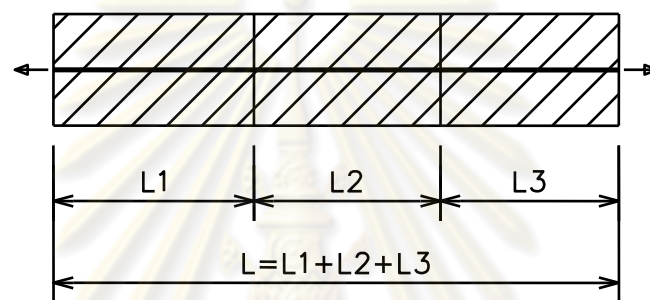
Figure 5.31 Damaged RC vicinity divided more than one element

Therefore, the damaged vicinity due the existing crack can be divided more than one element and each element within the same crack vicinity will has the same the existing crack strain.

Note:

1.) From the equation in the above, it is observed that the appropriated size of RED in the direction of the existing crack should be approximately less than or equal to two time of the envelope length.

2.) If the element size corresponding to the crack is very much larger than two time of the l_t, the result of the existing cracking strain calculated by Eq. (5.44) will be higher than element size equalled to $2l_t$. However this is acceptable, because the analysis results will be still in conservative.

3.) In case of RED element contains of many parallel cracks, the existing cracking strain can be calculated as average cracking strain, $\varepsilon_{cri} = \Sigma w_{cri}/L_{acri}$. Where w_{cri} is the individual crack width, and L_{acri} is the average cracks spacing.

Tension stiffening model for RED element:

In this section the tension stiffening model for RED element will be defined by using existing crack strain derived in the above. For the smeared concept of NLFEM, when RC element is cracking, the tension stiffening effect of that RC element will be reduced, and the material stiffness of corresponding to element will be reduced as well. Therefore, in the same way for the COD element, the tension stiffening effect and its stiffness will be reduced corresponding to existing crack width. The method to reduce the tension stiffening effect for RED element is that the existing crack width can be implied to cracking strain smeared over the RED element (at crack vicinity) by using Eq. (5.44) or (5.51). After that the remaining tension stiffening effect for RED element (σ_{tci}) can be calculated by substituting the total strain of RED which equals to sum of average existing crack strain and elastic recovery strain into the original tension stiffening model of Maekawa, then σ_{tci} can be defined as below:

$$\sigma_{tci} = f_t \left(\frac{\varepsilon_{tu}}{\varepsilon_{tci}} \right)^c \qquad \qquad ….. (5.52)$$

Where, σ_{tci}: Remaining tensile strength of concrete for tension stiffing effect

c: Coefficient of bond property (0.4 for deformed bar, 0.2 for welded bar)

ε_{tu}: Strain of crack starting to open, given in section 5.6

ε_{tci}: Total strain at crack RED element which $\varepsilon_{tci} = \varepsilon_{cri} + \varepsilon_{er}$,

ε_{er}: Elastic recovery strain is defined the same concept for concrete damage element, therefore it can estimate by below equation.

$$\varepsilon_{er} = \frac{f_t}{E_c} \left(\frac{\varepsilon_{tu}}{\varepsilon_{cri}} \right)^c \qquad \qquad ….. (5.53)$$

For simplicity the reaming material stiffness in normal crack direction will be adopted as the concept of damaged model (see Figure 5.23) and can be defined as:

$$E_{tci} = \frac{\sigma_{tci}}{\varepsilon_{tci}} \qquad \qquad ….. (5.54)$$

The full stress-strain path (tension stiffening model) for RED element will be reduced less than original model as thick dot line shown in the Figure 5.32. This will be called tension stiffening model for existing flaw/crack of RED element in this study. However, using this model, some of the assumptions are noted such as the

crack is assumed to have the same width as at the surface though effective tension zone (Through the depth of RED element), the effect of the reinforcement due to existing crack is not considered, because these effects are too small to consider.
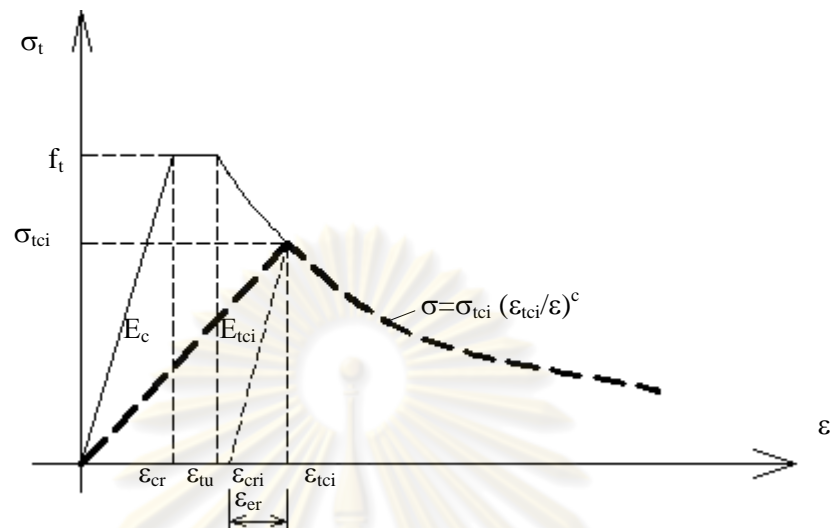
Figure 5.32 Tension stiffening model for exiting flaw/crack of RED element

5.8 Analysis Existing Notch Concrete and RC Beam

This section presents the analysis of concrete and RC notch beams in order to verify the proposed models, softening model for existing flaw/crack in concrete element (COD) and tension stiffening model for existing flaw/crack in reinforced concrete element (RED) which derived in the section 5.6.2 and 5.7.2, respectively. The concrete notch beam which tested by Karihaloo (1995) has been chosen to assume to contain COD element. The reinforced concrete notch beams which tested by Prasad (2002) and Sumarac (2003) have been chosen to verify RED element. The detail of the analysis model and result will be presented in the following section.
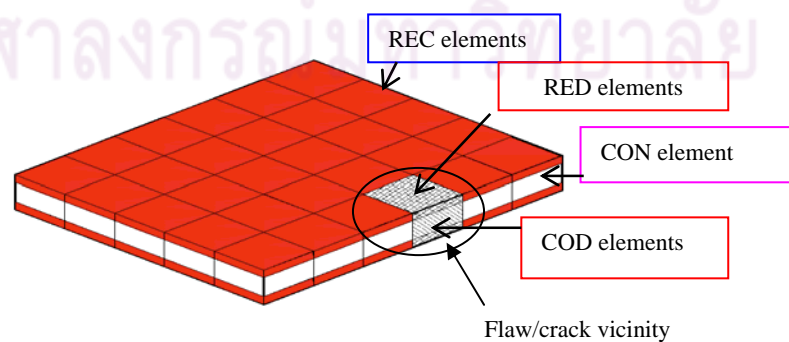
Figure 5.33 Solid elements of existing structure with flaw/crack

The 3D NLFEM, CAMUI program will be used to install the proposed models. For original program, two material element types such as concrete element type (CON), and reinforced concrete element type (REC) are used for analysis RC structure, and concrete structure. To adopt this program for analysis existing flaw/crack in concrete and RC structures, the author added two new material subroutines in the program. The first new material subroutine is for existing crack concrete element namely "COD", which is using constitutive law as tension softening model of COD element which derived in section 5.6.2. The second material subroutine is for existing crack reinforced concrete element namely "RED", which is using constitutive law as tension stiffening model for exiting flaw/crack of RED element which derived in section 5.7.2. The existing damaged RC structures can be now analyzed by this program. The material elements type in damaged RC structures can be modeled by four material types such as concrete element (CON) for normal (undamaged) region of concrete zone, reinforced concrete element (REC) for undamaged region of RC zone, flaw/crack concrete element (COD) for damaged/crack vicinity in concrete, and flaw/crack reinforced concrete element (RED) for damaged/crack vicinity in reinforced concrete zone (see Figure 5.33).

5.8.1 Analysis Existing Notch Concrete Beam

To verify the tension softening model for COD element which derived in section 5.6.2, the concrete notch beam tested by Karihaloo (1995) is chosen to analyze by CAMUI program. General method for analysis the concrete notch beam is that FEM element at the notch position is cut off, and the FE mesh size at near notch vicinity or the process zone are modeled in small element size or the same size of notch. For CBM is modeled element mesh size at the process zone as crack band with element as proposed Bazant and Oh (approximately three time of the maximum aggregate) (Van Mier, 1997). In this study, smear crack model concept is used the element size at the crack zone is about three time of maximum aggregates or higher can be used as explain in section 5.6. However, in this study, element at notch will not be cut off, and it is modeled by COD element (assumed as flaw/crack vicinity), and other zone are modeled by normal concrete element (CON). Both CON and COD are 3D solid elements, 20 nodes, and 8 Gauss points. Three major cases will be analyzed for comparison, case one is full beam without notch (no damaged assumed), case two is notch beam and element at notch position is cut off as conventional method for analysis notch beam, case three is beam with including damage presented

by COD element. The case three is also analyzed for two more cases, case 3.1 is assumed small crack (0.05mm) occurred at notch position by COD element. Case 3.2 is assumed large crack (2.5mm) at COD element to represent notch (this large crack will neglect concrete tensile strength of element at notch position). Case 3.2 also will represent that notch can be modeled by COD element. All of the results are compared to each other, and test result. The detail of analysis and results are presented in the below.

(1) Beam parameters

The dimensions of the beam are 80x200x800mm, total length 900 mm, notch size 60x6 mm, (Figure 5.34). The material parameter are fc'= 268 ksc, Ec= 245,073 ksc. ft'=25.8 ksc, G_F= 0.07 kg/cm.
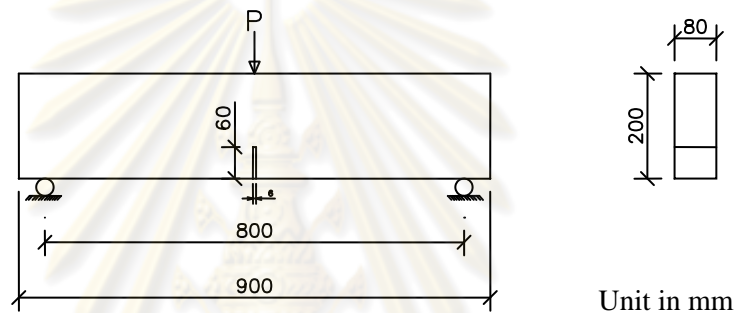
Figure 5.34 Notch beam (Tested by Karihaloo, 1995)

(2) FEM model

a) FE mesh

b) 3D FE mesh, case 1

c) 3D FE mesh, case2

d) 3D FE mesh, case3.1 and case3.2
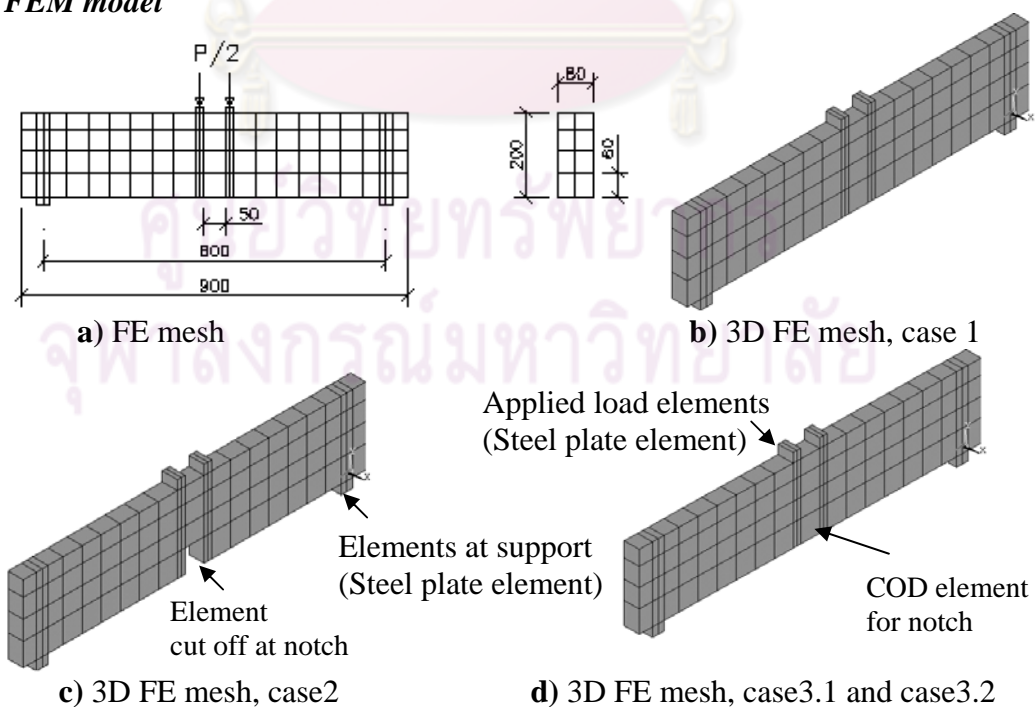
Figure 5.35 FE mesh of notch beam

Case 1: Full beam (No notch)

Case 2: Notch beam and notch element has cutting off

Case 3.1: Notch beam and notch element assumes as COD element

contained small crack (0. 05 mm)

Case 3.2: Notch beam and notch element assumes as COD element

contained large crack (0.25 mm)

3D solid element has been modeled for both CON, and COD elements. Due to symmetry, only half of beam in longitudinal direction has modeled. The steel elements have been added for applied load and supported to prevent local stress concentration. The model geometry is illustrated as below, Figures 5.35. The element size at notch is 5 cm in width and 6 cm in height; this width is appropriated for crack band theory or smear crack element as explaining in the above.

 (3) Analysis and results

All cases have been analyzed using load displacement control method, and the analysis result of each case has been compared to tested result. To compare the results of analysis cases, load and deflection curve at midspan of all analysis results, and tested result of notch beam have been plotted in Figure 5.36. In this figure, fives curves have been plotted to compare. The first curve is thick dash line represented analysis case 1 which is full beam model (no damage), the second curve is thick line represented analysis case 2 (notch beam with cutting element at not position as Figure 5.35 (b)), the third curve is thin dot line represented analysis case 3.1 (COD element occurred small crack of 0.05 mm), the fourth is thin dash line represented analysis case 3.2 (COD element occurred large crack of 0.25 mm for representing notch), and the fifth curve is thin continues line represented test result by Kariholoo (1995).

 Case1 is indicated that when beam has no any flaw, the peak load is up to 900 kg. If existing flaw/crack has occurred, even a small crack the peak load will be reduced significantly as case 3.1. For case 3.2, COD element at notch position is assumed to occurred large crack (0.25 mm), it is seen that the result is very close to test result (thin continues line) and analysis result of case 2 which is cutting element at notch position, results of case 3.2, case 2 and testing are very closed to each other, especially at the beginning of load. This is evident that notch can be presented well by COD element which is implied that the existing flaw/crack in concrete structure can

be represented by COD element. As proposed in this study using this method, the mesh topology is not changed during the flaw/crack presented. The number of FE mesh can be reduced which will be convenient to analyze large scale structure.
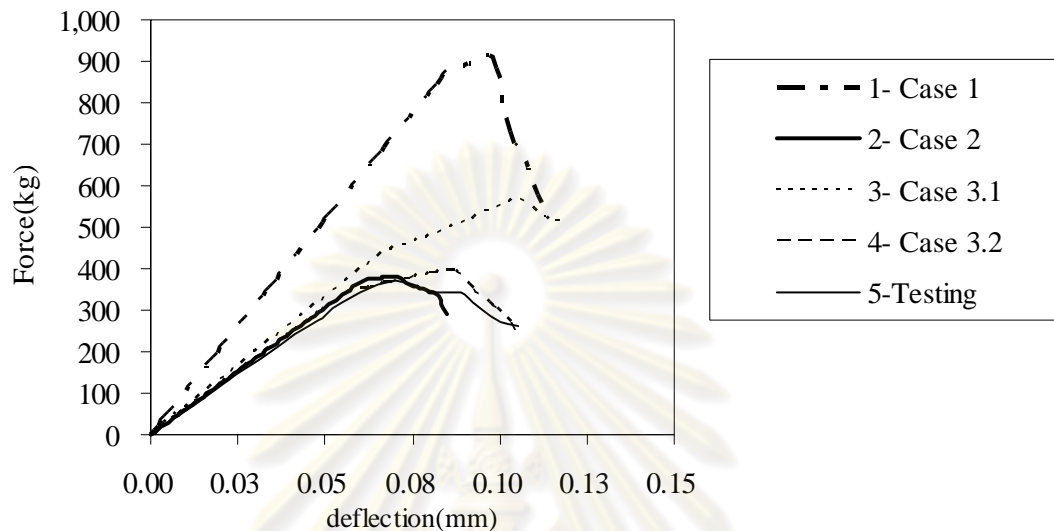
Figure 5.36 Results of load vs deflection curve for analysis cases and testing

Figure 5.37 represented the stress-strain path at element of notch position for case 1 (full beam without damage), case 3.1 (small crack in element at notch position), and case 3.2 (large crack in element at notch position). The case 1 is represented the tress-strain of concrete element without existing damage; the full stress-strain path can be obtained which peak stress is reached tensile strength of concrete. For case 3.1, when small crack occurred in concrete element (COD element) some tensile strength is still remain in COD element. Case 3.2 represented that when crack width is high up to 0.25 mm, the tensile strength of concrete is mostly vanished, and this case is also can be represented as real notch beam. These curves also show the manner of softening model for non damaged element (case 1), and softening model of damaged element or COD element (case 3.1 and 3.2). The softening behavior of COD element is depended on crack opening displacement as explained in section 5.3.

From this result, it is also implied that the proposed concept by using COD element at crack vicinity could be applied to assess exiting flaw/crack for old damaged concrete structure.
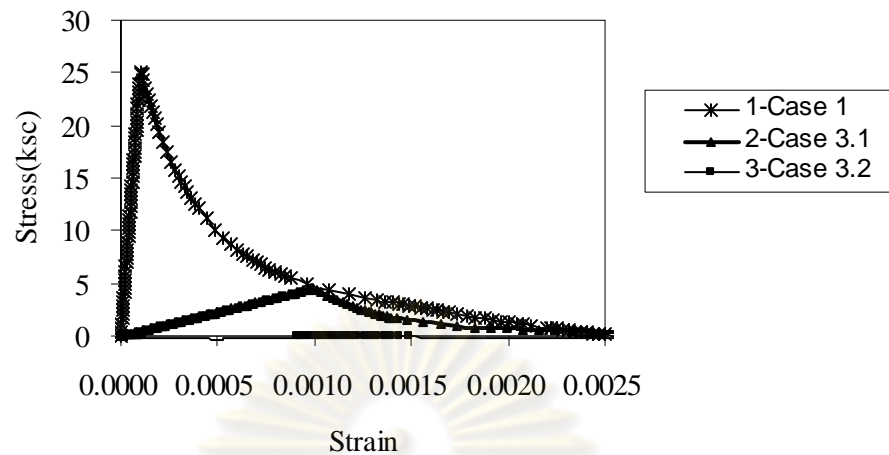
Figure 5.37 Stress strain at notch position for case 1, case 3.1 and case 3.2

5.8.2 Analysis Existing Notch RC Beam

In this section, to verify the tension stiffening model for RED element which is derived in section 5.7.2, two notched reinforced concrete beams which were tested by Prasad (2002) and Sumarac (2003) will be analyzed by 3D NLFEM.

(1.1) Reinforced concrete notch beam tested by Sumarac (2003).
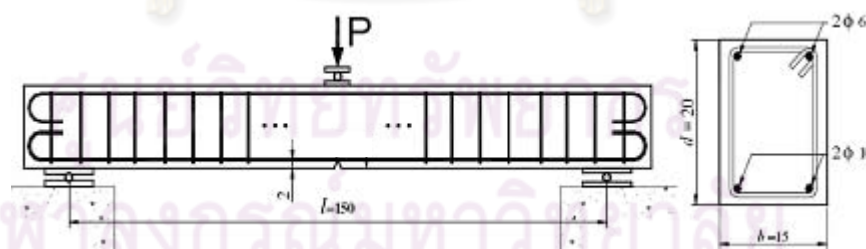
Figure 5.38 Notched reinforced concrete beam by Sumarac (2003)

The simply-supported notched reinforced concrete beam specimen which was tested by Sumarac as shown in Figure 5.38 was chosen. The beam parameters are length of 1.5 m, width of 15 cm and height of 20 cm. The notch is a edged notch located at the bottom of the cross section at the midspan with depth of 2 cm and width (at bottom surface of beam) of 2 cm. The concrete parameters are 330 ksc, 27.7 ksc,

and 272,488.53 ksc for compressive strength, tensile strength, and modulus of elasticity, respectively. The yield strength and modulus of elasticity of the steel reinforcement are 4,300 ksc, and 2,000,000 ksc, respectively.

(1.2) FEM analysis models

The beam will be analyzed in three difference cases. Case 1 is the model of full RC beam (no any damaged), case 2 is model of real notch which notch at the mid-span is represented by neglected element (2x2cm) at notch position, and case 3 is that notch is modeled by RED element (this case is the proposed approach for this study). The analysis results of all cases will be compared to test result of notched reinforced concrete beam tested by Sumarac (2003). As explaining in the above, the flaw/crack in RC is unlike crack in plain concrete structure, the crack in the RC will be influence to tension stiffening effect from the crack face up to enveloped length, l_t. This enveloped length can be calculated by Eq. (5.47). Therefore, RED elements for case 3 will be the elements within the length of *2l_t* at the bottom middle of beam as shows in the Figure 5.41(c), *2l_t* = 29 cm. The initial crack of 0.4 mm is assumed at RED elements for representing affect of notch. The way to select this crack width is done the same way as concrete notch beam that analyzed for different crack width, then select one that result is matched to test result. The effective area of the RC zone is defined by CEB-FIB recommendation (see Figure 5.29). In this example the height of RC zone is 6 cm form bottom face of beam. Due to the depth of the existing notch is 2 cm from concrete bottom face of beam, the RC zone is divided in two layers, layer one is 2 cm from bottom face of beam, and layer two is 4 cm. The RED elements are at the layer one as shows in Figure 5.39. The tension stiffening model of RED element is using Eq. (5.52). The element types for case 3 are consisted of CON, REC, and RED, while other cases are consisted of only CON, REC element types.
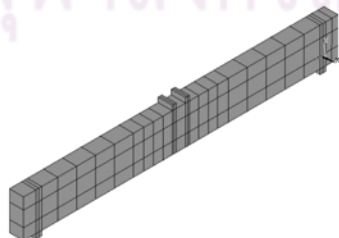
a) 3D FE mesh, case 1   **b)** 3D FE mesh, case 2
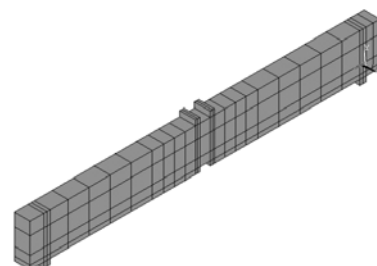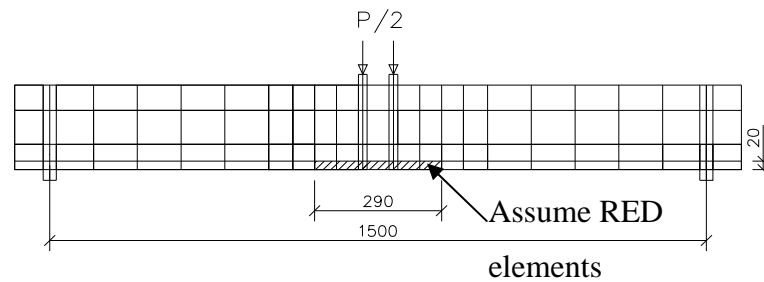
c) FE mesh size, case 3
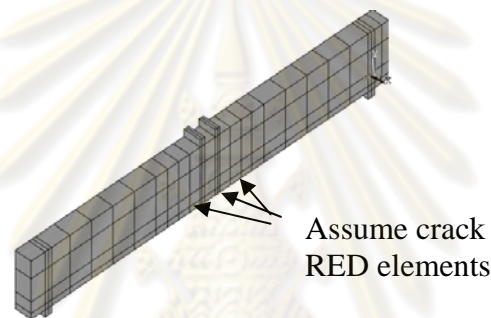
d) 3D FE mesh size, case 3

Figure 5.39 FE mesh of the reinforced concrete beams

(1.3) Analysis and results

Three cases have been analyzed. To compare the analysis results and test result, load deflection curves at the midspan of analysis and test results are plotted in the same figure as shows in the Figure 5.40. The test result is represented by thick line; the analysis result of case 1 (full beam without any damaged) is represented by thick dash line; the result of the case 2 (element at notch position is neglected) is represented by thin dot line; and the result of beam which notch assumed as RED elements, case 3 is represented by thin continues line. It can be seen that the result of case 3 is very closed to the test result; while notch beam which is cutting off element at notch position, case 2 is closed to test result at the only begin of the load, but after the applied load higher than about 2,000 kg, it is lower than test result. This implies that the RC zone could not omitted for representing notch for smear crack NLFEM concept, because the ultimate load is depended on steel ratio and effective depth of

beam. At the beginning and up to about 3,000 kg of the applied load, the results of case 3 (RED element for notch) and test result are not closed to the result of case 1 (full beam without damaged element). This is due to the affect of notch at the bottom of midspan beam for test result and affect of RED element for analysis result case 3. This is evident that the proposed model (case3) can be used for presenting notch or flaw/crack in RC structure. Tension stiffening effect is reduced when flaw/crack existed in RC structure. At the applied load higher than 3,000 kg, the result of case 3 and test are closed to case 1. This is due to that the beam is already in full crack state, tension stiffening effect is vanished.
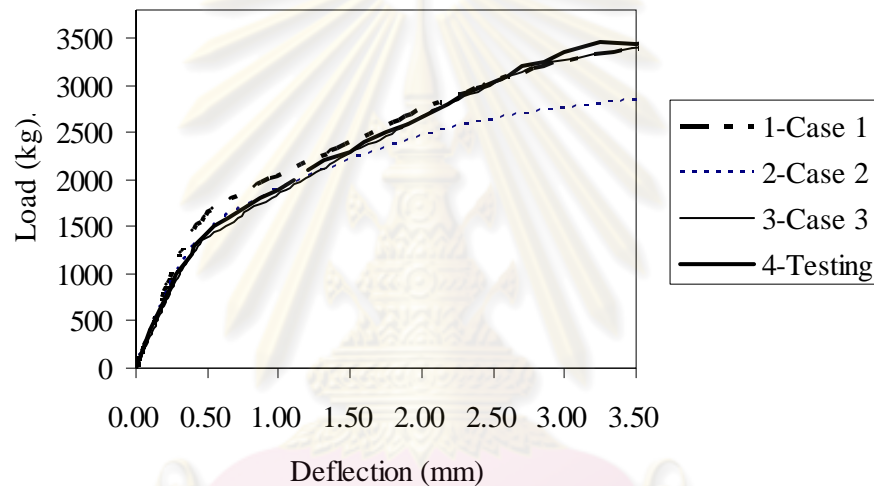
Figure 5.40 Comparison of load-deflection at midspan for analyses and test results

The strain of the element at steel reinforcement level at notch position of analysis results case1, case 2, and 3 are plotted versus applied load as shown in Figure 5.41. The characteristic of the load and strain curves at steel reinforcement level at notch position is also the same manner as load deflection curves. It is seen that the strain at the steel level of results case 2 is higher than that result of case 3 at the same applied load, and the strain result of case 3 is also higher than case 1 at the applied load lower than about 3,000 kg. This is due that element at notch position is neglected for case 2, the effective depth at midspan of the beam is less than full beam. While case 3 is that only tension stiffening effect is reduced, the stiffness of element at the existing crack is also less than beam without any flaw/crack (case 1). The analysis result from the case 3 is also indicated that the tension stiffening effect is very

important especially at the beginning of applied load up to load that induced strain of the steel closing to yield point (this example yield strain is 0.0021). Beyond yield point, the strain results of both cases (case 1 and 3) are closed to each other, as the beam is already in full crack state, and the tension stiffening effect is vanished, strain of element for both cases are reach yielding strain reinforced steel.

For this example, as shown in the Figure 5.40 and 5.41, it is indicated that the tension stiffening effect is one of important factor for NLFEM analysis of existing flaw/cark in RC structure. While normal model for NLFEM are not account for this effect, the full behavior of old RC structure with flaw/crack existed could not be presented closed to actual behavior. Therefore, the proposed model is one method that can analyze for assessment of old reinforced concrete structure with flaw/crack occurred.
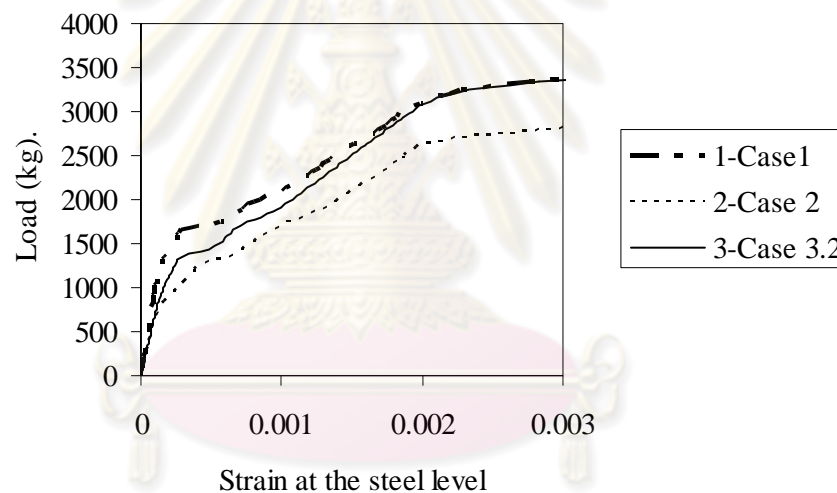
Figure 5.41 Applied load vs element strain at the steel level at notch position

(2.1) Reinforced concrete notch beam tested by Prasad (2002)

Second example is notched reinforced concrete beam which tested by Prasad, et al. (2002) for study RED model. The beam is a simply supported beam with initial notch at midspan as shown in Figure 5.42. The beam parameters are such as length of 150 cm, width of 15 cm and height of 20 cm. The edged notch is located at the bottom of the cross section at the midspan with depth of 60 mm. The concrete parameters are 301 ksc, 41.1 ksc, 292,700 ksc for compressive strength, tensile strength, and modulus of elasticity of the concrete, respectively. The yield strength and modulus of elasticity

of the steel reinforcement are 3,950 ksc, and 2,000,000 ksc, respectively. There are two reinforcement bar with 8 mm in diameter as shown in the Figure 5.42.
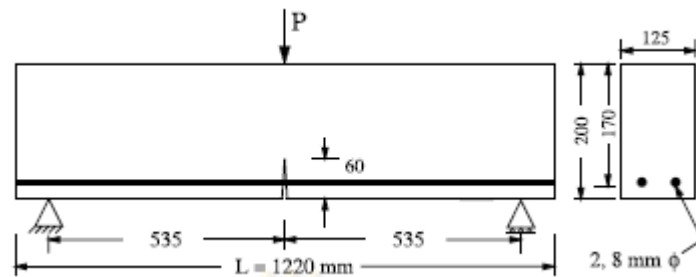
Figure 5.42 Notched reinforced concrete beam by Prasad (2002)

(2.2) FEM analysis models

a) 3D FE mesh, case 1   **b)** 3D FE mesh, case 2

c) FE mesh size, case2
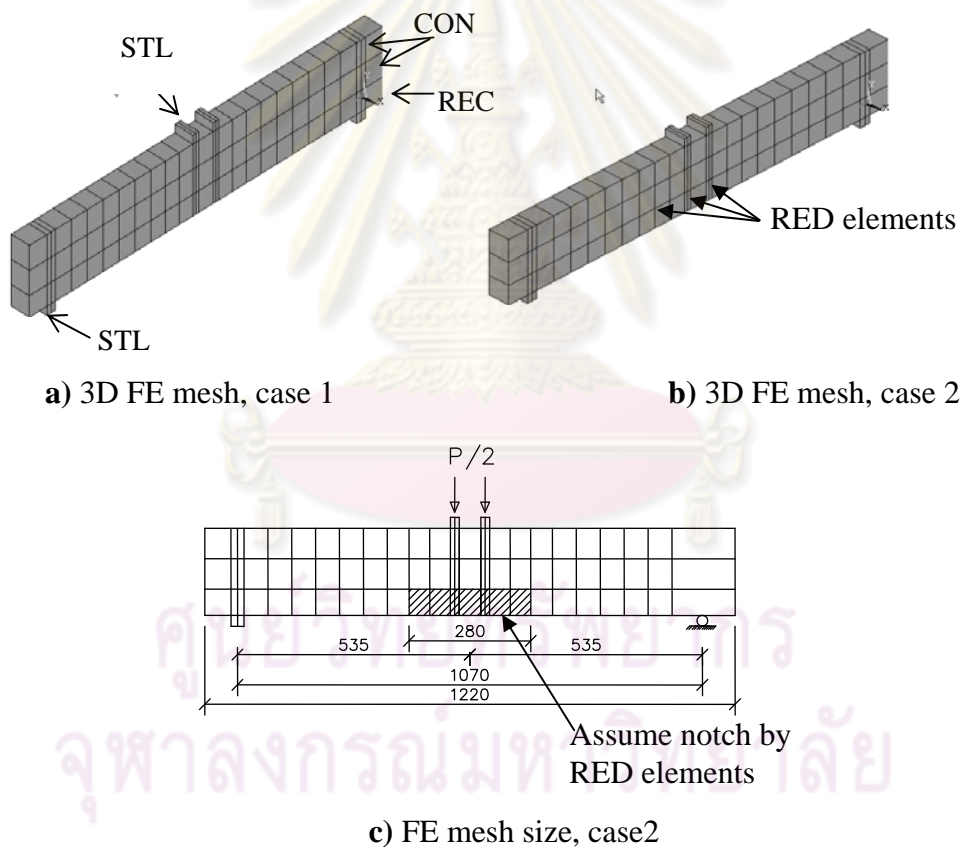
Figure 5.43 FE mesh of the reinforced concrete beams

In this example, the beam has been analyzed for two cases, case 1 is full beam (no any damaged element), case 2 is using RED element at notch position for representing the notch. As explained in the last example, the RED elements are distributed at the vicinity of $2l_t$. In this example the depth of notch is up to 6 cm from

the bottom face of beam, therefore the height of RED element is also the same as notch depth. The l_t is 140 mm as shown in Figure 5.42. For presenting initial flaw, crack width 0.1 mm has been assumed for RED elements. The way to select this crack width is that analyzed for different crack width, then select one that result is close to test result. This example is differ from the last example is that the depth of notch is through the reinforcement bar. Similar to the previous example there are mainly two material element types for case 1, CON element for concrete zone, REC with 6cm of depth for RC zone. There are three material element type for case 2 which RED elements are added at damaged vicinity as shown in Figure 5.43. Additional steel elements are added at supports and applied load position for both cases. Full 3D models of beam are shown in Figure 5.43 below.

(2.3) Analysis and results

The results of the analysis are compared to test result with similar manner as last example. The analysis and test results for load and deflection curves at midspan beam are shows in the Figure 5.44. The test result is represented by thick line, thick grey color line L1 and thick black color line L2 (there are two lines from test, this is due to the upper bound and lower bound of test result data). The analysis result of case 1 (full beam with no any damaged) is represented by thick dash line, and the analysis result of case 2 (RED elements represented initial notch) is represented by thin continue line. The results of analysis in this example are also the same manner as previous example. Analysis result, case 2 is fall in to test results (curve, L1 and L2), while analysis result case 1 is higher than test results. This is due to that there is the initial notch for tested beam, and tension stiffening effect for RED elements is reduced. At the applied load higher than 3,000 kg, the analysis results of case 1 and case 2 is closed to each other, this is as explain in the above example, the concrete beam is in full crack state. This example is also evident that crack in RC structure can be presented by reduction of the tension stiffening effect. Therefore the proposed RED element can be presented for exiting flaw/crack in RC structure.

The analysis result of the applied load and element strain at the steel level at the element of the notch position for case 1, and case 2 are shown in Figure 5.45. These analysis results are also similar to load and displacement curve. When the applied load lower than about 2,500 kg, the strain of element at the steel level at notch position for analysis result case 1 is less than analysis result case 2. This is due to the

flaw/crack, the tension stiffening effect is reduced, and beam stiffness is also reduced. After the applied load higher than about 2,500 kg, as it is explain in the above, the beam for both cases are in the full crack state, the strain results are reach yielding strain of the steel (this example yield strain is 0.0020), than strain results from both analysis cases are closed to each other.
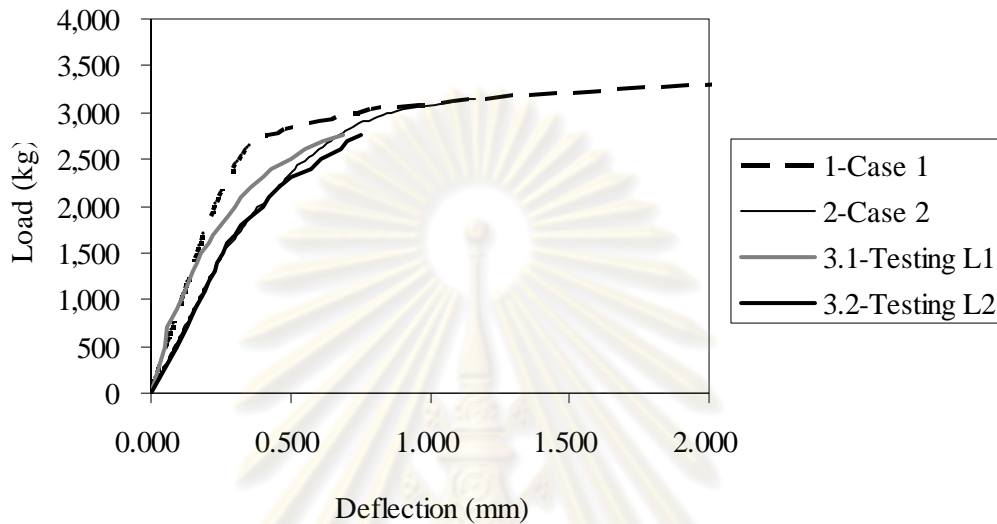
Figure 5.44 Comparison of load-deflection for analyses and testing results
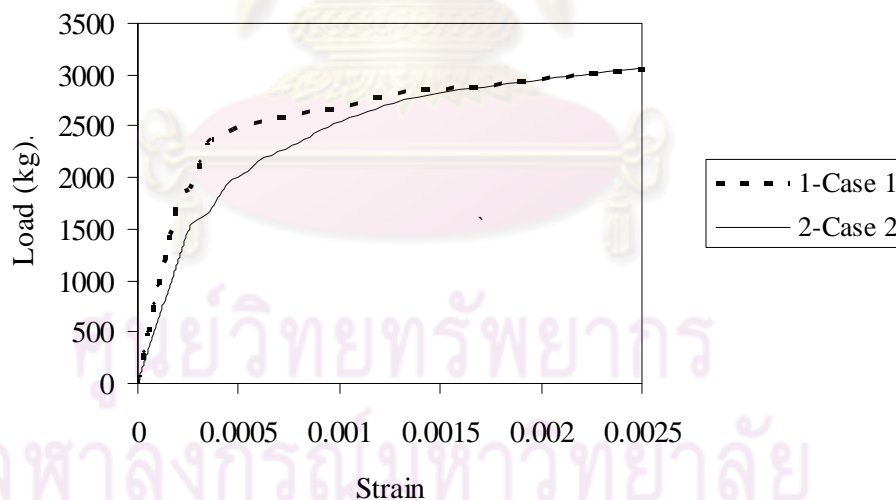
Figure 5.45 Results of load vs element strain at steel level at notch position

From both examples, it is found that the analysis models which are used RED elements for representing initial notch given the deflection results closed to test results of notched RC beams. The RED elements can be also represented the strain at steel reinforcement level, when existing flaw/crack occurred in RC element, the tension stiffening effect in vicinity of this flaw/crack will be reduced leading to strain at the

steel level is higher than no existing flaw/crack existed. It is implied that the steel stress at flaw/crack element will be higher than no flaw/crack element.

The analysis results from three examples in this section it could be evident that the proposed model in this study could be one method that can use for analysis to assess old concrete and RC structures with existed flaw/crack. In the next chapter, this models will be applied for analysis assessment full concrete slab bridges.

5.9 Summary

In this chapter, the properties and mechanics behavior of concrete are summarized. The general properties, mechanics behavior and NLFEM of concrete and RC structure are presented. The model for tension softening and tension stiffening for analysis exist flaw/crack at tension region in concrete and reinforced structure are also derived. The example of notched concrete and RC beams using proposed models in this study are also presented which notch is assumed as existing crack (small flexural crack).

Concrete is very high capacity in compression but very low in tension. In the conventional concrete design methods, the tension strength of concrete is neglected in both concrete and RC structure. However at the recent decades the effect of concrete in tension has been studied, and found that it is very important to structure behavior and NLFEM. Especially when crack occurred in RC structure, concrete will still further to carry some tension load. To account for tension strength behavior in the concrete structure, Fictitious crack model (FCM) by Hillerberg, and Crack Band Model (CBM) by Bazant can be used which known as tension softening model. CBM or smear crack concept is popular used for NLFEM analysis concrete and RC structure, especially for analysis large scale of concrete structure. For crack in the RC structure, the most important is envelopment length for first single crack, and crack spacing for multi crack. The tension stiffening affect plays important factor for crack in RC structure. Many models for NLFEM have been developed in previous researches; however, most of these models are not account for the existing flaw/crack in analysis concrete and RC structure. In this study, the softening and tension stiffening models for COD element and RED element, respectively are proposed for analysis existing flaw/crack in concrete and RC structures. These material subroutines are added in the NLFEM, CAMUI Program.

Three examples for verification the proposed models are analyzed. One example of notched concrete beam has been analyzed for checking softening of COD element, and two examples of notched reinforced concrete beams have been analyzed for checking tension stiffening models of RED element. Many cases are analyzed to compare the results and test result. From the analysis results of these examples using the proposed models (the softening and tension stiffening models for existing flaw/crack) for analysis flaw/crack concrete and RC beams, the results are well closed to the test results. The peak load of the concrete structure is strongly effect by flaw/crack; while RC structure is mainly effect by existing flaw/crack at beginning of applied load up to full crack state. From the analysis results of these examples, it is evident that the proposed models can be used to assess old concrete and RC structures with flaw/crack existed. Therefore, these models will be applied to analyzed full scale of concrete slab bridges in next chapter.

CHAPTER VI

ASSESSMENT EXISTING CONCRETE BRIDGE

6.1 General

The assessment of the existing bridge structures is still difficult to the bridge engineers at the present time, because many data and information are needed to complete this works, i.e. actual truck loading, actual bridge conditions, accuracy of the modelling for structural analysis etc. Figure 6.1 shows the procedure for evaluation of existing bridge structures. In this figure, the first and third steps are very difficult steps, because the actual truck load data is mostly not available, and general model for analysis of the bridge structure is still difficult to account actual bridge conditions (damaged condition, composite of secondary structures etc.). Especially, the aged concrete bridges are the most difficult than other type of bridges, because existing flaw/crack generally existed in old concrete structure. Therefore, this chapter is extended from last chapter that the damaged element represented existing flaw/crack will be applied to analyze diagnosis old concrete bridge structure.

Several old existing concrete slab bridges with span length 7 m to 10 m, in Thailand will be taken as cases study in this chapter. As explaining in chapter 3, in Thailand, the legal limit trucks loads have been increased in recent years; whereas, bridges are not changed, and some are deteriorated. Moreover in the actual situation there are many trucks that loaded higher than legal limited truck as shown in monitored data in chapter 4. Therefore, the precise approach to evaluate the capacity of the existing bridges is very vital to bridge engineers. In this section, the 3D NLFEM will be used for analysis diagnosis these concrete slab bridges. The bridge condition as step two in the Figure 6.1 has also conducted by visual inspection and testing. Bridges information have been collected from bridges site such as crack mapping and site dimension measurement (this works have been collected by author), concrete material testing and load test (these works have done by the inspection company). The flaw/crack in concrete and RC vicinity will be included in the analysis model by COD and RED elements, respectively. Because damaged and cracks are mostly occurred at the tension region or bottom surface of main slab, therefore the

COD and RED elements will be used at flaw/crack vicinity in this region. The detail and analysis procedure of the bridge will be presented in the following section.
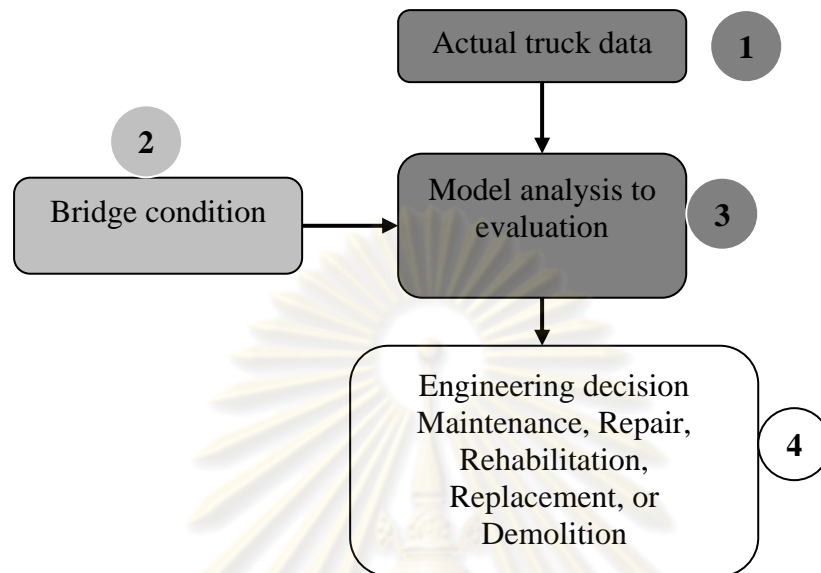
Figure 6.1 Procedure for the completed bridge assessment and evaluation

6.2 Bridge Structures in Thailand

There are many types of the bridge constructed in Thailand. According to the construction material, bridge can be classified into concrete bridge, steel bridge and wooden bridge. The concrete bridge is the most popular constructed in over the country which arranged from small to long span bridges, for the steel bridge is mostly using along the rail ways, while the wooden bridge is mostly constructed at the rural area. According to the superstructure, bridge can be classified into slab bridge, plank girder, multi-beam, box beam, I-girder, T-girder, and combination types (see Figure 6.2). In which the slab bridge is most popular used, i.e. bridge data along highway No. 14 (at the southern part of Thailand), the amount of concrete slab bridge type is up to 64.3 % of the total bridges; Highway No. 5(at the Northeast part of Thailand), the amount of concrete slab bridge is 53% of the total bridges (see report of Department of Highways, Thailand, 2008). In the same report, most of the bridges constructed more than 20 years are higher than 50% of all total bridges. All of these bridges have been design by AASHTO specification, and the allowable stress design method and HS20-44 design truck were used.

a) Slab bridge **b)** Box Girder Bridge **c)** Plank Girder Bridge

d) Multi-Girder Bridge **e)** I-Girder Bridge **f)** T-Girder Bridge
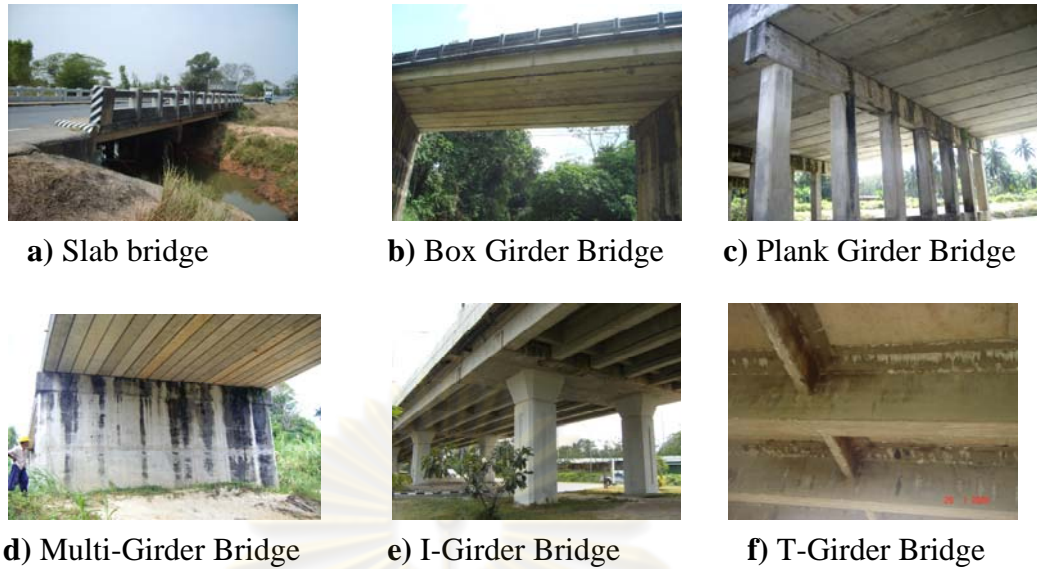
Figure 6.2 Picture of bridge for different type

In this study, only concrete slab bridge has been chosen to be case study. Due to the slab bridge type is most critical types. The slab bridge type is mostly used for short span length which ranges from 5 m to 15 m. There are two different barrier types popularly constructed for slab bridge that are railing barrier and solid barrier types. The height of both barrier types is about 80 cm to 90 cm. The main structure is solid concrete slab which the thickness is varying between 35 cm to 55 cm depending on the span length. The main reinforcement is arranged parallel to the traffic direction at the bottom layer, other reinforcements are used as shrinkage and temperature change purposed. The secondary structures of slab bridge type are such as walkway and barrier at the both sides of the bridge. Some solid barrier type doesn't have additional walk way (see Figure 6.3).

a) Slab bridge railing barrier **b)** Slab bridge railing barrier
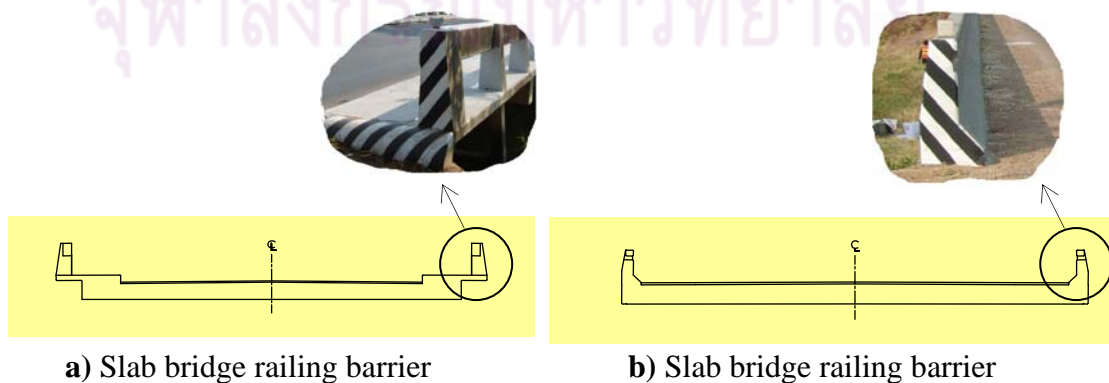
Figure 6.3 Concrete slab bridge section

6.3 Method for Evaluation of Existing Bridge.

   The conventional method for evaluation capacity of the exiting bridge is using AASHTO Manual for bridge evaluation (1994), AASHTO Guide for Strength Evaluation of Existing Bridge (1989). These conventional method is based on the rating factor RF, when RF >1, the bridge is within safety limits, whereas when RF < 1, additional evaluation and analysis is required and precautionary strengthening should be preformed (Chen 2007).

   There are two levels for rating bridge using this manual namely inventory level and operating level. The Inventory level is for as the design level, and the operating level is used for over weight permits check. There are also two methods that can be used for checking bridge member that are Allowable Stress (AS) method, and Load Factor (LF) method. The Eq. (6.1) is representing for RF formula, and only some factors in the formula are changed when applies for different rating level and method.

$$RF = \left(\frac{C - \gamma_d D}{\gamma_L L (1+I)} \right) \qquad \text{.....(6.1)}$$

Where, RF: Rating factor

  C: The capacity of the member/nominal strength

  D: The dead load effect on the member

  L: The live load effect on the member

  I: The impact factor to be used with the live load

  γ_d: Factor for dead load

  γ_L: Factor for live load

   For the AS rating method, the factors γ_d, ϕ and γ_L are equal to one. The capacity of member, *C* is according to the allowable stress design. For the *LF* method, γ_d is equal to 1.3, γ_L is depend on rating level, 1.3 for operating level. The capacity of the member can be calculated as $C = \phi R_n$, where R_n is the nominal strength of the material, and ϕ is the strength reduction factor and this value should also consideration the effect of deterioration from inspection, for example loss of concrete or steel section area, loss of the composite, or consideration from deterioration factor

that given from inspection. Normally, the conventional method of AASHTO for strength evaluation of the existing bridge is mostly lower than actual bridge strength, the NLFEM is the most reliable method comparing to conventional method of AASHTO, and Linear FEM (Huria, 1994).

6.4 Concrete Bridge Inspection and Testing in This Study

Two concrete slab bridge at the Highway No. 5 at Northeast part of Thailand (namely bridge CB7 and CB6), and one slab bridge at Highway No. 14 at Southern part of Thailand (namely CB4S) have been chosen for analysis using NLFEM in this study. The bridge CB7 and CB4S are railing barrier types with total length 8 m and 7 m, respectively. While the bridge CB6 is the solid barrier type. These bridges are involved in part of the project of Bridge Investigation and Testing for Load Carrying Capacity of Road Research Development Division (Department of Highways, Thailand, 2008). Therefore many information and testing have been conducted under this project.

The conditions of the bridge are collected by detail visual inspection, site material testing, and nondestructive load test. The visual inspection was done by author. Material testing and load test were conducted by the inspection company. The visual inspection works are included such as section measurement, flaw/crack mapping. The testing works are included such as testing of material strength which conducted by Rebound hammer method, coring test, rebar locator, tension test of cutting bar; and nondestructive load test. The results of inspection and test data are presented in the below.

Inspection procedure (by the author):

The inspection works is mainly detail visual inspection and bridge dimension measurement. The bridge measurements are included longitudinal bridge dimension, main slab width, slab thickness, barrier dimension, number of lane, lane and walkway width. The rebar diameter was also measured at the time installation of the steel strain gauges. The honey comb, steel corrosion has been measured and skated on the inspection note. The cracks width and its direction have been mapped.

The crack width is measured by oscilloscope for crack that less than 0.2 mm, and crack card for crack that larger than 0.2 mm (Figure 6.4). The technique to map the crack at the bottom sure face of the bridge is that draw the grid lines in the spacing

about 50 cm on the both longitudinal and transverse direction of the bridge over the crack patterns at bottom slab. The main grid lines are set up at the center longitudinal and transverse directions. After grid line was drawn, the coordinates of each crack line ware recorded at every 25cm corresponding to grid lines. And widths of cracks were also measured at every 25 cm. Most of the cracks that observed in this inspection are occurred at the bottom of the bridge, and only cracks that higher than 0.05 mm has been recorded. The difficulties to measure cracks have been found such that some bridge have no working area, the fine crack (crack which less than 0.1 mm) is difficult to be seen. In this study only the structure crack and crack that occurred at the tension zone has been considered, because the small none structure crack at the other zone may less influence the stiffness of the bridge. The details of crack on each bridge are also presented at the each analysis example in this chapter.
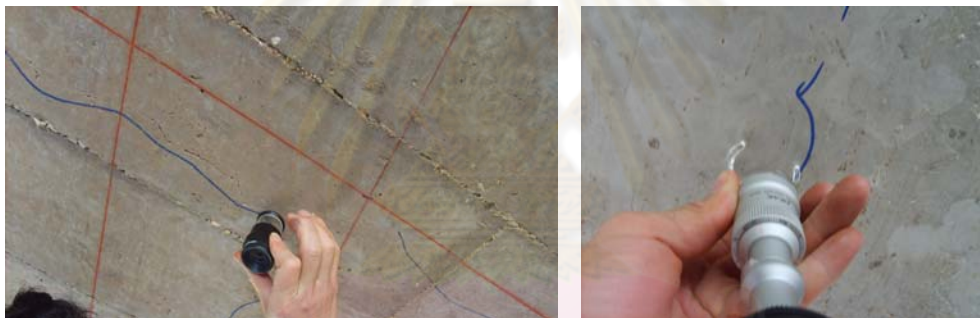
a) Draw grid line 50 cm   **b)** Oscilloscope for crack <0.1
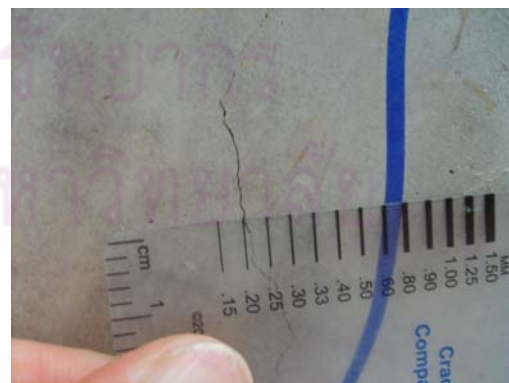
c) Oscilloscope for crack 0.1~0.2 mm   **c)** Crack card for crack >0.2 mm

Figure 6.4 Crack mapping

Figure 6.5 Measured the rebar diameter

Material testing (by Inspection Company):

The material testing conducted for estimate the concrete compressive strength and modulus of elasticity, and steel reinforcement strength. Two methods are used for estimate concrete compressive strength at each bridge, i.e. Rebound hammer, and coring test. These works were done by the inspection company under the project of Road Research and Development Division. Therefore, the more detail of these tests are referred to full report of this project.

Due to that the coring is simi-destructive bridge structure, after coring the concrete structure has to be replaced. Therefore, only few sample that were taken. For more other locations for estimating concrete strength were done by the Rebound Hammer. However, the Rebound Hammer may not accurate as coring test. The results of the tests for concrete compressive strength for each bridge are shown in the Table 6.1. In this study, the coring test results are used for concrete compressive strength of the concrete.

a) Rebound hammer test　　　　　　**c)** Ultrasonic test

d) Concrete coring   **e)** Coring diameter target 2"x4"

Figure 6.6 Material sampling and testing

Table 6.1 Concrete strength from testing

Bridge	Location	Rebound hammer		Core Drilling
		R, average	f^1_c *(ksc)*	f^2_c *(ksc)*
CB6	Slab	57	530	204
CB7	Slab	43	326	195
CB4S	Slab	59	550	305

Steel reinforcement of the existing bridge has been also tested for its tension strength. The steel strength has tested such that the three rebar samples with about 50 cm in length were cut off from the bridge site to test by direct tension test at the laboratory. The results of testing for the steel strength are in the Table 6.2 (a) and (b) below:

Table 6.2a Steel strength from test using for bridge CB6 and CB7

No	Size	Yield strength	Maximum strength	Elongation
		ksc	*ksc*	
1	DB25	3,293	5,027	30%
2	DB25	3,171	4,874	32%
3	DB25	3,243	4,996	24%
Average		3,235	4,965	

Table 6.2b Steel strength from test using for bridge CB4S

No	Size	Yield strength	Maximum strength	Elongation
		ksc	ksc	
1	DB25	4,010	6,380	31%
2	DB25	4,260	6,710	33%
3	DB25	4,070	6,080	29%
Average		4,113	6,390	
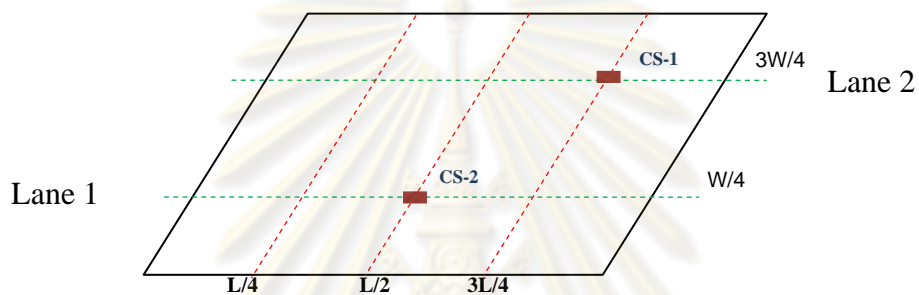
a) Concrete gauges on bridge top surface
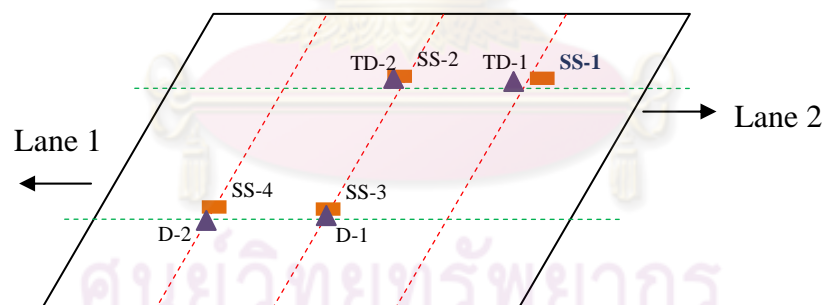
b) Sensor installed on bridge bottom surface

Figure 6.7 Layout of sensors

CS-1, CS-2: Strain gauges on the top surface of concrete bridge slab

SS-1, SS-2, SS-3, SS-4: Stain gauges on the main steel at bottom slab bridge

TD-1, TD-2: LVDT measurement bridge deflection at the bottom slab bridge

D-1, D-2: Dial gauges

Load testing (by Inspection Company):

The static non-destructive load test was conducted for diagnosis bridge behavior. These tests were also done by Inspection Company under project of Road Research and Development Division. The installation of the equipments for load test were conducted such that two embedded concrete stain gauges were installed at about 3 cm in depth on the concrete bridge top surface at position 3L/4 of lane 1 and L/2 of lane 2; steel strain gauges, accelerometers, displacement transducers (LVDT) were installed on the bottom surface of main slab bridge at 3L/4 lane 1, L/4 lane 2, and at L/2 of both lanes as shown in the Figure 6.7. The concrete strain gauges were used for providing concrete strain at the top concrete surface, steel gauges were used for providing strain at the reinforcement, transducer for displacement at corresponding location. All of these sensors were connected to the data acquisition (DAQ, KYOWA PCD 300A) for signal interpretation and save by computer note book. The standard ten wheels truck of Thai truck with GVW about 25 tons was used for tested truck. The static test cases were done by placing the second axle on the line of location L/4, L/2 and 3L/4. The test results for each bridge are provided at the appendix B of this manuscript.

In this study only static test results is needed to verify the proposed model, and the tested truck at the position L/2 is more concentrated. Because the proposed model is mainly focused on flaw/crack at tension region of the bridge structure members.

6.5 Procedure of NLFEM Analysis in This Study

The simplified method for evaluation of the bridge mostly gives the results far from the actual load testing, because many actual bridge conditions could not be included in the conventional method. The NLFEM is the most reliable method if the bridge can be modelled (geometry, material, and boundary) properly (Huria, 1994, Azizinamini et al 1994). However, there are still no any previous research that accounted for existing flaw and crack in old RC structure using NLFEM. As in the conventional method of AASHTO for strength evaluation, the data from bridge inspection mostly interprets to be reduction factor of the material strength. In this section, the existing flaw/crack will be accounted into the 3D model of bridge using NLFEM. However, this study is limits that it will mainly consider the flaw/crack at the tension region of the concrete and RC structure only.

6.5.1 Method Applied the Defects (flaw/crack) to The Model

Definition using in this study:

Some definitions in this study are made such that theoretical crack mean crack calculated from flexural theory representing unseen crack during inspection; visible crack, or observed crack is crack that taken from crack mapping; observed flaw/damage, or visible flaw/crack means that represents of any type of damage from inspection such as crack, corrosion, etc; existing crack means included both visible and theoretical cracks.

*Theoretical Crack***:**

As it is known that crack could not be avoidable in the concrete and RC structure. From the experience of inspection by the author, the fine crack, about 0.1 mm or smaller is difficult to be observed during inspection. However, even fine crack it will be also influential to behavior of concrete structure and NLFEM results as well. Therefore for accounting of unseen crack, the flexural crack due to traffic load will be accounted and given name as theoretical crack for this study. The theoretical crack is estimated as crack at tension region of main slab due to moving truck load. Standard ten wheel truck of Thailand, Figure 3.6 in chapter 3 is assumed as traffic load that will induce the theoretical crack in this study. The truck is assumed moving along the bridge for calculating bending moment at different sections. The equivalent width for slab bridge of AASHTO is used for distribution of loading (See Eq. (6.2) and (6.3)). From the equivalent width, then the total internal bending moment due to all loading (Live load, impact factor of live load, and dead load) for slab bridge in one meter width can be defined.

After theoretical bending moment is defined, the crack width can be calculated using Eq. (5.12) and (5.13), Gergely & Lutz equations in chapter 5. These equations estimate crack width depending on the stress at the reinforcement steel that also depend on the moving truck load induced stress at reinforcement bar. Formula of Gergely & Lutz is selected, because it is not complicated for applying and it is acceptable by the ACI code for many years. Other important parameter for theoretical crack is crack spacing. The crack spacing defines as explaining in the section 5.3.2, the crack spacing is varied between l_t and $2l_t$. l_t is an enveloped length which can be calculated by Eq. (5.20). To apply this theoretical crack to NLFEM for concrete slab bridge in this study, the elements at the section occurred theoretical crack are defined

and RED elements which their constitutive models will be altered corresponding to crack width and crack spacing as explaining in the section 5.7.2.

Equivalence width for slab bridge by AASHTO, (Chen, 2000)

Single lane loaded, interior strip   (SI unit)

$$E_{int} = 250 + 0.42\sqrt{L_1 W_1} \qquad\qquad ....(6.2)$$

Multilanes loaded, interior strip   (SI unit)

$$E_{int} = 2100 + 0.12\sqrt{L_1 W_1} \qquad\qquad ....(6.3)$$

Live load impact factors

$$I = \frac{15.24}{L + 38} < 0.3 \qquad\qquad \text{(L in m)} \qquad ....(6.4)$$

where E is equivalent width (mm); L_1, span length (mm), taken to be the lesser of the actual span or 18,000 mm; and W_1, edge-to-edge width (mm) of bridge, taken to be the lesser of the actual width or 18,000 mm for multilane loading, or 9,000 mm for single lane loading.

*Crack from inspection (crack mapping)***:**

The crack from inspection is also included to nonlinear finite element analysis model of the slab bridge in this study which will be defined as visible crack, or observed crack. The finite element meshes at the crack location can be meshed appropriately corresponding to crack. As explaining in the section 5.7, the crack will be influenced in the vicinity of about $2l_t$ perpendicular to crack direction, therefore at the crack path the most appropriated elements width should be about $2l_t$. However, it can be less or higher than this size as explaining in the section 5.7. Therefore, in this study the selection of element size can be considered according to parameters such as cracks location, envelopment length, l_t, bridge dimension, applied load location, and measurement point. For this study, the element mesh size between 5 and 60 cm is used.

*Steel corrosion***:**

Many studies have indicated that the corrosion will reduce section area of reinforcement bar (Shahrooz , 1994 Cabrera 1996,). For the smeared RC element for NLFEM, the steel ratio, ρ is used; therefore, the steel ratio will be reduced together

with tension stiffening effect at the element that corrosion exited. The reduction of steel ratio can be defined corresponding to the actual remaining steel section measured from site. For the tension stiffening, the corrosion will ruin bond strength between steel bars and concrete; therefore, the corrosion will also reduce the tension stiffening effect.

***Honey comb, spalling, scalling (at tension zone)*:**

If some defects such as honey comb, spalling, scalling are occurred at tension zone of concrete bridge structure, theses defects may reduce the section area of the concrete member. When concrete section is reduced, it means that the stiffness and strength capacity of element will be reduced as well. To account these affects for NLFEM, it may be done by implicit way that these defects may reduce the element stiffness at corresponding defect location. Therefore reduction in softening effect or tension stiffening effect of element at defect vicinity may also represent these affects.

6.5.2 Analysis procedures

This section will summarize the procedure for using NLFEM in this study which can be done carefully by the following steps:

1. Define the material properties data. In this study, these data are taken from test results in section 6.3.2, there are compression strength of the concrete f_c', yield strength of the reinforcement steel, Fy. The tensile or rupture strength of concrete f_r, and young modulus of elasticity E_c can defined from fc' as equation 5.5 and 5.1 of ACI-318.

2. Define element layer or zoning. The effective tension layer is defined as CEB-FIP formulas, as Figure 5.29 in chapter 5. For RC layer at the compression can be determined as two times of distance from concrete surface to reinforcement center.

3. Calculate the rebar perimeter, p for the transfer length.

4. Calculate theoretical crack. This step refers as section 6.4.1.

5. Define location of crack, and defects (scalling, spalling, corrosion) which inspected from site.

6. Defined finite element (FE) mesh size. This section is referred to section 6.4.1. The FE mesh size is considered from many parameters such as: crack and flaw location, crack spacing for muilti-cracks and envelopment length for single crack, location of applied wheel truck loads, measurement position (in case of results need to compare with testing). Meshing model can be done by 3D sigma

(Meshing program) or other meshing software that can mesh 20 nodes solid element. The different properties of elements have to define in different material type and number, i.e. CON elements for no damage concrete zone, REC elements for RC with no damaged RC zone, COD for existing flaw/crack concrete vicinity, and RED for flaw/crack in RC vicinity. The difference crack width or flaw vicinities are also needed to define in different material number.

7. Prepare the input format file for CAMUI program.

8. Run program as FORTRAN language. This step is needed to include the input file and source code file of the program in same directory.

9. View the results. After running completed, the results can be viewed. The results information are deformation of nodes, stress-strain at the Gauss point, and crack pattern.

6.6 Application of NLFEM for Concrete Slab Bridge due to Tested Truck

In this section, three concrete slab bridges will be analyzed and compared the analysis results to static load test results. The detail of each example will be presented hereinafter.

6.6.1 Analysis for bridge No. CB7

(1.1) Bridge information

The CB7 bridge is located at Route No 2054, khm 16+980.0, Xaiyaphome province, Thailand. The bridge is reinforced concrete slab, railing barrier type with total length 8 m, span length (support to support) 7.6 m, slab thickness 0.45m, total slab width 8.8 m, lane width 7m, walk way at both side 1.5 m (see Figure 6.8). The material data are collected from the testing as in the table 6.1 with concrete parameters are: fc'=195 ksc, ft= 28 ksc, Ec= 212,396.10 ksc; Steel parameter are: fy = 3,235 ksc, Es= 2,000,000 ksc, and fy of RB = 2,400 ksc. The main reinforcement at the bottom is parallel to the traffic direction which reinforced by DB 25 mm @ 11cm, and at transverse direction is DB12 mm @14cm. The top reinforcement layer is RB9 mm @ 25 cm in both longitudinal and transverse directions.

(1.2) Bridge condition

From the inspection, this bridge is not in good condition. At the bottom bridge surface, large and continues crack (0.2 to 0.4 mm) can be observed at the bridge midspan started from left to right (see crack mapping and inspection picture in the

appendix C). Some honey comb and corrosion have occurred at the bottom of the bridge. The bridge top surface can not be observed, because it is paved by asphalt concrete.
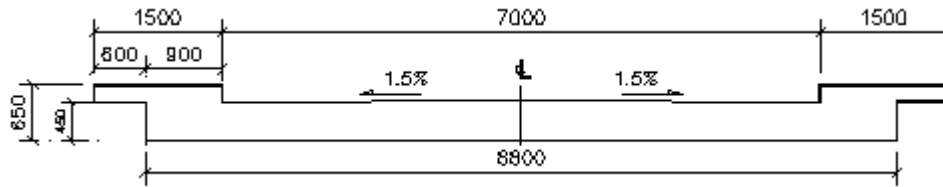
Figure 6.8 Section of bridge CB7

(1.3) Testing set up and truck load

The testing equipments have been installed as explaining on section 6.4 and shown in Figure 6.9 below.

a) Concrete strain gauges on top surface

b) Steel strain gauges and LVDT on bottom surface
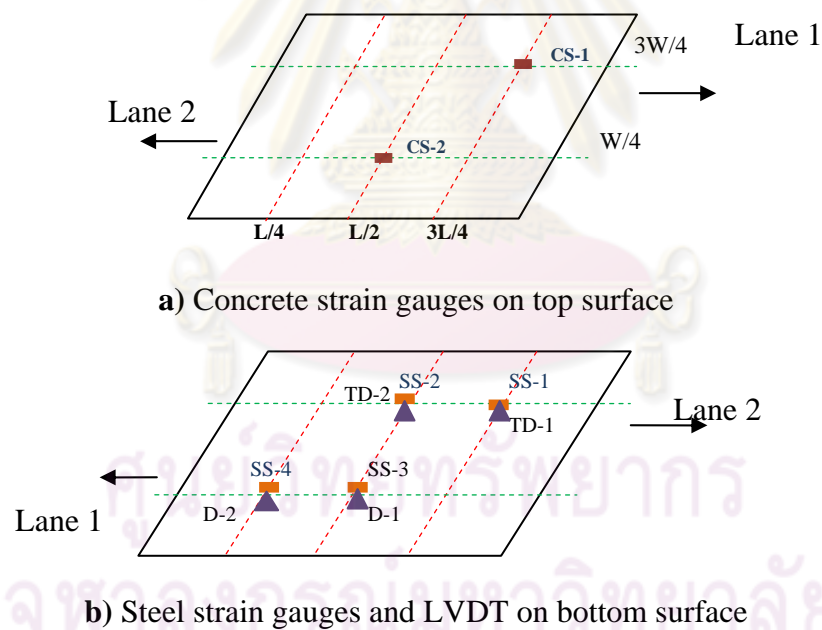
Figure 6.9 Layout of sensor for CB7

CS-1, CS-2: Strain gauges on the top surface of concrete slab bridge

SS-1, SS-2, SS-3, SS-4: Stain gauges on the main steel at bottom slab bridge

TD-1, TD-2: LVDT at the bottom slab bridge

D-1, D-2: Dial gauges

Standard ten wheels truck of Thai truck was used as tested truck, its configuration and distribution load for testing of CB7 are show in the Figure 6.10a. Two cases of position of the tested truck have done by stopping the second axle at the line position L/4, and L/2 at lane one. The load test results for CB7 are shown at the appendix B.
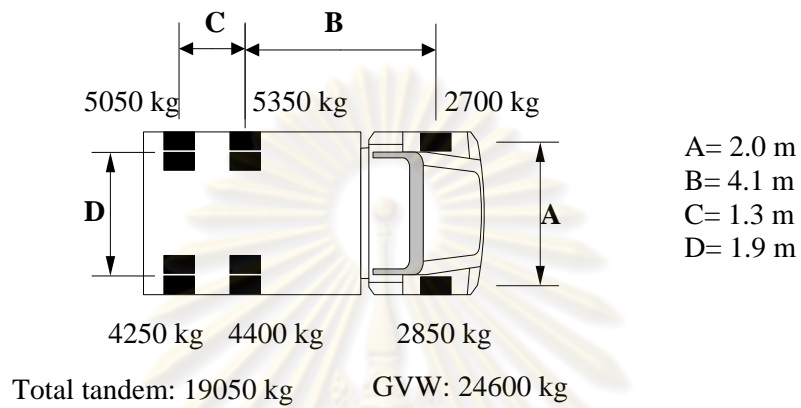
Figure 6.10a Configuration of tested truck
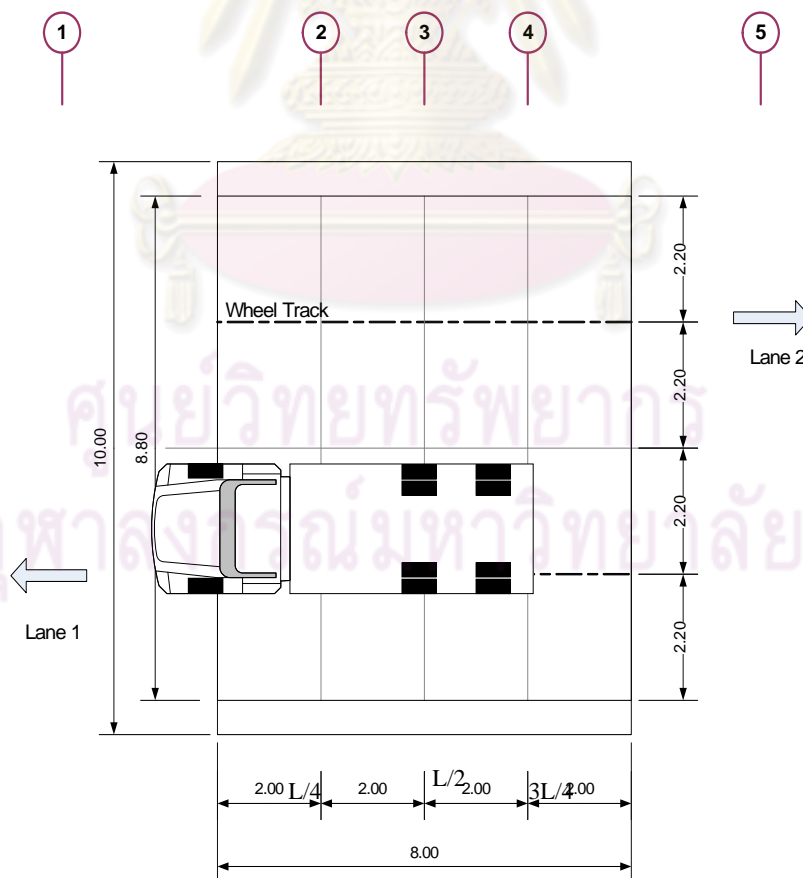
Figure 6.10b Position of truck load testing at L/2, CB7

(1.4) Calculate theoretical crack

The theoretical crack at the bridge has been calculated as indicating in the section 6.2.1. The applied loads for calculating theoretical crack are included dead load of bridge slab and standard ten wheels truck with axle weights of 5 tons, 10 tons and 10 tons for first, second, and third axles, respectively. The axle spacing between these axles are 4.1 m and 1.3 m (see Figure 3.6). This truck type is one of heavy legal limit truck load from Department of Highways and popularly used in Thailand. The distribution of truck load on 1 m width for slab bridge is according to simplified equivalence width slab bridge of AASHTO, Eq. (6.2). To calculate crack at different bridge section, truck load is assumed moving from left to right supports, and cracks width are defined for every section according to crack spacing. Theoretical crack will occurred when bending moment is higher than rupture moment of concrete as explaining in section 5.3.2 and Figure 5.7. The crack widths then can be calculated by Eq. (5.13). The crack spacing is considered from envelopment length, l_t which is calculated by Eq. (5.20).   The cracks width is calculated by this equation are at the bottom concrete surface; however the bridge is already old and serviced for many years. Therefore, it is assumed that these cracks will affect through effective tension zone of RC layer.

The results of theoretical crack for CB7 are summarized below:

Rupture moment of the concrete Mcr = 12,020.68 kg.m

Envelopment length l_t=19.01 cm

Theoretical crack spicing vary between l_t to $2l_t$, and decision crack spacing for calculated crack width is 33 cm. This value is about $1.75l_t$ and it is appropriated FE mesh model as explaining in section (1.5) below.

Theoretical crack widths at different section are for CB7:

From support	w_{cr}
m	mm
1.50	0.090
1.70	0.100
2.12	0.117
2.54	0.131
2.96	0.141
3.38	0.147
3.80	0.149

(1.5) FE mesh model

FE mesh type, boundary condition and applied load step is the basic step for FEM. In this example, full scale bridge is model in 3D solid elements, reinforcements are smeared corresponding to effective zoning. Boundary is assumed as simple supports, and the total applied load is the same as tested truck.

FE mesh:

As explaining in the section 6.4.1 and 6.4.2, the element sizes have to consider from flaw and crack mapping, theoretical crack, location of applied load, and bridge geometry. The FE meshes for this bridge are that the elements size in longitudinal direction (Z direction) at near the middle span are about 33 cm, at near the supported are 50 cm. Because steel plate elements need to provide at applied load elements for preventing local stress effect, the elements at applied load are 5 cm in Z direction. The dimensions of the element in the transverse direction (X direction) are about 30 cm. In the vertical direction (Y direction) from bottom to top surface of bridge is 45 cm, and this vertical direction is divided into three zones (three layers). Firs layer is tension reinforced concrete layer which calculated by CIB-FIP formula and has 13 cm depth from the bridge bottom surface, second layer is CON, and the third is top layer which is compression RC zone with 9 cm in depth. At the tension RC zone, there are REC elements for non damaged vicinity; and RED elements at vicinities that occur theoretical crack, observed flaw/crack, and corrosion. The difficulty for crack vicinity is that the crack depth is not known; therefore all theoretical and visible cracks at bottom surface are assumed through out the thickness of effective tension layer. The bridge curbs at both sites are also included in the model as solid REC elements. The different properties of elements are defined in different material names. The properties of smear REC elements are depended on concrete properties, ratio of the reinforcement in X, and Z direction. The properties of RED are also the same as REC element, but this element type is included crack width in each direction (see in put file format at appendix). The Figure 6.11 shows the complete 3D FEM geometry model.

Reinforcement ratios for CB7 bridge after zoning divided are: at bottom layer at Z direction (main reinforcement parallel to traffic direction), $pz = 0.0340$; at bottom layer X direction (sub reinforcement perpendicular to traffic direction), $px = 0.0061$; at the top layer, both direction Z and X direction, $p = 0.0032$. The envelopment length at

of main reinforcement at the bottom layer is l_t = 19.01 cm, and unit steel perimeter is 0.707 cm/cm.

a) FEM and visible crack at bottom surface

b) Complete 3D FEM for Case 1.2 and 1.3 test truck on L/2

c) Complete 3D FEM for Case 2.2 test truck on L/4
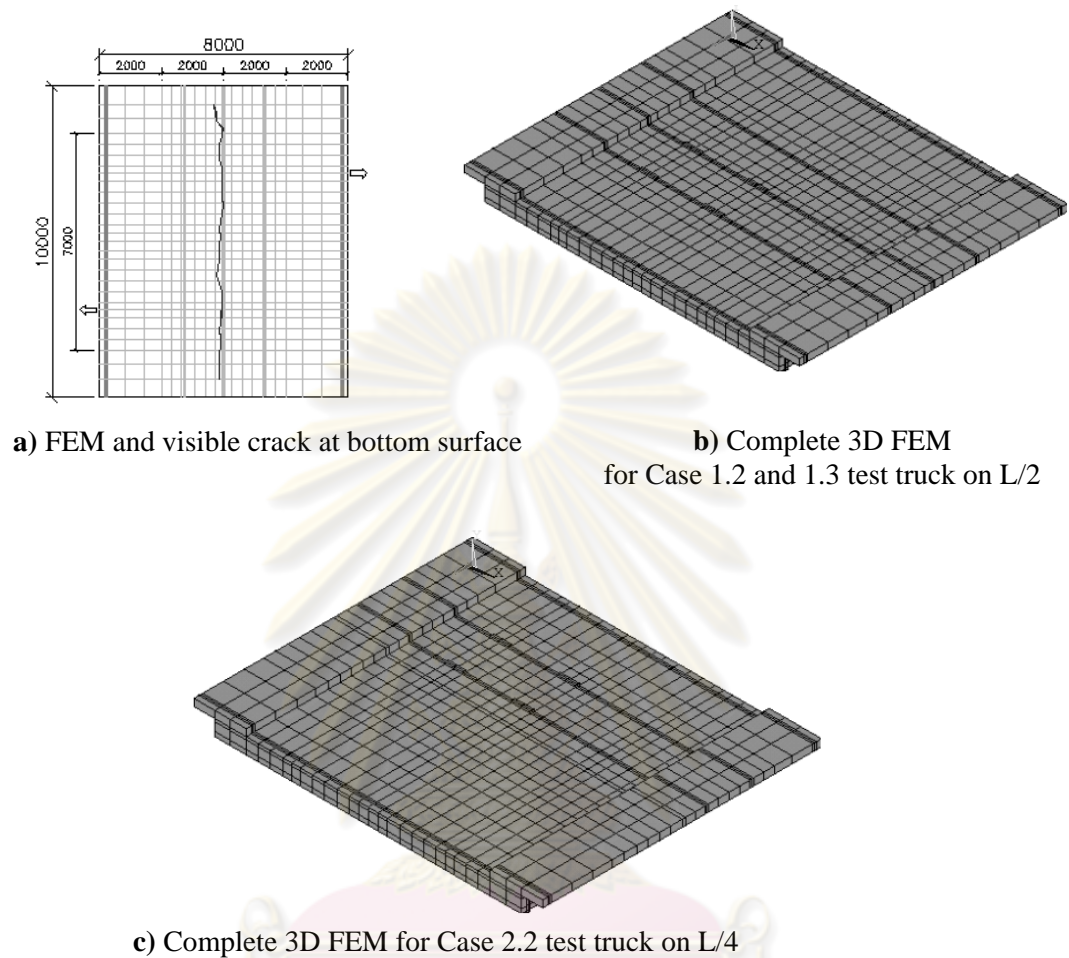
Figure 6.11 Full scale 3D FEM model for CB7

Support condition:

The bridge is simply supported bridge, therefore the supports are assumed as hinge at the left (restrained Y, Z directions at supported nodes) and roller (restrained Y direction at supported nodes) at the right supports. The supported nodes locate at 20 cm from bridge ends. The steel elements have been added at the support nodes as conventional NLFEM for preventing local failure.

Applied load:

The wheel truck load has been assumed as line load in 50 cm in length, and than divides to the corresponding nodes. At the wheel truck position, steel plate elements are assumed to prevent local failure during interaction analysis. Therefore at

the applied wheel truck load, the elements size in longitudinal of bridge is only 5cm width. NLFEM analysis is using interactive method of Modified Newton-Raphson as it is explained in section 5.5. Each wheel truck load is divided into load step, 15 load steps have been used for each. The method to divided load into FE nodes is show in the Figure 6.12, which P is total applied load to an element, 1/6P will be divided to edge nodes, and 2/3P divided mid-nodes (Zienkiewicz. O. C, 2005, book).
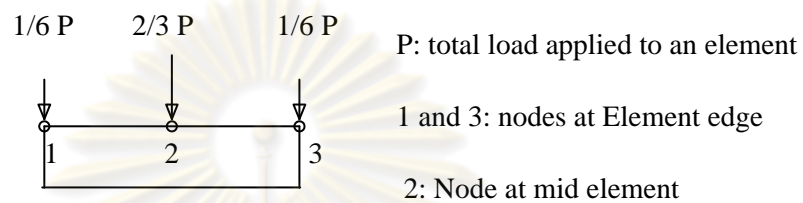
Figure 6.12 Load applied to FEM nodes

(1.6) Analysis case:

To compare the proposed approach which existed flaw/crack is included in model, five cases have been analyses for this bridge as below:

1. Truck on the middle span (L/2)
    Case 1.1 no damage elements
    Case 1.2 Included visible flaw/crack elements
    Case 1.3 Included visible flaw/crack and theoretical crack elements

2 Truck on the L/4 span
    Case 2.1 no damage elements
    Case 2.2 Included visible flaw/crack and theoretical crack elements

The group of case one is represented that tested truck stopped at the middle span (second axle on the L/2, Figure 6.10). To compare the influence of existed flaw/crack model to original model of NLFEM and test results, three different analysis cases (case 1.1, 1.2, 1.3) have been analyzed for this truck position. Case 1.1 is assumed for no flaw/crack model, this is also original NLFEM analysis. Case 1.2 is included only crack and flaw that from inspection (from crack mapping) or call observed damage. Case 1.3 is included both visible flaw/crack and theoretical crack calculated in section (1.4). For truck on position L/4, two analysis cases are analyzed (case 2.1 and 2.2) which material model of case 2.1 is similar to case 1.2 and case 2.2 is similar to case 1.3.

For case 1.2, the visible flaw/crack from crack mapping is included in those elements at the vicinity of crack path. The tension stiffening effect for exist flaw/crack in the perpendicular of crack direction of these elements are reduced due to amount of crack width as explaining in section 5.6 and 5.7. For bridge CB7, there is one large crack on direction perpendicular to traffic at the bridge midspan (see Figure 6.11 (a)), therefore the elements at region of crack path (with in l_t of crack face) are modeled as RED elements. This crack is structure flexural crack, by using RED elements, the flexural bridge stiffness at this section will be reduced.   Other observed defect in this bridge is corrosion at bottom slab surface near the middle edge of lane one (see crack mapping in appendix C). To account for this defect, the steel ratio of elements at this location is reduced by 30% of normal steel ratio (this consider from measuring the reaming steel section at this location) and tension stiffening is reduced by given large crack width, 0.5 mm. For the case 1.3 is included both observed flaw/crack and theoretical crack. The theoretical cracks are calculated as flexural cracks at the bottom layer with perpendicular to traffic direction. RED elements are used in this region to represent tension stiffening for flaw/crack model corresponding to those cracks width. Therefore for case 1.3, RED elements of observed crack are at the middle vicinity, and RED elements of theoretical cracks are at the region from 150 the supports to vicinity of observed crack.

(1.6.1) The analysis results of case1.1, 1.2, and 1.3:

The deflection and strain results of each analysis for tuck on L/2 (Case 1.1, 1.2, 1.3) are shown in the Tables 6.3.1 to 6.3.6, and compared to each other and the test results. Figure 6.13 to 6.22 are plotted the data of the results in the tables. In each table, the first column is indicated the equipment types corresponding position on Figure 6.9 for tested information. D-1, D-2 are LVDT measurement deflection at L/2 and L/4 of lane 1, TD-2, TD-1 are LVDT measurement deflection at L/2 and 3L/4 of lane 2, respectively. SS-4, SS-3 are steel strain gauges at L/2 and L/4 of lane 1, and SS-2, SS-1 are steel strain gauges at L/2 and 3L/4 of lane 2, respectively. CS-2 and CS-1 are concrete gauges at top slab surface at L/2 of lane 1 and 3L/4 of lane 2, respectively (See Figure 6.9).   The test results are available from these devices at corresponding position. Therefore, the analysis results shown in each tables are also taken from the same positions for verification analysis results.

The results of deflection from analysis comparing with the test results for case 1.1 (no any flaw/crack included), case 1.2 (Included visible flaw/crack case), and case 1.3 (Included visible flaw/crack and theoretical cracks case) are shown in the Tables 6.3.1, 6.3.2 and 6.3.3, and Figure 6.13 to 6.14, respectively. The important locations to compare the results are at location of applied load. The location D-1 (*X*(280), *Z*(400)) and D-2 (*X*(280), *Z*(200)) are at the position and lane that truck load applied for this analysis. Therefore, the results of these locations are most critical.

The value D-2 and D-1 in Table 6.3.1 indicated that the original model of NLFEM (case 1.1) is given deflection less than that test result up to 20%, when visible flaw/crack included (case 1.2) in Table 6.3.2, the deflection at D-1 is improved which it is less than test result 15.65%. In Table 6.3.3, results of analysis case 1.3 with included both visible flaw/crack and theoretical crack, the deflection at D-1 is more improved which differs to test result only 0.80%. The results of case 1.3 is the most closest to test result. The results of case 1.1 is using general NLFEM model which have been developed at the laboratory by calibration from new and good concrete condition, when using these general model, it may mean that the concrete structure is in good condition. This may be not correct for existing concrete structure, especially old concrete bridge which usually existed flaw/crack. Therefore case 1.1 is given results less than test results. The proposed RED model which reduces the tension stiffening effects due to existing flaw/crack in old concrete structures is close to test results. It is implied that this concept is more closed to real behaviour of old concrete structure. For the case 1.2, only visible flaw/cracks are included, and the deflection results are improved fairy good (not much close to test results). This may be the crack from inspecting mostly only large crack can been seen, while many small crack that less than 0.10 mm may be difficult to be seen and may be neglected by inspector. Moreover, the some structure crack is may closed when has no applied load during inspection. However in realistic and NLFEM, small structure crack will be influent to concrete and RC behaviour. Therefore if the more realistic results are needed, the small crack could not be neglected. To account for this, it may difficult to inspection all small structure crack and closed crack; therefore, the theoretical crack in this study may one alternative that is reasonable to account for this affect. Therefore, accounting small crack addition to the visible crack is more closed to realistic behaviour of old RC structure.

As compare to all results, it is indicated the analysis case 1.3 yield very good results for deflection, and it is evident that our proposed RED model for existing flaw/crack element can be reasonable and acceptable for assess full scale existing structure as concrete bridge.

Table 6.3.1, Deflection Case 1.1 no damaged elements, CB7

Device	Position			Analysis	Test	% Differ
		Z (m)	X (m)	mm	mm	
D-2	L/4-Lane 1	2.00	2.80	-0.48	-0.57	16.39%
D-1	L/2-Lane 1	4.00	2.80	-0.78	-0.99	20.84%
TD-2	L/2-Lane 2	4.00	7.20	-0.45	-0.45	-0.16%
TD-1	3L/4-Lane 2	6.00	7.20	-0.31	-0.30	-4.71%

Table 6.3.2, Deflection Case 1.2 included only visible flaw/crack, CB7

Dev	Position			Analysis	Test	% Differ
		Z (m)	X (m)	mm	mm	
D-2	L/4-Lane 1	2.00	2.80	-0.50	-0.57	12.67%
D-1	L/2-Lane 1	4.00	2.80	-0.83	-0.99	15.65%
TD-2	L/2-Lane 2	4.00	7.20	-0.49	-0.45	-8.61%
TD-1	3L/4-Lane 2	6.00	7.20	-0.33	-0.30	-10.97%

Table 6.3.3, Deflection Case 1.3 included theoretical and visible flaw/cracks, CB7

Dev	Position			Analysis	Test	% Differ
		Z (m)	X (m)	mm	mm	
D-2	L/4-Lane 1	2.00	2.80	-0.59	-0.57	-3.24%
D-1	L/2-Lane 1	4.00	2.80	-0.98	-0.99	0.80%
TD-2	L/2-Lane 2	4.00	7.20	-0.60	-0.45	-32.72%
TD-1	3L/4-Lane 2	6.00	7.20	-0.41	-0.30	-35.99%

In the Figure 6.13 to 6.14 are the plots the data in the Table 6.CB7.1 to 7.3 respectively. Each case of analysis is plotted in graph, i.e. Case1.1 L1 is analysis result of deflection from case 1.1 at position of device at lane 1, and so on for other cases. It can be observed from graphs and Tables that the deflection of the lane two (value of TD-1 and TD-2) which is the opposite lane of truck load applied, are closed to testing at the case 1.2, and higher than testing for case 1.3. This may be due to the effect of distribution of transverse stiffness of the slab bridge. The transverse stiffness from analysis model may stiffer than usual, there for the deflection results of case 1.3 at opposite lane (lane 2) are higher than that testing, and this effect are not consider in this study. In the assessment works, the critical location is applied load location.
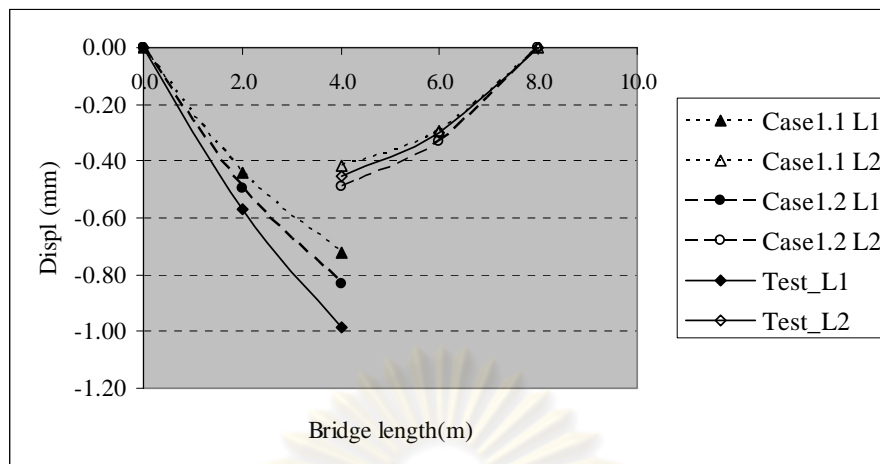
Figure 6.13 Deflection case 1.2 compare to case 1.1 and testing
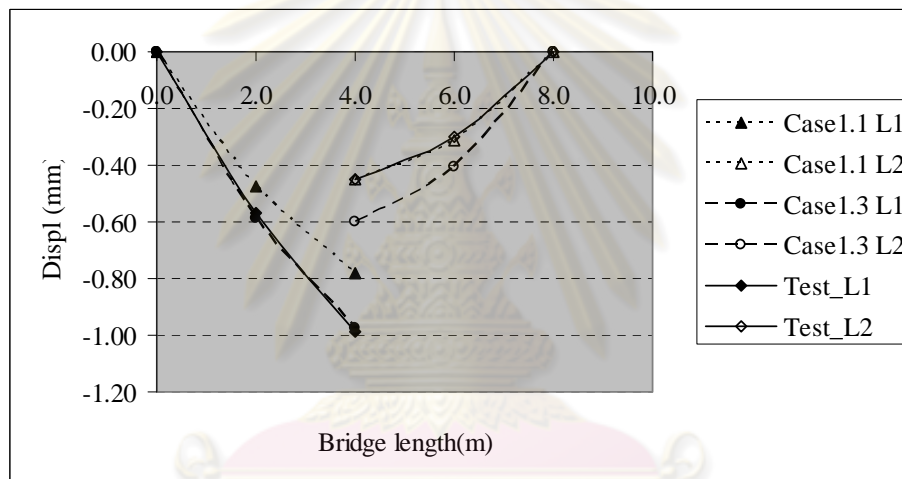
Note: in the figure, L1 means result at Lane 1

Figure 6.14 Deflection case 1.3 compare to case 1.1 and testing

The results of strain from analyses comparing with the test results for case 1.1 (no any flaw/crack included), case 1.2 (Included visible flaw/crack crack case), and case 1.3 are shown in the Tables 6.3.4, 6.3.5 and 6.3.6, and Figures 6.15 to 6.18, respectively. Similarly as explaining in the above, the critical locations are applied load locations which need to pay more attention. The location SS-3 (X(280), Z(400) and SS-4 (X(280), Z(200), Z and X are longitudinal and transverse bridge direction respectively) are at the position and lane that truck load applied for this analysis. Therefore, the results of these locations are more critical. Observing results in all tables, it is seen that the results of the strain at SS-3, and SS-4 of analysis given the same manner of results of deflection. Especially the results for SS-3, strain at the steel

level under location of the applied truck load. In the Table 6.3.4, result from analysis case 1.1 is 31.8 micro strains, while test result is 71.31 micro strains, the analysis result is less than test result up to 55.41 %. When visible flaw/crack is added (case 1.2) as in Table 3.5, the result from analysis of case 1.2 is improved by less than test result 15.72%. And case 1.3, theoretical cracks included together with visible flaw/crack, the result is more closed to the test result as value of SS3 of case 1.3 in Table 6.3.6 which only 8.29 % that differs from testing. Other value for SS4 is shown the same manner differ from test result, case 1.1 about 16.99%, case 1.2 about 9.23%, and case 1.3 about -12.49%. This indicated that the strain of the steel is strongly sensitive to cracking. The results from this analysis are agreed well with mechanical theory of the interaction between steel and concrete that has been explained in many previous researches such as Chen (1983), Manfred (1988), Kawak (1991). When there are no cracks presented, the stress from applied load in RC member will be transferred to both concrete and steel section. When cracks presented, concrete tensile capacity is reduced, and the stress will be transferred to steel section which infer that stiffness of RC member is reduced as well. Therefore, when existing crack included in the FEM model, the strain at crack section is much more than uncrack section. This evident that the proposed model in this study is reasonable and acceptable, the results are matched well with testing from old concrete bridge with already existed cracks. And other reason for case 1.3 is that in the actual bridge, the crack may be occurred much more as the same assumption (small cracks are existed in this slab bridge); therefore case 1.3 is more accurate to present actual bridge behaviour than other cases.

As it is explained in the above for other location at opposite applied load lane as in position SS-1, and SS-2, the analysis stresses at the steel level are higher than those test results. This may be due to the effect of transverse stiffness in FEM model is stiffer than that in the actual (this effect is not yet studied in this study). Other observing is strain at the concrete surface, the all analysis strain results at measuring position at the concrete surface, CS-1, and CS-2 are differed from the test results. This may be that the strains at the concrete from test are measured from new filled up mortar. The concrete strains from measurement may be lower than the actual usual values, because the way to measure concrete strain is such that pitting concrete surfaces about 2.5 cm in depth, then embedding concrete the gauge at pit and replacing by new mortar. New replacing mortar may not deform strictly with original

existed concrete. However, the strains at the top surface of concrete from analysis are also not high value i.e. analysis Case 1.3 is -12.8 micro strain. It is also seen that the different values between analysis results and test results are less than 10 micro strain which is still very low strain value.

Table 6.3.4, strain Case 1.1 no damage elements, CB7

Device	Position			Analysis	Test	Differ	% Differ
		Z (m)	X (m)	mstrain	mstrain		
SS-4	L/4-Lane 1	2.00	2.80	10.7	12.89	2.19	16.99%
SS-3	L/2-Lane 1	4.00	2.80	31.8	71.31	39.51	55.41%
SS-2	L/2-Lane 2	4.00	7.20	14.8	23.47	8.67	36.94%
SS-1	3L/4-Lane 2	6.00	7.20	10.3	8.93	-1.37	-15.34%
Concrete strain							
CS-1	3L/4-Lane 2	6.00	-7.20	-11.1	-2.97	8.13	-273.74%

Table 6.3.5, strain Case 1.2 included only visible flaw/crack, CB7

Device	Position	Analysis	Test	Differ	% Differ
		mstrain	mstrain		
SS-4	L/4-Lane 1	11.7	12.89	1.19	9.23%
SS-3	L/2-Lane 1	60.1	71.31	11.21	15.72%
SS-2	L/2-Lane 2	29.9	23.47	-6.43	-27.40%
SS-1	3L/4-Lane 2	10.9	8.93	-1.97	-22.06%
Concrete strain					
CS-1	3L/4-Lane 2	-11.5	-2.97	8.53	-287.21%

Table 6.3.6, strain Case 1.3 included theoretical and visible flaw/cracks, CB7

Dev	Loc	Analysis	Test	Differ	% Differ
		mstrain	mstrain		
SS-4	L/4-Lane 1	14.5	12.89	-1.61	-12.49%
SS-3	L/2-Lane 1	65.4	71.31	5.91	8.29%
SS-2	L/2-Lane 2	31.2	23.47	-7.73	-32.94%
SS-1	3L/4-Lane 2	16.1	8.93	-7.17	-80.29%
Concrete strain					
CS-1	3L/4-Lane 2	-12.8	-2.97	9.83	-330.98%

Figure 6.15 and 6.16 show the strain distribution of analyses results and test results through the depth of the slab at the measured location, SS-1, SS-2, SS-3, SS-4, respectively. The results of strain are such explaining in the above, the case 1.3 (Figure 5.16) gives the result closed to test result than other cases. However, the distribution of the analysis strain through out the depth of slab section may can not compare to test results; because there are only one or two points collecting from test,

and concrete strain from test results were measured from new filled up mortar which may lesser than usual. Therefore, only the strain measurement from steel at the bottom bridge surface can be observed. Therefore it is implied that the existing flaw/ crack model in this study can be observed the strain distribution in the bridge section as well. The all cases of analyses results give strain at the concrete are higher than test results.

a) Strain at section SS-3 (L/2, lane 1)

b) Strain at section SS-4 (L/4, lane 1)

c) Strain at section SS-2 (L/2, lane 2)

d) Strain at section SS-1 (3L/4, lane 2)
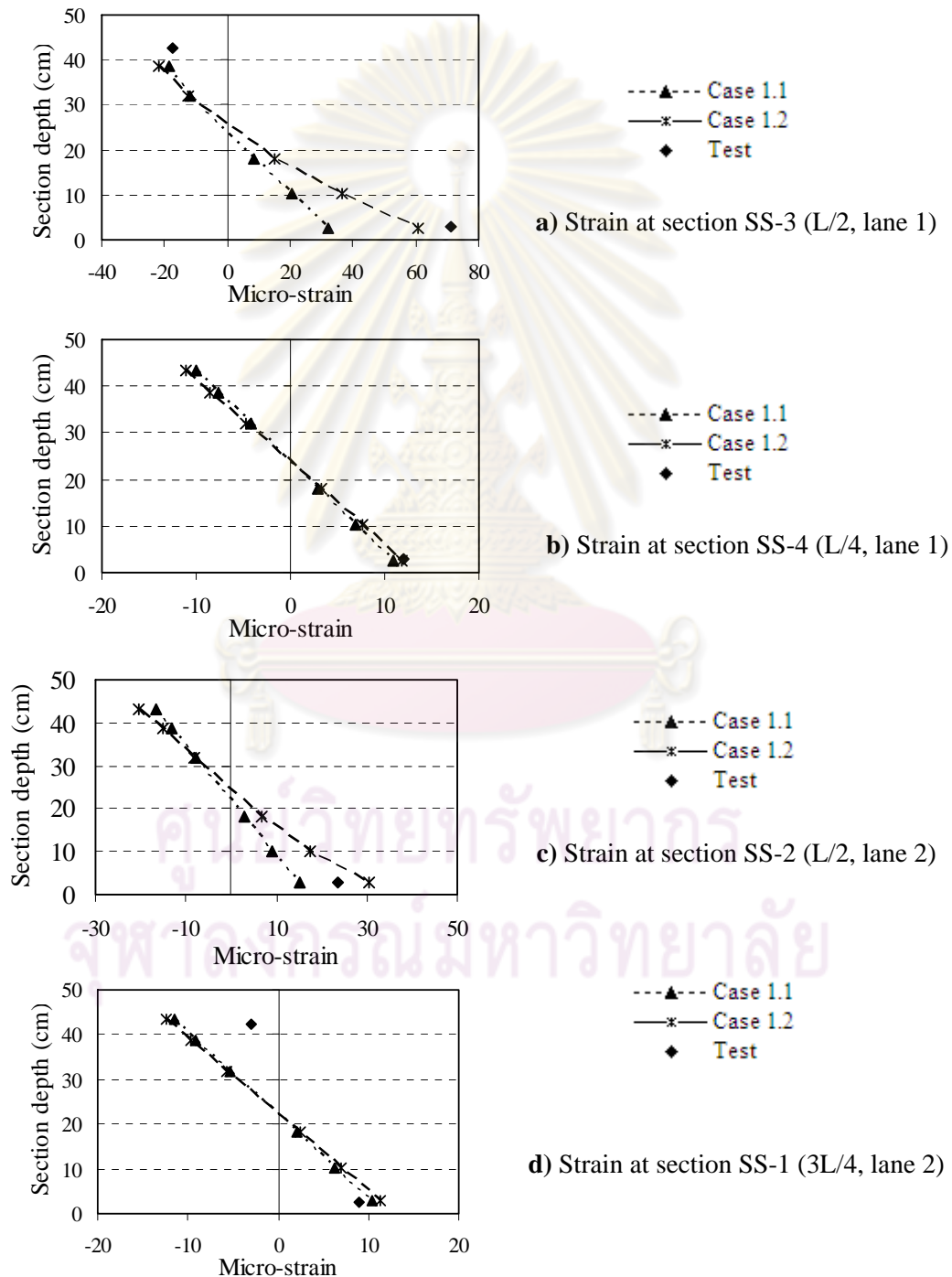
Figure 6.15 Strain comparisons among case 1.2, case 1.1 and testing

a) Strain at section SS-3 (L/2, lane 1)

b) Strain at section SS-4 (L/4, lane 1)

c) Strain at section SS-2 (L/2, lane 2)

d) Strain at section SS-1 (3L/4, lane 2)
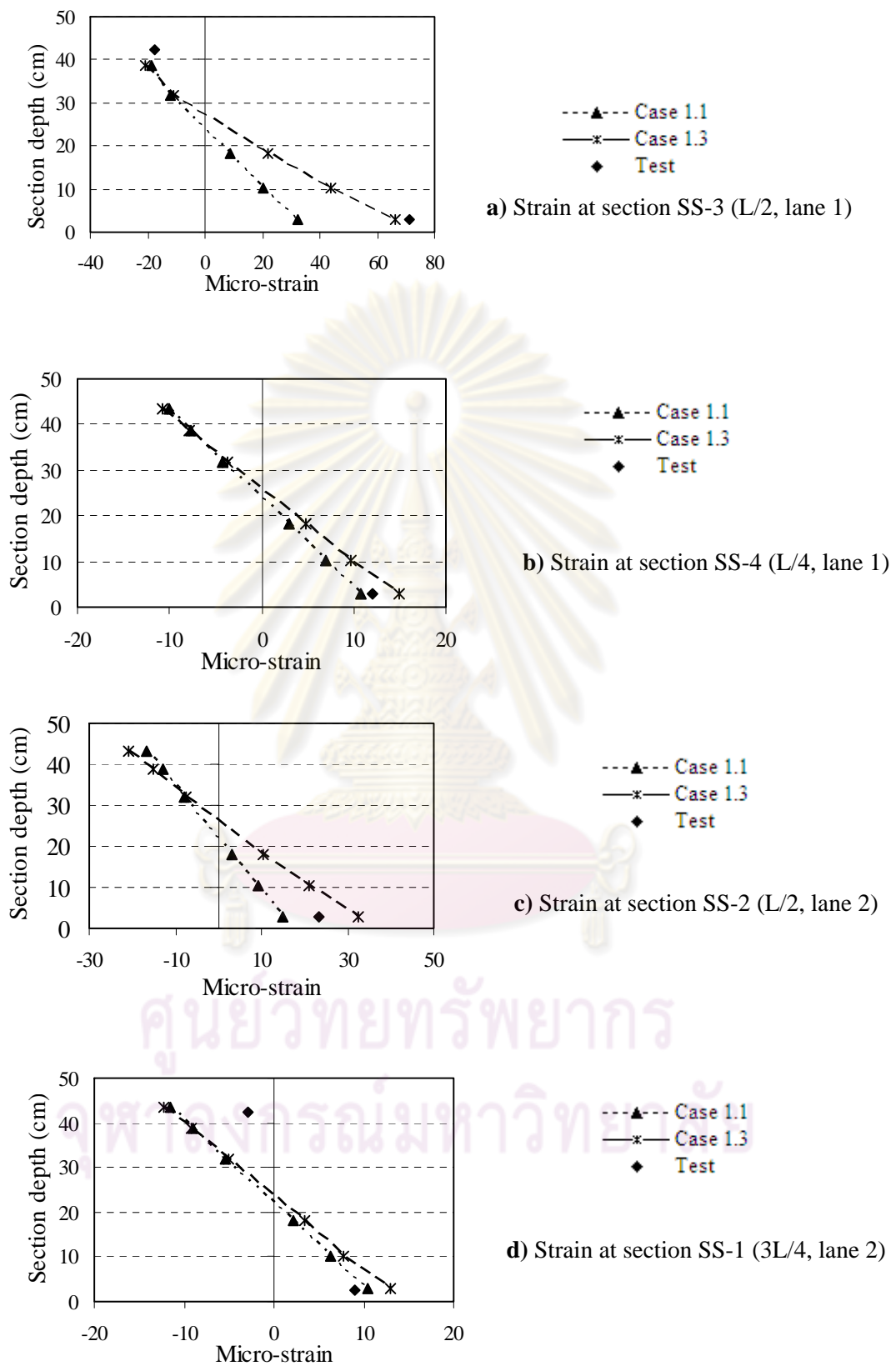
Figure 6.16 Strain comparisons among case 1.3, case 1.1 and testing

(1.6.2) The analysis results of case 2.1, 2.2:

This section will present the results of the test and analyses for case 2.1, and 2.2 for truck test at position L/4 (lane 1) the FE mesh for this case is shown in Figure 6.11. Case 2.2 is model that included theoretical and visible flaw/crack which is similar to case 1.3.

The results of deflection from testing comparing with the analyses for case 2.1 (no any flaw/crack included), case 2.2 (Included theoretical and visible flaw/crack) are shown in the Tables 6.3.7 and 6.3.8, and Figure 6.17, respectively. The important location to compare respond is concentrated at the applied load positions. The location D-2 (X(280), Z(200)) and D-1 (X(280), Z(400)) are the positions at lane that loads are applied. Therefore, the results of these locations are most critical and will be paid more attention. The values D-2 and D-1 for case 2.1 in Table 6.3.7 are less than that test results up to 21%. When exiting flaw/crack included, case 2.2, Table 6.3.8, the deflection at D-1 and D-2 from analysis results are improved which differ from test results only -8.1 % and -5.9 %, respectively. The comparisons are also the same manner as results of previous case (truck on L/2). As explaining that the original NLFEM (case 2.1) will give the results less than those from test results, because this case does not consider for existing flaw/crack in old RC structure. Therefore the case 2.2 is reasonable to represent actual bridge conditions.

For the results *TD1*, and *TD2* for case 2.1 in the Table 6.3.7 that differ from testing about 1.8%, and -3.6% , while theses values for case 2.2 (using proposed model) in the Table 6.3.8 are higher as -42%, and -47%. This different may be due to the distributions of the transverse stiffness of the actual slab bridge which is softer than FEM model. However, these are not critical values form testing, because they are at other lane from applied tested truck, and on the assessment condition, the case 2.2 give results higher than those test results. In this study, this effect is not yet considered and can be neglected at this study. Therefore, when applied this model to assessment concrete bridge structure, it is still in safe condition.

The Figure 6.17 plots to show the results in the tables comparing deflection at different bridge location at bottom slab bridge. The dot thick line is plot for case 2.2, and at the applied load lane, line Case 2.2_L1 is very closed to testing line Test_L1 at both location L/4 and L/2 for lane 1. As explaining that line Case 2.2_L2 which is plotted results at the lane 2 is higher than testing at the L/2.

Table 6.3.7, Deflection Case 2.1 no damage elements, CB7

Device	Position			Analysis	Test	% Differ
	Lane	Z (m)	X (m)	mm	mm	
D-2	L/4-Lane 1	2.00	2.80	-0.52	-0.63	17.21%
D-1	L/2-Lane 1	4.00	2.80	-0.67	-0.85	21.06%
TD-2	L/2-Lane 2	4.00	7.20	-0.39	-0.40	1.82%
TD-1	3L/4-Lane 2	6.00	7.20	-0.25	-0.24	-3.65%

Table 6.3.8, Deflection Case 2.2 included theoretical and visible flaw/cracks, CB7

Device	Position			Analysis	Test	% Differ
	Lane	Z (m)	X (m)	mm	mm	
D-2	L/4-Lane 1	2.00	2.80	-0.68	-0.63	-8.10%
D-1	L/2-Lane 1	4.00	2.80	-0.90	-0.85	-5.99%
TD-2	L/2-Lane 2	4.00	7.20	-0.57	-0.40	-42.45%
TD-1	3L/4-Lane 2	6.00	7.20	-0.35	-0.24	-47.17%
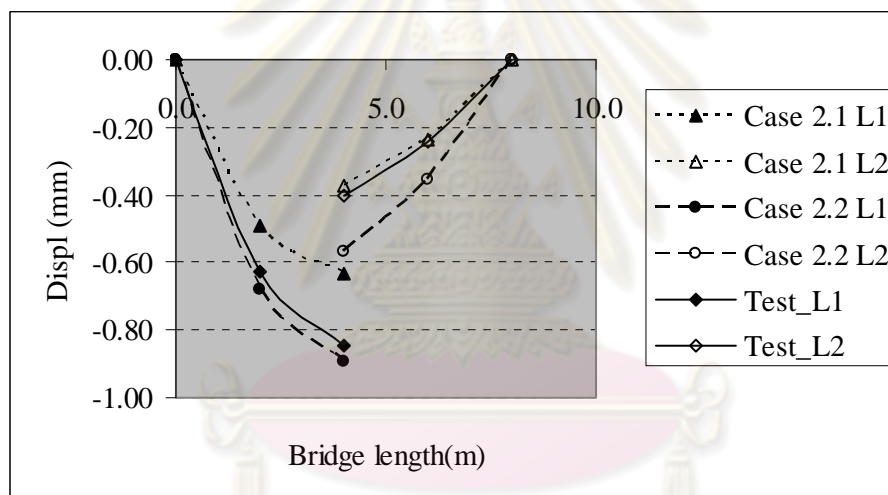
Note: in the figure, L1 means result at Lane 1

Figure 6.17 Deflection case 2.2 compare to case 2.1 and testing

Strain from test results comparing with the analyses results for case 2.1 (no any flaw/crack included), case 2.2 (Included existing flaw/crack case), are shown in the Tables 6.3.9, 6.3.10 respectively. The locations of applied load are at SS-4 and SS-3, the results of the strains at these locations are similar manner to deflection that case 2.2 gives results most closely to test results. The test results at SS-4 and SS-3 are 30.37 and 45.38 micro strain, respectively. The analysis result of case 2.1 are less than test results which are different up to 55.58% (SS-3, Tables 6.3.9); when crack are

included to the model (case 2.2), the results are closed to test results which is differ only 7.43% (Tables 6.3.10). This is tension stiffening effect due to cracking, when cracks present local steel stress at the crack will be increased. The results of case 2.2 are also agreed well with the case 1.3. Therefore, it is indicated that the proposed approach using RED elements at the crack vicinities are possible to apply for analysis diagnosis old concrete structures. Even though, the results from analysis at the opposite applied load lane are higher than those testing, but this effect can be neglected as explaining in the above. All analysis results for truck on *L/4* are similar manner for truck at *L/2*, therefore it may refer as the same reason as explaining in last example. The values of the strains at the concrete surface CS-1, CS-2 from all cases also have similar manner as last example for truck at *L/2*.

Table 6.3.9, Strain Case 2.1 no damage elements, CB7

Device	Position			Analysis	Test	Differ	% Differ
	Lane	Z (m)	X (m)	mstrain	mstrain		
SS-4	L/4-Lane 1	2.00	2.80	25.90	30.37	4.47	14.72%
SS-3	L/2-Lane 1	4.00	2.80	20.20	45.48	25.28	55.58%
SS-2	L/2-Lane 2	4.00	7.20	12.10	21.08	8.98	42.60%
SS-1	3L/4-Lane 2	6.00	7.20	6.15	3.77	-2.38	-63.13%
Concrete strain							
CS-2	L/2-Lane1	4.00	2.80	-20.40	-7.70	12.7	-164.94%
CS-1	3L/4-Lane2	6.00	7.20	-6.10	-1.38	4.72	-342.03%

Table 6.3.10, Strain Case 2.2 include theoretical and visible flaw/cracks, CB7

Device	Position			Analysis	Test	Differ	% Differ
	Lane	Z (m)	X (m)	mstrain	mstrain		
SS-4	L/4-Lane 1	2.00	2.80	35.80	30.37	-5.43	-17.88%
SS-3	L/2-Lane 1	4.00	2.80	42.10	45.48	3.38	7.43%
SS-2	L/2-Lane 2	4.00	7.20	27.80	21.08	-6.72	-31.88%
SS-1	3L/4-Lane 2	6.00	7.20	7.20	3.77	-3.43	-90.98%
Concrete strain							
CS-2	L/2-Lane 1	4.00	2.80	-23.80	-7.70	16.1	-209.09%
CS-1	3L/4-Lane 2	6.00	7.20	-6.07	-1.38	4.69	-339.86%

a) Strain at section SS-3 (L/2, lane 1)

b) Strain at section SS-4 (L/4, lane 1)

c) Strain at section SS-2 (L/2, lane 2)

d) Strain at section SS-1 (3L/4, lane 2)
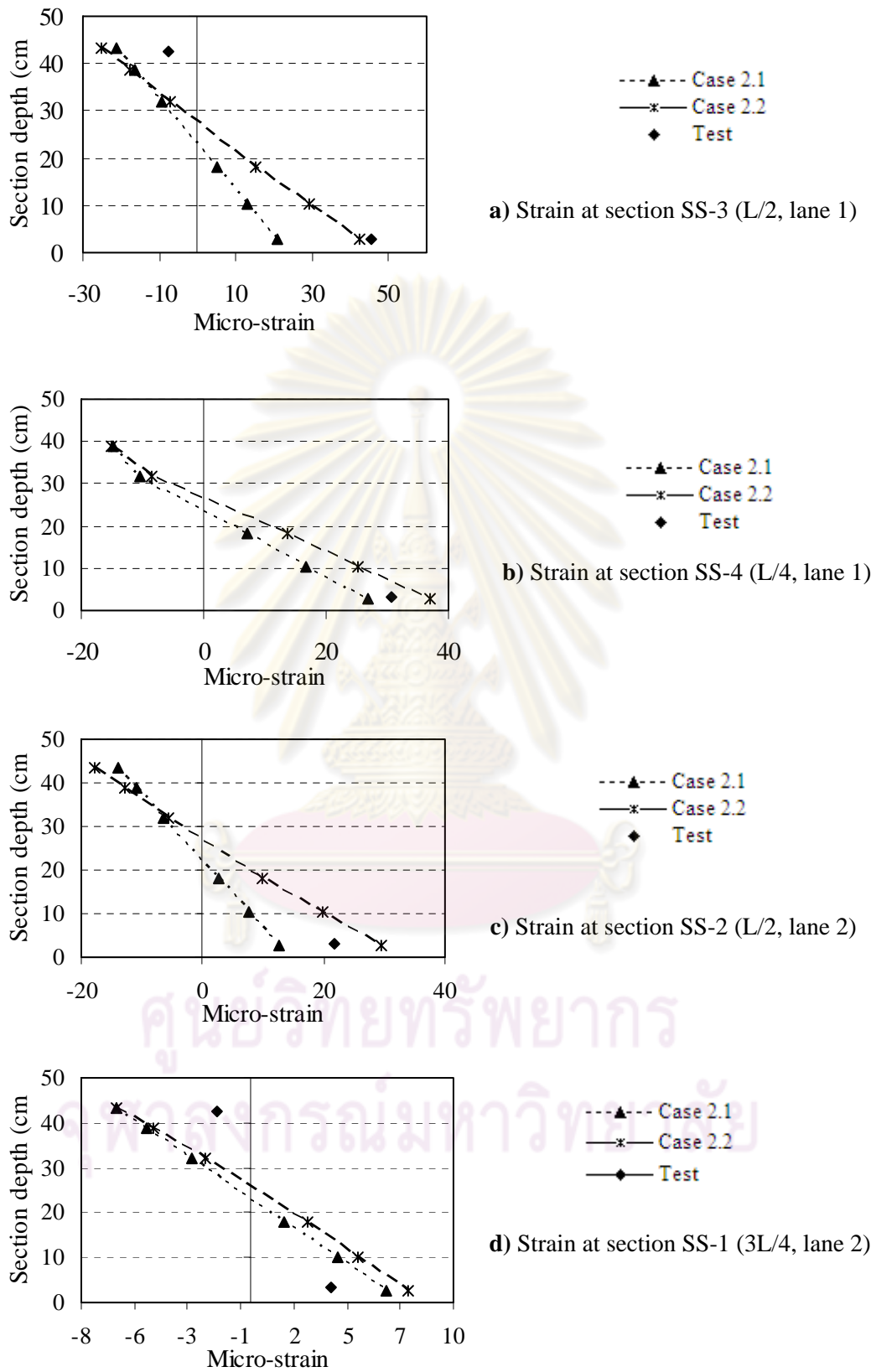
Figure 6.18 Strain comparisons among case 2.1, case 2.1 and testing

Figure 6.18 shows the strain distribution for analysis and test results through the depth of the slab at the measured locations, SS-1, SS-2, SS-3, SS-4, respectively. The distribution from both analyses case 2.1 and case 2.2 are not explicitly compared with test results, because the test results have only strain of the steel at the bottom surface and strain of concrete at the top bridge surface, while the strain results in between middle section points could not record. Moreover, there are few data for the strain of the concrete at top surface from testing. However, it is can implicitly observed strain at the reinforcement, i.e Figure 6.18 (a), strain at reinforcement level case 2.2 are closed to strain of the steel from testing. Further more, the strain distribution of analysis case 2.2, it is indicated that when crack occurs, the neutral axis of the section is higher than those no damaged case (case 2.1).

Five analyzed cases for concrete slab bridge, CB7 due to tested truck on the *L/2* and *L/4* are yielded satisfied results, and both position of truck give the same characteristic of the results. No existing damaged model or using original NLFEM give the results are much less than those test results for both deflection and the strains at the steel level. While the proposed model which included existing flaw/crack (theoretical and visible flaw/crack) have the results much closed to the test results. It is evident that the method of analysis existing concrete structure in this study could be applicable.

6.6.2 Analysis for Bridge No. CB6

(2.1) Bridge information:

The bridge No. CB6 is located at Route No 2096, km 43+887.0, Undonthani province, Thailand. The bridge is type of concrete slab, solid barrier with total length 8 m, span length (support to support) 7.5 m, slab thickness 0.52 m, total slab width 9 m, lane width 7m, walk way at both side 1 m (see Figure 6.19). The material data are collected by the testing as shown in the Table 6.1 which concrete parameters are: f_c'= 204 ksc, ft= 28.6 ksc, Ec= 217,242.25 ksc; Steel parameter for DB are: fy = 3,235 ksc, Es= 2,000,000 ksc; and steel parameter for RB is fy = 2,400 ksc. The main reinforcement at the bottom is parallel to the traffic direction which reinforced by DB 25 mm @ 12.5cm, and at transverse direction at the bottom layer is DB12 mm @14cm. The top reinforcement layer are RB9 mm @ 25 cm in both longitudinal and transverse bridge directions.
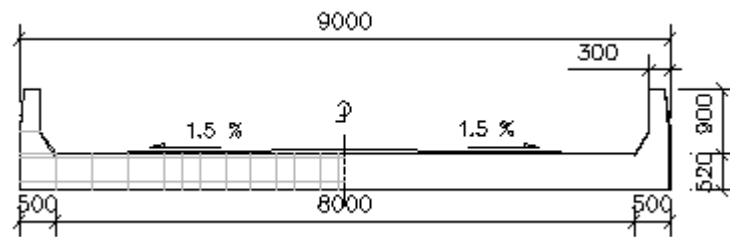
Figure 6.19 Section of bridge CB6

(2.2) Bridge condition:

From the inspection, the main slab of bridge is still is in a good condition. There are some medium cracks (0.2 to 0.3 mm) at the bottom surface in the direction of traffic and one small crack (0.2 to 0.25 mm) at the middle perpendicular to traffic lane (see Figure 6.20 and crack mapping in the appendix C). There is no asphalt pavement at the top surface.

a) Concrete strain gauges on top surface

b) Steel strain gauges and LVDT on bottom surface
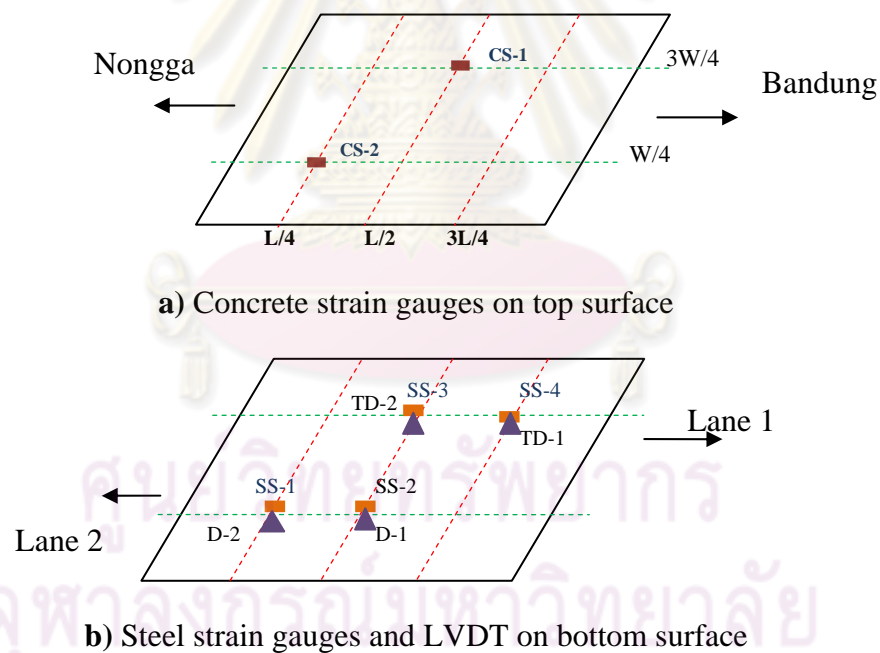
Figure 6.20 Layout of sensor for CB6

CS-1, CS-2: Strain gauges on the top surface of concrete bridge slab

SS-1, SS-2, SS-3, SS-4: Stain gauges on the main steel at bottom slab bridge

TD-1, TD-2: LVDT at the bottom slab bridge

D-1, D-2: Dial gauges

(2.3) Testing set up and truck load

   The testing equipments have been installed as explaining on section 6.4 above and shown in Figure 6.20.

   This bridge will be analyzed by applied load as tested truck position at the midspan, lane one as shown in the Figure 6.21 in the below. For the analysis only third and second axle were on the bridge, while first axle was at out the bridge

   The configuration of applied truck load on this bridge is indicated as below:
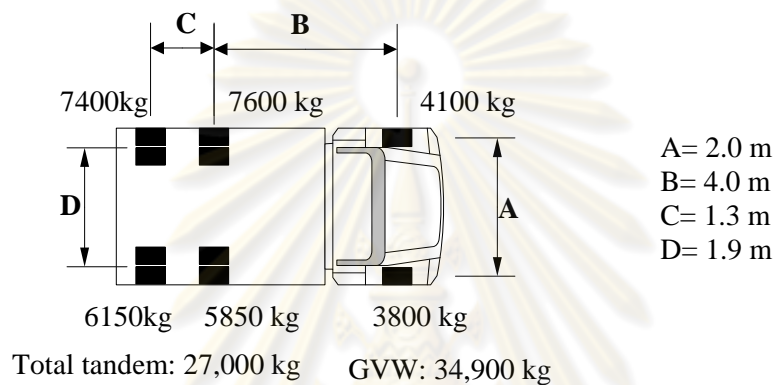
Figure 6.21a Configuration of tested truck for CB6
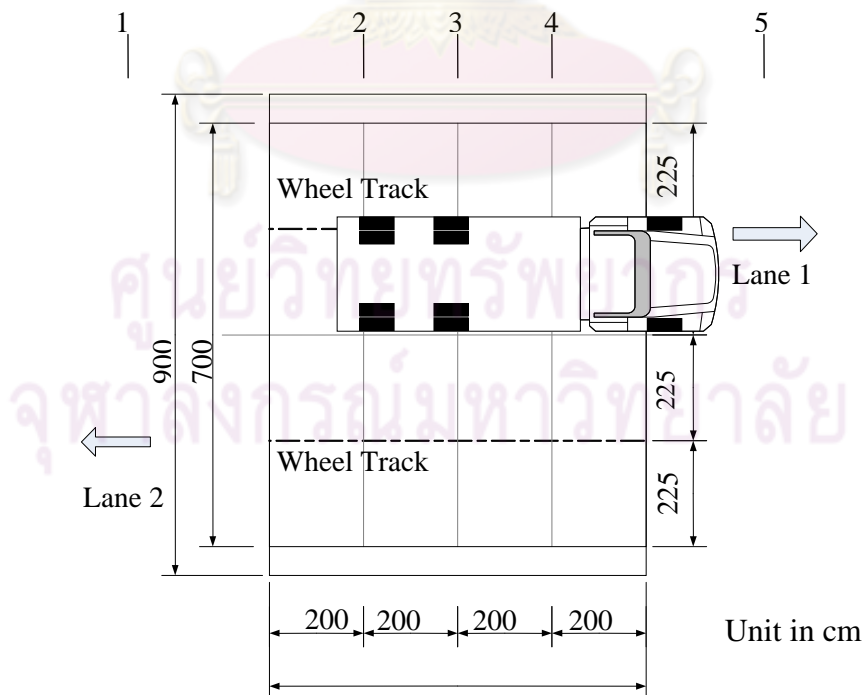
Figure 6.21b Position of truck load testing at midspan, CB6

(2.4) Calculate theoretical crack:

Similar to the last example, theoretical crack are calculated due to dead load of slab and standard Thai truck loading. The results are summarized in the below:

Rupture moment of the concrete Mcr = 14,526.40 kg.m

Enveloped length l_t=21.81 cm

Theoretical crack spacing is assumed varying between l_t to $2l_t$, therefore the decision crack spacing is selected as 35 cm. Selecting this value, because it is appropriated to bridge geometry and device location.

Theoretical crack widths at different section are:

From support	w_{cr}
m	mm
1.70	0.108
2.05	0.125
2.40	0.138
2.75	0.149
3.10	0.156
3.45	0.160
3.75	0.161

(2.5) FE mesh model

FE mesh type, boundary condition and applied load are referred to the same as previous example. The detail will be summarized as following:

The bridge is modeled in full scale 3D solid elements (the same way with CB7), all parts of bridge barrier are also integrated to the FE geometry model (see Figure 6.22). Total bridge thickness is 52cm, tension reinforcement zone is 13cm, compression reinforcement zone at the top layer is 8 cm. The steel ratios for reinforcement zoning are: at bottom layer parallel to traffic line, p = 0.0302; at bottom layer perpendicular to traffic line, p = 0.0061; at Top layer for both directions, p = 0.0032. and unit steel perimeter is 0.628 cm/cm.

(2.6) Analysis cases:

In this example, two cases have been analyzed which apply load as tested truck on the middle span (L/2) as Figure 6.21b. The two cases are given as:

Case B6.1 no damage elements

Case B6.2 Included theoretical and visible flaw/crack

The method to applied theoretical crack and visible crack for case B6.2 for this bridge are similar to those the last example for CB7, case 1.3 by using RED elements for representing theoretical and visible flaw/cracks. As it is explained that the depth of the cracks are not known, therefore the effect existing cracks is considered through the RED element thickness.

a) FEM and visible crack at bottom surface   **b)** Complete 3D FEM
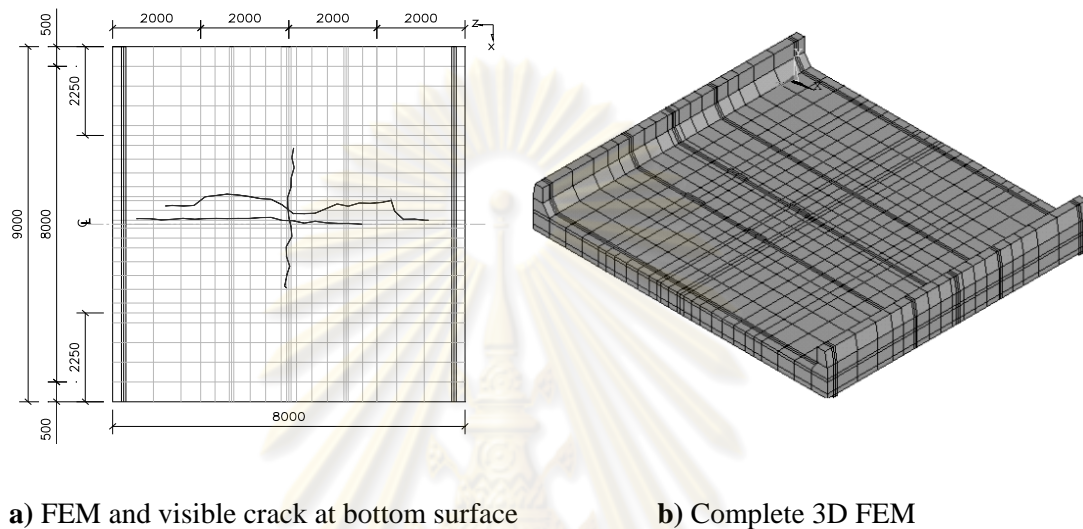
Figure 6.22 Full scale 3D FEM model for CB6

(2.6) The analysis results

The two cases have been analyzed for CB6, and results for deflection are given in the Table 6.4.1 to 6.4.2 for case B6.1 and case B6.2, respectively. The values shown in each column of the table are device names, device locations (Z in bridge longitudinal, X in bridge transverse directions), analysis results, test results, and percentage of analyses results to test results. The results of the strain are given in the table Table 6.4.3 to 6.4.4 for case B6.1 and case B6.2, respectively. The Figure 6.23 to 6.24 are represented the graphs corresponding to data in the tables. In the graphs, *Test_L1* is representing for test results for devices that are on lane one, and *Test_L2* is representing for test results of devices that are on lane two. The analyses results are also taken from the same position of measured devices for comparing.

The results in the Table 6.4.1 indicated that when there are no cracks included to the model, the defection at loaded lane TD-1 and TD-2 are 13.16% and 4.36% differed from test results. For case B6.2, both theoretical and visible cracks are

included; the different for the same devices are reduced to -2.05%, and -5.28% (Table 6.4.2). As explaining in the previous example, the reduction tension stiffening effect due to existing flaw/crack in old concrete structure will improve the analysis results of NLFEM to more close to the test results. Analysis results between case B6.1 (original NLFEM model) and case B6.2 (Included existing flaw/crack model) for this bridge are not much different. It may due to that only small crack occurred in the bridge, two cracks are parallel to the traffic lane, and only one small crack perpendicular to traffic lane (see Figure 22 (a)); and the crack in the longitudinal bridge direction may not much influence the bridge in main longitudinal flexural stiffness. And this bridge may still very stiff, even applied heavy load from test, but maximum deflection only 0.66 mm (at device TD-2). Other observing is that the bridge is still in stiff condition, the deflections of NLFEM at opposite of loaded lane (D-1 and D-2) are not much differed from test. It may indicate that bridge with stiff transverse stiffness may distribute load in transverse direction more than bridge with soft transverse stiffness.

Table 6.4.1, Deflection Case B6.1 no damage elements, CB6

Device	Position			Analysis	Test	% Differ
	Lane	Z (m)	X (m)	mm	mm	
TD-1	L/4-Lane 1	2.00	2.25	-0.35	-0.40	13.16%
TD-2	L/2-Lane 1	4.00	2.25	-0.57	-0.60	4.36%
D-1	L/2-Lane 2	4.00	6.75	-0.34	-0.28	-19.68%
D-2	3L/4-Lane 2	6.00	6.75	-0.23	-0.24	3.56%

Table 6.4.2, Deflection Case B6.2 included theoretical and visible flaw/cracks, CB6

Device	Position			Analysis	Test	% Differ
	Lane	Z (m)	X (m)	mm	mm	
TD-1	L/4-Lane 1	2.00	2.25	-0.41	-0.40	-2.05%
TD-2	L/2-Lane 1	4.00	2.25	-0.63	-0.60	-5.28%
D-1	L/2-Lane 2	4.00	6.75	-0.37	-0.28	-32.87%
D-2	3L/4-Lane 2	6.00	6.75	-0.27	-0.24	-14.24%

The Figure 6.23 plots to show the results of deflection in the Tables 6.4.1 and 6.4.2 versus bridge length. The curve case B6.1_L1 is shown the results of analysis case B6.1 at devices position on lane 1 (result at position of TD-1 and TD2), and Case B6.1_L2 is results of the same case at devices position on lane 2. And, it is similar manner for other cases. At applied load lane (lane 1), it is seen that the curve case B6.2 _L1 is very close to test results, curve Test_L1.
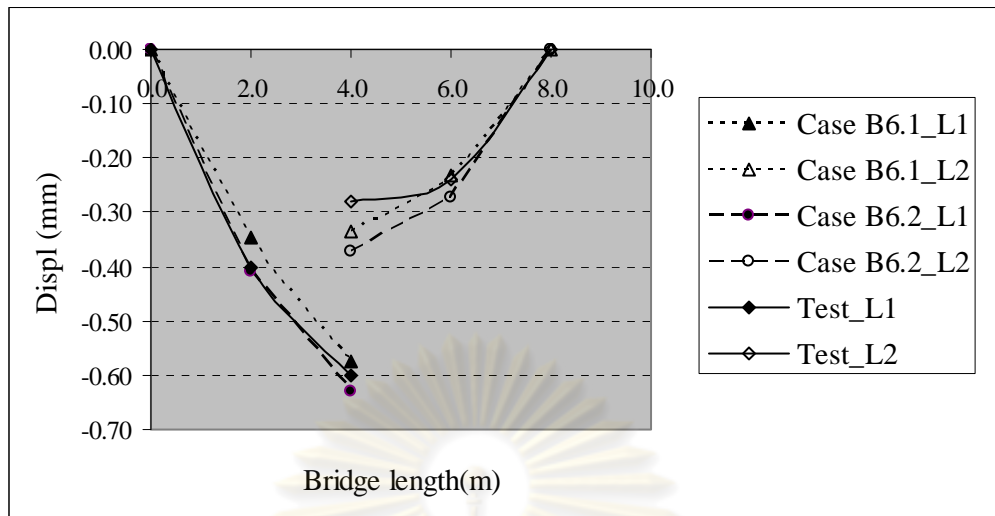
Figure 6.23 Load vs Deflection for CB6

The results of the strain at the steel level for each device location are shown in the Table 6.4.3 and 6.4.4. For non damage included case (Case B6.1), the analysis result of the steel strain under the load point is less that testing about 9% (Table 4.3, SS-3 value), when existing crack are included (Case 6.2), the analysis strain result at SS-3 is higher than the test result 24% which is lower bound value. This indicated that crack induces more strain in the RC members. In term of assessment, it is acceptable, while no crack included, NLFEM will given result less than usual which may dangerous to consider the behavior of the bridge. Other reason for model included the existing crack (Case 6.2) which the results of strain are higher than test results, it may be that the crack in slab bridge is more complicated than normal flexural crack in beam. In the good concrete slab bridge condition, the cracks may unlike as continue line across from left edge to right edge of the bottom bridge. During measurement, the strain gauges attached at section that existed crack may give strain value higher than that strain gauges attached at non crack section. In this study, theoretical cracks are assumed as the continue line at bridge bottom and averaged over element, hence the strain results is the average strain of an element. This may be one reason that the element strains at crack vicinity from analysis results are higher than testing results which in term of bridge assessment would be acceptable.

Table 6.4.3, Strain Case B6.1 no damage elements, CB6

Device	Position			Analysis	Test	% Differ
	Lane	Z (m)	X (m)	mcstrain	mcstrain	
SS-4	L/4-Lane 1	2.00	2.25	7.10	5.07	-40.40%
SS-3	L/2-Lane 1	4.00	2.25	26.70	29.50	9.49%
SS-2	L/2-Lane 2	4.00	6.75	13.20	10.50	-25.71%
SS-1	3L/4-Lane 2	6.00	6.75	8.50	7.45	-14.09%
Concrete strain						
CS-2	3L/4-Lane 2	6.00	6.75	-8.71	-5.74	-51.74%

Table 6.4.4, Strain Case B6.2, include theoretical and visible flaw/cracks, CB6

Device	Position			Analysis	Test	% Differ
	Lane	Z (m)	X (m)	mcstrain	mcstrain	
SS-4	L/4-Lane 1	2.00	2.25	7.14	5.07	-40.83%
SS-3	L/2-Lane 1	4.00	2.25	36.70	29.50	-24.41%
SS-2	L/2-Lane 2	4.00	6.75	18.20	10.51	-73.33%
SS-1	3L/4-Lane 2	6.00	6.75	8.80	7.45	-18.12%
Concrete strain						
CS-2	3L/4-Lane 2	6.00	6.75	-8.80	-5.74	-53.31%

The Figure 6.24 are shown the plot of the strain distribution trough the slab depth at the location of *SS-3*, (L/2, lane one), *SS-4*, (L/4, lane one), *S-2* (L/2, lane two), and *S-1*, (3L/4, lane two) (see also Figure 6.20 for these devices location on the bridge). All of the analysis results, strains distribution are lower bound values, strain from analyses are higher than test results. At the applied load point location can be more clearly to observe the distribution strain through slab bridge depth. The I ncluded existing crack model (case B6.2, Figure 6.24 (a)) is indicated that when crack occurs, the neutral axis (from bottom face) of the bridge will to higher than non crack section. This is reasonable that when flaw/crack happens, the compression zone of the concrete will be reduced, as the strain of the steel reinforcement will be increased. Observing strain distribution in other locations (Figure 6. 24 (b), (d)); the analyses results of case B6.1 and B6.2, and test results are not much different, this may be due to this bridge is still in a good condition. This is proved that the model accounting for existing flaw/crack in this study is reasonable having the results closed to test than no existing damage model when assesses existing bridge structure in the low applied load condition. This model also can be represented diagnosis load testing.

a) Strain at section SS-3 (L/2, lane 1)

b) Strain at section SS-4 (L/4, lane 1)

c) Strain at section SS-2 (L/2, lane 2)

d) Strain at section SS-1 (3L/4, lane 2)
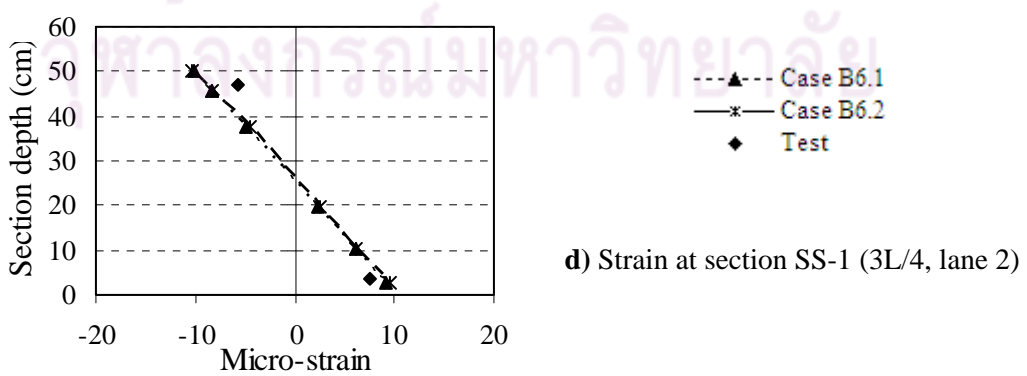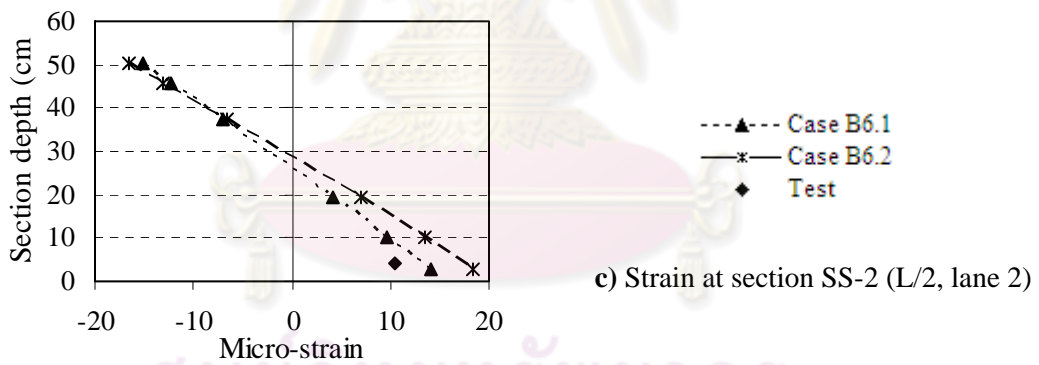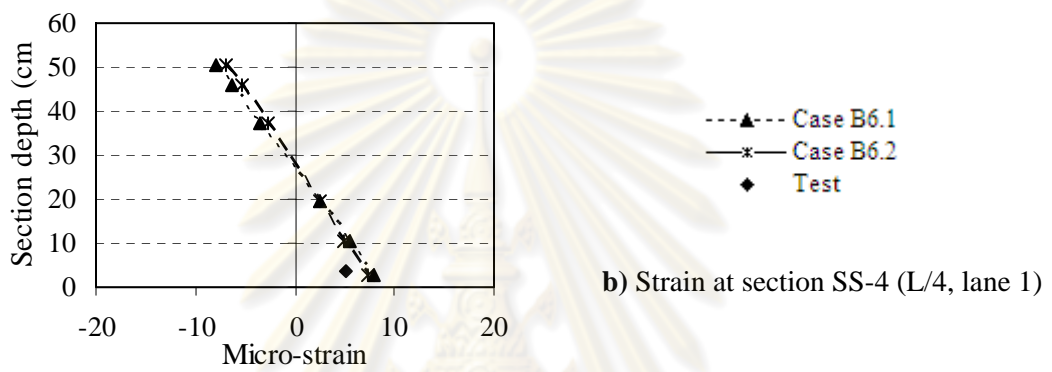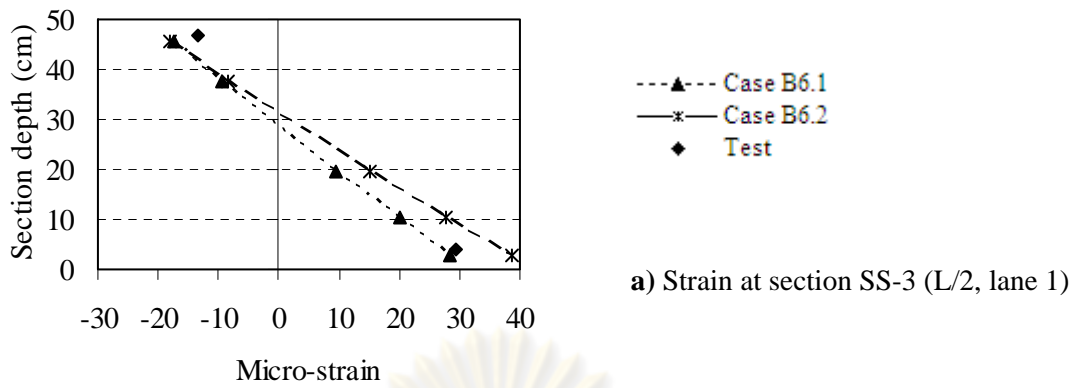
Figure 6.24 Strain comparisons among case B6.2, case B6.1 and testing

6.6.3 Analysis for bridge No. CB4S

(3.1) Bridge information

The bridge No. CB4S is located at Route No 14, km 38+684.0, Nakornsithammarat province, Thailand. This bridge is of concrete slab bridge, railing barrier type with total length 7 m, span length (support to support) 6.6 m, slab thickness 0.40 m, total slab width 8.8 m, lane width 7m, walk way at both side 1.5 m (see Figure 6.26). The material data are collected from the testing as in the table 6.1 with concrete parameters: f_c'= 305 ksc, ft= 34.92 ksc, Ec= 265,631.23 ksc; Steel parameter for DB: fy = 4,000 ksc, Es= 2,000,000 ksc; Steel parameter for RB: fy = 2,400 ksc, Es= 2,000,000 ksc. The main reinforcement at the bottom is parallel to the traffic direction which reinforced by DB 25 mm @ 12.5cm, and at transverse direction is DB12 mm @14cm. The top reinforcement layer is RB 9 mm @ 25 cm in both longitudinal and transverse directions.

Unit in mm
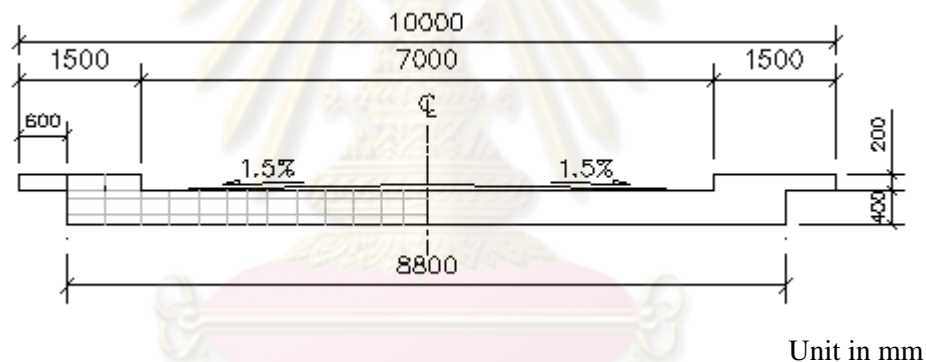
Figure 6.25 Cross section of the bridge CB4S

(3.2) Bridge condition

The bridge data are taken from report of Bridge Inspection and Load Testing (Nakornsithammarat) of Road Research Development Division, Department of Highways, Thailand. This bridge was not inspected by the author; therefore crack mapping is not available for this bridge. Therefore, only theoretical crack will be included in analyses model of this bridge. However, from rating of inspection company is indicating that this bridge is still in good condition by rating rate of 95%.

(3.3) Testing set up and truck load

Testing setup is also similar to previous examples, and will be summarized in the below:

a) Concrete strain gauges on top surface

b) Steel strain gauges and LVDT on bottom surface
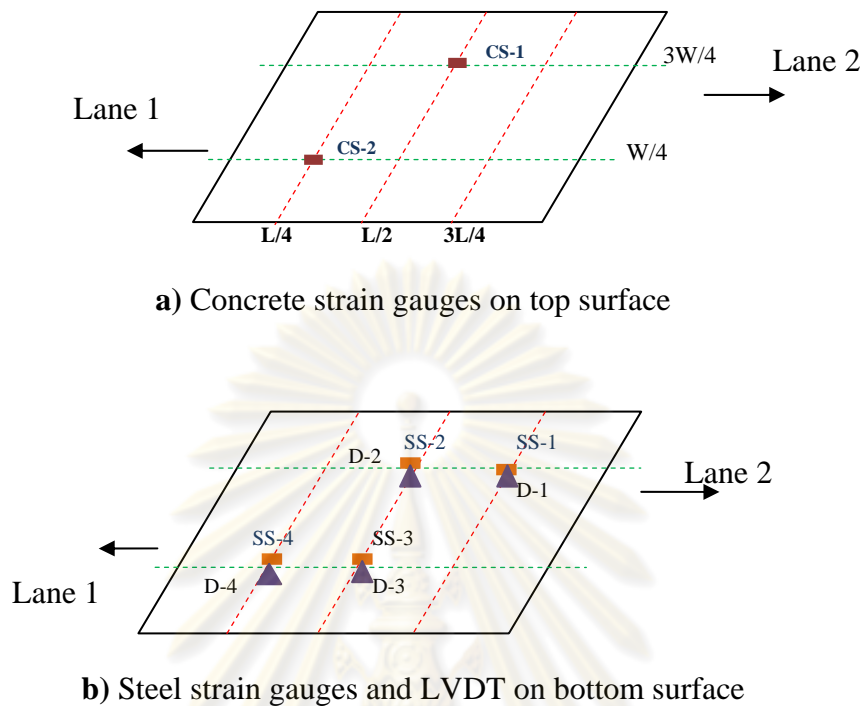
Figure 6.26 Layout of sensor for CB4S

This bridge will be analyzed by applied load as tested, the position of applied analysis loads are also at the position of wheel truck test with at the midspan, lane one. For the analysis only third and second axles of truck were on the bridge, while first axle was out off the bridge. Configuration and load of tested truck are shown in the Figure 6.27 (a) and (b).

(3.4) Calculate theoretical crack

The method of calculation theoretical crack is referred as explaining in example CB7. The results are summarized in the below:

Rupture moment of the concrete $\quad$ Mcr =11,255.16 kg.m

Envelopment length $\qquad$ l_t=24.61 cm

The spacing of theoretical crack can be determined between l_t to $2l_t$, therefore, in this example, crack spacing is about 35 cm. Selecting this value because it may appropriate to FE mesh model for this bridge geometry.

Summarized theoretical crack width at different sections for CB4S are:

From support	w_{cr}
m	mm
1.25	0.000
2.05	0.114
2.40	0.128
2.75	0.139
3.10	0.145
3.50	0.151
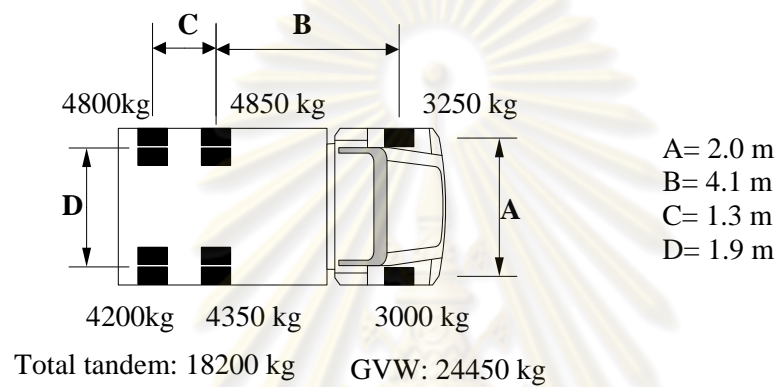
Figure 6.27a Configuration of tested truck for CB4S
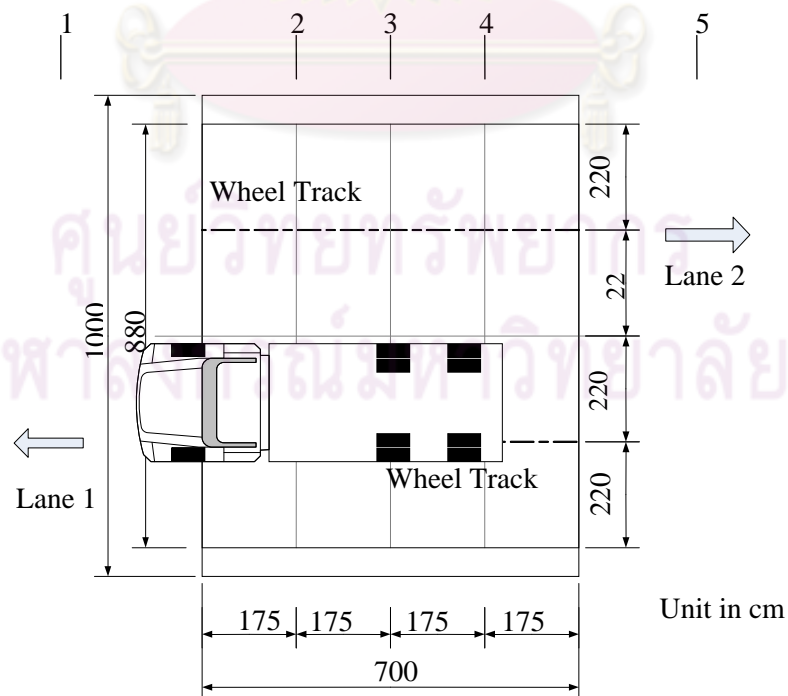
Figure 6.27b Position of truck load testing at midspan, CB4S

(3.5) FE mesh model

FE mesh type, boundary condition and applied load are also taken similar to previous examples. Therefore only important information are given briefly as following.

The bridge is modeled in full scale 3D solid elements, all parts of bridge barrier are also integrated to the analysis model (see Figure 6.28). Total bridge thickness is 40cm, tension reinforcement zone is 12cm, compression reinforcement zone at the top layer is 8 cm. The steel ratios for reinforcement zoning are: at bottom layer parallel to traffic line, $p = 0.0327$; at bottom layer perpendicular to traffic line, $p = 0.0066$; at Top layer for both directions, $p = 0.0032$. The FEM elements mesh size dimension in the vicinity of theoretical crack and visible crack in the direction perpendicular to crack direction should be between l_t to $2l_t$ preferably. The full model of this bridge is shown in the Figure 6.28.
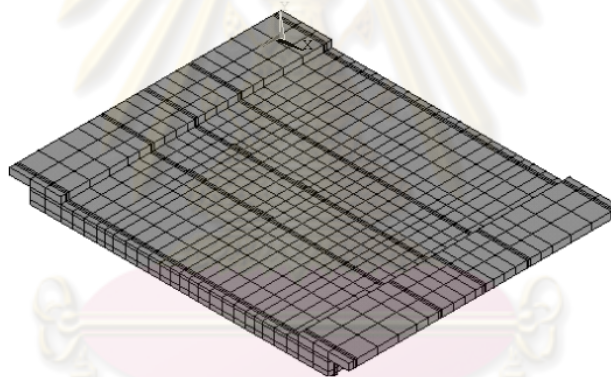
Figure 6.28 Full scale 3D FEM model for CB4S

(3.6) Analysis case:

In this example, two cases have been analyzed in the same test truck position, i.e. truck is at the middle span (L/2) as Figure 6.27b. The two cases are defined as:

Case B4.1 no flaw/crack elements

Case B4.2 Included theoretical crack elements

The analysis load is the same as axle load and position as shown in the Figure 6.27b.

(3.7) The analysis results

The deflection results are given in the Table 6.5.1 to 6.5.2 for case B4.1 and case B4.2, respectively. Table 6.5.3 to 6.5.4 are represented the strain at measurement

locations. The values in each column of the table are the same as that has been explained in the previous example.

The value *D-3* in the Table 6.5.1 is the deflection at applied load location. For no any damage included model, case B4.1, the analysis result is 18.92% differed from test result. For case B4.2, cracks (theoretical cracks) are included, the analysis result at the same device location (*D-3*) is reduced to 8.14% differed from test result, Table CB4.2. This is indicated that when the existing flaw/cracks are included in the model, the results are improved and closed to truck test results; this is implied that the proposed approach (case B4.2) can represent more realistic bridge behavior. As explaining in last two examples, the effect of existing flaw/crack is very important for NLFEM results, especially at the low applied load (service load). The data of the visible crack is not available for this example, only the theoretical cracks are included; therefore, the results are still in higher value by 8.14% and 25.58 % differ from test. However, this example may be represented that if the crack mapping is not available, when using NLFEM analysis old concrete bridge, the theoretical crack should be used for this proposed model.

Table 6.5.1, Deflection Case B4.1 no damage elements, CB4S

Device	Position			Analysis	Test	% Differ
	Lane	Z (m)	X (m)	mm	mm	
D-4	L/4-Lane 1	1.75	2.80	-0.26	-0.39	32.59%
D-3	L/2-Lane 1	3.50	2.80	-0.45	-0.55	18.92%
D-2	L/2-Lane 2	3.50	7.20	-0.24	-0.22	-7.04%
D-1	3L/4-Lane 2	5.25	7.20	-0.16	-0.15	-7.83%

Table 6.5.2, Deflection Case B4.2 included theoretical crack, CB4S

Device	Position			Analysis	Test	% Differ
	Lane	Z (m)	X (m)	mm	mm	
D-4	L/4-Lane 1	1.75	2.80	-0.29	-0.39	25.58%
D-3	L/2-Lane 1	3.50	2.80	-0.51	-0.55	8.14%
D-2	L/2-Lane 2	3.50	7.20	-0.27	-0.22	-24.68%
D-1	3L/4-Lane 2	5.25	7.20	-0.18	-0.15	-21.31%

Figure 6.30 is plotted the deflection versus span length of all analysis results and test results, the subscript *L1* is represented the deflection at lane one with data point *D-3* and *D-4*, and *L2* is represented the deflection at lane two with data at point *D-1* and *D-2* respectively. The curve Case 4.2_L1 (analysis results at applied load

lane, lane 1) is more close to the test results (curve Test_L1) than those results Case 4.1_L1.

Figure 6.29 Load vs Deflection Case 4.2 compare to Case 4.1 and testing

Table 6.5.3, strain Case B4.1 no damaged elements, CB4S

Device	Position			Analysis	Test	Differ	% Differ
	Lane	Z (m)	X (m)	mcstrain	mcstrain		
SS-4	L/4-Lane 1	1.75	2.25	6.77	6.00	-0.77	-12.83%
SS-3	L/2-Lane 1	3.50	2.25	21.07	26.00	4.93	18.96%
SS-2	L/2-Lane 2	3.50	6.75	9.01	10.00	0.99	9.90%
SS-1	3L/4-Lane 2	5.20	6.75	6.77	7.00	0.23	3.29%
Concrete strain							
CS-1	3L/4-Lane 2	5.20	6.75	-7.61	-7.00	0.61	-8.71%

Table 6.5.4, strain Case B4.2 included theoretical crack, CB4S

Devce	Position			Analysis	Test	Differ	% Differ
	Lane	Z (m)	X (m)	mcstrain	mcstrain		
SS-4	L/4-Lane 1	1.75	2.25	6.84	6.00	-0.84	-14.00%
SS-3	L/2-Lane 1	3.50	2.25	32.10	26.00	-6.1	-23.46%
SS-2	L/2-Lane 2	3.50	6.75	13.80	10.00	-3.8	-38.00%
SS-1	3L/4-Lane 2	5.20	6.75	6.70	7.00	0.3	4.29%
Concrete strain							
CS-1	3L/4-Lane 2	5.20	6.75	-8.15	-7.00	1.15	-16.43%

The results of the strain at the steel level at each device location are shown in the Table 6.5.3 and 6.5.4. The analysis result at applied load point (*SS-3*) of case B4.1 (non crack included case, Table 6.5.3) is that less than the test result about 18.9%. After included theoretical crack, case B4.2 (Table 6.5.4), the result of strain at the same position is 32.1 micro strains, while testing is 26 micro strains, the different about -23 %. Even though this percentage is higher than case CB4.1, but case CB4.2 gives the result higher than that test result. This is due to that this bridge is still in good condition, therefore the strain results from included existing flaw/crack model gives the results higher than the actual. This may be that the cracks in the actual slab bridge with in good condition are distributed uncertainly and may not continually like theoretical assumption as explaining in the above. Therefore, the strain results at the reinforcement level from analysis are higher than measurement, especially at the low applied load. However, the analysis results from proposed model which accounts for existed flaw/crack gives the strain distribution is reasonable, and can be represented more accurate than general model (no included existing flaw/crack in old RC structure) as shown in the Figure 6.30, most results of strain at steel level from case B4.1 are less than those test results. While the included existing crack model (case B4.2), the stain distribution will be higher than those test results. The strain distribution between these models can be obviously in the Figure 6.30 (a) and 6.30 (c) for middle bridge span and applied load lane. Therefore, it can be concluded that the strain distribution in the old concrete slab bridge structure is influence by crack pattern.

a) Strain at section SS-3 (L/2, lane 1)

b) Strain at section SS-4 (L/4, lane 1)

c) Strain at section SS-2 (L/2, lane 2)
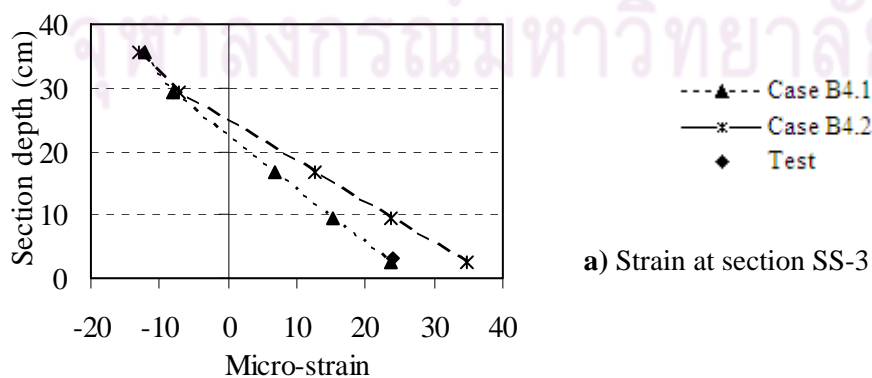
d) Strain at section SS-1 (3L/4, lane 2)
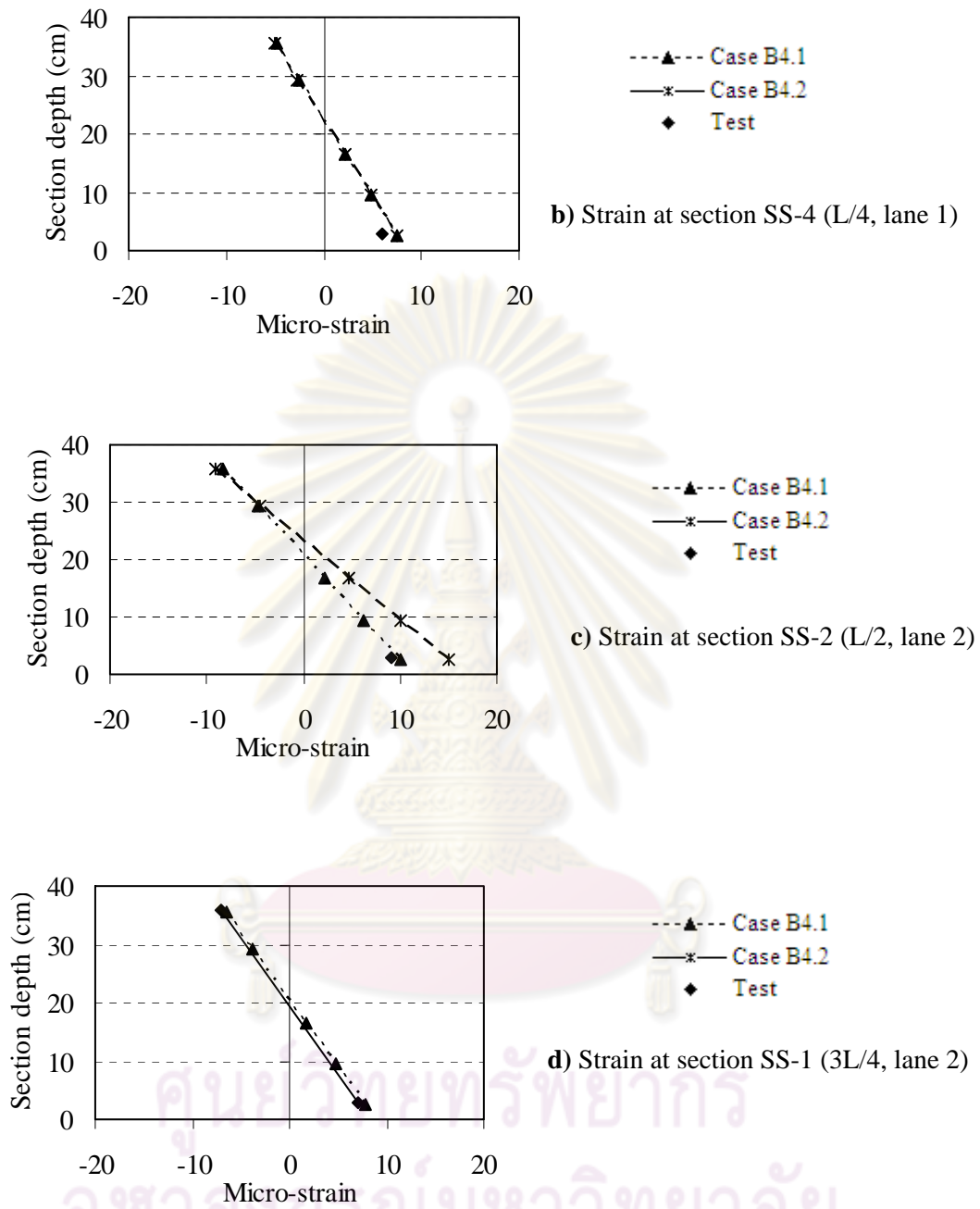
Figure 6.30 Strain comparisons among case 4.2, case 4.1 and testing

6.7.Evaluation of Rating Factor

The concrete slab bridges, CB7 and CB6 as presented in the section 6.1 and 6.2 respectively, in this chapter will be continued to analyze observing their performance due to maximum truck load from monitored data in Chapter 4, and load that induces bridges to fail. Their capacity will be also evaluated according the rating equation of AASHTO Manual, 1994.

6.7.1 Analysis for CB7

The bridge dimension and material parameters, the material model, the geometry model, and boundary condition of CB7 are already given in the section 6.1. Only analysis loads that are different from previous examples (section 6.1); therefore, only the applied loads that will be explained in this section.

(1) Applied load

In the actual, the majors load on the bridge are dead load and live load; therefore, loads for analysis the bridge are included both dead load, and live load which is truck load (TL) for this study. For studying bridge capacity, loads at the truck wheels position will be furthered to increase to induce bridge up to ultimate load.

Dead load (DL): The dead load has been assumed as the surface area load applying at the elements areas that are at bridge surface. The area loads than distribute to corresponding nodes as general FEM concept (See Figure. 6.31). The material unit weights for calculating the dead load are 2,400 kg/m^3, and 2,000 kg/m^3 for concrete and pavement material, respectively. The dead load for this bridge are 1,180 kg/m^2, 480 kg/m^2, and 60.29 kg/m applied at main slab, bridge curbs, and railing, respectively. The total dead load (DL) after multiplying to their corresponding areas is 97,156.57 kg, and total factor load of 1.3DL is 126,303.54 kg.
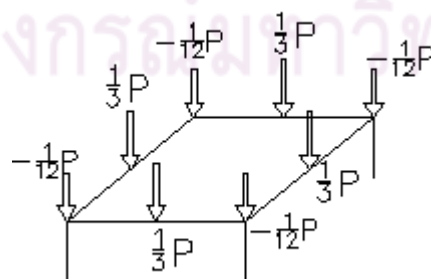
Figure 6.31 Area load divided to the nodes for FEM

Truck load (TL): To evaluate performance of the bridge due to present truck loading, the maximum truck, TR-05 from the monitoring data in the chapter 4 is selected to represent actual truck effect to the bridge. The configuration and axle weights of this truck type are shown as Figure 6.32. There are two lanes for this bridge, therefore two trucks running parallel have been assumed to crossing the bridge. Normally, truck effect to the bridge is moving load; therefore, the critical positions of the truck on the bridge have been selected for presenting maximum responses. In this bridge only second and third truck axles (P1 and P2) are on the bridge deck with the total two truck weights on the bridge is 52.4 kg. In the bridge longitudinal direction, position of truck is defined such that the center gravities of the truck places at distance *LGp/2* form the bridge midspan (see Figure 6.33 (b)). Where *LGp* is the distance between third axle to the center gravity of the truck. In the bridge transverse direction, the right axle load of the first truck is placed at distance 0.6 m from the bridge curb, and right axle load of the second tuck places at 1.2 m apart from the first truck (see Figure 6.33(a)). Each load of truck wheel is assumed to have width as 0.5 m, and then it is divided to corresponding nodes.
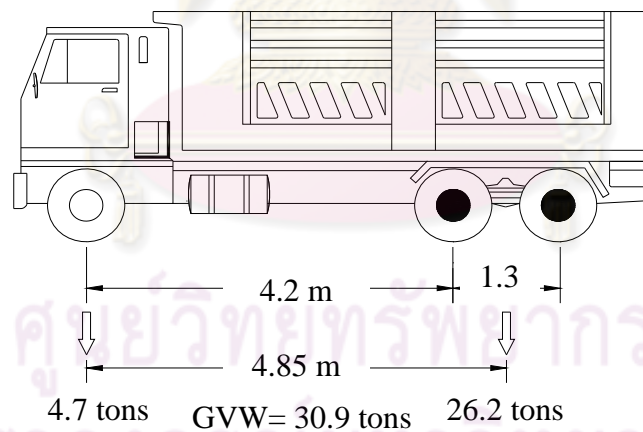
Figure 6.32 Configuration for maximum TR-05
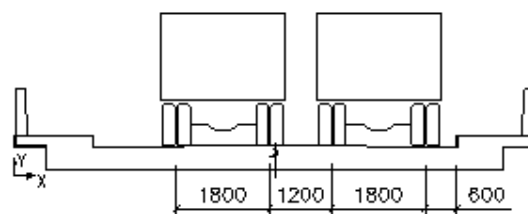
Figure 6.33 (a) Transverse position of truck on the bridge, CB7
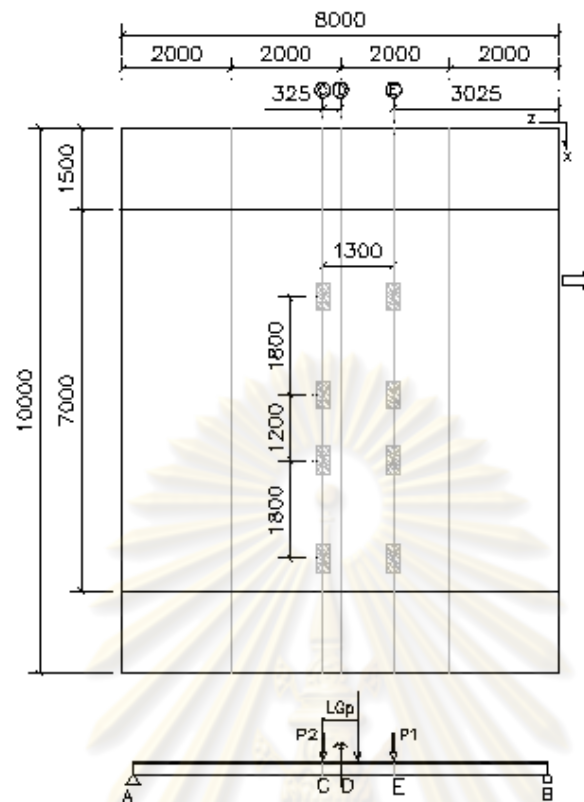
Figure 6.33 (b) Bridge plan and position of truck on longitudinal of bridge

According to NLFEM, the analysis procedure is conducted as interaction manner and the applied analysis loads have to divide into many small load steps to capture the nonlinear behavior of the material model. Therefore in this example, the dead load factor *1.3DL* is divided in to 50 load steps. After that the load from step of 51 are represented as axle truck loads and further to induce bridge up to fail. The factor dead load (*1.3DL*) for each analysis load step is 2,526.07 kg applied on the corresponding nodes at the bridge surface, and after load step 50, each load step of 2,116.52 kg is applied at nodes corresponding to positions of truck wheels to represent axle truck load and load induced bridge to failure (see Figure 6.33b).

(2) Analysis case

Two cases have been analyzed for comparison the model of no damage element using original NLFEM model and including existing flaw/crack model which is proposed in this study such as case7.1 no damage element model, and case7.2 including existing flaw/crack model (both theoretical and visible flaw/cracks are included). The method to include crack in to the model is also refer to section 6.1.

(3) Geometry mesh model of bridge CB7

The bridge geometry model for analysis is also the same as explaining in the above which considers from parameters such as material zone, crack location and applied load location. Both geometry models for case7.1 and case7.2 are the same as shown in Figure 6.34 below.
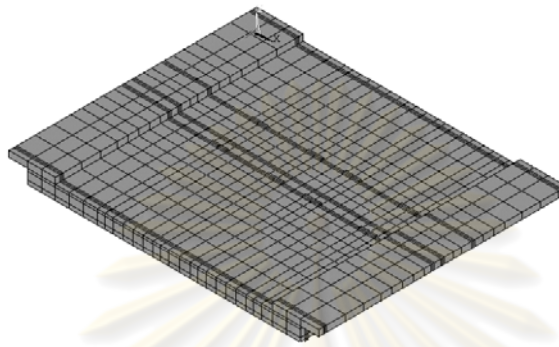
Figure 6.34 Geometry model for bridge CB7

(4) Analysis results

Because the aim of this section is to study the performance of old concrete slab bridge, therefore the results of case 7.2 (included crack using models proposed in this study) will be more attended and compare to case 7.1.

(4.1) Observe results case 7.2 to case 7.1

The deflection at section *C*, applied load section (see Figure 6.33b) for case 7.1 (no included crack model) and case 7.2 (included flaw/crack model) are shown in Figure 6.35 (a). The meaning of subscripts -1, -2, -3 in name of each graph are represented applied load levels; i.e. Case7.2-1, Case7.2-2, and Case7.2-3 are analysis results for model case 7.2 at applied load for DL, DL+TL, and 1.3DL+1.3TL(1+I), respectively. Where I is bridge impact factor which equals to 0.3 for this bridge. For other cases are also similar to this manner. At the same load level, the deflections of case 7.2 are all higher than case 7.1. It is seen also that the transverse deflection at right edge is higher than left edge, because the truck wheel is closer to the bridge right edge than left edge (Figure 6.33). For the deflection at the longitudinal section of case 7.2 is also higher than that case 7.1 as shown Figure 6.35 (b); in this figure shows only case 7.2-2 and case 7.1-2, because other load levels also have the similar manner. It is seen that the deflections of included crack model (case 7.2) are higher than that original model (case 7.1). This different is as high as up to 23.53 %.
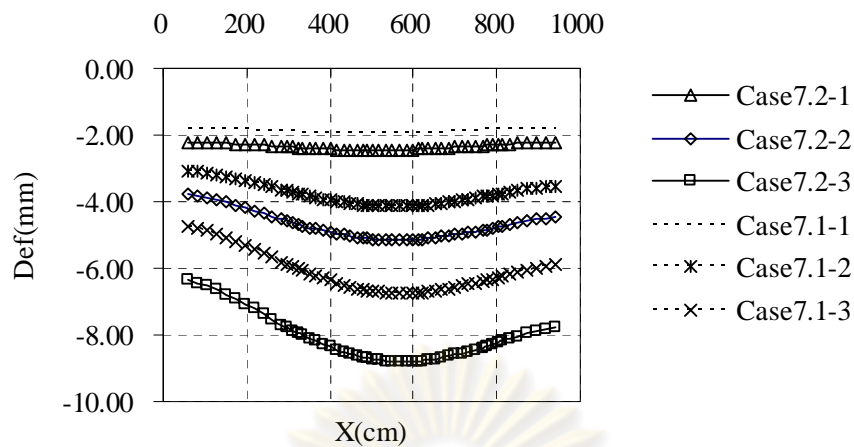
Figure 6.35(a) Compare transverse deflection for case 7.2 and case 7.1
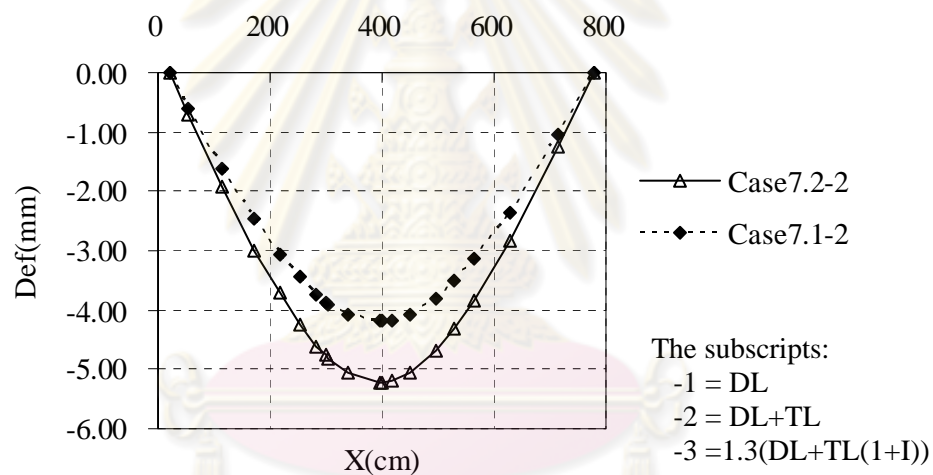
Figure 6.35(b) Compare longitudinal deflection for case 7.2 and case 7.1

The applied loading versus deflection at the bridge center (at the coordinate *X*=525 cm, *Z*=400 cm) for case 7.2 and case 7.1 are shown in Figure 6.36. The model which included existing cracks (case 7.2) is occurred deflection higher than that no crack model (case 7.1) through the applied loads. This different is about 20%. It is implied that cracks at the bottom slab may reduce the stiffness of the bridge structure. This is also identical to the beam theory of reinforced concrete member subjected to flexural, when cracks present at the tension zone, the moment of inertial at crack section will be decreased leading to increase deflection of the member.
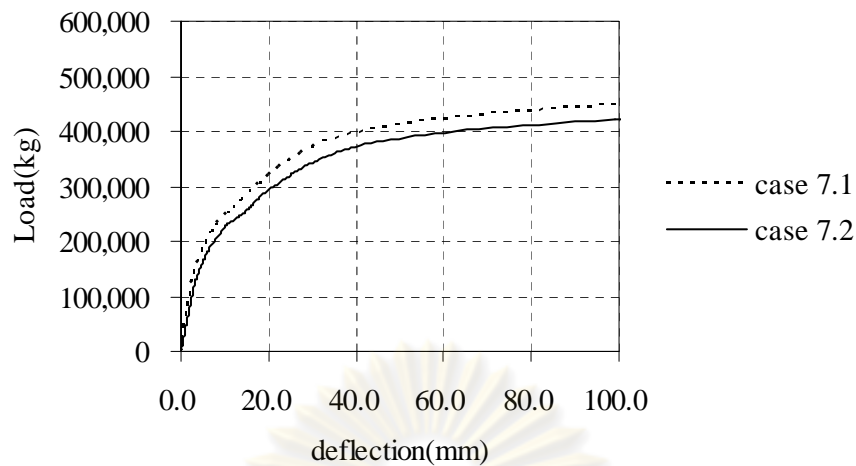
Figure 6.36 Load vs deflection for case 7.2 and case 7.1

Similar to the deflection, the strain at the mid point of bottom surface for case 7.2 is higher than the strain of case 7.1 at the same applied load. As Figure 6.37 shows the load and strain curves at the bottom mid point of the bridge (Z=431, X=495). At the yield strain of the steel ($\varepsilon y=0.0016$), the total applied load for case 7.1 (Py_case7.1) is 395,615.50 kg while case 7.2 (Py_case7.2) is 292,519.50 kg. The other load level are also given in the figure with P1=1.3DL=126,303.50 kg, P2=1.3DL+1.3TL(I+0.3)= 214,859.12 kg, and Pul=250,797.69 kg. Where Pul is the ultimate applied load according to simplify beam theory (see appendix-D). It seen that the ultimate load from conventional method (Pul) is less than Py from both cases.
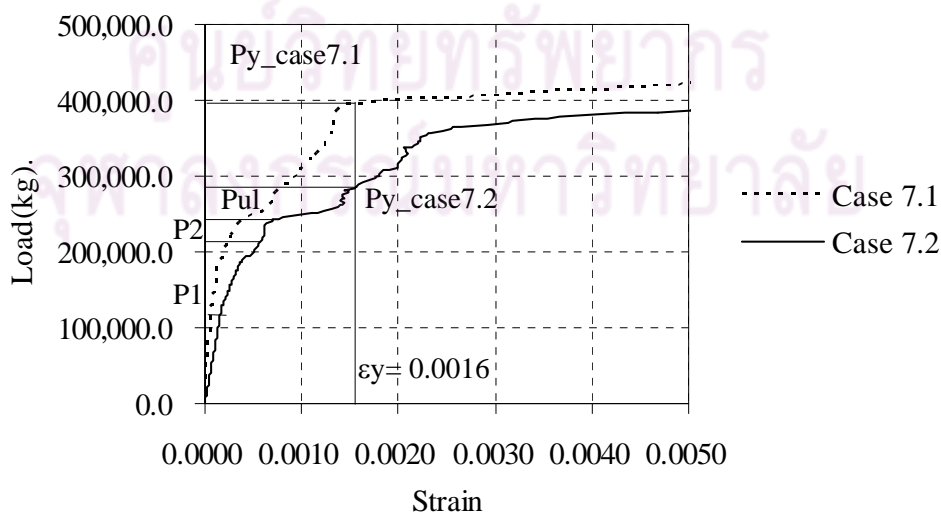
Figure 6.37 Load vs strain at bottom mid point (Z=431, X=495)
for case 7.2 and case 7.1

(4.2) Observe results case 7.2

The transverse deflection curve for case 7.2 at service load (DL+TL) at different section such as at section *C* (*Z*=432.5, applied second axle load point, see Figure 6.33), section *D* (*Z*= 400 cm, midspan section), and section *E* (*Z*=432.5, applied second axle load point) are shown in the Figure 6.38. The maximum deflections at these sections are -5.15 mm, -5.23 mm, -4.79 mm at section *C*, *D*, and *E*, respectively. It is seen that the deflection is highest at the midspan section (point *D*). The deflection at applied load section, point *C* is a little bit less than point *D*.
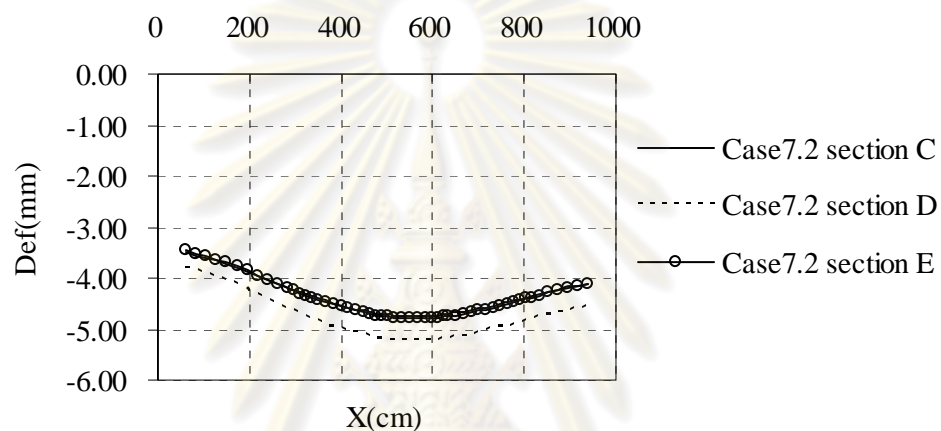
Figure 6.38 Transverse deflections at different sections
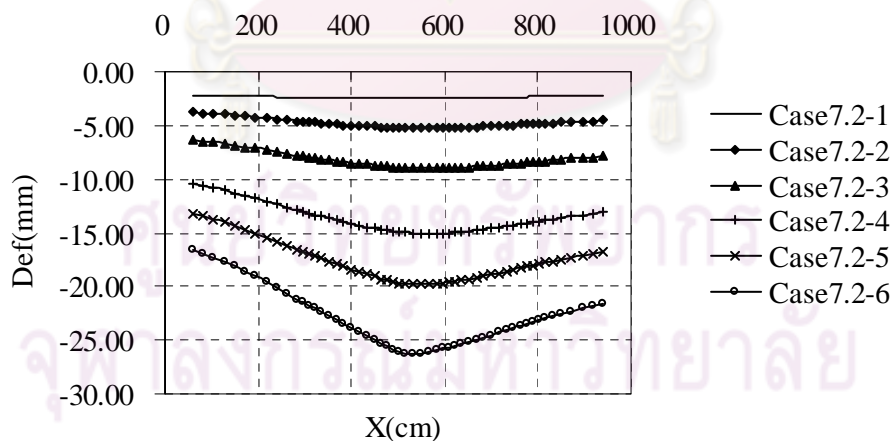
Figure 6.39 Transverse deflections at different load levels, case 7.2

Figure 6.39 needs to show the behavior of deflection at midspan section (section *D*) for different applied loads. The subscripts of line names are represented applied load levels: -1 =DL= 97,156.57 kg, -2 =(DL+TL)=149,556.57 kg, -3 =1.3(DL+TL(1+I)=214,671.54 kg, -4 = 256,751.50 kg, -5 = 292,519.50 kg, and -6 =

326,183.50 kg. It is seen that at the load up to 292,519.50 kg (Line case7.2-5), the deflections along transverse direction are smooth curves. After applied load is increased at about 326,183.50 kg (Line case7.2-6), the transverse deflection curves become sharp peak at the near bridge center and the deflections rate is increased as well. This may be that the bridge becomes failure at the mid point of the slab.

The strain distributions along bridge longitudinal axis (Z axis) at different section C, D, and E (see Figure 6.33 (b)) are also shown in Figure 6.40 at the applied load is approximated to 1.3DL +1.3TL(1+I). It is seen that the strain at section C (applied load point) is highest than other sections. This is also identical to simplify beam theory, the maximum internal force mostly occurred at the applied load section, while maximum deflection may occur at midspan section.
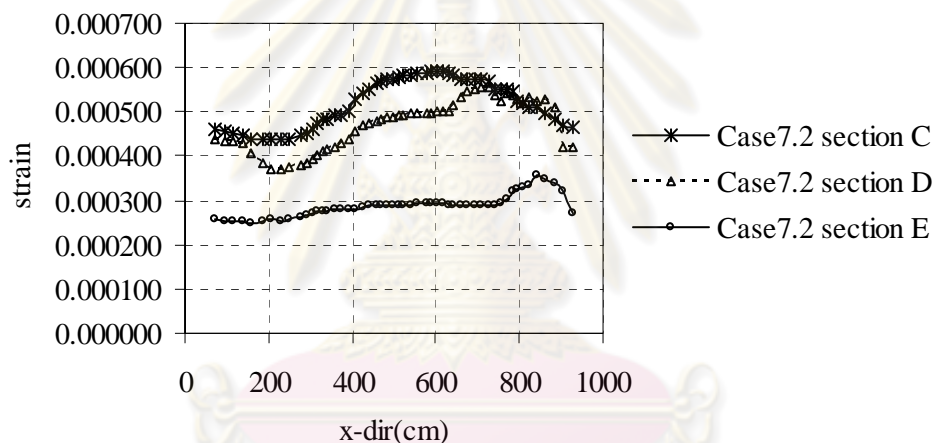
Figure 6.40 Strain distributions along Z axis at bridge bottom for different section at load 1.3DL+1.3TL(1+I)

The strain distribution along transverse axis (X axis) at sections C, D, and E, respectively are plotted in Figure 6.41. It is seen that the strain distribution along this direction at different bridge section are not much different. Maximum strain at all section is occurred at bridge center under applied load point, and the slab bridge tends to fail at the center.

Figure 6.42 presents the strain distribution through concrete slab depth at midpoint of section C (at point X= 495, Z=432) for different applies load level. The curves in this figure such as Case7.2-1, Case7.2-2, Case7.2-3, Case7.2-5 are representing for dead load (DL), dead load and live load (DL+TL), factored load

(1.3DL+1.3TL(1+I)), and yield point, respectively. It is seen that during service load (DL+TL) the strain distribution through slab depth are straight line, but at applied factored load strain distribution is not linear (Case7.2-3). At the applied load abourt 292,519.50 kg (Py), curve Case7.2-5, the strain is closed to yield strain of the reinforcement steel which yield strain of steel for this bridge is 0.0016 strains (1600 micro-strain). This strain distribution is also indicated that the bridge will be fail due to steel reinforcement, be cause the strain at top surface is still much less than that concrete crushing strain with about -0.003 strain (300 micro-strain).
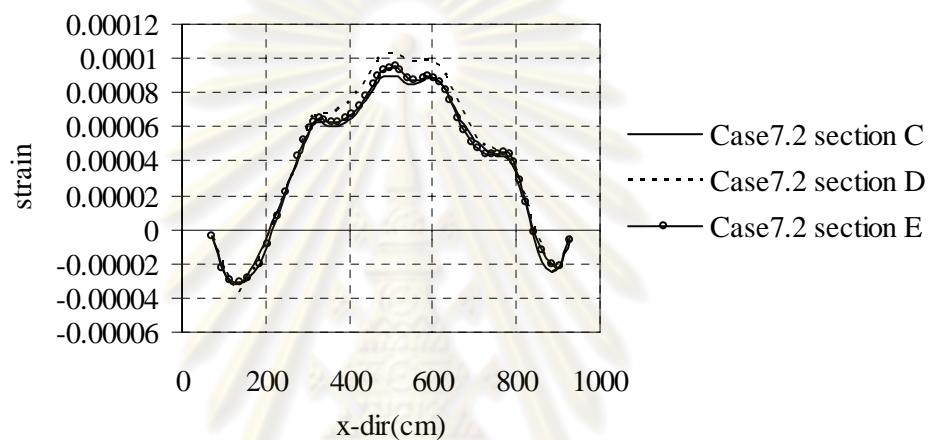
Figure 6.41 Strain distributions along X axis at bridge bottom for different section at load 1.3DL+1.3TL(1+I)
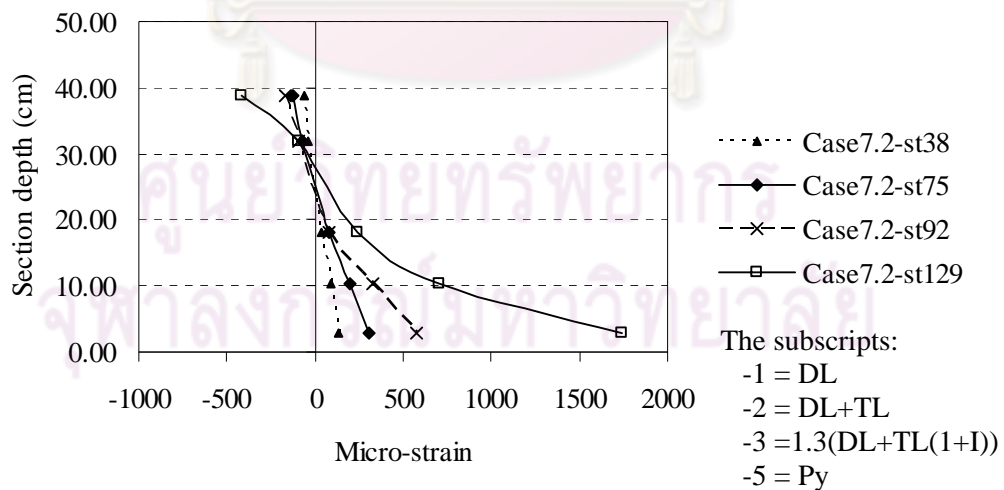
Figure 6.42 Strain distributions through slab depth

Figure 6.43 shows the longitudinal strain and transverse strain at mid point, Z(431) and X(495) at the bottom slab for case 7.2 (model included existing

flaw/crack). It is seen that strain along transverse direction is less than that strain along longitudinal directions of the slab bridge at the same applied load level. The slope of transverse strain curve is quite steep at the beginning of the applied loads and suddenly plateaus at higher load at about 380,000 kg. This due to that there is small steel ratio at transverse bridge. When the area of the concrete surrounding a reinforcing bar become large (small ratio of reinforcing bar volume to the concrete), the bar will be yielded sooner after concrete cracking since larger stress previously carried by concrete is immediately transferred to the bar (Maekawa et al., 2003).
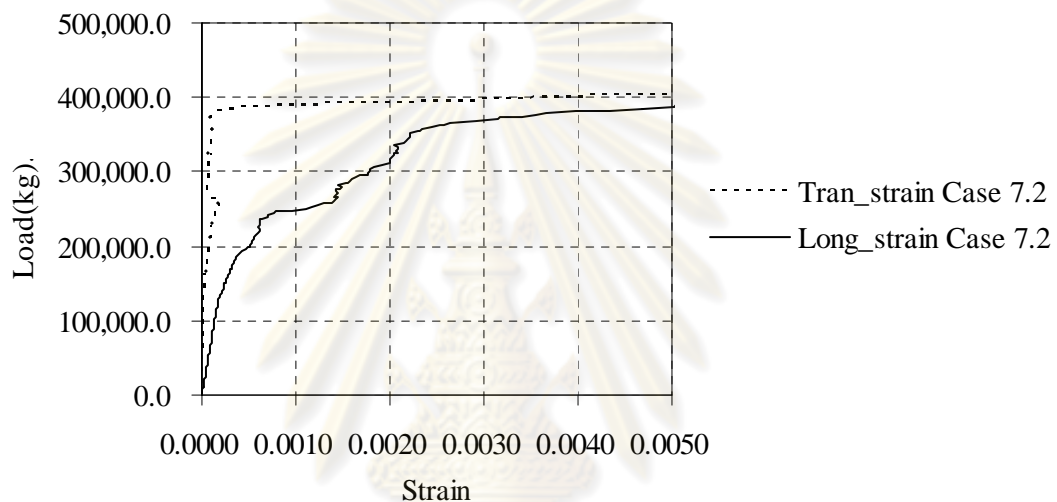
Figure 6.43 Load vs longitudinal strain and transverse strain

(5)Evaluation for rating factor (RF), CB7

According to Manual for condition evaluation of bridge of AASHTO, 1994, there are two level of the bridge capacity evaluation, inventory level and operating level. The Inventory level is for as design level, and the operating level is used for over weight permits checks. The equation for calculation rating factor is as Eq. (6.1). There are different between two evaluation level only the load and material factor.

Evaluation equation for bridge capacity of AASHTO:

As Eq.(6.1) can rewrite as

$$RF_{opr} = \frac{C - A_1 * DL}{A_2 * TL * (1+I)} \qquad .....(6.5)$$

The condition is that if $RF >= 1$, bridge will be safe

For the operating level:

A_1 = 1.3, factor for dead loads

A_2 = 1.3, factor for live load

$C = \phi*Rn$, capacity of the bridge element

ϕ = Strength reduction factor, 0.9 for bending moment, and 0.85 for shear force

Rn= Nominal bridge strength. This value may included damaged condition

DL = Dead load effect

I = Impact factor

TL = Truck load effect

For the inventory level:

The inventory level can be calculated as

$$RF_{(inv)} = \frac{3}{5} R_{(opr)} \qquad \text{.....(6.6)}$$

Where:

$RF(opr)$: Rating factor for operating level using above factors

$RF(ivn)$: Rating factor for inventory level

Using equation of AASHTO for NLFEM results

Using NLFEM results in this analysis, the concrete slab bridge capacity, C will be determined from the analysis results. The available results from analysis are applied load and average element strain. Therefore, the way to define value C is determined from total applied load that induces maximum strain at reinforcement location reached yielding strain of reinforcing bar. The total bridge capacity is considered to be the same as total applied load by $C=Py$, where Py is the total applied load (see Figure 6.43 and 6.44).
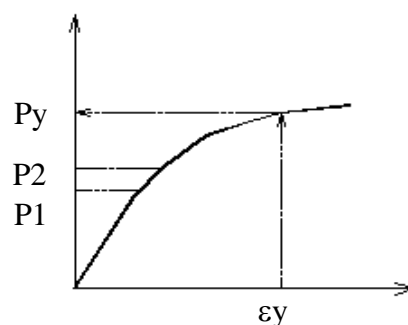
Figure 6.44 Results from NLFEM for evaluation bridge

From the Figure 6.44, and to accommodate with AASHTO formula, the bridge rating factor formula can be rewritten by.

$$RF = \frac{P_y - P1}{P2 - P1}$$ .....(6.7)

Where:

C = Py   correspond to εy
1.3*DL = P1
1.3*DL + 1.3*TL(1+0.3) = P2

The results for calculation rating factor of this bridge are summarized in the Table 6.6.1 below. In the table, the rating factor calculated by conventional method of AASHTO is also given to observe with proposed approach (see appendix-D for calculation procedure of conventional method). The rating factors of both operating level and inventory level from including crack model (Case 7.2) are less than that no any damage model (Case 7.1), but higher than conventional method. The conventional method is given inventory rating level (RF (inv)) less ten one; however, this method is could not realistic model of the bridge. From the results of case 7.2, RF (inv) is about 1.13; therefore it is still implied that bridge is still safe to the monitored truck.

Table 6.6.1 Rating factor for bridge CB7

No	P1	P2	Py	RF(opr)	RF(inv)
	kg	kg	kg		
Case 7.1	126,303.50	214,859.12	395,615.50	3.04	1.82
Case 7.2	126,303.50	214,859.12	292,519.50	1.88	1.13
AASHTO			250,797.69	1.60	0.90

7.2 Analysis for CB6

The bridge dimension and material parameters, the material model, the geometry model, and boundary condition of CB6 are also given in the section 6.2. The applied analysis load is also similar to bridge CB7. Therefore for the parameters of the bridge using in this section are referred to 6.2, and applied analysis load is referred to last example for CB7.

(1) Applied load

Dead load (DL): The applied dead loads are included main slab, and bridge curbs at the both edges of the bridge. The area dead load of main slab is 1,300 kg/m^2 and curb at the each bridge edge is 778.4. kg/m^2. Total dead load (DL) after multiplying to area is 106,488.06 kg, and the total factor load, 1.3DL is 138,434.48 kg. This dead load has than dived into 50 steps loads, with 2,768.69 kg for each step.

Truck load (TL): The applied truck load is also similar manner as previous example. The locations of applied truck axle loads are shown in the Figure 6.45. The load will be also further applied to ultimate load.

(2) Analysis case

Two cases have been analyzed for comparison the models of including crack and not including crack namely case 6.1 for no including crack model and case 6.2 for including existing cracks model.
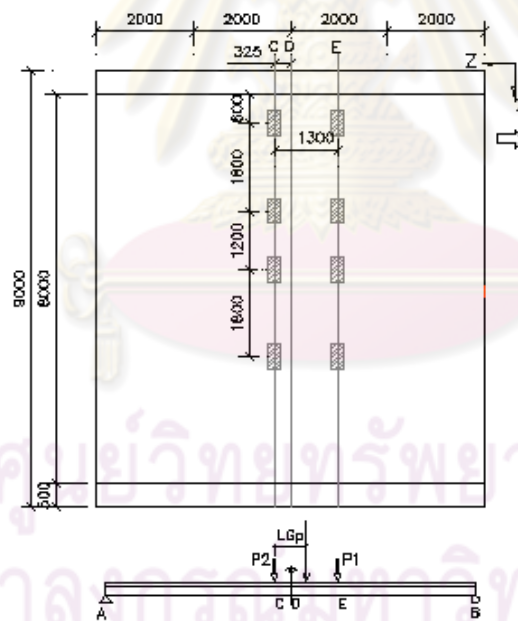
Figure 6.45 Bridge plan and position of truck axles for CB6

(3) Geometry mesh model of bridge CB7

The 3D bridge geometry model for analysis is also based on concept as explaining in the previous section. Both geometry models for case6.1 and case6.2 are the same as shown in Figure 6.46.
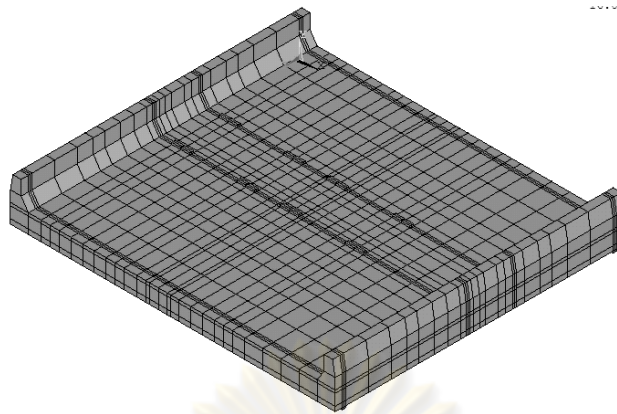
Figure 6.46 Geometry model for bridge CB6

(4) Analysis results

(4.1) Observe results
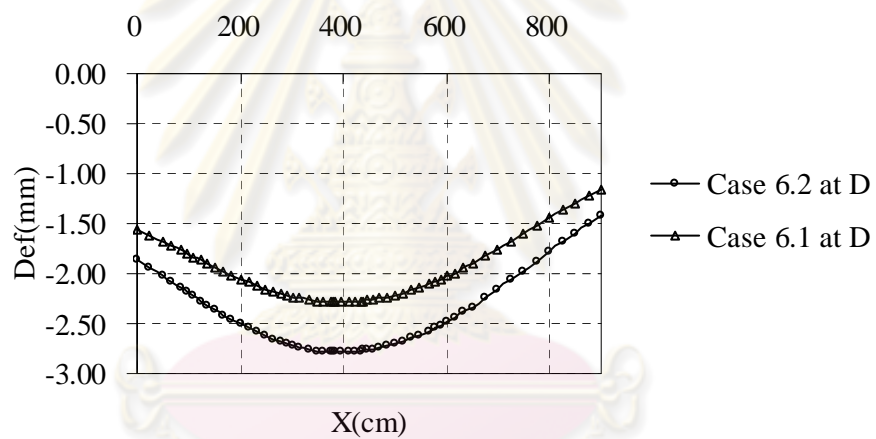
Figure 6.47(a) Transverse deflection for case 6.2 and case 6.1
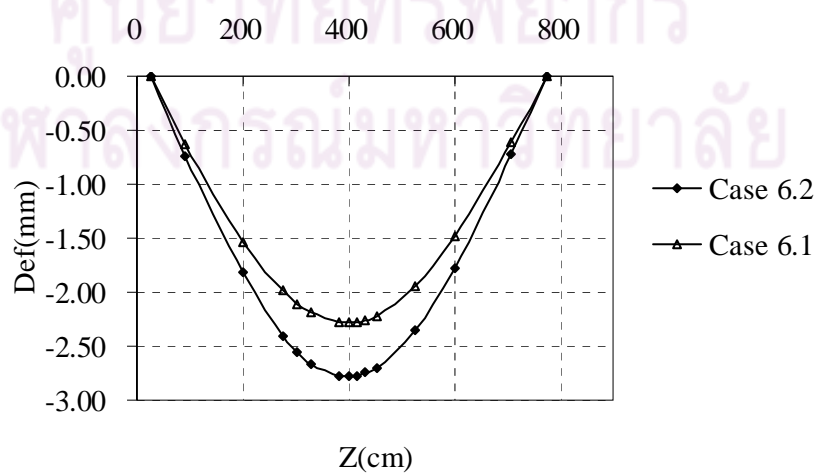
Figure 6.47(b) Longitudinal deflection for case 6.2 and case 6.1

The results from analyses for case 6.2 (including existed cracks model) and case 6.1 (no existing crack model) are observed in this section. The same manner as CB7 that the result of deflection of case 6.2 is higher than results of case 6.1 as shown in the Figure 6.47 (a) and Figure 6.47 (b) for transverse and longitudinal deflections at service load level (DL+TL). The results between these models are different about 17%. This is not much different, because due to that this bridge is still in the good condition, the main slab bridge is still very stiff as explaining in the section 6.2. At the transverse direction Figure 6.47 (a), the maximum values are obviously at the bridge center, this may be due to that the bridge curbs at bridge both sides are solid and very stiff. It is normally for longitudinal direction, Figure 6.47 (b), the maximum deflection is at the midspan of the bridge.

The applied load versus deflection at the slab mid point (Z=400 cm and X= 380 cm) for case 6.2 and case 6.1 are shown in the Figure 6.48. Similar explanation as previous example, deflection case 6.2 is higher than case 6.1 about 17%. This is due to that cracks at the bottom slab may reduce the stiffness of the bridge structure. Therefore, the existing crack is vital for NLFEM for analysis old concrete structure. This effect may influence since small applied load to failure load.
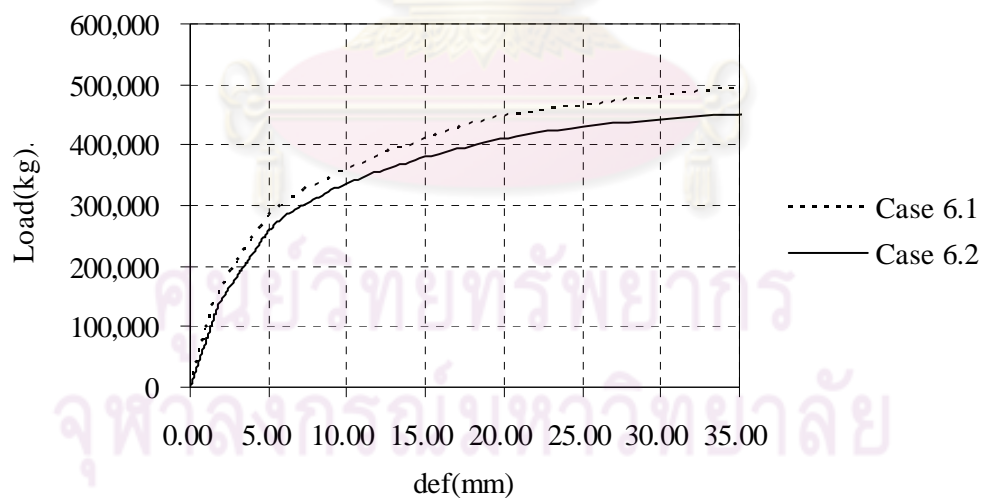
Figure 6.48 Load vs deflection for case 6.2 and case 6.1

Figure 6.49 (a) and (b) show the applied load versus strain of element at mid point of the bridge. Figure 6.49 (a) are plotted the applied load versus longitudinal stains at bridge mid point (Z=431. X=370, using this point to present, because this is critical point). The same as deflection, the analysis strain result from case 6.2 is

higher than that the strain result from case 6.1 for the same applied load level. It is seen that the longitudinal strain of both cases are not obviously yield, this may be due to that the yield strain is occurred at the transverse direction as shown in the Figure 6.49 (b), load versus longitudinal strain and transverse strain of case 6.2 and case 6.1. The curbs of transverse strain for both cases are plateau since the longitudinal strain of case 6.2 are still increase. The curve of transverse stain for case 6.2 become plateau suddenly when applied load is about 300,000 kg, while case 6.1 become plateau at applied load bout 400,000 kg. The suddenly plateau of the curves for load versus strain is due to that the reinforcement ratio to the concrete area in the direction is very small (Maekawa et al, 2003).
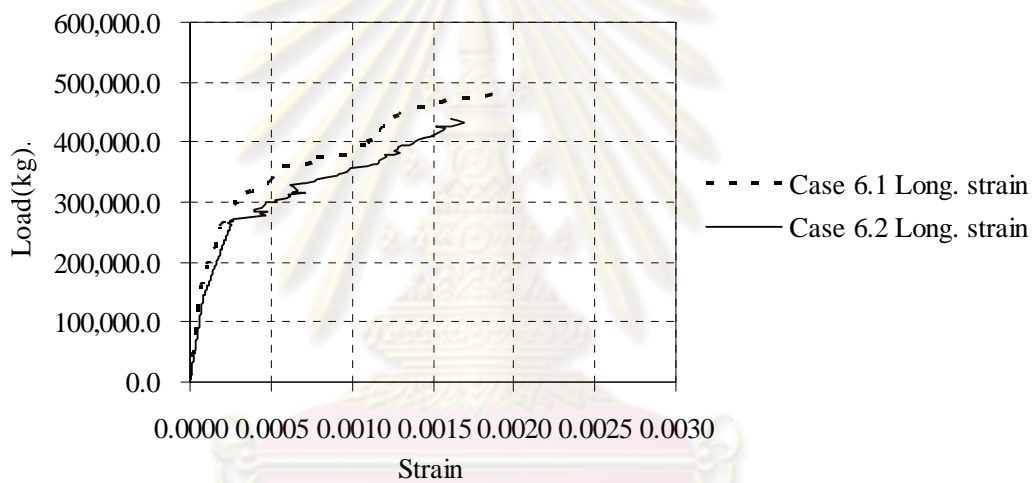
Figure 6.49(a) Longitudinal strain for case 6.2 and case 6.1
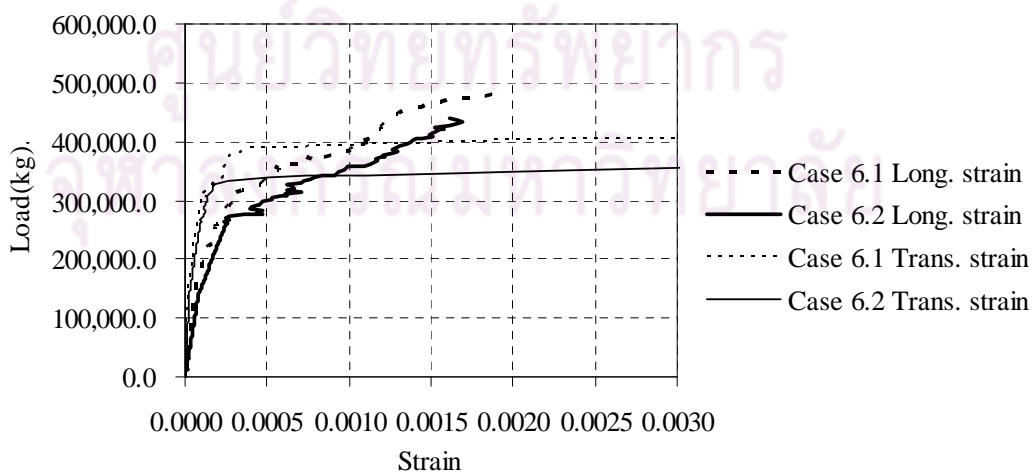
Figure 6.49(b) Load vs longitudinal strain of case 6.2, and transverse strain of case 6.2 and case 6.1

Figure 6.50 shows the different analysis load level for case 6.2. It is seen that at the lower load applied load which applied load equal to LP1=1.3DL+1.3TL(1+I), the transverse curve is very smooth (Line case 6.2-LP1). After applied is increase (LP2 = 346,204.5 kg), the maximum transverse deflection is obviously at near the bridge mid point (Line case 6.2-LP2). When applied load is continued to increase (with LP3=414,584.5 kg), the transverse deflection become sharp peak at mid point of the slab (Z=400 cm, X= 383 cm). From these figures (Figure 6.50 and Figure 6.49(b)), it may evident that bridge is fail at transverse direction. This due to this direction has small reinforcement ratio, and bridge curbs is very stiff, slab bridge behaves unlikely one way RC slab.
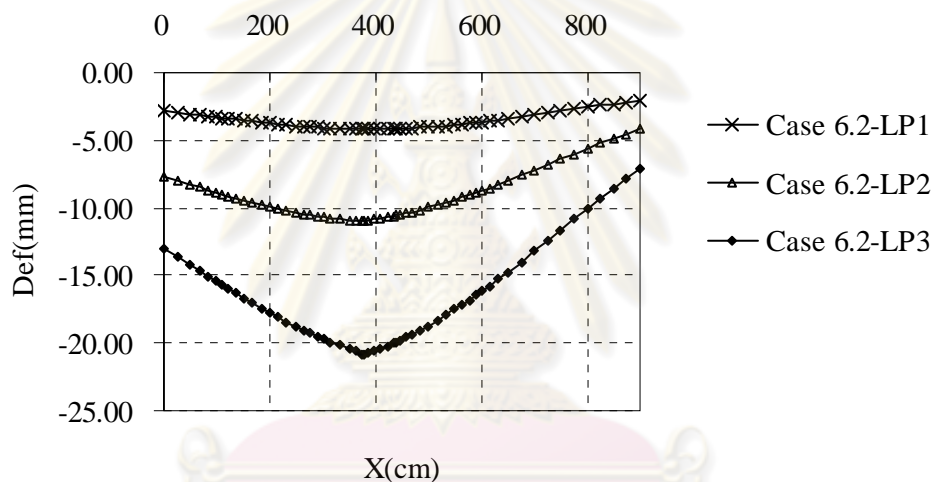
Figure 6.50 Transverse deflections at different load levels, case 7.2

(5)Evaluation for rating factor (RF), CB6

Due to analysis results of this bridge, the yield strain is not obvious in the longitudinal direction, but is seen in the transverse direction. Therefore the bridge capacity will be implied from transverse strain as shown in the Figure 6.51 below. In this figure also shows the applied load level similar to applied load for CB7, with P1 (1.3DL), P2 (1.3DL+1.3TL(1+0.3)) and Pul (Ultimate load calculated by simplify beam theory) (see these value in the Table 6.6.2)

After the load factor and bridge capacity have been determined, rating factors are calculated similar to the previous example, the calculation results then are summarized in the Table 6.6.2 below. The RF for case 6.1 are 2.94 and 1.76 for operating and inventory levels, respectively. The RF for case 6.2 are 2.35 and 1.41

for operating and inventory levels, respectively. It is seen that the model which included cracks gives RF less than that no crack included model and higher than conventional method. Even though the rating factor is calculated according to transverse strain; however it still gives the results higher than that simplify analysis. It is implied that the bridge is still safe for maximum monitoring truck data.
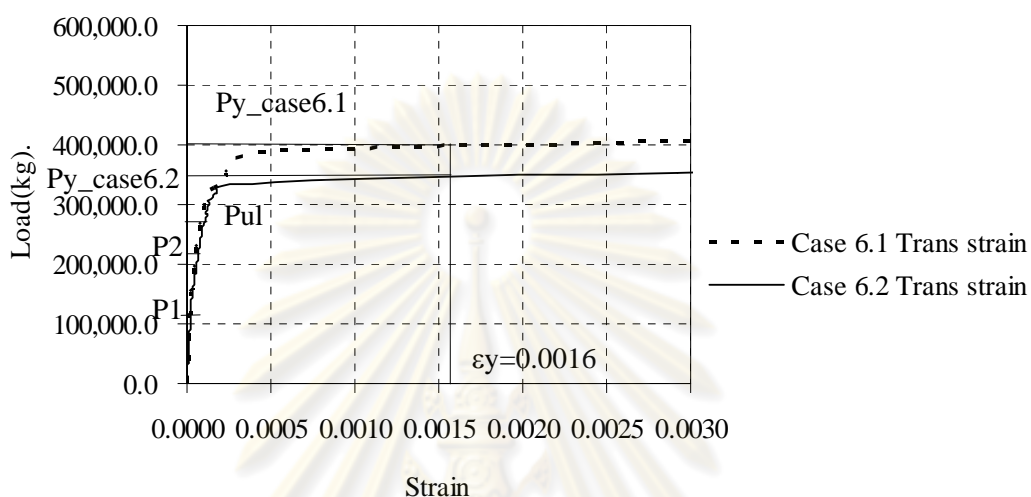
Figure 6.51 Load vs transverse strain of case 6.2 and case 6.1 for considering bridge capacity

Table 6.6.2 rating factor for bridge CB6

No	P1	P2	Py	RF(opr)	RF(inv)
	kg	kg	kg		
Case 6.1	138,434.48	226,990.48	398,804.50	2.94	1.76
Case 6.2	138,434.48	226,990.48	346,204.50	2.35	1.41
AASHTO			271,323.97	1.76	1.06

The full analyses for bridge CB7 and CB6 have been conducted in this section, the results from the proposed model (including exiting crack for analysis old concrete bridge), deflection and strain measurement are higher than those from general NLFEM model. This is identical to structure theory that when cracks present in RC member the moment inertia of section or stiffness of the member may be reduced. The capacities of the bridges have been evaluated based on analysis results. Both bridges have rating factor higher than one and higher than conventional method of AASHTO, which *RF(inv)* are 1.13 and 1.4 for CB7 and CB6 respectively. The conventional method could not model actual bridge. Therefore according to proposed

approach, these bridges are safe for truck load from monitoring data. The response in transverse direction is also important for failure behaviour of the bridge, especially solid parapet type. The curbs or parapets at edges of the slab bridge may act as supported beam for the slab leading to fail at direction of small reinforcement such as bridge CB6.

6.8 Observing NLFEM results to beam theory results for different fc'

As known that the important parameters for mechanical property of the concrete are compressive strength, *fc'*, modulus of elasticity, *Ec*, and tension strength or rupture strength (*ft* or *fr*). However, many research accepted that *Ec*, and *fr* can be interpreted by *fc'* as shown in Eq. (5.1) and (5.5). Therefore in this section will present the influence of different value of *fc'* for both NLFEM and simplify beam theory method.

6.8.1 Observing the results of bridge CB7

In this section, the bridge CB7 will be calculated due to beam theory method to observe influence of fc' value, and the beam theory results will be also observed to NLFEM. Therefore all bridge parameters are the same as presented in the section 6.6.1; however only that some analysis cases in this section will change fc' value.

(1) Assumption

Due to two states of uncrack and crack sections from beam theory will be calculated to observe bridge behaviour; therefore the results of NLFEM as case 7.1 at above will be brought to compare with this beam theory method. The conventional method for analysis concrete slab bridge behaviour is that slab bridge will be implied as beam with one meter in width, which the applied loads (DL and TL) can be used as equivalent width from of AASHTO. To observe the results to NLFEM, therefore the applied load for beam theory is similar as load that applied to NLFEM model which truck load (TL) is similar to TR-05 and further applied up to ultimate load.
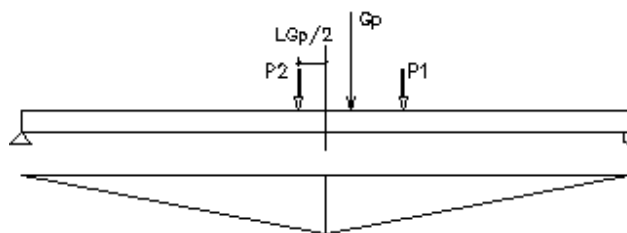
Figure 6.52 Applied truck load for beam theory method

(2) Analysis case

To observe the influence of fc' value, two different values of fc' will be used to compare the results. For beam theory method analysis cases are case BT.1 for fc'= 195 ksc, and case BT.2 for the fc'= 260.5 ksc. And NLFEM are case 7.1 for fc'= 195 ksc, and case 7.12 for fc'= 206.5 ksc, respectively. The model of case 7.12 is similar to that case 7.1, but it is different only fc' value. For the calculation detail using beam theory is given in appendix-D.

(3) Analysis results for different value of fc' for beam theory method and NLFEM

The result of load and defection curve for the case BT.1 and case BT.2 are shown in Figure 6.53. In the figure, it is also indicating the applied load level such as P11 = DL+TL =149,556.54 kg, P2 = 1.3DL+1.3TL(1+I) =214,856.50 kg, and Pul=250,797.69 kg for fc'=195ksc. Where Pul is ultimate load calculated by beam theory (see appendix-D), and the value of fc' is not influence to Pul because ultimate capacity of beam section depending on steel reinforcement. The deflection case BT.1 are higher than case BT.2 such as at beginning of applied load up to P11, about 12%; at P2 about 10%, and at Pul about 7.5%. This indicated that when applied load is increased, the effect of fc' is less important for beam theory method.
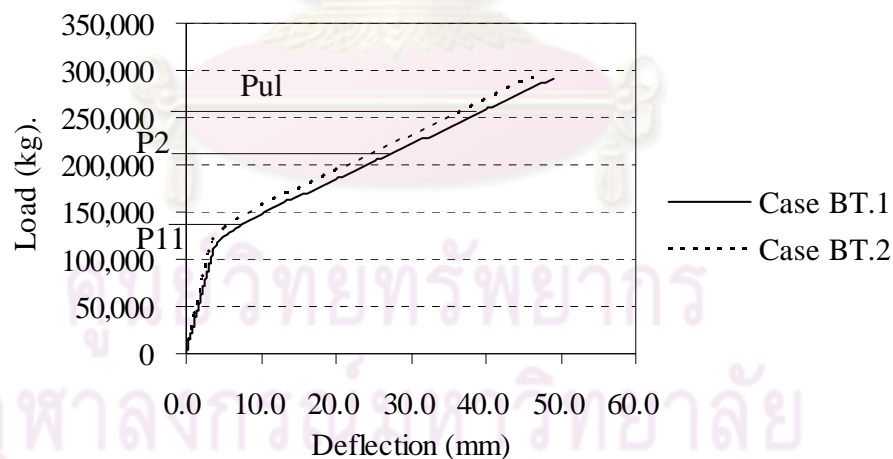
Figure 6.53 Applied load vs deflection curves for case BT.1 and BT.2

Figure 6.54 shows the stain at the steel level for calculation case BT.1 and BT.2. It is seen that at the uncrack state (the applied load induces moment less than cracking moment) the strain case BT.1 are higher than case BT.2 about 11%, at the crack state, the strain case BT.1 are differed case BT.2 only 0.75%. This due to that

from the conventional beam theory, at crack section the concrete at tension zone is not considered.
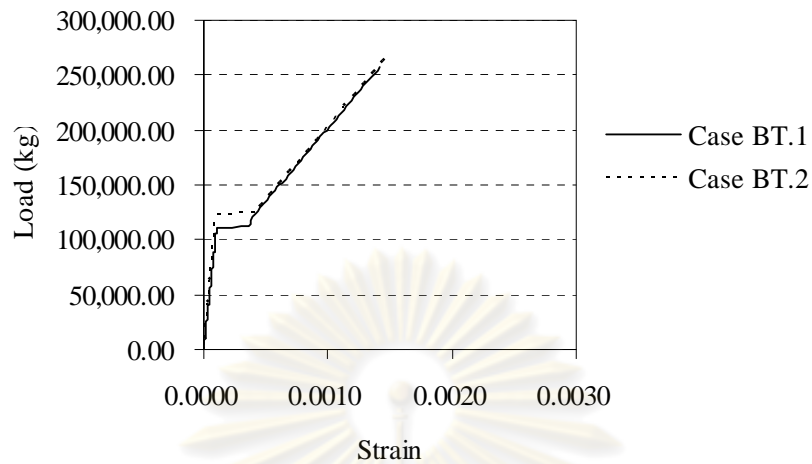
Figure 6.54 Applied load vs strain at steel level for case BT.1 and BT.2

The influence of fc' for NLFEM are shown in Figure 6.55 and 6.56 for load-deflection and load-train curves, respectively. The load and deflection for case 7.1 is higher than case 7.12 about 8% through the applied load. This due to that NLFEM is accounting for concrete as tension stiffening effect at crack section; therefore even crack occurred, concrete strength still influence to the stiffness of element at tension zone.
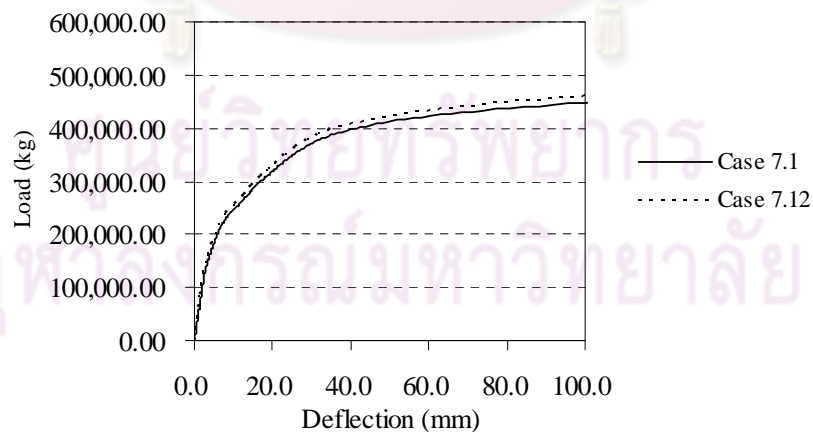
Figure 6.55 Applied load vs deflection curves for case 7.1 and 7.12

The results of the strain at the steel reinforcement level of NLFEM also has similar manner as deflection, the strain results from case 7.1 is higher than case 7.12

(see Figure 6.56). At the applied load less than 149,556.54 (P11), results case 7.1 is higher than case 7.12 about 8% ; after load higher than 214,856.50 (P2), results case 7.1 is higher than case 7.12 about 12%; and at the applied load about 350,000 kg, results case 7.1 is higher than case 7.12 about 17%. It seen that results case 7.1 is still differed than case 7.12 at higher load. The Py_case 7.1 and Py_case 7.12 are 395,615.50 kg, and 421,611.50 kg, respectively. This because the manner of the NLFEM is that even crack occurred, the effect of tension stiffening due to tension strength of concrete is still accounted and it will be gradually reduced. Unlike conventional beam theory, once section is crack, concrete at tension region is neglected; therefore in crack section of beam theory, the strains at the steel level are not influenced by value of fc'.
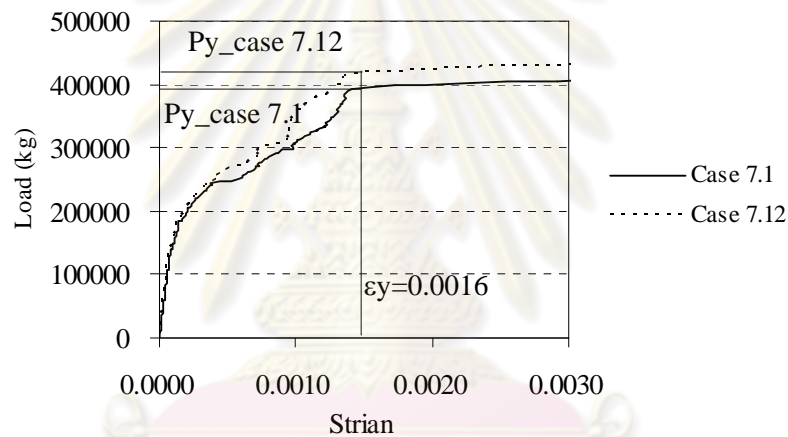
Figure 6.56 Applied load vs strain at reinforcement level for case 7.1 and 7.12

(3) Observing result for beam theory method and NLFEM
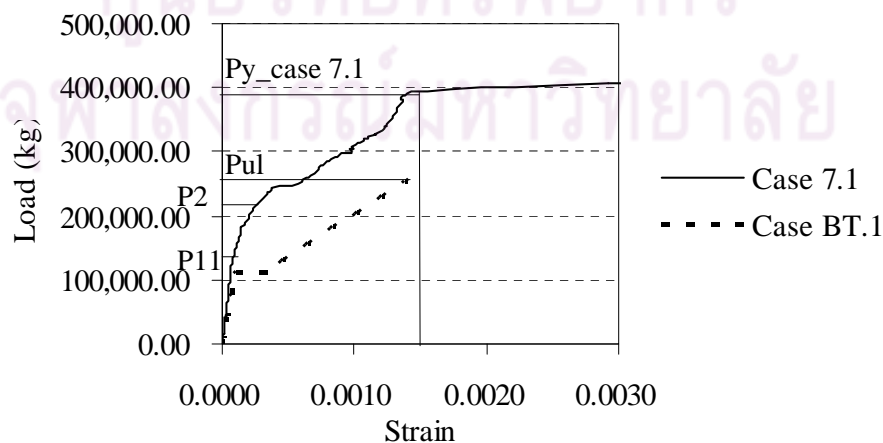
Figure 6.57 Applied load vs strain at reinforcement level for case 7.1 and BT.1

Figure 6.57 shows the comparison of beam theory method and NLFEM for strain at the reinforcement level. At the beginning of the load (uncrack section for beam theory), the strain results from beam theory is higher than that results of NLFEM about 35%; 80%, and 55% at applied load of P11, P2, and Pul, respectively. This because after bending moment reached cracking moment, the crack section is used for conventional beam theory; while tension stiffening effect is still accounted to carry tensile force and gradually reduced for NLFEM. Other reason is the geometry model which geometry model for NLFEM in this study is accounted all part of bridge such as bridge curbs is assumed full composite with main slab. Using this assumption, because this bridge has been checked and met the ACI requirement for composite concrete beam section 17.5.3.

a) Strain at applied load P_DL

b) Strain at applied load P2

c) Strain at applied load reach εy
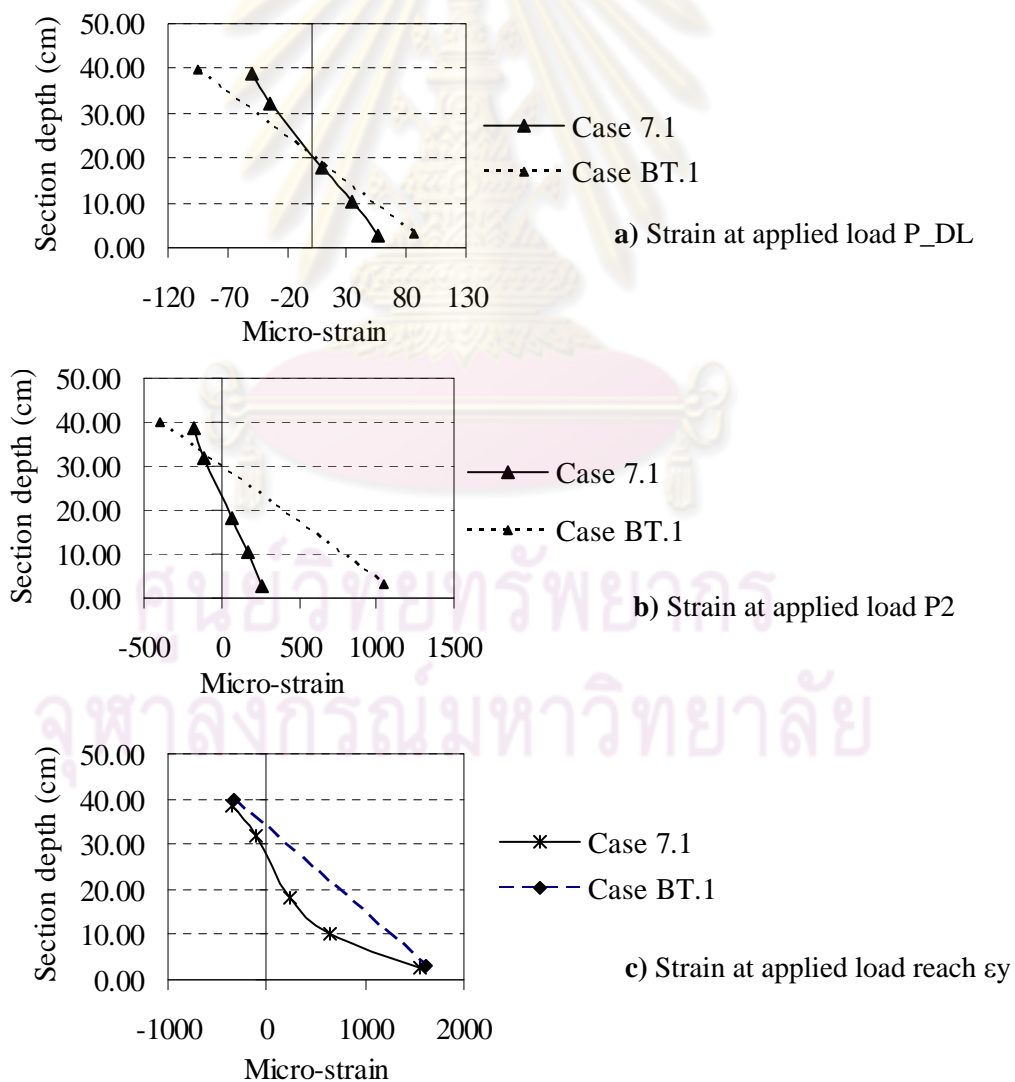
Figure 6.58 Strain distribution at different load levels for case 7.1 and BT.1

The strain distributions through the depth of the slab bridge for beam theory method and NLFEM are shown in Figure 6.58. Figure 6.58 (a), (b), and (c) are strain distribution due to different applied load level of P_DL (Dead load only and in uncrack section), P2 (1.3DL+1.3TL(1+I), and at strain at steel reinforcement reached yield strain, respectively. For the all applied load levels, the strain due to beam theory method are higher than that NLFEM, i.e. strain at the steel level of case BT.1 (beam theory method) is higher than case 7.1 (NLFEM) about 35%, and 80% at applied load of P_DL (Figure 6.58 (a)) and P2 (Figure 6.58 (b)), respectively.   In Figure 6.58 (a), it is seen that the neutral axis depth from both cases are very closed to each other with 23.8 cm and 24 cm for case BT.1 and case 7.1, respectively. This may be that the section is still in uncrack state. However, when load is increased up to P2 (Figure 6.58 (b)), the neutral axis depth of case BT.1 is much less than case 7.1 with about 14.72 cm and 21 cm for case BT.1 and case 7.1, respectively.

At the strain reach yield strain of the steel (Figure 6.58 (c)), it is seen that the distribution strain of case BT.1 is linear and the neutral axis is reduced with about 10.14 cm, while strain distribution of case 7.1 is nonlinear, and neutral axis is higher than case BT.1. This is due to that concrete at tension zone of section still remains the tension stiffening effect, concrete at tension region still can carry small tension force.

6.8.2 Observing the results of bridge CB6

In this section, the bridge CB6 will be calculated due to beam theory to observe different value of fc', and the beam theory results will be also observed to NLFEM model. The detail and procedure of calculation is similar to CB7. Two different values of fc' will be used such as fc'_1=204 ksc, and fc'_2=367 ksc.

(1) Assumption

For beam theory method, slab bridge is assumed as simply supported beam with one meter in width, which the applied loads (DL and TL) will be used from equivalent width of AASHTO as explaining in the last example. For NLFEM is also refer to section 6.7.2 as case 7.1; however two different value of fc'_1 and fc'_1 are used to compare the results.

(2) Analysis case

Similar to last example of CB7, beam theory method analysis cases are case BT6.1 for fc'= 204 ksc, and case BT6.2 for the fc'= 367 ksc. And NLFEM are case 6.1 for fc'= 204 ksc, and case 6.12 for fc'= 206.5 ksc, respectively.

(3) Analysis results for different value of fc' for beam theory method and NLFEM

The result of load and defection curve for the case BT6.1 and case BT6.2 are shown in Figure 6.59. In the figure is also indicating the applied load level such as P11 = DL+TL =158,888.06 kg, P2 = 1.3DL+1.3TL(1+0.3) =226,990.48 kg, and Pul=271,323.97 kg (Pul is ultimate applied load calculated by beam theory, see appendix-D). The deflection case BT6.1 are higher than case BT6.2 such as at beginning of applied load up to P11, about 22%; at P2 about 19%, and at Pul about 13%. This indicated that when applied load is increased, the effect of fc' is less influence to the beam deflection.
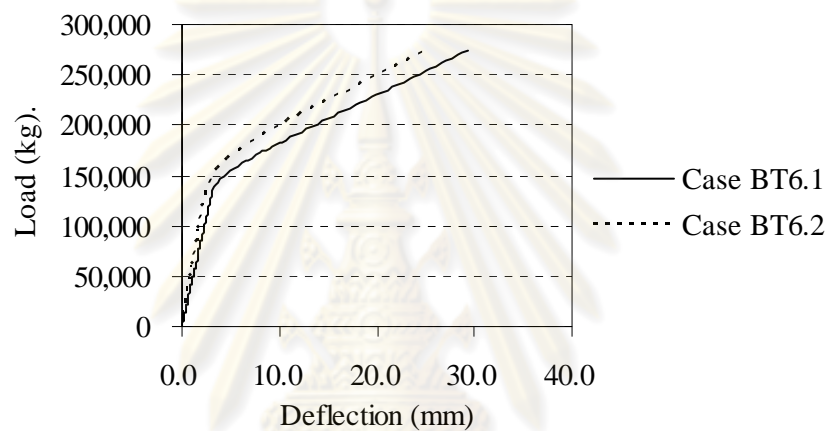
Figure 6.59 Applied load vs deflection curves for case BT6.1 and BT6.2
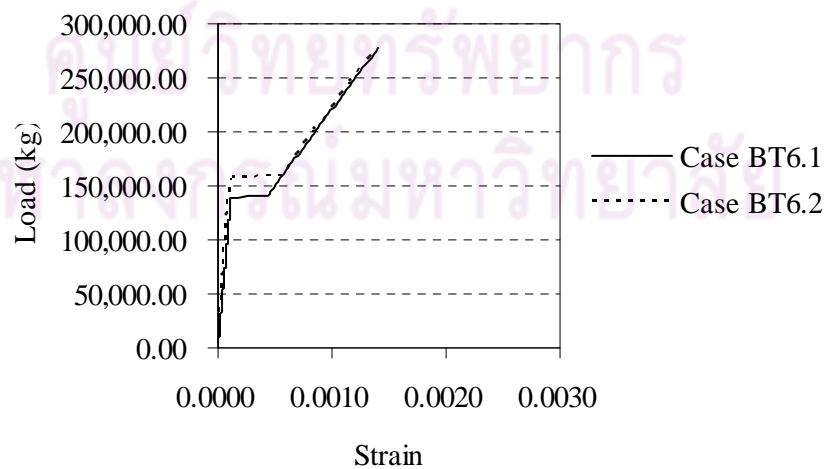
Figure 6.60 Applied load vs strain at steel level for case BT6.1 and B6T.2

Figure 6.60 shows the stain at the steel level for calculation case BT6.1 and BT6.2. Similar to example of CB7 that results of case BT6.1 are higher than case BT6.2 about 21% and 1.34% for uncrack section state and crack section state, respectively. The fc' less important to strain at still level when section occurs cracking.

The influence of fc' for NLFEM are shown in Figure 6.61 and 6.62 for load-deflection and load-train curves, respectively. The load and deflection for case 6.1 is higher than case 6.12 about 17% at applied up to about P11, and about 20% at about Pul. This is indicated that higher fc' will be higher tension strength of concrete as well which leading to increase tension stiffening; therefore even crack occurred, concrete strength still has influence to result of NLFEM.
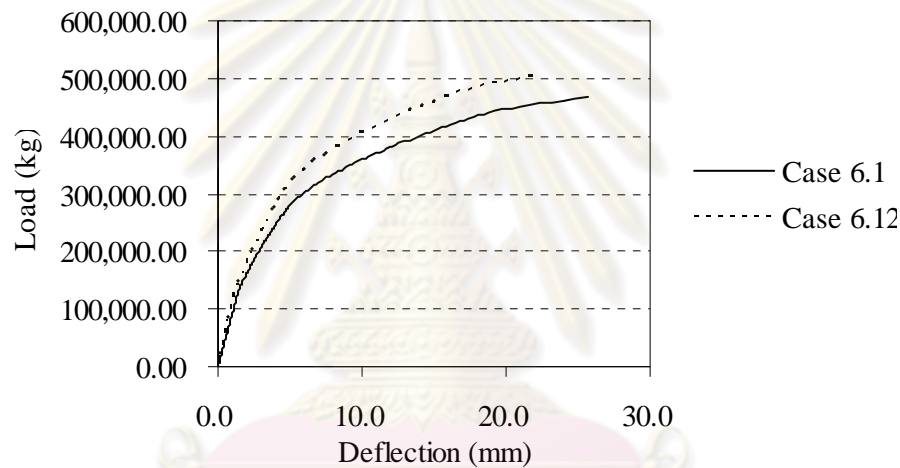
Figure 6.61 Applied load vs deflection curves for case 6.1 and 6.12

The results of strain at the steel reinforcement level (Figure 6.62) for different concrete strength of NLFEM also has similar manner to previous example. At the applied load less than P11, results case 6.1 is higher than case 6.12 about 15%; after load higher than 226,990.48 (P2), results case 6.1 is higher than case 6.12 about 20%; and at the applied load about 271,323.97 kg (Pul), results case 6.1 is higher than case 6.12 about 24%. As explaining that the NLFEM is accounting for tension strength of concrete as tension stiffening effect, the concrete strength is still influence to strain of element even cracking occurred. The yield state is not obvious in this figure, because the bridge is fail due to reinforcement at transverse direction as explaining at section 6.7.2.
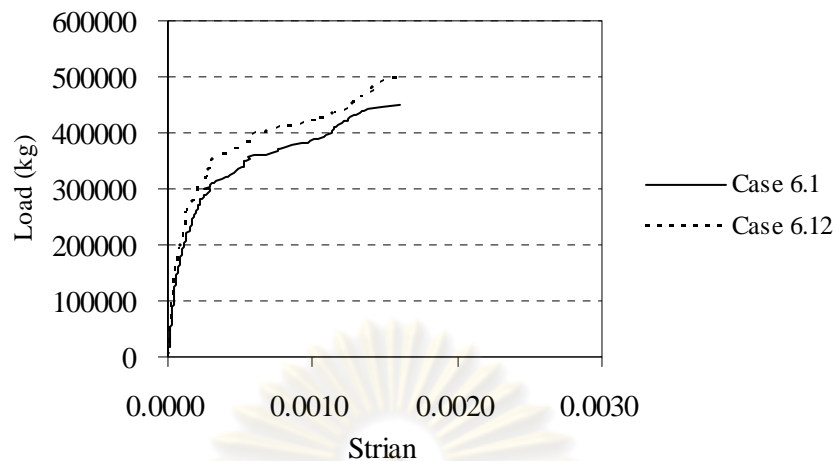
Figure 6.62 Applied load vs strain at steel level for case 6.1 and 6.12

(3) Observing result for beam theory method and NLFEM
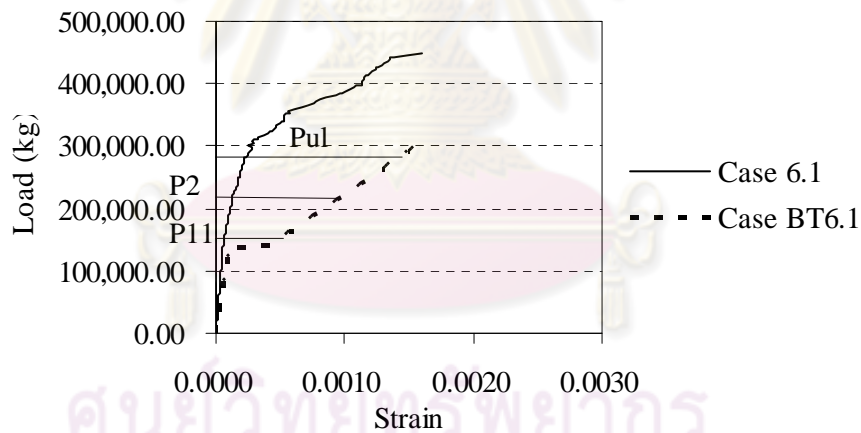
Figure 6.63 Applied load vs strain at reinforcement level for case 6.1 and BT6.1

Figure 6.63 shows the comparison of beam theory method and NLFEM for strain at the reinforcement level. At the beginning of the load (uncrack section for beam theory), the strain results from beam theory is higher than that results of NLFEM about 55%; and 87%, at applied load of P11, and Pul, respectively. This because after bending moment reached cracking moment, the crack section is used for conventional beam theory and concrete part at tension region is neglected. The beam theory method is also analyzed by 1D simple supported beam. While NLFEM is

accounting to the concrete tension strength as tension stiffening effect, and geometry model for 3D NLFEM in this study is included all parts of the bridge such as bridge curbs. Therefore the results from NLFEM are much less than those the beam theory method.

a) Strain at applied load P_DL

b) Strain at applied load P2

c) Strain at applied load reach ey
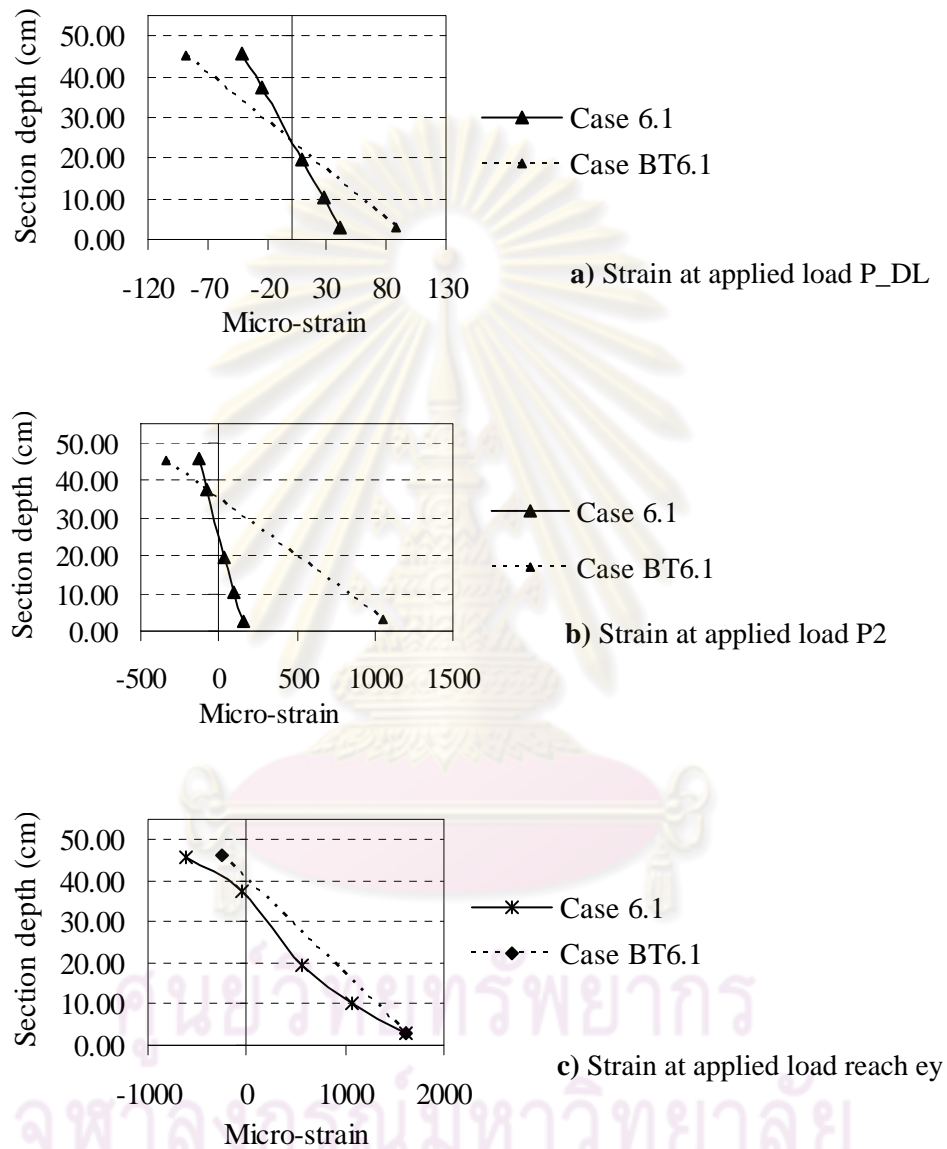
Figure 6.64 Strain distribution at different load levels for case 7.1 and BT.1

The strain distributions through the depth of the slab bridge for beam theory method and NLFEM are shown in Figure 6.64 which Figure 6.64 (a), (b), and (c) are strain distribution due to different applied load level of P_DL (Dead load only and in

uncrack section), at P2 (1.3DL+1.3TL(1+I), and at strain at steel reinforcement level reached yield strain, respectively. These results are similar to CB7 that strain distribution due to beam theory is much differed from NLFEM, and only that at low applied load (Figure 6.64 (a)) the neutral axis from beam theory is closed to neutral axis from NLFEM results. For higher applied load, the neutral axes from beam theory are higher from NLFEM.

It is seen that the different values of fc' is also influence to deflection of concrete structure. For beam theory, this effect is important at small applied load. However, the value of fc' is less important for crack section of beam theory method. For NLFEM, the fc' is important to behavior of the concrete structure since small to higher applied loads, because the effect of tension stiffening depending mainly on tension strength of the concrete which interpreted from fc'. The NLFEM can present concrete slab behavior very well, at uncrack section state the neutral axis from NLFEM is very closed to neutral axis from beam theory. However when crack occurred, the neutral axis from both are different from each other, because beam theory method neglect concrete section at tension zone.

6.9 Conclusion

This chapter is applied from the chapter 5 by application the softening and tension stiffening models with account for existing flaw/crack to apply analysis full scale bridge structure. The purpose is to verify that the proposed model approach which accounted for existing flaw/crack in this study can be used to assessment performance of existing concrete structure.

The old existing concrete bridge are not the same as new concrete condition, the flaw/crack are generally existed. This effect will be influence the concrete structure performance, especially at the service load. There are many NLFEM program has been developed in the worldwide, but most of the models do not account for existing flaw/crack in old RC structure. Therefore, the main purpose in this section is that the existing flaw/cracks at tension region of old bridge structure are considered using 3D NLFEM. The COD and RED element together with their constitutive models, softening model and tension stiffening model for existing flaw/crack which derived in chapter 5 are used for elements at flaw/crack vicinities in existing concrete bridge. Using these models, the effect of softening and tension stiffening in the

normal direction of crack will be reduced. The cracks consider in this study are visible crack and theoretical crack. The visible crack is taken from crack mapping during bridge inspection. Normally the small cracks are difficult to observe during inspection, moreover some cracks may close when no applied load. If it is the structure crack, even fine crack it will influence to concrete behavior. Therefore the theoretical crack has been assumed for representing invisible crack during inspection.

Three concrete slab bridges, standard types in Thailand namely CB7, CB6, CB4S are taken to be example study. Many cases have been analyzed to compare to each other and testing results. The analysis cases are included general NLFEM case (no crack included) for all bridge, visible crack included case for CB7, theoretical and visible cracks included case for CB7 and CB6, and only theoretical crack included case for CB4S (because there is no crack mapping for this bridge). The results of general NLFEM at the critical point (applied loaded point) are much less than that testing results for both deflection (differed up to 30 %, CB7) and strain at the steel level (differed up to more than 55%, CB7). While the proposed model which included theoretical and visible crack case gives every satisfied results. At the same poison (applied loaded point) the deflection differs to testing only 5%, and strain at the steel level is differed from testing result only 7%. This due to the cracks have been occurred in old reinforced concrete bridge structures, the tension stiffening effect is reduced promotional to flaw/crack, and the proposed model can present more closely to real behaviour of the actual bridge structure.

The propose model can be proved that at service load, the analysis results are closed to testing results while general NLFEM model are not. Even though there is effect of transverse stiffness distribution that makes some analysis results of proposed NLFEM at opposite applied load lane are not matched that testing results. But analysis results of proposed model at this positions are higher than those testing results. If this effect is neglected, it is still in safe condition for assessment of bridges.

Two type of the concrete slab bridge have been analyzed using maximum truck load from monitored data in Chapter 4 and load further up to ultimate load. The behaviour and capacity of the bridges can be obtained based on NLFEM results. Both bridges have rating factor for inventory level higher than one and higher than conventional method of AASHTO. Therefore, these bridges are safe for truck load from monitoring data. The crack in concrete slab bridge is influent not only at the low

applied load (service load) but also at the higher loads. The global stiffness of the bridge structure may reduce due to existing crack leading to bridge being lower capacity. The concrete slab bridge may not has behaviour like one way concrete slab, especially when there are solid curbs or parapets at bridge edges. Such as bridge CB6, the bridge may fail at the transverse reinforcement, while longitudinal reinforcement does not yet reach yield point.

In this chapter, the effect of different values of fc' is also study for the concrete slab bridge using beam theory method (For applied load distribution is using AASHTO equivalent width method), and NLFEM. For beam theory method, fc' value is important at small applied load, but less important at higher load or when crack section is used, especially strains at the reinforcement level are not much change among difference of fc' values. For NLFEM, different values of fc' has effect to behavior of the concrete structure since small to higher applied load for both deflection and strain at the steel reinforcement level. This effect is implied that tension stiffening model effect is also influent from value of fc', which fc' is increased leading to increase concrete tension strength as well. In this section, the results from beam theory method are also observed to NLFEM results. At the beginning of applied load (assume uncrack section), the results from beam theory are higher the results from NLFEM about 36%; however, when applied load increase (crack section assumed for beam theory), the results of beam theory are very much higher than those results of NLFEM. The NLFEM can present more reality behavior of concrete slab bridge very well. Therefore, if the result of beam theory is not satisfied or more completed behavior of concrete slab bridge is needed, the NLFEM should be used.

CHAPTER VII

CONCLUSION AND RECOMMENDATION

7.1 Discussion and Conclusions

Dealing with existing structure is more difficult than design new structures, especially existing concrete structure such as bridges. The first difficulty is the uncertainly of the applied loading, and the second is actual structure condition (damage condition and material properties), i.e. presented truck loading may be higher than previous truck; material properties are altered with time and environment of the bridge location. This research has been studied into two major parts, the first part is about development of truck loading monitoring system based on B-WIM algorithm to record actual truck configuration and load, and the second part is studying about the method for analysis diagnosis existing concrete bridge structure using 3D NLFEM which actual existed damaged such as flaw/cracks can be accounted. Many advantages and difficulties have been found. The discussion and conclusion for these study are summarized in the below.

7.1.1 Discussion

Truck loading monitoring system

The system can estimate truck parameters well for one truck on the bridge, for many trucks on the bridge, the system may can not estimate truck parameters accurately. Therefore, the case of more than one truck on the bridge is not considered in this study.

The truck axle parameters estimated by the system in this study is only the longitudinal axle spacing, while the width of the axle truck can not be estimated by the system. However the axle widths for different truck types are not different, and the longitudinal axle spacing from system is one of the most important parameters for developing of bridge truck load model.

It can be observed only 3% in each truck type that loaded higher than the legal limit. This may be due to that there is a weight control station on this highway. For other highway without weight control station, more data of overweight truck may be found.

NLFEM for existing flaw/crack in concrete structure and bridge

Only critical cracks at tension region observed in the bridges are considered in this study. However, if the old concrete structures are found occurring serious flaw/cracks at other critical location such as at compression or shear zones, other models such as compression and shear models accounting for existing damage or flaw/cracks may need to develop and apply at those damaged vicinities.

Even though there is effecting of transverse distribution that makes some analysis results of proposed NLFEM at opposite applied load lane are higher than those test results. For assessment of the bridge, if this effect is neglected, the results may be still acceptable; because the bridge is still in safe condition and the results at these locations are not maximum value as the applied load locations. Therefore this effect can be neglected for this study.

7.1.2 Conclusion

Truck loading monitoring system

The alternative system of truck load monitoring based on B-WIM is developed, which consists devices such as: strain gauges, photoelectric sensor and CCTV. The system is uncomplicated, inexpensive, but gives reliable truck load data. There is no any equipment exposing to road way surface to reflecting to truck drivers, and it is not interrupted traffic during installation, which is leading to convenient for installation, maintenance and getting unbiased. From the calibration truck, the system error in estimation of axle spacing is less than 2%, the error in estimation of axle weight and axle group weight is less than 13%, and error in estimation of the GVW is within 6% to 10%.

Bridge in the Bangkok Eastern Ring Road (BK-ERR) in Thailand was selected for monitoring actual truck configurations and loads. From the results of this test about 10,621 numbers of the actual trucks data have been collected, these truck data can be classified to seven types. The configurations of trucks can be grouped such as 2-axle truck, 3-axle truck, semi-trailer truck, and full trailer truck. The varying of truck configurations is given as standard deviation (SD) of axle spacing. The median value of axle spacing for 2-axle truck is about 5 m, and the 3-axle truck are about 4.1 m, and 1.3 m, respectively. The axle spacing of semi-trailer truck groups are very varied with SD higher than one; however, the individual axle spacing in axle groups for each truck type are similar by median value is 1.30 m for heading truck, and 1.35 m for trailing truck. This individual axle spacing in axle groups is also agreed with

data collected from truck manufactures in Thailand. The frequencies of GVW of each truck type are also presented. Most of the truck was loaded less than the legal GVW limit, as the mean value of GVW from monitored data are for 2-axle truck about 11 tons, 3-axle truck about 20 tons, 4-axle truck about 25 tons and 5-axle truck about 55 tons.

Based on the nominal analysis method for one lane short to medium span bridge, it is observed that all heaviest monitored trucks (or actual Thai trucks) generate force to the bridges higher than standard design truck. The heaviest truck load can reach as high as high as 48% and 35% for bending moment and shear forces, respectively above that of the HS20-44 design truck. The effect of truck load to the bridge is not only axle weight but also axle spacing, which limit of axle spacing are not yet defined in legal limit of truck load in Thailand.

NLFEM for existing flaw/crack in concrete structure and bridge

Most of the NLFEM model for concrete structure have been developed from the empirical model with using concrete experiment at the laboratory, therefore many models do not consider existing flaw/crack which general exist in existing concrete and reinforced concrete structure such as concrete bridges. Therefore, this research have been studied and proposed the models for accounting for existing flaw/crack at tension region of the old concrete and reinforced concrete structures.

In this study, the tension softening and tension stiffening models for concrete and reinforced concrete members accounting for existing flaw/crack at the tension region of concrete and reinforced concrete member are respectively proposed. The characteristic of the model are such that the tension capacity and stiffness of the damaged elements which are in the crack vicinities will be reduced corresponding to amount or crack width of the existing flaw/crack. In concrete, the vicinity of the existing flaw/crack can be smeared over an element and defined as 'COD' element which its characteristic in tension is defined as tension softening model for existing flaw/crack. In reinforced concrete member, the vicinity of the existing flaw/crack can be smeared over an element and defined as 'RED' element which its characteristic in tension is defined as tension stiffening model for existing flaw/crack. These elements and models than have been installed into the 3D NLFEM, CAMUI program for analysis old concrete and reinforced concrete structures.

To verify the proposed models, several notched concrete and reinforced concrete beams which tested by other investigators have been analyzed in 3D and the

results from the proposed models have been then compared with those general NLFEM results and test results. For notched concrete beam, COD element is used at notched vicinity; and for notched reinforced concrete beam, RED element is used at notched vicinity. The analysis results of these example beams using proposed models are very closed to those test results, while results from general NLFEM models are not. The peak load of the concrete beam is strongly affected by amount of flaw/crack, while in reinforced concrete beam the amount of flaw/crack is mainly affected at beam under full crack state.

To apply the proposed models, three concrete slab bridges have been taken to be examples for application using COD and RED elements which existing flaw/crack of the actual bridge can be accounted. Two types of flaws are used for existing concrete bridge namely visible flaw/crack which is crack or other defects taken from bridge inspection, and theoretical crack which is calculated by theory to represent small or invisible crack during inspection. The analysis results at the service load (tested truck load) from the proposed models have been compared to those results from the general NLFEM (no any existing flaw/crack included in model) and from test results. At the applied load location, the results of the general NLFEM are much less than those test results for both deflection and strain at the steel level, while the proposed model (included existing flaw/crack as RED elements) gives satisfied for both results, i.e. for CB7, the results from general model are less than those test results up to 20% and 55%, while results using proposed models are very close to the test results with about 0.8% and 8% for defection and strain at the steel level, respectively. These due to that the flaw/crack generally have been existed in the old concrete and reinforced concrete structures. Therefore, the proposed model for accounting for existing flaw/crack in this study can be close to realistic behaviour of old concrete slab bridge.

Two types of the concrete slab bridge have been further analyzed to evaluate their capacities. The bridge capacity evaluates from the proposed approach gives reasonable results which rating factor for inventory level *(RF(inv))* of both bridges are less than those from original NLFEM results and higher than those results from simplified method of AASHTO. Finally, both bridges are still safe for maximum monitored truck which have *RF(inv)* values of 1.13 and 1.41 for bridge CB7 and CB6, respectively.

The crack in concrete slab bridge is influent to the bridge behaviour not only at the service load but also at the higher loads. The global stiffness of the bridge structure may be reduced due to the existing flaw/crack leading bridge to lower capacity. The concrete slab bridge may not has behaviour fully like one way concrete slab, especially when there are solid curbs or parapets at bridge edges. This effect can lead the bridge failure in transverse direction.

7.2 Recommendation for further study

1. Further employing this B-WIM to monitor more actual truck data at different highway network is recommended, and furthering using the truck load data from monitoring system of this study to develop bridge design truck load model for Thailand is also recommended.

2. The monitoring system that can estimate truck load even more than one truck presented on the bridge is also recommended to research.

3. If the old concrete structures are found occurring serious flaw/cracks at different critical location such as at compression or shear regions, the constitutive models for compression and shear accounting for existing damage or flaw/cracks are needed to develop to apply at those damaged vicinities.

4. The effect of difference ratio of the transverse reinforcement of concrete slab bridge with composite curbs is also recommended to further study.

REFERENCES

AASHTO (1989). <u>Guide Specifications for Strength Evaluation of Existing Steel and Concrete Bridges</u>. Washington, DC., 2th Edition.

AASHTO (1994). <u>Manual Condition Evaluation of Bridges, 1994.</u> Washington, DC., Second Edition.

AASHTO (1998). <u>AASHTO LRFD Bridge Design Specification.</u> Washington, D.C., SI Unit, 2nd Edition.

AASHTO (2002). <u>Standard specification for highway bridges.</u> Washington, D.C., 17th edition.

ACI Committee 318 (2002). <u>Building code requirements for structural concrete,</u> American Concrete Institute, Farmington Hills, MI.

Anun, P. (2005). <u>Structural Identification of Concrete Girder Bridge for Strength Evaluation.</u> Ph.d Dissertation, Asian Institute of Technology.

Azizinamini, A., Ashekar, Y., et al (1994). Old Concrete Slab Bridges. II: Analysis. <u>Journal of Structural Engineering ASCE</u> 120(11): 3284-3304.

Azizinamini, A., Boothby, T, et al (1994). Old Concrete Slab Bridges. I: Experimental Investigation. <u>Journal of Structural Engineering ASCE</u> 120(11): 3305-3319.

Bathe, K.J. (1996). <u>Finite Element Procedure.</u> Prentice-Hill, Inc.

Bazant, Z. P., and Oh, B. H. (1983). Crack band theory for fracture of concrete <u>RILEM Material and Structures</u> 16(93): 155-177.

Bhattacharjee, S.S., and Leger, P. (1993). Finite Element Modeling of Tensile Strain Softening Behaviour of Plain Concrete. <u>Engineering Computation</u> 10: 205- 221

Bouteldja, M., Jacob B., and Dolcemascolo, V. (2008). Test of a B-WIM system on integral and steel orthotropic deck bridges in France. <u>Proceedings of the International Conference on Heavy vehicles</u> HVParis2008-ICWIM5: 311-322.

Cabrera, J.G. (1996). Deterioration of Concrete Due to Reinforcement steel corrosion. <u>Cement and Concrete composite</u> : 47-59.

Cai, C.S., and Mohsen, S. P. (2002). Predict and Measure Performance of Prestressed Concrete Bridges. <u>Journal of Bridge Engineering ASCE</u> 9(1): 4-13.

Červenka, J., Jendele1, L., and Saouma, V. (2001). On the choice between discrete or smeared approach in practical structural FE analyses of concrete structures. <u>Fourth International Conference on Analysis of Discontinuous Deformation,</u> UK, 6-8th June.

Chamchuenwong, A. (1998). Weigh-In-Motion analysis and fatigue assessment of a steel overpass bridge under normal traffic condition in Bangkok. Master's Thesis, Department of Civil Engineering, Graduate School, Asian Institute of Technology.

Chan, T.H.T., and Ashebo, D.B. (2006). Theoretical study of moving force identification on continuous bridges. Journal of Sound and Vibration 295(3-5): 870-883.

Chan, T.H.T., Law, S.S., and Yuan, X.R. (1999). An interpretive method for moving force identification. Journal of Sound and Vibration 219(3): 503-524.

Chan, T.H.T., Law, S.S., and Yung, T.H. (2000). Moving Force Identification Using Existing Prestresses Concrete Bridge. Engineering Structures 22(10): 1261-1270.

Chapman, S.J. (2004). Fortran 90/95 for Scientists and Engineers. McGraw-Hill, Inc.

Charles, M., Bala S, Fred M. (2004). New AASHTO Guide Manual for Load and Resistance Factor Rating of Highway Bridge. Journal of Bridge Engineering ASCE 9(1): 43-54.

Chen, W.F. (1982). Plasticity In Reinforced Concrete. McGraw-Hill, Inc.

Chen, W.F., and Lian D. (2000). Bridge Engineering Handbook. CRC Press, Inc.

Choi, C. K., and Kwak, H.G. (1990). The effect of finite element mesh size in nonlinear analysis of reinforced concrete structures. Computers & Structures 36 (5): 807-815.

Chowdhury, M.R., and Ray, J.C. (1995). Further Consideration for Nonlinear Finite Element Analysis. Journal of Structural Engineering, ASCE, 121(9): 1377-1379.

CIB-FIP (1990). Design of concrete structures – Part 1-1: General rules and rules for buildings, ENV 1992-1-1: 1991.

Colin O'Connor, and Peter, A.S. (2000) Bridge Loads, an International Perspective, Spon Press.

COST 323 (1999). Weigh-In-Motion of Road Vehicles. Final Report, Ver. 3, Aug., 1999

Dahlblom, O., and Ottosen, N.S. (1990). Smear Crack Analysis Using Generalized Factious Crack Model. Journal of Structural Engineering, ASCE, 116(1): 55-76.

Dede, T., and Ayvaz, Y. (2009). Nonlinear analysis of reinforced concrete beam with/without tension stiffening effect. Materials and Design 30: 3846–3851.

Dempsey, A.T., O'Brien, E.J., and O'Connor, J.M. (1995). A bridge weigh-in-motion system for the determination of gross vehicle weights. In Post Proceedings of First

European Conference on Weigh-In-Motion of Road Vehicles, eds. B. Jacob et al., ETH Zurich: 239-249.

Department of Civil Engineering, Chulalongkorn University (2003). Report of Study Project for Probability Factor for Increasing Truck Weight in Thailand. Project Report, Civil Engineering Chulalongkorn University. (In Thai).

Department of Highways, Thailand (2008). Project of Exiting Bridge Investigation and Testing for Load Carrying Capacity Report, Dec. (In Thai).

Department of Highways, Thailand (2005). Limit of Axle and Gross Weight of Vehicles, Dec., (In Thai).

Diprisco, M., Ferrara, L., and Meftah, F. (2000). Mixed Mode Fracture In Plain And Reinforced Concrete: Some Results On Benchmark Tests. International Journal of Fracture (103): 127–148.

Eamona, C.D., and Nowak, A.S. (2004). Effect Of Secondary Elements On Bridge Structural System Reliability Considering Moment Capacity. Structural Safety 26: 29–47.

Elenas, A., Vasiliadis, L., and Emmanouilidou, N. (2006). Influence of Tension Stiffening Effect On Design And Behavior of RC Structure. Measuring, Monitoring and Modeling Concrete Properties, Springer: 215-220.

European Commission 4th Framework Programme Transport (2001). Weighing-in-motion of Axles and Vehicles for Europe (WAVE) – Bridge WIM systems (B-WIM). University College Dublin.

Floegl, H., and Mang, H.A. (1982). Tension stiffening concept based on bond slip. Journal of Structural Engineering ASCE 108(12): 2681-2701.

Florinda, C. (1990). Chlorine Iron Distribution in Twenty-Years-Old Prestressed Bridge Girder. ACI Material Journal. 87(5): 479-488.

Getachew, A., and Obrien, E.J. (2005). Simplified Site Specific Models for Determination of Characteristic Traffic Load Effect for the Bridges. Proceeding of ICWIM4, Taiwan:312-320.

Gilbert, R.I., and Warner, R.F. (1978). Tension stiffening in reinforced concrete slabs. Journal of Structural Division ASCE 104(12): 1885-1900.

Gonzalez, A. (2001) Development of Accurate Methods of Weighing Trucks in Motion. Ph.d Dissertation,Trinity College Dublin, Ireland.

Hakan, T. (2006). <u>Assessment of Fatigue Resistance and Strength in Existing Concrete Structures</u>. Ph.D. Thesis, Department of Civil Engineering, Luleå University of Technology.

Hambly, E.C. (1991). <u>Bridge Deck Behaviour.</u> John Wiley & Sons, Inc.

He, X.G. (1999). <u>Constitutive Modeling of Reinforced Concrete for Nonlinear Finite Element Analysis</u>. Ph.D. Thesis, Department of Civil Engineering, The University of Hong Kong.

Heywoo, R. J., and O'Connor, C. (1992). A Bridge Design and Evaluation Method Derived from Weigh-In-Motion Data. <u>Canadian Journal of Civil Engineering</u> 19:423-431.

Hu, X., and Shenton, H.W. (2003). Damage Identification in a two span continuous beam. <u>Proceeding of Structural Heath Monitoring and Intelligent Infrastructure</u>.: 1040-1047.

Huria, V., Lee, K.L., and Aktan, A. E. (1993). Nonlinear Finite Element Analysis of RC Slab Bridge. <u>Journal of Structural Engineering ASCE</u> 11(1): 88- 107.

Huria, V., Lee, K.L, and Aktan, A. E. (1994). Different Approaches to Rating Slab Bridges. <u>Journal of Structural Engineering ASCE</u> 120(10): 3056- 3062.

Jacob, B., and Obrien, E.J. (2005). WIM – Recent development in Europe. <u>Proceeding of ICWIM4, Taiwan</u>:3-13.

James, M., Hao, H., and Pan, T C. (2001). Assessment of Structural Condition of Bridges by Dynamic Measurements. <u>App Rep. research, Nangyang Technology University</u>.

Jiang, J.J., and Kuang, J.S. (1995). <u>Nonlinear Finite Element Analysis of Concrete Structure.</u> Department of Civil Engineer, Tsinghua University.

Kanham, J.A., and Dagher, H.J. (1995). Nonlinear Finite Element Analysis of Skew Slab Bridge. <u>Journal of Structural Engineering ASCE</u> 121(9): 1338- 1345.

Karihaloo, B. (1995). <u>Fracture Mechanics and structural Concrete.</u> Longman Group Limited.

Karuomi, R., and Wiberg, J. (2005). Monitoring Traffic Load and Dynamic Effect Using Instrumented Railway Bridge. <u>Engineering Structures.</u> July: 1813-1819.

Kevin, L., and Carnot L. (2005). Bridge Management and Nondestructive Evaluation. <u>Journal of performance of Constructed Facilities ASCE</u> 19(9): 3-16.

Kwak, H.G., and Plippou, F.C. (1991). Finite Element Analysis of Reinforced Concrete Structure Under Monotonic Loads. Department of Civil Engineering University of California, Berkeley Rep. No. 90/14.

Kwak, H.G., and Plippou, F.C. (1996). Nonlinear FE Analysis of R/C Structure Under Monotonic Loads. Depart. Computers & Structures 65(1): l-16.

Kwak, H.G., and Song, J.Y. (2001). Cracking Analysis of RC Members Using Polynomial Strain Distribution Function. Engineering Structures 24: 455–468.

Law, S.S., and Chan, T.H.T. (1997). Moving Force Identification: A Time Domain Method. Journal of Sound and Vibration: 1-22.

Law, S.S., Bu, J.Q., Zhu, X.Q., and Chan, S.L. (2004). Vehicle axle loads identification using finite element method. Engineering Structures 26(8): 1143-1153.

Law, S.S, Bu, J.Q., Zhu, X.Q., and Chan, S.L. (2007). Moving load identification on a simply supported orthotropic plate. International Journal of Mechanical Sciences 49(11): 1262-1275.

Law, S.S., Ward, H.S., and Shi, G.B. (1995). Dynamic Assessment of Bridge Load-Carrying Capacities II.   Journal of Structural Engineering ASCE 121(3): 488-495.

Lindquist, W. (2006). Effect of Cracking on Chloride Content in Concrete Bridge Decks. ACI Materials Journal 103(6): 467-473

Mabsout, M., Tarhini, K., and Awwad, E. (2004). Wheel Load Distribution in Simply Supported Concrete Slab Bridges. Journal of Bridge Engineering ASCE 9(2): 147-155.

Maekawa, K., Pimanmas, A., and Okamura, H. (2003). Nonlinear Mechanics of Reinforced Concrete. Spon Press, London, UK.

Małecki, T., Marzec, I. Bobinski, J., and Tejchman, J. (2009). Effect of a characteristic length on crack spacing in a reinforced concrete bar under tension. Mechanics Research Communications 34: 460–465.

Mehta, P.M., and Moterio, P.J.M. (2006). Concrete Microstructure, Properties, and Materials. McGraw-Hill 3th Edition.

Meschke, G., Mang, H.A., and Kosza, P. (1991). Finite Element Analysis of Crack Cooling Tower Shell. Journal of Structural Engineering ASCE 117(9): 2620-2639.

McCall, B., and Vodrazka, W.C. (1997). Weigh - In- Motion Hand Book. US, Department of Transportation Technical report.

Miao, T.J., and Chan, T.H.T. (2002). Bridge live load models from WIM data. Engineering Structures 24: 1071-1084.

Michel, G. (1985). Bridge Loading. Journal of Engineering Mechanics ASCE 111(9): 1093-1104.

Miller, R.A., Aktan, E.C., and Sharoon, B.M. (1994). Destructive Testing of Decommissioned Concrete Slab Bridge. Journal of Structural Engineering ASCE, 120(7): 1276- 2198.

Moses, F. (1979). Weigh-In-Motion system using instrumented bridges. Journal of Transportation Engineering ASCE 105:233-249.

Ngo, D., and Scordelis, A.C. (1967). Finite element analysis of reinforced concrete Beams. ACI Material Journal 64(3): 152-163.

Noh, S.Y., Kratzi, W.B., and Meskouris, K. (2003). Numerical Simulation of Serviceability, Damage Evolution and Failure of Reinforced Concrete Shells. Computers & Structures 81: 843–857.

Nowak, A.S., and Hong, Y.K. (1991) Bridge live-load models. Journal of Structural Engineering ASCE 117(9): 2757-2767.

Nowak, A.S., Nassif, H., and DeFrain, L. (1993). Effect of truck loads on bridges. Journal of Transportation Engineering ASCE 119: 853-867.

Nowak, A.S. (1993). Live load model for highway bridges. Journal of Structural Safety 13: 53-66.

Nowak, A.S. (1995). Calibration of LRFD bridge code. Journal of Structural Engineering ASCE 121(8): 1245-1251.

Oh, B.H., and Kang, Y.J. (1988) New Formulas For Maximum Crack Width and Crack Spacing in Reinforced Concrete Flexural Members. ACI Structural Journal. 84(10): 103-112.

Okamura, H., and Maekawa, K. (1991). Nonlinear Analysis and Constitutive Models of Reinforced Concrete. Gihodo-Shuppan Co. Tokyo.

Ojio, T., and Yamada, K. (2005). Bridge WIM by reaction force method. Proceeding of ICWIM4, Taiwan. : 97-108.

Omron Industrial Automation (2006). Standard Photoelectric Sensors.

Palermo, D., and Vecchio, F.J.(2004). Compression field modeling of reinforced concrete subjected to reversed loading: Verification. ACI Structural Journal 101(2): 155-164.

Park, R., and Paulay, T. (1975). Reinforced Concrete Structure. John Wiley & Son.

Patrick, P., Jean, P., and Martin, T. (1995). Dynamic Testing Procedure for Highway Bridges Using Traffic Load. Journal of Structural Engineering ASCE 121(2), Feb.: 362-374.

Peters, R.J. (1986). CULWAY – an unmanned and undetectable highway speed vehicle weighing system. In Proc. 13th AARB Conference, Australian Road Research Board 13(6).

Peter, R.J. (1995). The accuracy of the Australia and Europe Culvert WIM system. National Traffic data acquisition conference, New Mexico : 647-656.

Pinkaew, T. (2006). Identification of vehicle axle loads from bridge responses using updated static component technique. Engineering Structures 28(11): 1599-1608.

Pin-Qi Xia, and James, M.W.(2004). Bridge Structure Condition Assessment using Systematically Validated Finite-Element Model. Journal of Bridge Engineering ASCE 9(5): 418-423.

Piyasena, R. (2002). Crack Spacing Crack Width Tension Stiffening Effect In RC Beam and One Way Slab. Ph.d Dissertation, Faculty of Engineering, University of Griffith, Gold Coat Campus.

Phoonsak, P. (2003) Bridge Design Based On Thai Truck Loading. JSCE-EIT Joint Seminar on Advanced Eng. for Long-Life Steel Bridge, Bangkok, Thailand: 107-121, 2003. (In Thai)

Potisuk, T., and Higgins, C. (2007). Field Testing and Analysis of CRC Deck Girder Bridges. Journal of Bridge Engineering ASCE 12(1): 53-63.

Prasad, M.V., and Krishnamoorthy, C.S. (2002). Computational model for discrete crack growth in plain and reinforced concrete. Comput. Methods Appl. Mech. Engrg. 191: 2699–2725.

Raina, V.K. (1994). Inspection, Repair, Strengthening for concrete bridge. McGraw-Hill.

Reinhardt, H.W., Cornelissen, H.A.W. and Hordijk, D.A. (1986). Tensile tests and failure analysis of concrete. Journal of Structural Engineering ASCE 112(11): 2462-2477.

Renata, S.B.S., and Henriette, L.L.R. (2008). An efficient tension-stiffening model for nonlinear analysis of reinforced concrete members Engineering Structures 30: 2069–2080.

Rodriguez, J., Ortega, L.M., and Casal, J. (1997). Load Carrying Capacity of Concrete Structure with Corroded Reinforcement. Construction and Building Materials. 2 (4): 239-248.

Schnobrich, W.C. (1977). Behaviour of reinforced concrete structures predicted by the finite element method. Computers & Structures (7): 265-376.

Schultz, G.G., and Seegmiller, L.W. (2006). Utah Commercial Motor Vehicle Weigh-In-Motion Data Analysis. Utah Department of Transportation Research, Report No. UT-06.10.

Shahrooz, B.M. (1997). Finite Element Modeling of Deteriorated RC Slab Bridge: Lession Learn and Recommendations. Journal of Structural Engineering and Mechanics ASCE 6(3): 259- 274.

Shahrooz, B.M., Ho, I.K., and Aktan, A.E. (1994). Nonlinear Finite Element Analysis of Deteriorated RC Slab Bridge. Journal of Structural Engineering ASCE 120(2): 422- 440.

Shahrooz, B.M., Saraf, V., and Miller, R.A. (2002). Response of Slab Bridges Before, During, and After Repair. Journal of Bridge Engineering ASCE 7(5): 267-275.

Shi, Z., and Nakano, M. (1999). Three-Dimensional Finite Element Analysis On Crack Behaviors of RC Cantilever decks. Construction and Building Materials 13:33-47.

Smith, I.M, and Griffiths, D.V. (1999). Programming The Finite Element Method. John Wiley & Sons, 3th Edition.

Somayaji, S., and Shah, S.P. (1982). Bond Stress Versus Slip Relationship and Cracking Spacing Response of Tension Member. ACI Structural Journal 78(20): 217- 225.

Somkuan, W. (1963). Analysis and Rating of Existing Highway Bridges in Thailand. Ms. Thesis, Graduate School of Engineering, Asian Institute of Technology, Bangkok, Thailand.

Stalling, J.M., and Yoo, C.H. (1993). Test-and rating of short span steel bridge. Journal of Structural Engineering ASCE 119(7): 2150-2168.

Stramandinolia, R.S.B. and Rovereb, H.L.L. (2008). An Efficient Tension-Stiffening Model For nonlinear Analysis Of Reinforced Concrete Members. Engineering Structures 30: 2069- 2080.

Sumarac, D. and Sekolovic, M. (2003). Fracture of Reinforced Concrete BeamsSubjected to Three Point Bending. International Journal of Damage Mechanics 12: 31-44.

Tao, S., and Fillip, D.V. (2005). A simplified isotropic damage model for concrete under bi-axial stress states. Cement and Concrete Composites 27: 716–726.

The Committee on Bridges of the Structural Division (1982). Bridge Loading Research Need. Journal of Structural Division of ASCE 108(5), May: 1012-1020.

Tokyo Sokki (2005). Strain Gauge Users' Guide.

Tonias, D.E. (1995). Highway Bridge Engineer. McGraw-Hill, Inc.

Van Mier, J.G.M. (1997). Fracture Processes of Concrete. CRC Press, Inc.

Val, D.V., and Melchers R.E. (1997). Reliability of Deteriorating RC Slab Bridge. Journal of Structural Engineering ASCE 123(12): 1638-1644.

Vecchio, F.J., and Collins, M.P. (1986). The modified compression field theory for reinforced concrete elements subjected to shear. ACI Structural Journal, 83(2):219-231.

Vecchio, F.J. and Collins, M.P. (1988). Predicting the response of reinforced concrete beams subjected to shear using modified compression field theory. ACI Structural Journal, 85(3): 258-268.

Vecchio, F.J., and Selby, R.G. (1991). Towards compression field analysis of reinforced concrete solids. Journal of Structural Engineering ASCE 117(6): 1740-1758.

Vecchio, F.J., and Collins, M.P. (1993). Compression response of cracked reinforced concrete. Journal of Structural Engineering ASCE 119(12): 3590-3610.

Wang, T. L., et al. (2005). Truck Loading and Fatigue Damage Analysis for Girder Bridge Base on Weigh-In-Motion Data. Journal of Bridge Engineering ASCE 10(1): 12-20.

Wirat, L. (2000). Bridge Damage Detection Using a System Identification Method. Ph.d Dissertation, University of Florida.

Withit, P. (2004). Shear Resisting Mechanism of RC T-Beam. Ms. Thesis, Graduate School of Engineering, Hokkaido University.

Wu, Z., Yoshikawa, H., and Tanabe, T. (1991). Tension stiffness model for cracked reinforced concrete. Journal of Structural Engineering ASCE 117(3).

Yamaguchi, E., and Masuki, Y. (2006). Bridge Weigh-In-Motion and Heavy Truck Flow in Fukuoka, Japan. Symposium on Recent Advances in Structural Engineering, Mechanics and Materials, AIT, August 2006: 51- 57.

Yang, S., and Chen, J. (1988). Bond Slip and Crack Width Calculations of Tension Members. ACI Structural Journal 85(38): 414-422.

Zhang, J., Li, C., Xu, F., and Yu, X. (2007). Test and Analysis for Ultimate Load-Carrying Capacity of Existing Reinforced Concrete Arch Ribs. Journal of Bridge Engineering ASCE 12(1): 4-12.

Zhu, X.Q., and Law, S.S. (2000). Identification of Vehicle Axle Load From Bridge Responses. Journal of Sound and Vibration: 705-724.

Zhu, X.Q., and Law, S.S. (2002). Moving loads identification through regularization. Journal of Engineering Mechanics ASCE 128(5): 989-1000.

Zidaric, A., Lavric, I., and Kalin, J. (2005). Nothing-On-The-Road axle detection with threshold analysis. Proceeding of ICWIM4, Taiwan: 86-96.

ศูนย์วิทยทรัพยากร
จุฬาลงกรณ์มหาวิทยาลัย

APPENDICS

Appendix A-1
Example Truck Monitored Data

This is the example of the trucks data that monitoring at the Bangkok Eastern Bangkok Eastern Ring Road (BK-ERR) at the eastern part of Bangkok during April, to May, 2007 using system developed in this study. There are may sheets of the data that may could not presented all, therefore only some data example of each truck type are presented.

The meanings of the head of column name are:

TR-n: Truck type number, i.e TR-02 is mean truck type TR-02

A, B, C, D, E, F : Truck axle spacing

1_SA: Single axle weight

1_AG: Axle group weight

GVW: Gross vehicle weight

Example data TR-02
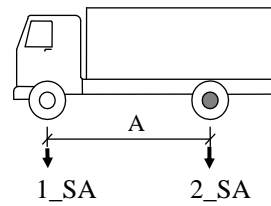
TR_n	A	1_SA	2_SA	GVW
	m	kg	kg	kg
2.00	3.37	2,496.32	5,240.76	7,737.08
2.00	3.19	3,281.15	4,458.86	7,740.01
2.00	4.15	3,518.13	4,226.10	7,744.24
2.00	5.50	3,905.92	3,838.34	7,744.26
2.00	5.53	2,898.81	4,846.69	7,745.50
2.00	4.26	2,814.03	4,932.72	7,746.75
2.00	4.88	2,639.41	5,107.96	7,747.37
2.00	3.95	3,405.87	4,343.14	7,749.00
2.00	5.55	2,243.26	5,763.39	8,006.65
2.00	3.80	2,145.31	5,608.67	7,753.98
2.00	5.52	2,762.66	4,992.22	7,754.88
2.00	5.48	2,496.43	5,259.76	7,756.19
2.00	5.48	2,496.43	5,259.76	7,756.19
2.00	5.53	2,618.08	5,138.73	7,756.81
2.00	3.35	2,881.67	4,877.46	7,759.13
2.00	5.53	3,715.27	4,044.46	7,759.73
2.00	4.20	3,432.62	4,328.15	7,760.77
2.00	4.03	2,318.40	5,447.10	7,765.49
2.00	5.48	2,343.68	5,426.40	7,770.08
2.00	5.53	3,214.78	4,557.41	7,772.18
2.00	3.29	2,674.25	5,348.49	8,022.74
2.00	6.10	2,591.32	5,182.64	7,773.96
2.00	5.00	3,381.07	5,323.51	8,704.59
2.00	5.03	3,582.00	4,194.16	7,776.16
2.00	5.04	3,289.77	4,490.25	7,780.02
2.00	5.55	3,452.45	5,620.27	9,072.72
2.00	5.53	3,299.83	4,485.24	7,785.07
2.00	5.49	2,075.39	5,710.35	7,785.74
2.00	4.35	3,063.11	4,723.47	7,786.58
2.00	5.53	2,505.44	5,282.31	7,787.75
2.00	4.02	2,487.75	5,303.94	7,791.69
2.00	3.11	2,597.93	5,195.86	7,793.79
2.00	4.77	2,599.33	5,198.66	7,798.00
2.00	4.03	1,153.59	6,650.62	7,804.21
2.00	5.58	3,118.24	4,686.29	7,804.54
2.00	4.93	4,090.75	3,718.41	7,809.16
2.00	5.53	3,262.02	4,549.67	7,811.69
2.00	5.53	3,262.02	4,549.67	7,811.69
2.00	5.00	3,118.36	4,697.97	7,816.34

Example data TR-05
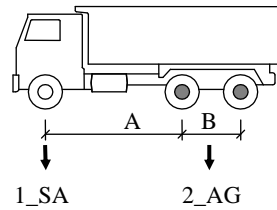
TR-n	A	B	1_SA	2_AG	GVW
	m	m	kg	kg	kg
5.00	4.13	1.31	5,045.87	18,776.55	23,822.42
5.00	4.97	1.32	4,237.98	19,591.01	23,828.98
5.00	4.12	1.30	4,425.75	19,411.33	23,837.09
5.00	4.14	1.30	3,999.30	19,841.91	23,841.20
5.00	4.14	1.30	4,393.85	19,462.06	23,855.90
5.00	4.01	1.31	5,230.34	18,802.40	24,032.75
5.00	4.15	1.30	4,665.15	19,375.53	24,040.68
5.00	4.02	1.30	5,972.81	18,070.10	24,042.91
5.00	3.94	1.32	4,372.74	19,677.56	24,050.30
5.00	5.04	1.31	4,903.26	19,154.17	24,057.43
5.00	4.14	1.30	4,140.81	20,516.88	24,657.69
5.00	3.93	1.33	5,145.07	19,514.97	24,660.04
5.00	4.06	1.34	4,420.50	20,248.04	24,668.55
5.00	4.17	1.29	4,779.69	20,297.46	25,077.15
5.00	4.13	1.33	5,037.40	20,046.31	25,083.71
5.00	4.03	1.30	3,513.94	21,578.17	25,092.11
5.00	4.20	1.30	5,339.30	19,757.59	25,096.89
5.00	4.01	1.13	4,878.68	20,223.94	25,102.61
5.00	4.07	1.31	4,743.09	20,362.34	25,105.43
5.00	4.15	1.30	5,223.36	19,905.07	25,128.43
5.00	4.13	1.32	5,606.89	19,531.81	25,138.69
5.00	4.16	1.31	3,628.61	21,543.67	25,172.29
5.00	3.93	1.30	4,585.55	20,590.53	25,176.08
5.00	4.13	1.32	5,691.51	19,503.16	25,194.68
5.00	4.14	1.33	3,256.13	21,998.46	25,254.58
5.00	4.12	1.32	6,258.54	19,018.66	25,277.20
5.00	3.73	1.18	5,123.15	20,164.13	25,287.28
5.00	4.15	1.30	3,097.69	22,192.52	25,290.22
5.00	4.13	1.31	4,770.92	20,522.45	25,293.37
5.00	4.12	1.34	5,809.29	19,487.56	25,296.85
5.00	4.11	1.32	5,260.73	20,063.51	25,324.23
5.00	4.12	1.34	5,734.95	19,591.54	25,326.50
5.00	3.94	1.30	5,873.50	19,454.25	25,327.75
5.00	4.07	1.30	5,222.81	20,105.15	25,327.96
5.00	4.14	1.30	4,636.81	20,719.65	25,356.46
5.00	4.99	1.31	4,976.23	20,393.15	25,369.38
5.00	4.00	1.30	4,697.32	20,675.42	25,372.74
5.00	4.13	1.30	5,939.79	19,629.27	25,569.06
5.00	4.00	1.16	5,898.08	19,752.14	25,650.22
5.00	4.14	1.31	4,907.49	20,573.26	25,480.75

Example data TR-07
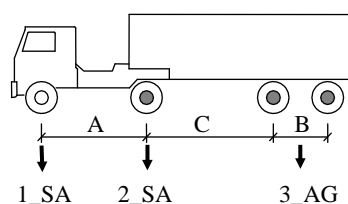
TR-n	A	C	B	1_SA	2_SA	3_AG	GVW
	m	m	m	kg	kg	kg	kg
7.00	5.54	8.88	1.35	2,672.78	9,460.20	7,883.08	20,016.06
7.00	3.38	8.36	1.35	2,143.76	10,232.79	7,936.90	20,313.45
7.00	3.78	7.96	1.38	3,911.94	7,585.31	9,589.74	21,086.99
7.00	3.78	7.96	1.38	3,911.94	7,585.31	9,589.74	21,086.99
7.00	3.79	7.96	1.38	3,210.95	6,954.67	11,045.14	21,210.76
7.00	7.40	5.76	1.34	1,538.49	4,504.93	15,583.59	21,627.00
7.00	3.75	7.79	1.36	3,191.83	9,698.74	8,754.61	21,645.18
7.00	3.76	7.90	1.37	3,655.82	6,746.60	11,805.31	22,207.73
7.00	5.02	7.84	1.39	4,413.07	9,185.63	8,687.99	22,286.69
7.00	5.53	8.87	1.36	3,757.54	9,163.86	9,630.85	22,552.25
7.00	5.53	8.87	1.36	3,757.54	9,163.86	9,630.85	22,552.25
7.00	3.70	9.62	1.34	2,708.55	8,374.42	12,178.69	23,261.66
7.00	3.70	9.62	1.34	2,796.65	8,347.71	12,165.73	23,310.08
7.00	3.08	8.64	1.33	7,165.64	6,610.29	9,534.70	23,310.63
7.00	3.69	9.63	1.36	3,226.54	9,164.74	10,929.71	23,321.00
7.00	3.98	7.81	1.43	4,536.38	8,485.46	10,664.23	23,686.07
7.00	3.71	9.62	1.35	2,944.73	8,661.55	12,085.90	23,692.18
7.00	3.68	9.63	1.36	2,971.65	8,596.73	12,372.51	23,940.89
7.00	3.70	9.65	1.35	3,525.35	8,491.71	12,044.35	24,061.41
7.00	3.69	9.63	1.36	3,498.70	8,581.25	12,030.97	24,110.92
7.00	5.54	8.85	1.35	3,902.56	6,953.43	13,455.32	24,311.31
7.00	3.02	7.80	1.49	4,122.94	8,133.20	12,172.12	24,428.26
7.00	5.54	8.84	1.35	3,389.58	11,206.57	11,316.98	25,913.13
7.00	5.53	8.83	1.36	2,911.78	11,433.26	12,412.61	26,757.64
7.00	3.77	9.57	1.37	4,071.50	9,512.89	13,179.96	26,764.35
7.00	5.53	8.85	1.35	3,837.31	10,706.26	12,372.86	26,916.43
7.00	5.54	8.85	1.36	3,609.16	9,725.22	13,633.69	26,968.07
7.00	5.52	8.85	1.37	3,565.67	10,533.24	13,000.07	27,098.98
7.00	5.54	8.85	1.35	3,259.47	10,615.63	13,284.31	27,159.42
7.00	5.53	8.83	1.36	4,123.32	11,078.59	12,152.16	27,354.06
7.00	3.67	4.02	1.35	3,927.42	11,086.46	12,435.72	27,449.60
7.00	3.68	4.02	1.36	4,151.36	12,555.50	10,970.35	27,677.21
7.00	5.52	8.86	1.35	4,315.83	11,163.03	12,444.74	27,923.60
7.00	5.52	8.86	1.35	3,171.82	10,387.68	14,423.74	27,983.24
7.00	5.53	8.85	1.34	3,567.43	10,262.01	14,444.12	28,273.56
7.00	4.58	7.63	1.37	5,241.25	11,043.75	12,801.54	29,086.54
7.00	4.68	6.43	1.36	5,185.53	10,580.01	13,737.83	29,503.37
7.00	3.74	5.64	1.36	4,157.26	5,891.55	20,183.02	30,231.83
7.00	3.75	5.63	1.36	4,183.35	2,896.08	23,160.68	30,240.10
7.00	5.53	8.85	1.34	4,074.76	10,917.87	15,295.08	30,287.70
7.00	3.78	4.14	1.36	3,991.01	11,969.23	14,444.06	30,404.31

Example data TR-09
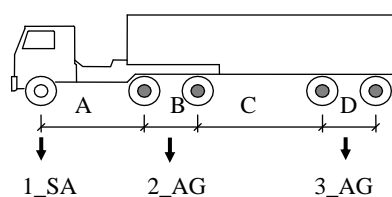
TR-n	A	B	C	D	1_SA	2_AG	3_AG	GVW
	m	m	m	m	kg	kg	kg	kg
9.00	3.07	1.32	7.25	1.30	3,608.04	9,946.50	12,361.62	25,916.16
9.00	3.39	1.30	7.37	1.36	4,194.17	10,961.53	10,818.39	25,974.09
9.00	3.39	1.30	7.37	1.36	4,194.17	10,961.53	10,818.39	25,974.09
9.00	4.16	1.31	7.59	1.36	5,978.65	10,003.97	10,059.59	26,042.21
9.00	3.18	1.29	7.71	1.37	4,269.77	10,265.25	11,528.67	26,063.69
9.00	3.38	1.31	7.21	1.33	3,901.20	10,351.54	12,790.01	27,042.76
9.00	3.30	1.31	7.65	1.35	4,093.46	10,683.19	12,278.52	27,055.18
9.00	3.28	1.32	7.44	1.35	4,518.57	10,481.07	12,068.78	27,068.43
9.00	3.09	1.31	7.36	1.34	4,864.70	11,449.60	11,736.01	28,050.30
9.00	3.28	1.32	7.63	1.37	4,581.50	10,754.15	12,749.60	28,085.24
9.00	3.32	1.30	7.50	1.35	4,070.64	12,499.94	12,461.25	29,031.83
9.00	3.39	1.32	7.44	1.36	4,287.73	11,238.90	13,525.74	29,052.37
9.00	2.89	1.11	6.48	1.13	6,867.44	12,433.72	9,752.43	29,053.59
9.00	3.39	1.30	7.69	1.37	4,253.60	10,524.69	15,268.80	30,047.08
9.00	3.41	1.30	7.14	1.34	3,584.46	12,685.81	13,820.27	30,090.54
9.00	3.67	1.41	7.91	1.39	4,466.28	9,011.80	16,689.10	30,167.18
9.00	3.17	1.30	7.37	1.34	4,489.92	12,872.01	13,682.06	31,044.00
9.00	3.39	1.37	7.39	1.35	6,582.60	12,110.87	13,291.77	31,985.25
9.00	3.28	1.31	7.23	1.35	2,761.93	12,717.11	16,538.08	32,017.13
9.00	3.24	1.30	8.21	1.36	5,168.87	6,325.43	22,478.67	33,972.97
9.00	3.35	1.31	7.56	1.34	4,157.87	13,153.90	16,982.45	34,294.22
9.00	3.08	1.32	7.58	1.33	3,951.75	14,167.48	16,267.35	34,386.58
9.00	3.18	1.22	5.84	1.26	4,942.46	15,744.65	14,385.82	35,072.93
9.00	3.39	1.36	7.23	1.36	5,915.00	12,078.11	17,198.61	35,191.72
9.00	3.28	1.29	3.41	1.31	4,089.23	8,234.05	23,649.19	35,972.47
9.00	3.40	1.37	7.40	1.30	4,209.18	15,723.19	16,050.60	35,982.96
9.00	3.40	1.30	3.33	1.35	4,238.59	7,169.90	24,942.71	36,351.20
9.00	3.40	1.37	7.01	1.33	4,710.00	13,611.40	18,035.55	36,356.95
9.00	3.34	1.31	6.27	1.38	4,118.81	15,747.05	17,146.57	37,012.43
9.00	3.34	1.31	6.55	1.36	4,499.24	17,115.79	15,400.05	37,015.08
9.00	3.39	1.31	7.44	1.35	4,664.19	14,201.14	19,167.33	38,032.66
9.00	3.40	1.30	6.43	1.35	4,857.35	16,643.47	16,960.33	38,461.15
9.00	3.29	1.32	3.63	1.33	3,311.82	15,168.03	19,988.74	38,468.59
9.00	3.34	1.34	7.07	1.35	5,047.20	16,412.78	17,913.94	39,373.92
9.00	3.20	1.36	8.73	1.36	4,635.51	14,858.26	19,894.22	39,387.99
9.00	3.10	1.33	5.52	1.36	4,676.30	16,401.79	19,181.02	40,259.11
9.00	3.35	1.42	7.91	1.47	4,548.14	17,361.20	18,379.91	40,289.26
9.00	2.94	1.33	7.25	1.35	5,298.64	14,855.51	21,263.45	41,417.60
9.00	3.38	1.29	6.28	1.36	4,278.98	16,513.06	21,475.92	42,267.95
9.00	3.27	1.31	6.16	1.33	4,454.83	20,379.68	18,488.34	43,322.86
9.00	3.25	1.30	7.37	1.34	7,023.71	18,006.76	19,374.21	44,404.68
9.00	3.39	1.30	7.45	1.24	6,105.24	19,089.62	20,135.20	45,330.06
9.00	3.38	1.30	7.31	1.36	5,838.54	19,430.18	20,434.24	45,702.96

Example data TR-10
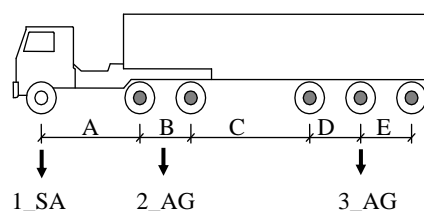
TR-n	A	B	C	D	E	1_SA	2_AG	3_AG	GVW
	m	m	m	m	m	kg	kg	kg	kg
10.00	3.09	1.34	6.59	1.36	1.34	6,634.00	9,490.25	20,352.56	36,476.82
10.00	3.37	1.30	4.82	1.38	1.35	4,485.08	9,465.93	24,507.11	38,458.12
10.00	2.71	1.05	7.83	1.10	1.30	7,600.22	12,797.55	18,159.51	38,557.29
10.00	2.71	1.05	7.83	1.10	1.30	7,600.22	12,797.55	18,159.51	38,557.29
10.00	2.71	1.05	7.83	1.10	1.30	7,600.22	12,797.55	18,159.51	38,557.29
10.00	3.39	1.30	6.86	1.37	1.36	4,995.96	11,235.37	22,449.24	38,680.57
10.00	3.39	1.35	4.97	1.35	1.37	6,051.39	16,620.43	16,666.49	39,338.31
10.00	3.40	1.38	5.10	1.36	1.36	5,359.07	14,843.16	19,220.73	39,422.96
10.00	3.10	1.33	6.37	1.37	1.35	3,976.38	15,653.43	19,937.54	39,567.35
10.00	3.38	1.31	5.19	1.36	1.32	5,498.09	14,315.57	20,412.05	40,225.71
10.00	3.39	1.37	5.05	1.36	1.36	5,239.82	13,928.64	21,812.47	40,980.93
10.00	3.39	1.31	6.55	1.35	1.37	5,040.47	15,509.67	20,736.31	41,286.44
10.00	3.14	1.34	6.52	1.29	1.30	5,490.36	9,078.47	28,043.97	42,612.79
10.00	3.40	1.38	5.24	1.34	1.36	5,511.12	15,242.63	24,291.47	45,045.22
10.00	3.96	1.31	6.83	1.36	1.36	4,152.89	13,470.75	27,667.78	45,291.42
10.00	3.29	1.31	7.23	1.35	1.36	3,672.37	17,762.49	24,683.97	46,118.83
10.00	3.28	1.30	7.24	1.33	1.38	4,316.06	18,771.07	23,071.50	46,158.63
10.00	3.24	1.31	6.76	1.33	1.42	4,769.40	18,788.39	23,474.90	47,032.69
10.00	3.30	1.31	6.54	1.35	1.36	6,163.84	17,127.25	24,750.72	48,041.81
10.00	3.19	1.32	6.29	1.37	1.38	4,723.22	17,856.23	25,477.15	48,056.60
10.00	3.37	1.31	3.30	1.32	1.32	5,561.96	18,371.52	25,125.81	49,059.29
10.00	3.40	1.37	6.57	1.35	1.37	5,826.49	19,642.69	24,863.35	50,332.53
10.00	3.41	1.36	3.17	1.34	1.39	5,945.28	14,584.82	29,856.74	50,386.83
10.00	3.40	1.36	4.63	1.38	1.36	6,278.70	17,998.84	26,114.25	50,391.78
10.00	3.39	1.30	6.68	1.35	1.35	4,940.03	19,456.89	26,214.97	50,611.89
10.00	3.11	1.31	6.39	1.37	1.35	8,507.17	18,618.34	23,493.31	50,618.81
10.00	3.37	1.31	6.66	1.36	1.34	4,829.37	19,728.46	26,120.33	50,678.16
10.00	3.37	1.31	6.66	1.36	1.34	4,829.37	19,728.46	26,120.33	50,678.16
10.00	3.37	1.31	5.58	1.36	1.36	5,462.02	18,960.41	26,258.61	50,681.04
10.00	3.40	1.35	4.56	1.36	1.35	8,476.14	15,817.38	26,777.72	51,071.24
10.00	3.40	1.35	4.66	1.35	1.35	6,370.53	16,732.74	28,082.69	51,185.96
10.00	3.41	1.35	4.66	1.37	1.34	6,762.48	16,973.93	27,529.60	51,266.01
10.00	3.37	1.30	5.61	1.36	1.35	5,756.32	19,539.16	26,026.84	51,322.32
10.00	3.29	1.31	6.49	1.33	1.35	7,878.96	19,387.74	24,079.35	51,346.04
10.00	3.36	1.31	5.60	1.35	1.36	6,100.42	17,923.65	27,429.07	51,453.14
10.00	3.38	1.30	4.85	1.36	1.34	6,396.46	18,142.52	27,634.38	52,173.36
10.00	3.39	1.36	4.61	1.39	1.36	6,146.46	17,118.60	28,917.71	52,182.76
10.00	3.39	1.35	3.18	1.34	1.39	7,578.63	16,973.98	27,664.54	52,217.14
10.00	3.38	1.31	5.58	1.37	1.35	6,216.59	20,211.98	25,809.46	52,238.03
10.00	3.37	1.30	5.61	1.35	1.35	5,729.25	19,321.50	27,367.77	52,418.52
10.00	3.27	1.31	2.67	1.20	1.32	5,524.04	16,486.74	30,536.48	52,547.26
10.00	3.44	1.38	4.68	1.40	1.37	9,509.30	20,558.64	22,605.10	52,673.05

Example data TR-11
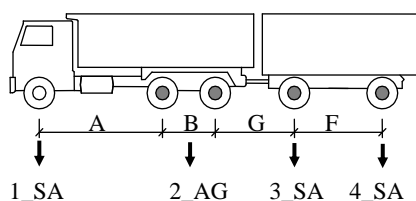
TR-n	A	B	G	F	1_SA	2_AG	3_SA	4_SA	GVW
	m	m	m	m	kg	kg	kg	kg	kg
11.00	4.63	1.30	5.18	4.90	4,380.00	13,109.71	6,962.10	6,650.22	31,102.03
11.00	3.99	1.30	5.08	4.69	2,836.24	16,156.23	5,366.93	8,213.75	32,573.14
11.00	4.89	1.30	5.49	4.48	4,396.59	13,869.57	7,201.35	7,583.03	33,050.53
11.00	4.14	1.30	4.68	4.72	4,520.86	14,536.07	6,610.55	7,398.36	33,065.84
11.00	4.12	1.31	4.39	4.42	4,542.21	13,927.04	7,989.02	6,623.25	33,081.52
11.00	4.15	1.30	4.65	4.75	3,916.78	14,651.40	8,305.91	7,536.39	34,410.48
11.00	4.14	1.31	4.68	3.83	2,618.14	15,986.50	3,454.71	12,643.31	34,702.67
11.00	4.93	1.61	6.27	5.76	2,025.85	15,575.08	7,520.18	9,776.47	34,897.59
11.00	3.38	1.09	3.41	3.66	5,059.38	17,152.47	6,255.39	6,580.35	35,047.60
11.00	4.01	1.31	4.35	4.30	4,569.99	15,278.99	7,356.08	8,087.50	35,292.56
11.00	4.13	1.31	4.30	4.63	3,565.42	20,566.98	5,737.62	5,779.49	35,649.50
11.00	4.02	1.17	4.25	4.40	3,124.19	16,180.09	7,400.34	9,121.76	35,826.38
11.00	4.00	1.25	4.51	4.31	4,455.14	17,017.62	6,818.88	7,734.44	36,026.08
11.00	4.01	1.31	4.45	4.31	4,331.08	17,261.68	6,586.07	7,887.17	36,066.01
11.00	3.39	1.08	3.41	3.66	4,369.96	16,963.21	8,704.88	6,890.67	36,928.72
11.00	4.90	1.29	5.50	4.48	4,686.78	16,046.36	9,350.61	6,997.14	37,080.88
11.00	4.91	1.30	5.45	4.47	4,687.41	16,788.19	9,486.71	7,089.30	38,051.62
11.00	4.00	1.31	4.45	4.32	5,261.63	17,158.60	7,481.17	8,354.18	38,255.59
11.00	3.97	1.32	4.87	4.33	4,496.00	16,974.06	8,545.34	8,713.42	38,728.83
11.00	4.42	1.35	4.60	4.30	5,579.42	17,279.48	8,230.96	8,145.70	39,235.57
11.00	4.12	1.30	4.53	4.36	4,010.15	17,378.20	10,259.60	8,579.49	40,227.44
11.00	4.14	1.31	4.55	4.59	4,927.31	18,407.42	9,663.21	7,268.93	40,266.87
11.00	4.00	1.32	4.35	4.43	4,931.75	17,821.96	8,901.86	8,666.36	40,321.93
11.00	4.13	1.31	4.44	4.72	3,688.99	20,287.56	8,287.20	8,093.10	40,356.85
11.00	4.57	1.19	4.17	4.40	3,807.57	16,476.68	10,243.87	10,190.52	40,718.65
11.00	4.41	1.37	4.60	4.31	6,420.67	17,513.96	8,649.10	8,602.20	41,185.92
11.00	4.14	1.31	4.39	4.50	4,191.24	18,023.09	10,714.64	8,282.94	41,211.91
11.00	3.99	1.31	4.78	4.59	3,468.21	19,083.41	8,707.82	9,985.02	41,244.47
11.00	4.00	1.31	4.51	4.70	5,113.56	18,392.07	8,999.56	9,155.61	41,660.80
11.00	4.13	1.30	4.30	4.44	5,696.17	18,310.37	9,321.12	8,515.35	41,843.01
11.00	4.02	1.15	4.35	4.40	4,040.50	18,986.98	9,440.42	9,629.13	42,097.03
11.00	3.39	1.30	4.72	4.45	6,161.40	18,623.56	8,361.17	8,976.68	42,122.81
11.00	4.10	1.32	4.80	4.61	3,749.19	20,200.00	8,633.06	9,861.56	42,443.81
11.00	4.11	1.30	4.18	4.42	3,436.63	18,483.50	10,397.28	10,232.89	42,550.29
11.00	4.08	1.31	4.24	4.38	3,629.51	18,425.00	10,173.85	10,845.86	43,074.22
11.00	4.14	1.30	4.23	4.30	6,666.44	19,277.47	8,832.22	8,352.65	43,128.78
11.00	4.11	1.31	4.17	4.49	5,360.71	18,892.63	9,480.07	10,227.71	43,961.12
11.00	4.13	1.30	4.15	4.36	3,086.40	18,525.10	11,884.75	10,532.46	44,028.70
11.00	4.03	1.31	4.55	4.30	5,304.73	19,160.09	9,157.02	11,403.63	45,025.47
11.00	4.11	1.30	4.20	4.42	5,010.16	18,398.09	10,661.92	11,158.65	45,228.83
11.00	4.14	1.31	4.15	4.37	5,743.18	19,151.99	10,766.16	10,715.02	46,376.35

Example data TR-12
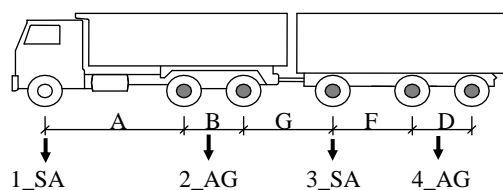
| TR-n	A	B	G	F	D	1_SA	2_AG	3_SA	4_AG	GVW
	m	m	m	m	m	kg	kg	kg	kg	kg
12.00	4.12	1.30	4.05	2.99	1.32	3,389.13	9,073.05	1,722.45	6,153.13	20,337.75
12.00	4.14	1.30	4.81	3.61	1.30	4,086.21	20,779.47	8,439.31	16,287.70	49,592.70
12.00	4.13	1.33	4.23	2.96	1.36	5,294.95	19,445.48	13,743.52	16,142.01	54,625.95
12.00	4.10	1.29	4.03	2.93	1.40	4,873.71	7,198.59	4,184.25	4,963.14	21,219.67
12.00	4.09	1.30	4.30	3.10	1.29	3,598.84	6,837.07	2,261.10	4,126.28	16,823.28
12.00	4.15	1.32	5.10	3.54	1.36	3,144.65	6,818.78	2,249.62	4,107.73	16,320.79
12.00	4.10	1.32	5.17	3.51	1.35	3,421.54	8,258.90	2,226.47	4,292.88	18,199.78
12.00	4.11	1.29	4.71	4.02	1.35	5,031.25	21,379.77	11,759.66	13,265.11	51,435.80
12.00	4.14	1.30	4.21	3.00	1.37	5,413.44	17,445.69	4,600.42	4,332.69	31,792.24
12.00	4.14	1.32	4.15	2.99	1.30	4,085.47	6,340.67	3,475.67	3,266.46	17,168.27
12.00	4.97	1.29	4.08	3.94	1.29	5,965.58	7,592.54	3,480.47	6,398.64	23,437.24
12.00	4.16	1.31	4.64	3.49	1.37	5,099.00	10,307.68	4,592.63	5,729.94	25,729.25
12.00	4.16	1.31	4.40	3.56	1.32	3,830.50	6,985.08	2,132.31	4,907.21	17,855.10
12.00	4.15	1.31	4.18	3.12	1.30	2,984.87	9,258.55	1,687.16	4,184.32	18,114.90
12.00	4.16	1.29	4.18	3.73	1.40	3,847.67	7,869.02	4,567.26	5,295.25	21,579.20
12.00	4.12	1.32	5.03	3.56	1.35	3,724.98	6,705.59	2,291.72	4,089.56	16,811.85
12.00	3.99	1.32	4.47	2.94	1.34	5,021.00	8,994.17	1,656.77	5,485.36	21,157.30
12.00	4.14	1.31	4.31	3.60	1.36	3,610.23	7,690.68	2,345.83	5,012.70	18,659.44
12.00	4.16	1.30	4.38	3.02	1.28	3,238.63	21,954.34	11,175.41	15,248.67	51,617.05
12.00	4.15	1.30	5.07	3.51	1.35	3,725.42	6,847.92	2,513.93	3,760.34	16,847.61
12.00	4.15	1.31	4.27	2.94	1.36	3,672.23	9,305.38	2,667.67	5,508.62	21,153.90
12.00	3.40	1.30	4.49	2.83	1.38	4,360.82	13,001.89	3,901.56	21,923.61	43,187.87
12.00	3.40	1.07	3.70	3.15	1.14	5,497.18	7,711.05	4,715.72	2,404.43	20,328.38
12.00	4.16	1.28	4.39	3.42	1.41	2,284.89	11,602.90	3,021.28	7,799.42	24,708.50
12.00	4.14	1.31	4.87	3.69	1.36	2,998.85	6,315.89	2,040.93	3,616.35	14,972.03
12.00	4.15	1.31	4.17	3.01	1.34	4,087.44	7,746.14	4,438.30	4,420.09	20,691.97
12.00	4.15	1.31	4.60	4.03	1.36	3,303.47	5,993.65	2,703.09	3,007.89	15,008.10
12.00	4.17	1.31	4.38	3.57	1.36	3,710.33	5,361.33	2,504.74	2,918.30	14,494.70
12.00	4.16	1.29	4.71	3.09	1.36	4,813.07	8,645.93	1,634.36	4,968.51	20,061.87
12.00	4.16	1.30	4.40	3.21	1.28	6,750.88	21,039.34	12,536.70	12,381.57	52,708.49
12.00	4.12	1.32	4.81	3.72	1.36	3,098.54	8,519.56	1,630.47	5,481.79	18,730.36

Appendix A-2
Distribution diagram for axle spacing and axle weight from of monitored truck data
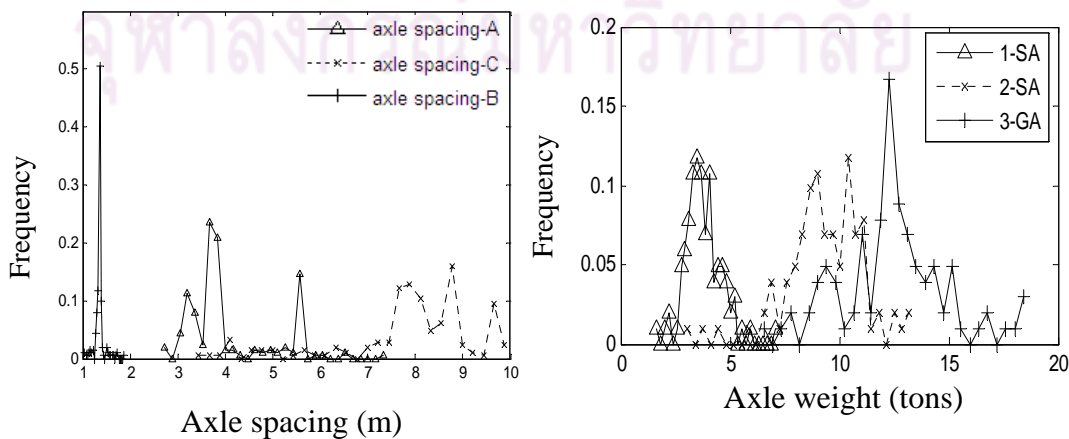
1. Distribution of axle spacing and weight for TR-02
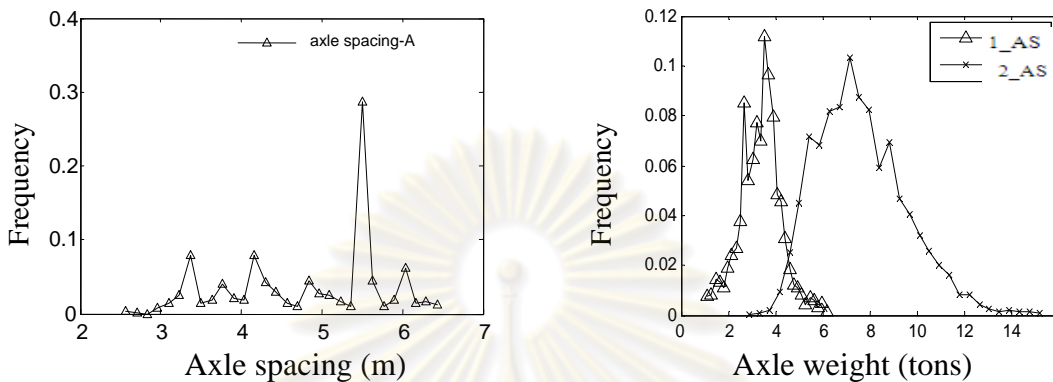
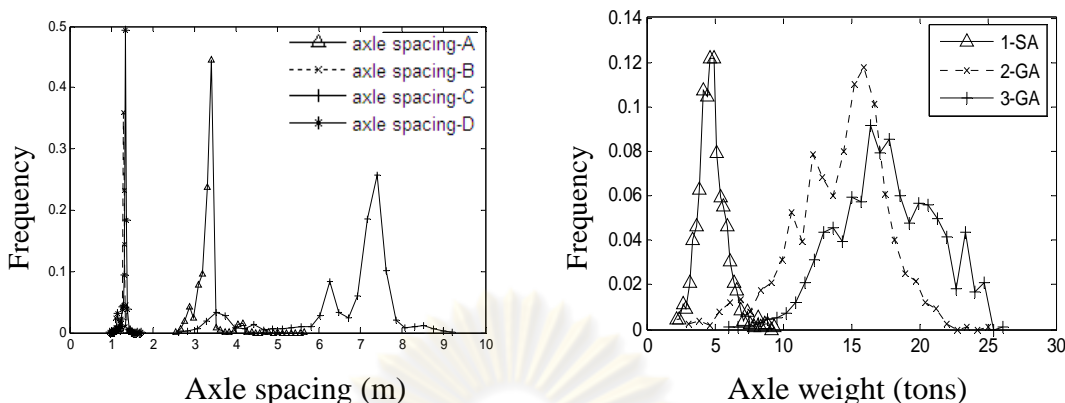2. Distribution of axle spacing and weight for TR-05
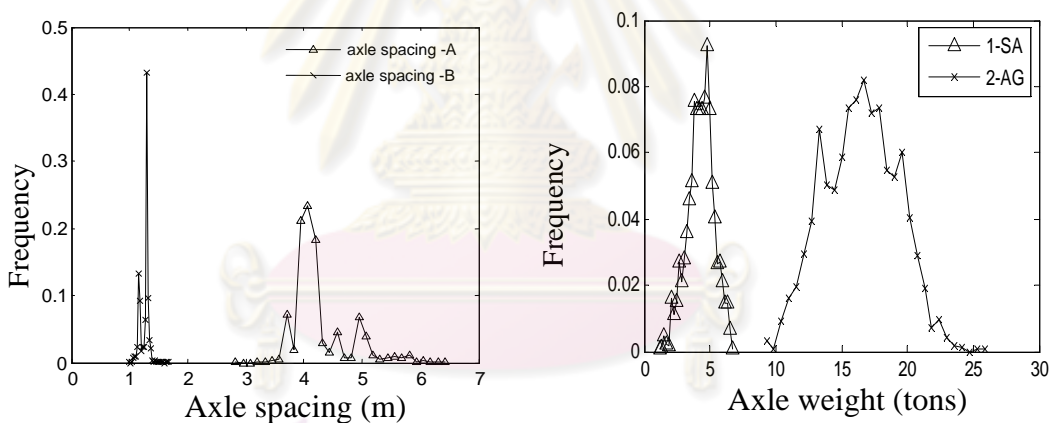
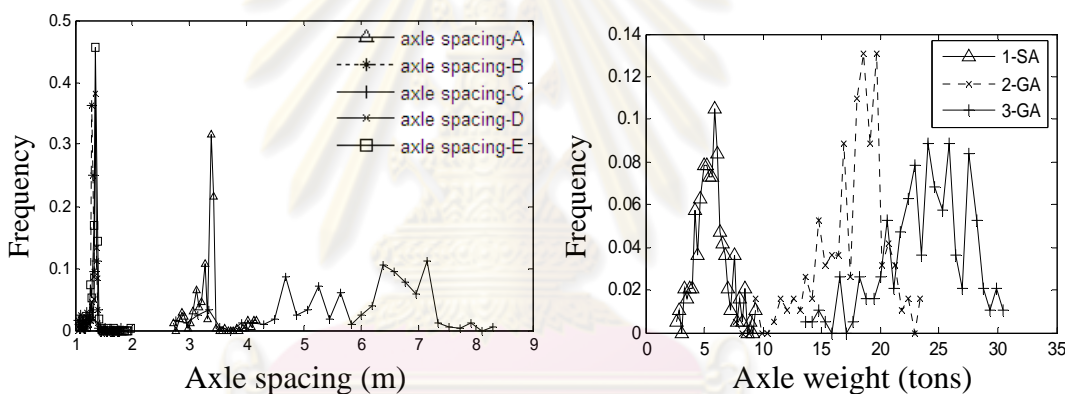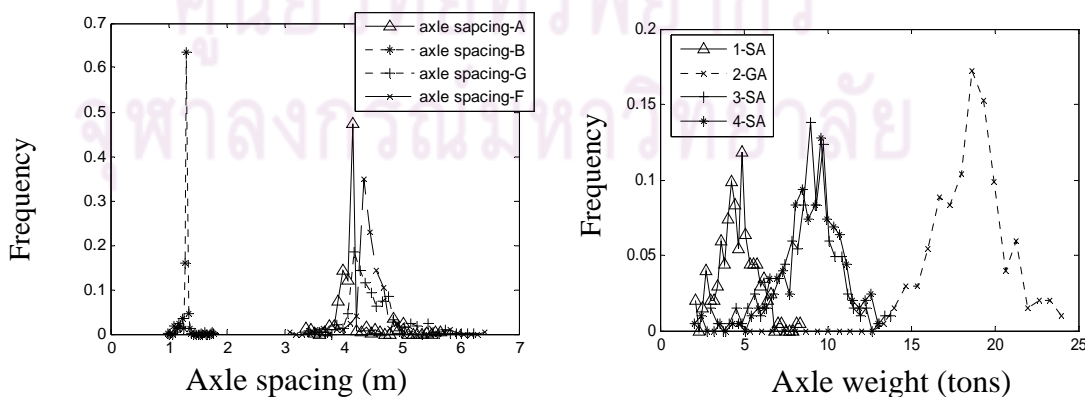3. Distribution of axle spacing and weight for TR-07

4. Distribution of axle spacing and weight for TR-09

5. Distribution of axle spacing and weight for TR-10

6. Distribution of axle spacing and weigh for TR-11

Note: For TR-12 is not enough data for plotting for axle spacing and axle weight distribution graph.

Appendix B
Truck Load Tested results for CB7, CB6, CB4S

B.1 Bridges and equipments installation for testing

Slab bridges railing barrier type, CB7

Slab bridges solid barrier type, CB6

Equipments setup, CB7

Equipments setup, , CB6

Concrete strain gauges embed on road surface, CB7

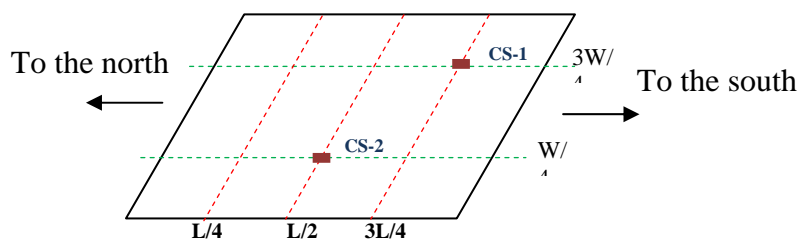Steel strain gauges embed on bottom of slab, CB6
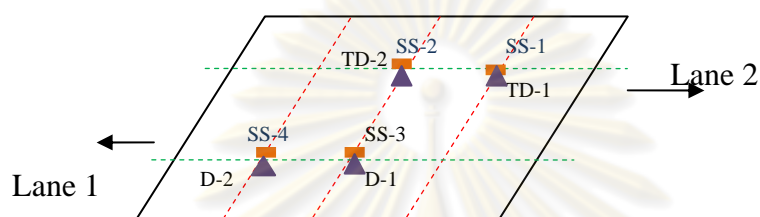

Truck test, CB7

DAQ of Kyowa PCD 300A, CB6

B.2 Truck load test results

Truck Test result for Bridge CB7:

a) Concrete strain gauges on top surface

b) Steel strain gauges and LVDT on bottom surface

CS-1, CS-2: Strain gauges on the top surface of concrete bridge slab

SS-1, SS-2, SS-3, SS-4: Stain gauges on the main steel at bottom slab bridge

TD-1, TD-2: LVDT measurement bridge deflection at the bottom slab bridge

 D-1, D-2: Dial gauges

Test result for bridge CB7

Sensor		Truck on L/2, Lane 1	Truck on L/2, Lane 1
SS-1	Micro Strain (me)	8.93	3.77
SS-2		23.47	21.08
SS-3		71.31	45.48
SS-4		12.89	30.37
CS-1		-2.97	-1.08
CS-2		-17.64	-7.70
TD-1	Deflection (mm)	-0.30	-0.24
TD-2		-0.45	-0.40
D-1		-0.99	-0.85
D-2		-0.57	-0.63

Truck Test result for Bridge CB6:

a) Concrete strain gauges on top surface

b) Steel strain gauges and LVDT on bottom surface

CS-1, CS-2: Strain gauges on the top surface of concrete bridge slab

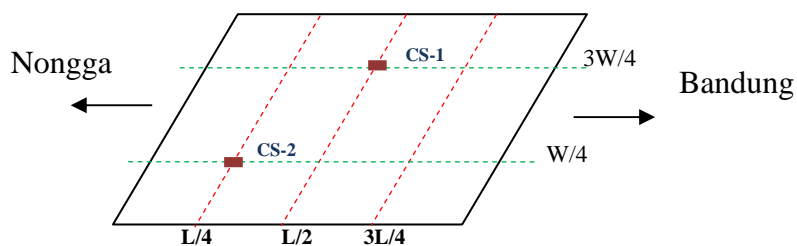SS-1, SS-2, SS-3, SS-4: Stain gauges on the main steel at bottom slab bridge

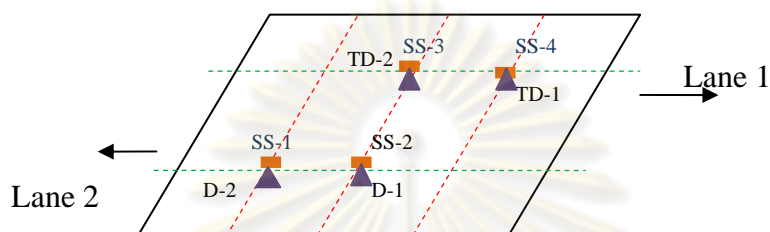TD-1, TD-2: LVDT measurement bridge deflection at the bottom slab bridge

D-1, D-2: Dial gauges

Test results for bridge CB6

Sensor		Truck on L/2, Lane 1
SS-1	Micro Strain (me)	7.45
SS-2		10.50
SS-3		29.50
SS-4		5.07
CS-1		-12.54
CS-2		-5.74
TD-1	Deflection (mm)	-0.40
TD-2		-0.60
D-1		-0.28
D-2		-0.24

Truck Test result for Bridge CB4S:

a) Concrete strain gauges on top surface
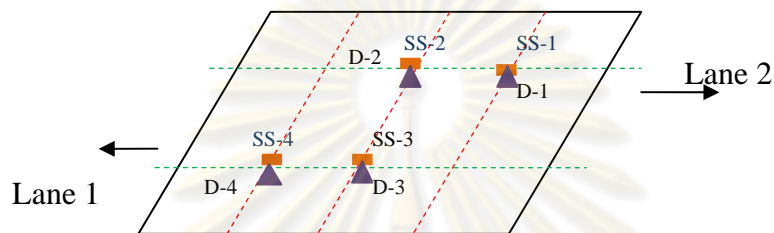
b) Steel strain gauges and LVDT on bottom surface

CS-1, CS-2: Strain gauges on the top surface of concrete bridge slab

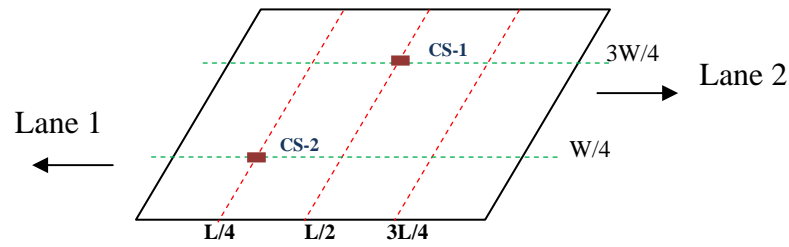SS-1, SS-2, SS-3, SS-4: Stain gauges on the main steel at bottom slab bridge

D-1, D-2: Dial gauges

D-3, D-4: Dial gauges

Test results for bridge CB4S

Sensor		Truck on L/2, Lane 1
SS-1	Micro Strain (me)	7.00
SS-2		10.00
SS-3		26.00
SS-4		6.00
CS-1		-7.00
CS-2		-20.00
D-1	Deflection (mm)	-0.15
D-2		-0.22
D-3		-0.55
D-4		-0.39

Appendix C
Crack Mapping for CB7, CB6

Crack mapping tool

a) Draw grid line 50 cm

b) Oscilloscope for crack <0.1 mm

c) Oscilloscope for crack 0.1~0.2 mm

c) Crack card for crack >0.2 mm
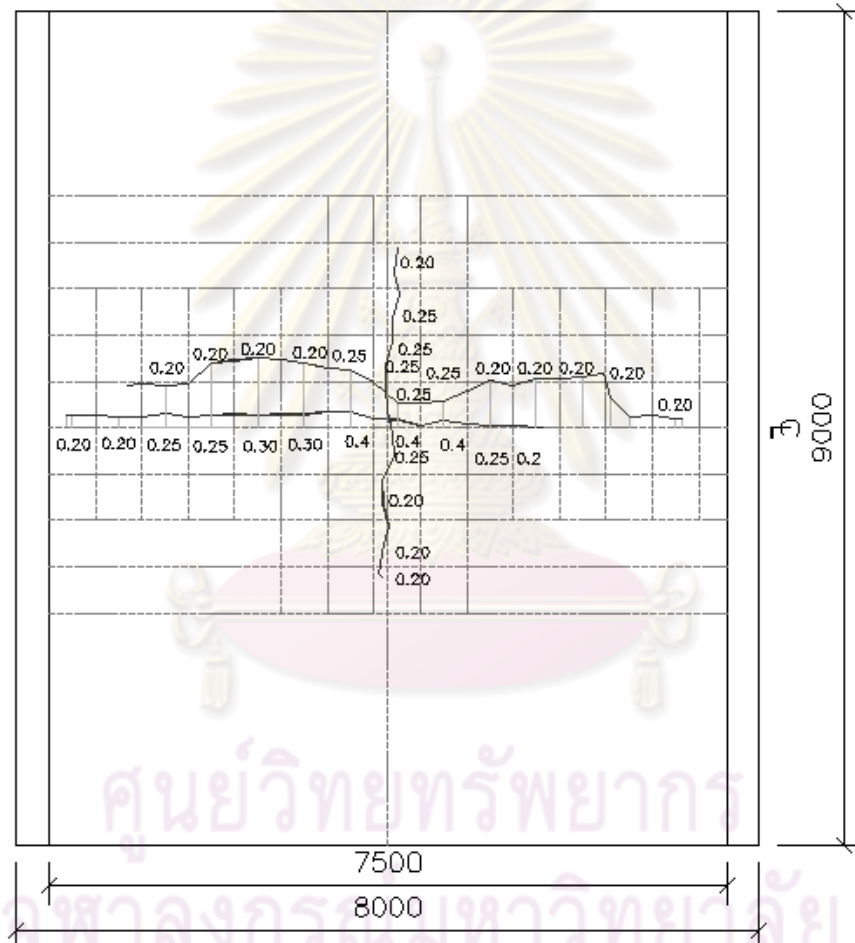
Crack mapping at the bottom slab for CB7:

CB7: Bridge picture, railing parapet type Corrosion at bottom slab, CB7

Crack mapping at the bottom slab for CB6:

CB6 : Bridge picture, solid parapet type

Appendix D-1

Example for evaluation bridge due to TR-05   **CB7**

I. Bridge data and Information
Bridge dimension

Total length	L'=	800.00	cm	8.00	m
Span length	L=	760.00	cm	7.60	m
Total width	B=	880.00	cm	8.80	m
Road way	W=	700.00	cm	7.00	m
Thickness	h=	45.00	cm	0.45	m
	d=	40.75	cm	0.41	m

Material information

Compressived strength of con	fc'= 195.00		Kg/cm2
	fr= 27.93		Kg/cm2
	Ec= 212,256.45		Kg/cm2
Yeild strength of Deform bar (DB)	fy= 3,235.00		Kg/cm2
Yeild strength of Round bar (RB)	fys= 2,400.00		Kg/cm2
Steel modulus of elasticity	Es= 2,000,000.00		Kg/cm2
	n= 9.42		

Reinforcement
Midle strip

 Longitudial reinforcement_bottom

	dia	25.00	mm
	@	11.50	cm
Area for 1m width	As=	44.16	cm2
Ratio for 1m width	p=	0.011	mm

 Transverse reinforcement_bottom

	dia	12.00	mm
	@	14.00	cm

Bridge section
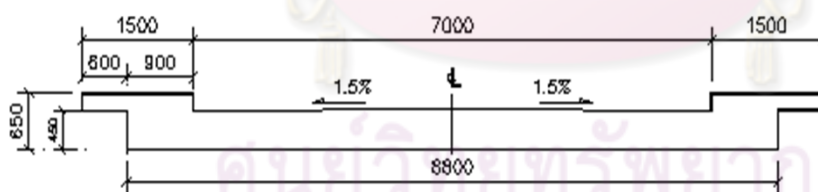
Section of bridge

II. Bridge Analysis
1 Bridge factor
Equilvalent strip by AASHTO

E=1.2+0.06S(m)<=2.1m

    E= 1.656 m

Select equilvalent width E= ***1.656*** m

Impact factor of live load I=50/(L+125)<=0.3

    I=50/(L+125)= 0.33 (L in feet)
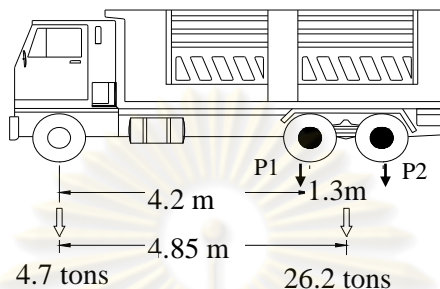
    Use   I= 0.3

2 Analysis

Dead load

Total load   DL=   1380.06 kg/m2

Truck load from monitored data, TR-05   (Thai truck, ten whells truck)

	Axle 1=	4700 kg
P1=	Axle 2=	13100 kg
P2=	Axle 3=	13100 kg
	Total=	30900 kg

Truck TR-05
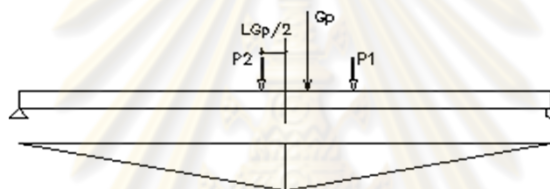
Critical truck position

Dead load

The bridge due to dead load has been assumed as beam in 1m width

Moment due to Dead load for 1m width

Distant from support

L'		BM in 1m	1.3DL
m		kgm	kgm
0.80	=	3,753.76	4,879.89
1.00	=	4,554.20	5,920.46
1.20	=	5,299.43	6,889.26
1.50	=	6,313.77	8,207.91
1.70	=	6,921.00	8,997.30
2.20	=	8,197.56	10,656.82
2.40	=	8,611.57	11,195.05
2.75	=	9,203.28	11,964.26
3.10	=	9,625.92	12,513.69
3.48	=	9,891.15	12,858.49
3.80	=	9,964.03	12,953.24

Bending moment due to truck load (All truck load)

BM, when P2 is at the midspan of the bridge, the maximu BM will be at midspan

Pi	Xi	L	X	li	LGp	Pi*li
kg	m	m	m			kgm
13,100.00	3.80	7.60	3.80	1.90	0.65	24,890.00
13,100.00	5.10	7.60	3.80	1.25	0.65	16,375.00
						41,265.00

BM, when P2 is at LGp/2 from midspan, the maximu BM will be at under position P2

Pi	Xi	L	X	li	LGp	Pi*li
kg	*m*	*m*	*m*			*kgm*
13,100.00	3.48	7.60	3.48	1.89	0.65	24,707.94
13,100.00	4.78	7.60	3.48	1.29	0.65	16,921.19
						41,629.13

Total Bending moment DL and LL for 1m width

	DL	LL in1m	DL+LL	1.3DL+LL(1+I)
	kgm	*kgm*	*kgm*	*kgm*
Bm at midspan=	9,964.03	12,459.24	22,423.27	29,150.25
Bm at section P2=	9,891.15	12,569.18	22,460.33	29,198.43

Select maximum ultimate forces from analysis result

		DL	LL	
Select	Mmax=	**9891.15**	**12569.18**	(kgm)

II. Bridge Capacity Evaluation (Load Factor method)

Rating equation and parameters

$$RF = \frac{C - A_1 * D}{A_2 * L * (1 + I)}$$

Where
RF = Rating factor for live load capacity
A1 = Factor for dead loads
A2 = Factor for live load
C = Capacity of the bridge
D = Dead load effect
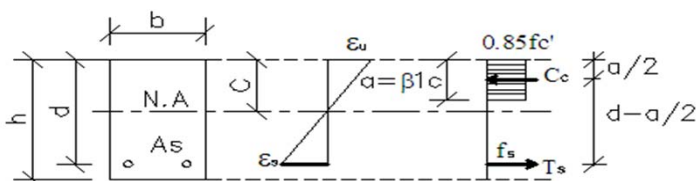I = Impact factor
C = Capacity of the member
L = Live load effect

Parameters and factors for load factor method

	Operating level
A1=	1.3
A2=	1.3

Capacity of the member

	Operating level
For flexural Cm=ϕ*Mn	ϕ= 0.9

Flexural bridge capacity

$$C_c = 0.85 * f_c' * a * b$$

$$T_s = As * f_s$$

Checking maximium tension bar ratio   0.75Pb= 0.75*0.85*B1*(fc'/fy)*(6000/(6000+fy)

Parameter   B1=
0.85	fc'<=280 ksc
0.85-0.05*(fc'-280)/70	280<fc'<=560
0.65	fc'>561

0.75Pb=   0.028
p=   0.011

Atual reinforced less than balance condition, this is underreinforcement slab

Flexural capacity of the slab
a=p*fy*d/(0.85f'c)=   8.62   cm
Mn=p*b*d*fy*(d-a/2)=   52,058.12   kgm

C=φ*Mn=   46,852.31   kgm

Rating for Operating level
Rating factor for flexural

$$RF_m = \frac{C - 1.3*Mdl}{1.3*Mll*(1+0.3)}$$

RFm=   1.60

Rating Factor for Inventory level

$$RF_{(inv)} = \frac{3}{5} RF_{(opr)}$$

Rating factor for flexural
RFm=   0.96

III. Bridge Ultimated load
Resistant moment of the slab bridge for one meter width

φ*Mn=   46,852.31   kgm

P1um_tr: applied load of one axle truck for one meter width (assuming truck load P1=P2)
P1um_tr= Mc*L/((2L-X1-X2)(L/2-LGp/2))
***P1um_tr=   10,697.29** kg*

Pue_tr: applied load of one axle truck for equivalent width
***Pue_tr=E*P1un_tr=   17,714.72** kg*

Pu_tr: Total applied axle truck for two lane bridge
***Pu_tr=4*Pue_tr=   141,717.75** kg*

Pmax=P1max=P2max: Maximum axle truck that can applied to bridge
***Pmax=Pue_tr/(1.3*(1+0.3))=   20,964.16** kg*

Total ultimate load 1.3DL+1.3TR(1+0.3)
***Pul=   250,797.69** kg*

Appendix D-2

Example meam theory method for analysis concrete slab bridge   CB7
1. General data
   Bridge data

Total length	l=	8.00	m	8000	mm
Bridge span	L=	7.60	m	7600	mm
Bridge lane road width	W1=	7.00	m	7000	mm
Walk way	W2=	1.50	m	1500	mm
Slab structure width	W=	8.80	m	8800	mm
Slab thickness	t1=	0.45	m	450	mm
Walk way thickness	t2=	0.20	m	200	mm
Asphalt surface	t3=	0.05	m	50	mm
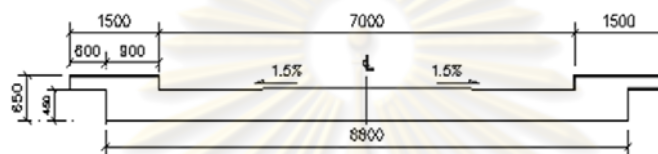
Section of bridge

   Material data

Concrete comp. strength	fc'=	195.00	ksc
Modulus of the conceret	Ec=	212,256.45	ksc
Yield strenght of the still	fy=	3,235.00	ksc
Modulus of the steel	Es=	2,000,000.00	
	n=	9.42	
Unit weigth of the concrete	gc=	2,325.00	kg/m3
Uniweigth of asphalt	ga=	1,800.00	kg/m3
Ruture concrete strength	fr=	27.93	ksc

   Reinforcement data

Reinforced steel at the bottom pararell to traffic at midle strip

dia	25	mm
@	11.5	cm

2. Calculate section properties
   Moment interia (for 1m of slab bridge)

H	=	45.00	cm
B	=	100.00	cm
As'	=	0.00	cm2
As	=	44.18	cm2
Transforma (n-1)As'	=	0.00	cm2
(n-1)As	=	372.10	cm2
Transforma nAs	=	416.28	cm2
p	=	0.011	
p'	=	0	

Moment inertia of transform section beforce concrete crack   *Ig*

Section	A	Y		AY	dt	Ad^2	Ixx	Iyy
	cm2	cm		cm3	cm	cm4	cm4	cm4
1	4,500.00	22.50		101,250.00	-1.39	8,742.18	759,375.00	
2	372.10	4.25		1,581.41	16.86	105,724.48		
	4,872.10	21.11		102,831.41		114,466.66	***873,841.66***	

Moment inertia of transform section after concrete crack **Icr**

	effetive depth	d	=	40.75	cm
	pn	=	0.102	
(Rec with comp steel)	k	=	(2pn+(pn)^2)^0.5 -pn	0.361
	Xc	=	k*d	14.72	cm
	j	=	1-k/3	0.88

Icr

Section	A	Y		AY	dt	Ad^2	Ixx	Iyy
	cm2	cm		cm3	cm	cm4	cm4	cm4
1	1,472.09	37.64		55,408.88	-7.36	79,752.69	26,584.23	
2	416.28	4.25		1,769.17	26.03	282,032.37		
	1,888.37	30.28		57,178.06		361,785.07	388,369.30	

Flectural cracking moment

Mcr= fr*Ig/yt

		fr	=	27.93	ksc
Gross moment inertia in 1m	Ig	=	873,841.66	cm4
	yt	=	21.11	cm
at con outer fiber	Mcr	=	11,562.99	kgm	1,156,299.15 kgcm

Effective moment of inertia

Ie = (Mcr/Ma)^3*Ig+(1-(Mcr/Ma)^3)*Icr

3. Bridge applied load

Bridge factor loads

The factor loads is according to AASHTO manual for bridge rating

Dead load factor	A1=	1.30
Live load factor	A2=	1.30
Impact factor	I=	0.30

Dead load

| Total load | DL= | 1,380.06 | kg/m2 |

| Total 1.3DL | 1.3DL= | 1,708.96 | kg/m2 |

Live load

Truck load from monitored data, TR-05   (Thai truck, ten whells truck)

	Axle 1=	4,700.00	kg
P1=	Axle 2=	13,100.00	kg
P2=	Axle 3=	13,100.00	kg
	Total=	**30,900.00**	**kg**
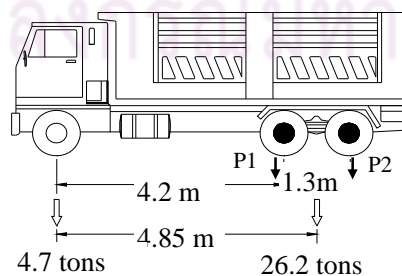
Truck TR-05

Equilvalent strip, AASHTO

$$E=1.2+0.06S(m)<=2.1m$$
$$E= \quad 1.656 \quad m$$

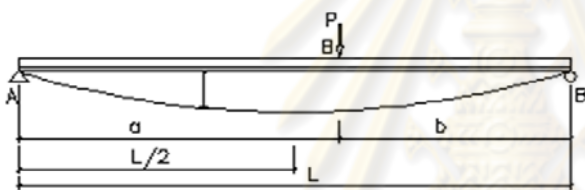Select equilvalent width   E=   ***1.656***   m

Impact factor of live load

$$I=50/(L+125)= \quad 0.33 \quad \text{(note L in feet)}$$
$$\text{Use} \quad I= \quad \textbf{0.3}$$

For mula for deflection due to applied DL for 1m width

$$\delta_x = \frac{wx}{24EI}(x^3 - 2Lx^2 + L^3) \qquad \delta_{L/2} = \frac{5wL^4}{384EI}$$
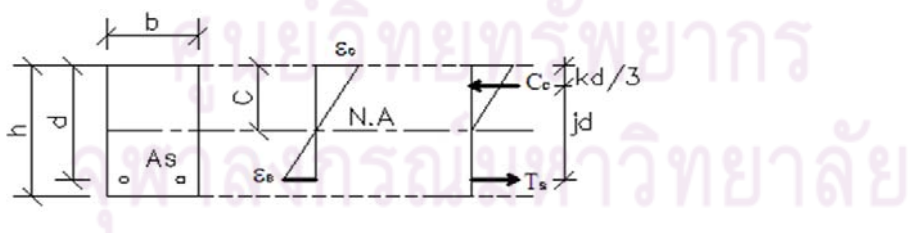
For mula for deflection due to TR-05

$$0 < x < a, \delta_x = \frac{Pbx}{6EIL}(L^2 - b^2 - x^2) \qquad a < x < L, \delta_x = \frac{Pa(L-x)}{6EIL}(2Lx - a^2 - x^2)$$

For mula for Stress and strain due to DL and TR-05

The linear section of beam is assumed

At the elestic state/ uncrack section   M<Mcr

Stress at steel lavel   ***σs= n*M*y/Igt***

At the crack section state   M>=Mcr

Stress at steel lavel   ***σs= M/As*Jd***

VITA

I was born in Xiengkhouang Province, Lao P.D.R, on April 14th, 1975. I graduated the high school level at Phonesavanh high school, Xiengkhuang Province. Then I finished the bachelor's degree of civil engineering at National University of Laos in 1999. After that in 2002, I attended my graduate level at Communication and Transport University, Hanoi, Vietnam and graduated the master's degree of civil engineering in 2004. In the academic year 2005, I began to study in Ph.D. at civil engineering, the structural division, Chulalongkorn University under supervisor by Associate Professor Doctor Phoonsak Pheinsusom who is a specialist in the field of my study.

ศูนย์วิทยทรัพยากร
จุฬาลงกรณ์มหาวิทยาลัย